



ПОЛИТЕХ
Санкт-Петербургский
политехнический университет
Петра Великого

Инженерно-строительный институт
Центр дополнительных профессиональных программ
195251, г. Санкт-Петербург, Политехническая ул., 29,
тел/факс: 552-94-60, www.stroikursi.spbstu.ru,
stroikursi@mail.ru

**Приглашает специалистов организаций, вступающих в СРО,
на курсы повышения квалификации (72 часа)**

Код	Наименование программы	Виды работ*
Курсы по строительству		
БС-01-04	«Безопасность и качество выполнения общестроительных работ»	п.1,2, 3, 5, 6, 7, 9, 10, 11, 12, 13, 14
БС-01	«Безопасность и качество выполнения геодезических, подготовительных и земляных работ, устройства оснований и фундаментов»	1,2,3,5
БС-02	«Безопасность и качество возведения бетонных и железобетонных конструкций»	6,7
БС-03	«Безопасность и качество возведения металлических, каменных и деревянных конструкций»	9,10,11
БС-04	«Безопасность и качество выполнения фасадных работ, устройства кровель, защиты строительных конструкций, трубопроводов и оборудования»	12,13,14
БС-05	«Безопасность и качество устройства инженерных сетей и систем»	15,16,17,18,19
БС-06	«Безопасность и качество устройства электрических сетей и линий связи»	20,21
БС-08	«Безопасность и качество выполнения монтажных и пусконаладочных работ»	23,24
БС-12	«Безопасность и качество устройства мостов, эстакад и путепроводов»	29
БС-13	«Безопасность и качество выполнения гидротехнических, водолазных работ»	30
БС-14	«Безопасность и качество устройства промышленных печей и дымовых труб»	31
БС-15	«Осуществление строительного контроля»	32
БС-16	«Организация строительства, реконструкции и капитального ремонта. Выполнение функций технического заказчика и генерального подрядчика»	33
Курсы по проектированию		
БП-01	«Разработка схемы планировочной организации земельного участка, архитектурных решений, мероприятий по обеспечению доступа маломобильных групп населения»	1,2,11
БП-02	«Разработка конструктивных и объемно-планировочных решений зданий и сооружений»	3
БП-03	«Проектирование внутренних сетей инженерно-технического обеспечения»	4
БП-04	«Проектирование наружных сетей инженерно-технического обеспечения»	5
БП-05	«Разработка технологических решений при проектировании зданий и сооружений»	6
БП-06	«Разработка специальных разделов проектной документации»	7
БП-07	«Разработка проектов организации строительства»	8
БП-08	«Проектные решения по охране окружающей среды»	9
БП-09	«Проектные решения по обеспечению пожарной безопасности»	10
БП-10	«Обследование строительных конструкций и грунтов основания зданий и сооружений»	12
БП-11	«Организация проектных работ. Выполнение функций генерального проектировщика»	13
Э-01	«Проведение энергетических обследований с целью повышения энергетической эффективности и энергосбережения»	
Курсы по инженерным изысканиям		
И-01	«Инженерно-геодезические изыскания в строительстве»	1
И-02	«Инженерно-геологические изыскания в строительстве»	2,5
И-03	«Инженерно-гидрометеорологические изыскания в строительстве»	3
И-04	«Инженерно-экологические изыскания в строительстве»	4
И-05	«Организация работ по инженерным изысканиям»	7

*(согласно приказам Минрегионразвития РФ N 624 от 30 декабря 2009 г.)

**По окончании курса слушателю выдается удостоверение о краткосрочном повышении
квалификации установленного образца (72 ак. часа)**

Для регистрации на курс необходимо выслать заявку на участие, и копию диплома об образовании по телефону/факсу: 8(812) 552-94-60, 535-79-92, , e-mail: stroikursi@mail.ru.

Инженерно-строительный журнал

НАУЧНОЕ ИЗДАНИЕ

ISSN 2071-4726, 2071-0305

Свидетельство о государственной регистрации: ПИ №ФС77-38070, выдано Роскомнадзором

Специализированный научный журнал. Выходит с 09.2008.

Включен в Перечень ведущих периодических изданий ВАК РФ

Периодичность: 8 раз в год

Учредитель и издатель:

Санкт-Петербургский политехнический университет Петра Великого

Адрес редакции:

195251, СПб, ул. Политехническая, д. 29, Гидрокорпус-2, ауд. 227А

Главный редактор:

Екатерина Александровна Линник

Научный редактор:

Николай Иванович Ватин

Выпускающий редактор:

Ксения Дмитриевна Борщева

Литературный редактор:

Крупина Анастасия

Редакционная коллегия:

д.т.н., проф. В.В. Бабков;
 д.т.н., проф. М.И. Бальзанников;
 к.т.н., проф. А.И. Боровков;
 д.т.н., проф. Н.И. Ватин;
 PhD, проф. М. Вельжкович;
 д.т.н., проф. А.Д. Гиргидов;
 д.т.н., проф. Э.К. Завадскас;
 д.ф.-м.н., проф. М.Н. Кирсанов;
 D.Sc., проф. М. Кнежевич;
 д.т.н., проф. В.В. Лалин;
 д.т.н., проф. Б.Е. Мельников;
 д.т.н., проф. Ф. Неправишта;
 д.т.н., проф. Р.Б. Орлович;
 Dr. Sc. Ing., professor
 Л. Пакрастиньш;
 Dr.-Ing. Habil., professor
 X. Пастернак;
 д.т.н., проф. А.В. Перельмутер;
 к.т.н. А.Н. Пономарев;
 д.т.н., доцент В.В. Сергеев;
 д.ф.-м.н., проф. М.Х. Стрелец;
 д.т.н., проф. О.В. Тараканов;
 д.т.н., проф. В.И. Травуш

Дата выхода: 25.06.2018

Содержание

Краснощеков Ю.В., Красотина Л.В., Пулидо-Делегадо Х. Модели прямой анкеровки арматуры в бетоне	3
Мандровский К.П., Садовникова Я.С. Характеристики движения капель жидкого противогололедного реагента	14
Орлов В.А., Дежина И.С., Орлов Е.В. Микротурбулентность потока и ее связь с рельефом внутренней поверхности трубопроводов	27
Травуш В.И., Конин Д.В., Крылов А.С. Прочность железобетонных балок с жесткой арматурой из высокопрочного бетона	36
Бушманова А.В., Харченко Д.К., Семенов К.В., Барабанщиков Ю.Г., Коровина В.К., Дернакова А.В. Термическая трещиностойкость массивных сталежелезобетонных конструкций	45
Тюкалов Ю.Я. Улучшенный стержневой конечный элемент для решения задач устойчивости	54
Федюк Р.С., Лесовик В.С., Свинцов А.П., Мочалов А.В., Куличков С.В., Стоюшко Н.Ю., Гладкова Н.А., Тимохин Р.А. Самоуплотняющийся бетон с использованием предварительно подготовленной золы рисовой шелухи	66
Саинов М.П., Котов Ф.В., Назаров Н.В. Работоспособность сверхвысокой каменно-набросной плотины с противофильтрационным элементом в виде комбинации железобетонного экрана и инъекционной завесы	77
Гравит М.В., Голуб Е.В., Антонов С.П. Огнезащитный штукатурный состав для конструкций в условиях углеводородного горения	86
Иванов К.С. Гранулированная пеностеклокерамика для защиты грунтов от сезонного промерзания и морозного пучения	95
Виейра Г.Б., Петриченко М.Р., Мусорина Т.А., Заборова Д.Д. Деревянный фасад с вентилируемыми каналами для тропического климата	103
Орлович Р.Б., Беспалов В.В., Деркач В.Н. Сжато-изгибаемые каменные стены, армированные композитными материалами	112
Лебедев В.В., Нуднер И.С., Беляев Н.Д., Семенов К.К., Щемелинин Д.И. Формирование рельефа донной поверхности у гравитационного объекта	120
Рассохин А.С., Пономарев А.Н., Фиговский О.Л. Сверхлегкие гибридные композитные древесно-полимерные конструкционные элементы в строительстве	132
Введенский Р.В., Гендлер С.Г., Титова Т.С. Влияние строительства тоннелей на окружающую среду	140

© ФГАОУ ВО СПбПУ, 2018

На обложке: иллюстрации авторов к статьям номера

Контакты:

Тел. +7(812)535-52-47 E-mail: mce@spbstu.ru

Web: <http://www.engstroy.spbstu.ru>

Magazine of Civil Engineering

SCHOLAR JOURNAL

ISSN 2071-4726, 2071-0305

Peer-reviewed scientific journal

Start date: 2008/09

8 issues per year

Publisher:Peter the Great St. Petersburg
Polytechnic University**Indexing:**Scopus, Russian Science Citation
Index (WoS), Compendex, DOAJ,
EBSCO, Google Academia, Index
Copernicus, ProQuest, Ulrich's Serials
Analysis System**Corresponding address:**227a Hydro Building, 29
Polytechnicheskaya st., Saint-
Petersburg, 195251, Russia**Editor-in-chief:**

Ekaterina A. Linnik

Science editor:

Nikolay I. Vatin

Technical editor:

Ksenia D. Borshcheva

Editorial board:

V.V. Babkov, D.Sc., professor
 M.I. Balzannikov, D.Sc., professor
 A.I. Borovkov, PhD, professor
 M. Veljkovic, PhD, professor
 E.K. Zavadskas, D.Sc., professor
 M.N. Kirsanov, D.Sc., professor
 M. Knezevic, D.Sc., professor
 V.V. Lalin, D.Sc., professor
 B.E. Melnikov, D.Sc., professor
 F. Nepravishita, D.Sc., professor
 R.B. Orlovich, D.Sc., professor
 L. Pakrastinsh, Dr.Sc.Ing., professor
 H. Pasternak, Dr.-Ing.habil.,
 professor
 A.V. Perelmuter, D.Sc., professor
 A.N. Ponomarev, PhD, professor
 V.V. Sergeev, D.Sc., associate
 professor
 M.Kh. Strelets, D.Sc., professor
 O.V. Tarakanov, D.Sc., professor
 V.I. Travush, D.Sc., professor

Date of issue: 25.06.2018

Contents

Krasnoshchekov Y.V., Krasotina L.V., Pulido-Delgado J.L. Models of direct anchoring of reinforcement in concrete	3
Mandrovskiy K.P., Sadovnikova Y.S. Characteristics of the droplet motion of a liquid antifreeze reagent	14
Orlov V.A., Dezhina I.S., Orlov E.V. Micro-turbulence of the stream and its connection with the roughness of the pipeline inner surface.	27
Travush V.I., Konin D.V., Krylov A.S. Strength of composite steel and concrete beams of high-performance concrete	36
Bushmanova A.V., Kharchenko D.K., Semenov K.S., Barabanshchikov Yu.G., Korovina V.K., Dernakova A.V. Thermal cracking resistance in massive steel-reinforced concrete structures	45
Tyukalov Yu.Ya. Thermal cracking resistance in massive steel- reinforced concrete structures	54
Fediuk R.S., Lesovik V.S., Svintsov A.P., Mochalov A.V., Kulichkov S.V., Stoyushko N.Y., Gladkova N.A., Timokhin R.A. Self-compacting concrete using pretreated rice husk ash	66
Sainov M.P., Kotov F.V., Nazarov N.V. Serviceability of ultrahigh rockfill dam with seepage-control element presented by combination of a reinforced concrete face and a grout curtain	77
Gravim V.V., Golub E.V., Antonov S.P. Fire protective dry plaster composition for structures in hydrocarbon fire	86
Ivanov K.S. Granulated foam-glass ceramics for ground protection against freezing	95
Vieira G.B., Petrichenko M.R., Musorina T.A., Zaborova D.D. Behavior of a hollowed-wood ventilated façade during temperature changes	103
Orlovich R.B., Bepalov V.V., Derkach V.N. Compressed-bent masonry walls reinforced with composite materials	112
Lebedev V.V., Nudner I.S., Belyaev N.D., Semenov K.K., Schemelinin D.I. The formation of the seabed surface relief near the gravitational object	120
Rassokhin A.S., Ponomarev A.N., Figovsky O.L. The formation of the seabed surface relief near the gravitational object	132
Vvedenskij V.R., Gendler S.G., Titova T.S. Environmental impact of the tunnel construction	140

© Peter the Great St. Petersburg Polytechnic University. All rights reserved.

On the cover: authors' illustrations

+7(812) 535-52-47

E-mail: mce@spbstu.ruWeb: <http://www.engstroy.spbstu.ru/eng/index.html>

doi: 10.18720/MCE.79.1

Models of direct anchoring of reinforcement in concrete

Модели прямой анкеровки арматуры в бетоне

Y.V. Krasnoshchekov,
L.V. Krasotina,
Siberian state automobile and road university,
Omsk, Russia
J.L. Pulido-Delgado,
Universidad Autónoma de San Luis Potosí
"UASLP", San Luis Potosi, Mexico

Д-р техн. наук, профессор
Ю. В. Краснощеков,
канд. техн. наук, доцент Л.В. Красотина,
Сибирский государственный автомобильно-
дорожный университет, г. Омск, Россия
канд. техн. наук, профессор
Х. Пулидо-Делегадо,
Автономный университет Сан-Луис-
Потоси, Сан Луиз Потоси, Мексика

Key words: reinforced concrete; stress-strain state; anchoring of reinforcement; modeling and theory of elasticity

Ключевые слова: железобетон; напряженно-деформированное состояние; анкеровка арматуры; моделирование; теория упругости

Abstract. When analyzing methods for calculating the anchoring of non-tension reinforcement of reinforced concrete structures, it has been established that there are two types of destruction of concrete in the anchoring zone by shearing or cracking. They are based on the results of research of the strength the adhesion of reinforcement with concrete and testing of specimens with the same type. A new model of anchoring has been created. This model initial moment is the equality of deformations of the elements of equality deformation elements. A new anchoring model was developed. This model is based on the equality of deformations of the elements. For theoretical substantiation were used the ideas of the theory of elasticity about the action of a concentrated force at the point of half-space and the results of computer simulation of the anchoring zone of reinforcement in concrete. Modeling of reinforced concrete samples was carried out using the finite element method.

Аннотация. При анализе методов расчета анкеровки ненапрягаемой арматуры железобетонных конструкций установлено, что существуют два вида разрушения бетона в зоне анкеровки срезом или расколом. Они основаны на результатах исследования прочности сцепления арматуры с бетоном и испытаниях однотипных образцов. Разработана новая модель анкеровки, исходным моментом которой является равенство деформаций элементов. Для теоретического обоснования привлекаются задачи теории упругости о действии сосредоточенной силы в точке полупространства и результаты компьютерного моделирования зоны анкеровки арматуры в бетоне. Моделирование образцов железобетонных конструкций производилось с использованием метода конечных элементов.

1. Introduction

It is accepted that the reliability of the anchoring of non-tensioning reinforcement depends basically on the factors determining the adhesion of the reinforcement to the concrete [1]. The empirical basis of the calculated dependencies are the "pull-out" tests of the reinforcing armature bar out of prisms, fixed to the surface [2]. In the last years very often was used the scheme which was recommended in 1983 by international organizations RILEM, FIP and CEB [3].

Tear-out tests are used to determine the adhesion of reinforcement to concrete and serve to compare the adhesion strength of reinforcement bars of different profiles. The effective bond length in the test samples is only 5 diameters of the reinforcement, therefore the results of the test cannot be a confirmation of the reliability of the calculated value of the anchoring length. The dimensions of the concrete samples ($200 \text{ mm} > 10 d$), the length of the section of the armature covered by plastic cuffs (the section with the removed coupling $5 d \geq (200 \text{ mm} - 5 d)$) and the loading speed are regulated.

During testing special samples according to this scheme, the destruction of anchoring occurs two ways both – by cutting the concrete surrounding the armature bar and by developing cracks along the reinforcement, with followed cracking of the concrete. Accordingly, the exhaustion of the anchoring

strength in the test samples is accompanied by a controlled displacement of the unloaded end of the reinforcement (up to 3 mm) or destruction of the concrete.

The theoretical model of the interaction of the reinforcement with concrete, which was realized with the destruction of the anchoring by shear, was placed in the basis of the technical theory of adhesion at VNIIZhilezobeton with a number of several of simplifying assumptions. One of the assumptions is linked to the neglect of the stressed-deformed state of concrete in the envelope shell surrounding the reinforcement beyond the contact layer, as result the destruction of the anchoring occurs only by shearing. Recognizing this deficiency, the authors of the theory of coupling allowed the possibility of removing it by special (constructive) methods. They believed that "accidental nature of the development of longitudinal cracks, their danger and the difficulty of their calculated make it necessary to widely apply transverse reinforcement" [5].

In Russian and European design standards has been adopted a model of destruction of the shear. The transition from the probabilistic model of Russian standard (SNIP 2.03.01-84*) to the physical model of Eurocode 2 [6] and SNIP 52-101-2003 made it possible to more accurately reflect the mechanism of interaction of reinforcement with concrete at the anchoring length, but at the same time it wasn't provide demands of the Russian design standards to need to consider the influence of the stressed state of concrete, the protective layer, group reinforcement, formation and development of cracks, and so on the anchoring length.

Destruction from cracking is considered unacceptable as very dangerous, and for its prevention provides structural events (transverse reinforcement, compression of concrete, etc.).

Destruction from cracking is usually associated with the formation and development of cracks along the reinforcement. In old Russian standard (SNIP 2.03.01-84*), constructive measures were provided to prevent the formation of cracks from stretching the concrete along the anchored rods. But the conditions of formation such cracks in the anchoring zone by design standards aren't described. In the current design standards the possibility of splitting concrete in the anchoring zone of non-tensioning reinforcement isn't mentioned at all.

It's known that the transition from calculated methods of ensuring reliability to constructive methods indicates about non-availability of development of the theory. For this reason and with the appearance of new types of reinforcement, the question of the reliability of anchoring in different conditions arises again.

In the United States and some other countries the concept of design model of the destruction anchorage failure of anchoring as a result of splitting the concrete shell around the reinforcement from ring stresses is common [7, 8]. The idea of this model (the analogy of hydrostatic pressure) was first time presented by R. Telfers in 1973 [9, 10]. On figure 1 shows the distribution of circular (splitting) stresses σ_t in a concrete shell with reinforcing bar located at the distance c from the surface of the shell or structural element. On figure 1 shows the distribution of circular stresses σ_t in a concrete shell with reinforcing bar located at the distance from the surface of the shell or structural element. R. Telfers considered the stressed-deformed state of the concrete shell in the elastic stage and took the stress distribution angle σ_t along the anchoring length $\alpha = 45^\circ$. Later the model was made more accurate by taking into account the plastic deformations and angle was decreased to $\alpha = 30^\circ$ [11, 12].

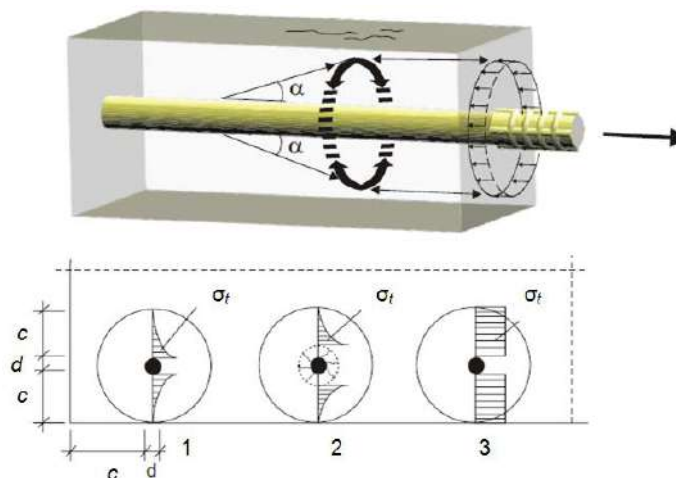


Figure 1. Tensile stresses in a concrete shell in the elastic stage – 1; stresses in the concrete shell in the elastic stage with cracks – 2; stresses in the concrete shell in the plastic stage – 3

The priority factor for breaking by splitting is the thickness of the protective layer of concrete but is not profile of armature [13, 14]. Cracks in the protective layer of concrete sharply reduce the adhesion strength, so their formation isn't allowed.

According to P. Telfers's model, the splitting occurs under the following condition: $\sigma_t = R_{bt}$, in which the stress σ_t for stage 3 (Figure 1) is determined by the following formula:

$$\sigma_t = Tdtg\alpha / 2c . \quad (1)$$

Research of the effect of puncturing cracks on the anchoring of reinforcing bars of periodic profiles was carried out in Russia [15, 16].

To obtain experimental data on the adhesion of reinforcement to the concrete of the protective layer, by standard EN 10080:2005 provides for the testing of special samples in the form of beams (Figure 2). Beam models were used, for example, when was researched models of the adhesion of rusted reinforcement to concrete [17].

Recently, attempts have been made to improve the theory of adhesion [13, 18, 20, 21], including using finite element models [19, 22, 23, 31]. But now the calculation models of anchoring used in design standards have an empirical basis. Different coefficients are used which characterize the adhesion of the reinforcement to the concrete. It should be noted that experimental researches of the interaction of reinforcement with concrete are mainly performed in order to clarify the strength of adhesion but this does not always match to the unfavorable conditions of the real work of the design. In the "pull-out" tests of the reinforcement bar from made of prisms supported by the butt, the researchers can't observe the development of cracks and deformation of the outside surface of the samples. This disadvantage defect is easily eliminated by computer simulation [30].

It should be noted that the theoretical basis of the existing design models is the stress state of reinforcement and concrete in the anchoring zone, without taking into account their joint deformations. Therefore, consideration of the joint operation of reinforcement and concrete in the anchoring zone is an actual task.

The purpose of this research is to improve the design model of anchoring taking into account the joint elastic deformations of reinforcement with concrete.

The objectives of this research are:

1. Using of FEM to observe the development of cracks and deformation of the face surface of the samples;
2. Determinate the dependence of the splitting stresses on the reinforcement anchoring length;
3. Evaluate the value of the splitting stresses on the anchoring when tested according to the recommendations of the RS-6 RILEM / CEB / FIP;
4. Make recommendations for estimating the value of splitting stresses;
5. Compare the results of calculating the length of the anchoring.

2. Methods

In [24], the equations of the theory of elasticity were used to theoretically substantiate an anchoring model, which was destroyed by the splitting of concrete. The dependencies of the theory elastic are applied, taking account that the tests are of a short time. The correctness of the calculation formulas was verified by experiments and Finite elemental modeling. The premise of quasi-elastic deformations of materials was used to justify the design models. This greatly simplifies the calculation and doesn't exclude the appearance of inelastic deformations.

In the research was used method of the computer's simulation and results of experiments given in the monograph [25].

In Figure 2 shows the scheme according to the standard EN 10080: 2005 [4], which was used in the test.

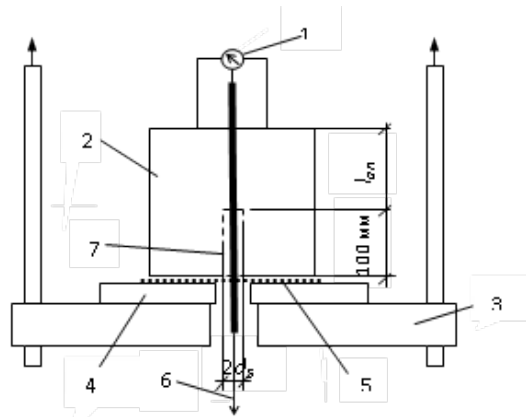


Figure 2. Scheme test of pull according to the recommendations of RS-6 RILEM / CEB / FIP, which was used in [23]: 1 – a strain gauge; 2 – test sample of concrete; 3 – base plate; 4 – steel plate; 5 – rubber lining; 6 – shows the direction of the pulling force; 7 – area with broken adhesion

The tests were conducted in the different organizations and had aim to determine the strength and deformation of the adhesion of the reinforcement of the periodic profile with concrete. A total of 335 samples with dimensions of $200 \times 200 \times 200$ mm by $l_{an} = 100$ mm, and $250 \times 250 \times 250$ mm and $300 \times 300 \times 300$ mm with $l_{an} > 100$ mm were tested. The length of the anchoring l_{an} was changed from $5d_s$ to $15d_s$. In the same, a zone with a length of 100 mm with broken adhesion in the tested samples was provided. The pulling of reinforcing bars when concrete was revealed during the cutting of concrete by profile ribs or from a concrete sample was split. The pulling was observed at low values of l_{an} or relatively low strength of concrete. At $l_{an} > 8d_s$ and the design compressive resistance of concrete to compression $R_b > 17$ MPa, destruction, as a rule, occurred during the splitting of concrete.

During modeling samples for concrete were used the universal solid eight-nodes isoperimetric finite elements (KE -36) with dimensions $10 \times 10 \times 10$ mm ($E_b = 30000$ MPa). The steel armature was modeled by the bar's elements (KE-10) with length 10 mm. During the simulation, all dimensions of the prototypes experience samples were taken as real (except for the borehole location on the broken's adhesion, which in all case dimensions was taken as 20×20 mm). The forces of pulling the reinforcement from the concrete were simulated by the node load N at the point with the coordinates $X = Y = Z = 0$.

For obtain a general idea of the computer model on the Figure 3 are shown characteristic isopolls of the splitting stresses σ_y in the planes XOZ (section $Y = 0$) and YOZ (section $X = 0$).

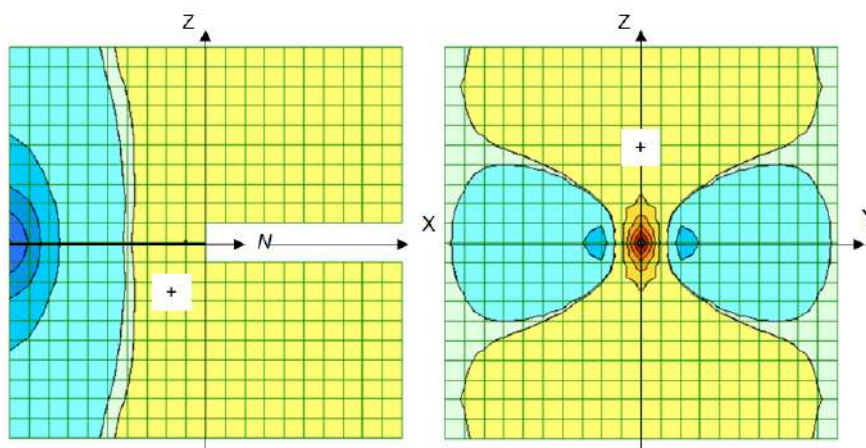


Figure 3. The isopoles of stress σ_y in computer models of experience samples from Pulling the reinforcing bar by force N (+ tension)

The main attention is drawn to the maximum stress σ_y in the concrete mass. When processing numerical results, the resistance of concrete to stretching at splitting is accepted $R_{tt} = 0.1R_b$ [26] into analyzing the results of the finite element method. It is known that under the condition $\sigma_y > R_{tt}$, crack's split are formed and most likely that samples are fracture from the split. Otherwise, the samples are

destroyed as a result of cutting concrete with reinforcement. If $\sigma_y = R_{it}$, the destruction by different schemes is equally probable.

3. Results and Discussion

The main conclusions from the analysis of stressed state of concrete prototypes:

- The area with the broken coupling of the reinforcement enters in the zone of probable splitting. If there are no antifricition pads this, the section is reduced by 2 to 3 cm and is approximately equal to 1/3 of the anchoring length;
- When the point of application of force N is shifted deep into the anchoring the qualitative picture of the distribution of splitting stresses does not change;
- The distance from the reinforcement, the splitting zone increases and extends over the entire width of the sample;
- The maximum values of the splitting stresses σ_y are obtained in the finite elements near to the point of application of the force N , and in all cases considerably exceed the resistance of the concrete to the stretching at splitting R_{it} ;
- Elements are found we call them critical (in figure 3, in all cases their coordinates are $X = -1.5$ cm, $Y = \pm 1.5$ cm and $Z = \pm 0.5$ cm., in which the values of the splitting stresses may exceed the value of R_{it} ;
- The value of the plitting stresses in the remaining elements are less than R_{it} ;
- Stress values in the critical elements decrease with increasing diameter of the reinforcement, anchoring length and transverse dimensions of the specimens, and also when the force N is displaced deep into the anchoring zone.

The values of some parameters of the stress state of the testing samples are given in Table 1.

Table 1. Results of analysis stress of the testing samples

No.	d_s , mm	N , kN	R_{it} , MPa	σ_y , MPa		Character of destruction		
				FEM	(2)	experience	FEM	(2)
1	2	3	4	5	6	7	8	9
1	12	16.25	1.7	0.9	1.0	section	cutting	cutting
2	12	34		1.9 (1.6)	2.1 (1.6)	cutting	cutting	split
3	14	32.4		1.6	1.7	cutting	cutting	cutting
4	16	68.3		2.7	3.2	split	split	split
5	18	35.5		1.3	1.5	split	cutting	cutting
6	18	66.5		2.3	2.7	split	split	split
7	25	82.5		2.1	2.6	split	split	split
8	12	26.8	3.5	1.5	1.6	cutting	cutting	cutting
9	12	48.3		2.7	3.0	cutting	cutting	cutting
10	14	49.1		2.4	2.6	cutting	cutting	cutting
11	16	90.3		3.6	4.2	split	split	split
12	18	65.5		2.4	2.7	cutting	cutting	cutting
13	18	97.2		3.4	4.0 (3.1)	cutting	cutting	split (cutting)
14	25	145		3.8	4.6	split	split	split
15	20	69.8	2.4	2.4 (2.2)	2.6 (2.4)	cutting	cutting	split (cutting)
16	20	84		2.6	3.2	split	split	split
17	20	83.5		2.9 (2.3)	3.2 (2.2)	split	split (cutting)	split (cutting)
18	20	87		2.7	3.3	split	split	split
19	25	101.6		2.7 (2.2)	3.2 (2.2)	split	split (cutting)	split (cutting)
20	25	111.3		2.8	3.5	split	split	split
21	25	145		3.9 (2.4)	4.6 (2.3)	cutting	split (cutting)	split (cutting)
22	25	116.9		2.9	3.7	split	split	split

Analysis of the stressed state of concrete showed that the nature of damage when using simulation in the elastic stage of deformation did not coincide with the experimental data in 5 cases out of 22. It is assumed that the results of the tests in these cases could be affected by inelastic deformation of the reinforcement and the formation of cracks in the concrete, especially when the samples are continuously loaded. The effect of inelastic deformations was taken into account in the calculation by replacing the concentrated force N by the force distributed along some part of the anchoring length (the corresponding values of σ_y are given in parentheses). Thus, with a force distribution of only 2 cm along the anchoring length, the cutoff condition $\sigma_y < R_{it}$ in series 2 and 15 is satisfied, with a 3 cm distribution in series 17 and 19. In series 21, the maximum value of the test force is recorded, the effect of which was obviously the longest. The followability of reinforcement in this case should extend to a length of at least 7 cm at $l_{an} = 12.5$ cm. Thus, the nature of failure in the simulation of the tests as a whole did not coincide with the experimental character in only 1 case (series 5) of 22 (less than 5 %).

To evaluate the effect of reinforcement of different sections on the stress state of the test samples, the calculated values of the splitting stress σ_y in the samples of the same dimensions $200 \times 200 \times 200$ mm and $l_{an} = 100$ mm were compared. In the column 3 of Table 2, these values are given at points with coordinates $X = -1.5$ cm and $Y = \pm 1.5$ cm (in parentheses are the maximum stress values for reinforcement A 500). In line 7, the stresses σ_{0y} are given under the action of the force $M = 10$ kN at the origin without taking into account the influence of the reinforcement excluding the effect of reinforcement.

Computer modeling let to allows to compare different various schemes of test and evaluate the errors of each of them. In the table 2 also shows the calculated values of the stresses σ_y in the absence of a region with broken coupling. When excluding such sections from the calculated models of samples, the maximum stress values σ_y are at points with coordinates $X = 1.5$ cm and $Y = \pm 0.5$ cm. In the absence of reinforcement, critical stresses $\sigma_{0y} = 0.38$ MPa were obtained at $X = 0.5$ cm and $Y = \pm 1.5$ cm.

Table 2. The values of the splitting stresses σ_y was calculated by the finite element method

No	d_s , mm	With areas with broken adhesion,		Without areas with broken adhesion,	
		σ_y , MPa	$k = \sigma_y/\sigma_{0y}$	σ_y , MPa	$k = \sigma_y/\sigma_{0y}$
1	12	0.57 (2.8)	1.64	0.50 (2.4)	1.32
2	14	0.48 (3.2)	1.40	0.46 (3.1)	1.22
3	16	0.43 (3.7)	1.23	0.43 (3.7)	1.14
4	18	0.38 (4.2)	1.10	0.41 (4.5)	1.08
5	20	0.35 (4.8)	1.01	0.39 (5.3)	1.03
6	25	0.29 (6.3)	0.85	0.35 (7.5)	0.94
7	0	$\sigma_{0y} = 0.35$	1.00	$\sigma_{0y} = 0.38$	1

On the Figure 4 was showed the characteristic stress lines σ_y in the concrete massif (the segment (area) with the broken coupling is absent). It should be noted that if you exclude the final elements of the reinforcement and the segment (area) with broken coupling (Figure 5-2), splitting is possible only outside the anticipated anchoring zone.

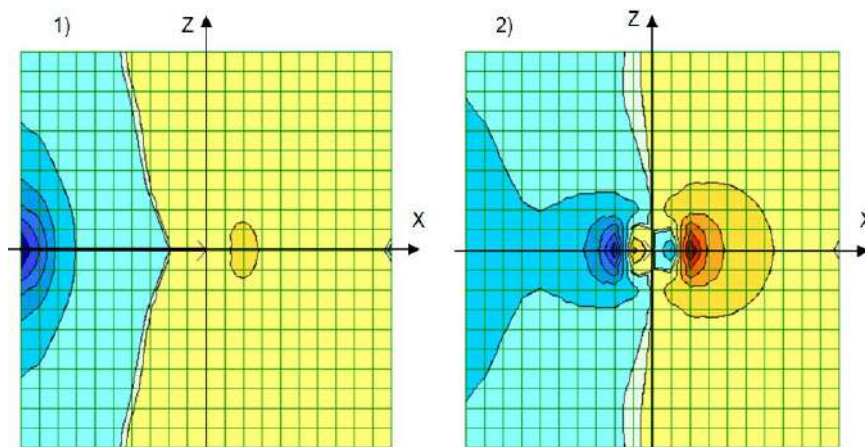


Figure 4. The stress line σ_y in a body of concrete. The concentrated force acts at the origin of coordinates: 1) with reinforcement; 2) without reinforcement

The results of the calculation with using the finite element models are approximate. The task of the action of the force applied at the point of an infinite body combined with the origin to evaluate the degree of approximation is considered.

The exact solution in cylindrical coordinates under the action of the force in the direction of the axis of symmetry x was obtained by Kelvin in the form of the equation of stresses in the circumferential direction [27]. Kelvin's equation is refined by introducing a coefficient k that takes into account the effect of the reinforcement and the segment with broken coupling (column 4 of Table 2).

$$\sigma_y = \frac{kN(1-2\nu)x}{8\pi(1-\nu) \cdot (x^2 + y^2) \cdot \sqrt{x^2 + y^2}}, \quad (2)$$

where $\nu = 0.2$ is the Poisson's ratio for concrete.

The values of stress values determined by formula (2), at the individual points completely coincided with the calculated values obtained by the finite element method. For example, on points with coordinates $X = 0.5$ cm and $Y = \pm 1.5$ cm, $k = 1$, $\sigma_y = 0.38$ MPa was obtained.

The results of calculating testing samples to formula (2) are given in Table 1. The overestimated values of the splitting stresses can be clarified by the distribution of the force N along the anchoring length. In this case, the calculation reduces to the solution of several equations (2) with an increase in unit coordinate x in each subsequent equation and using the average value of the force N .

For example, for series 2 (Table 1), the cut-off condition $\sigma_y < R_{tt}$ was obtained by a force distribution N of 5 cm with an anchoring length of 14.5 cm, for 13 series force N was distributed of 5 cm with an anchoring length of 12 cm, for 15 series – by 4 cm with an anchoring length of 10 cm, for 17 series – by 6 cm with an anchoring length of 10 cm, for 19 series – by 6 cm series with an anchoring length of 12.5 cm and 21 series – by 9 cm with an anchoring length of 12.5 cm.

The condition of joint operation of reinforcement and concrete is the equality of absolute deformations in the direction of pulling force, which is guaranteed by ideal connections of reinforcement and concrete.

$$w_s = w_b. \quad (3)$$

With the length of the l_{an} anchoring, the deformations of the reinforcement are determined by the formula

$$w_s = \sigma \cdot l_{an} / E_s. \quad (4)$$

The average stresses of the reinforcement at the anchoring length will be represented as a linear dependence on the resistance of the reinforcement to the stretching $\sigma = \alpha R_s$.

It is possible to use a theoretical model with a force at the boundary of an elastic half-space to determine the deformation of concrete during a short loading. The exact solution of this problem in cylindrical coordinates under the action of a force in the direction of the axis of symmetry x was obtained by Boussinesq [27]. The displacement of the point in which the concentrated force N is applied is determined by the formula:

$$w = N(1-\nu^2) / \pi \cdot E \cdot r, \quad (5)$$

where ν – is Poisson's ratio, E – is the modulus of elasticity, r – is the distance from the axis of symmetry.

According to equation 5, the displacement at the origin is infinite. This defect of equation 5 demand the replacement of the concentrated force by a statically equivalent load q distributed over a circular surface with radius r . Then the displacement at the boundary of the loaded circle of radius r can be determined by formula:

$$w_r = 4qr / \pi E. \quad (6)$$

The evenly distributed load acting on the armature pulled from the concrete is numerically equal to the stresses in the reinforcement.

From equation 6, it is possible to determine the absolute deformations of concrete on the boundary of a loaded circle with diameter d .

$$w_b = 2qd(1 - \nu_b^2) / \pi E_b \quad (7)$$

Taking into account that the maximum value of the load corresponds to the identity $q_{max} = R_s$, the following expression is obtained from the joint solution of equations (3), (4) and (7):

$$l_{an} = \frac{2(1 - \nu_b^2)n}{\alpha\pi} d \quad (8)$$

where $n = E_s / E_b$ is the coefficient of reduction.

Coefficient of average stresses α is determined by the distribution of stresses along the anchoring length. At the length of the anchoring of the stretched reinforcement, a gradual decrease of stresses occurs from the initial value $\sigma_s \leq R_s$ in the calculated section to $\sigma_s = 0$ at the free end of the reinforcing element. Usually, a uniform reduction in stress is taken as the reinforcement cross-sections are removed from the loading point.

The stress distribution coefficient α is equal to 0.5 if the stresses in the reinforcement at the anchoring length vary linearly.

Computer simulation was performed with using elastic finite elements to refine the calculated coefficient value (Figure 5).

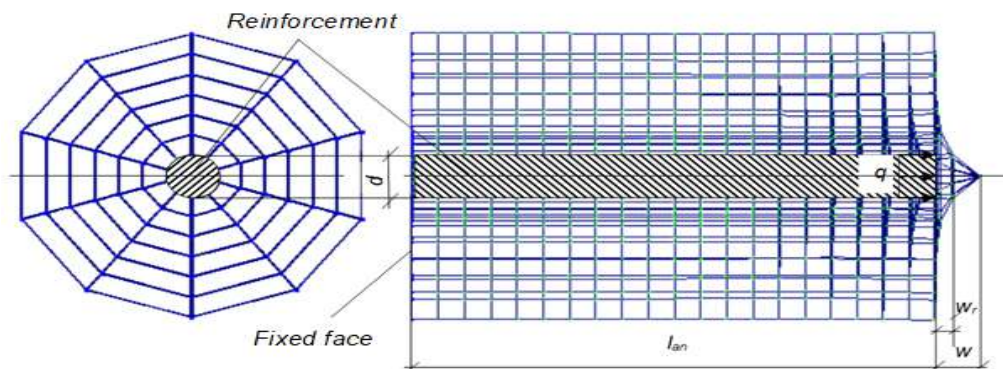


Figure 5. Axisymmetric finite element model and deformed fragment of scheme in the interaction of reinforcement with concrete

The result of the simulation were obtained data of changing stress in the reinforcing bar along the anchoring length $l_{an} = 10$ cm (Fig. 6) [28]. In this case, $\alpha = 0.3$.

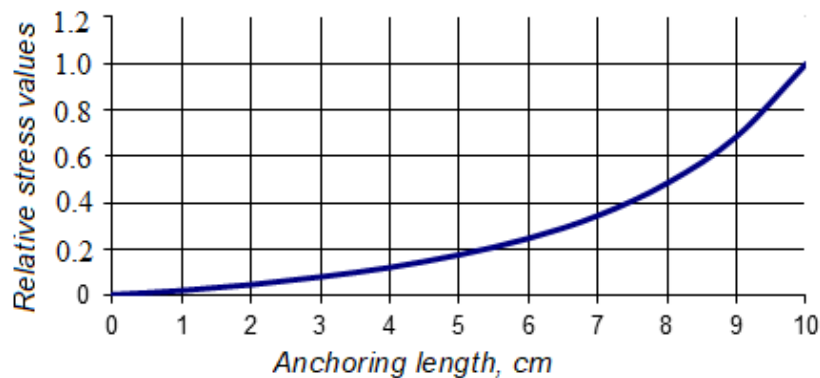


Figure 6. Relative stresses σ_s / R_s in the reinforcement along the anchoring length

Selected results of comparing the estimated anchoring lengths for a combination of concrete B 25 and reinforcement A 500 are shown in Table 3. Values l_{an} were calculated with using the formula 8

$E_b = R_{bt} / \varepsilon_{bt0}$ (tensile strength of the concrete = 1.05 MPa, ultimate tensile strength = 0.0001) and $\alpha = 0.3$. The normative data are taken from [29].

Table 3. Selected results of comparison of the calculated anchoring lengths

SNIP 2.03.01-84 (old Russian standards, 1984)	SP 52-101-2003 (Russian standards)	EN 1992-1-1 (6)	(7)
32 d	41.4 d	46 d	38.8 d

4. Conclusions

1. The method of computer modeling can be an effective means of predicting the destruction of direct anchoring.

2. There was no direct correlation between the splitting stresses and the anchoring length. On the value of splitting stresses is affected by the length of the anchoring section on which the pulling force is distributed, or the depth of displacement of the concentrated force in the anchoring zone. The formation of splitting cracks and breakage by a split depends mainly on the tensile strength of the concrete during the splitting of R_{tt} and the degree of distribution of the pulling force.

3. When testing the anchoring by scheme 1, the nature of the destruction of the samples is random and depends on the duration of the pulling force. Then longer the load application time, the greater the probability failure by shear.

4. The value of the splitting stresses on the anchoring is expedient to be estimated according to the scheme of the elastic half-space, taking into account the influence of the protective layer. The use of constructive methods of eliminating the split (transverse reinforcement) promotes a favorable distribution of pulling force.

5. The results of calculating the anchoring length according to the deformation model are bit (slightly) different from the data obtained by design standards.

References

- Pulido-Delgado J.L., Rodriguez Cuevas C., Martín Duran Garcia H. Seismic response of adjacent structures connected by linear viscous dampers. *Ingenieria Investigacion y Tecnología*. 2012. Vol. XIII. No. 2. Pp. 227–235.
- Tikhonov I.N. K diskussii po statie "O normirovanii ankerovki stershnevoi armature" [To the discussion on the article "On the Normalization of Anchoring of Core Valves"]. *Concrete and reinforced concrete*. 2007. No. 1. Pp. 28–30. (rus)
- RILEM/CEB/FIB. Recommendation on reinforcement steel for reinforced concrete. RC6. Bond test for reinforcement steel. 2. Pull-out tests. 1983. 8 p.
- EN 10080 Final Draft «Steel for the reinforcement of concrete» - Weldable reinforcing steel - General (January 2005).
- Holmyansky M.M. *Contact armatyri s betonom* [Contact of reinforcement with concrete]. Moscow: Stroiizdat, 1981. 184 p. (rus)
- EN 1992-1-1: 2004 Eurocode 2: Design of concrete structures. Part 1-1: General rules and rules for buildings.
- Bond of reinforcement in concrete. State-of-art report by Task group Bond models. FIB bulletin 10 (August 2000).
- FRP reinforcement in RC structures. Technical report prepared by a working party of Task group 9.3. FIB bulletin 40 (September 2007).
- Jansson A., Lofgren I., Lundgren K., Gylltoft K. Bond of reinforcement in self-compacting steel-fiber-reinforced concrete. *Magazine of Concrete Research*. 2012. Vol. 64(7). Pp. 617–630.
- Tepfers R.A. *Theory of Bond Applied to Overlapped Tensile Reinforcement Splices for Deformed Bars*. PhD thesis, Chalmers University of Technology. Goteborg, Sweden. 1973.

Литература

- Pulido-Delgado J.L., Rodriguez Cuevas C., Martín Duran Garcia H. Seismic response of adjacent structures connected by linear viscous dampers // *Ingenieria Investigacion y Tecnología*. 2012. Vol. XIII. № 2. Pp. 227–235.
- Тихонов И.Н., Мешков В.З., Судаков Г.П. К дискуссии по статье «О нормировании анкерovки стержневой арматуры» // *Бетон и железобетон*. 2007. № 1. С. 28–30.
- RILEM/CEB/FIB. Recommendation on reinforcement steel for reinforced concrete. RC6. Bond test for reinforcement steel. 2. Pull-out tests. 1983. 8 p.
- EN 10080 Final Draft «Steel for the reinforcement of concrete» - Weldable reinforcing steel - General (January 2005).
- Холмянский М.М. Контакт арматуры с бетоном. М.: Стройиздат, 1981. 184 с.
- EN 1992-1-1: 2004 Eurocode 2: Design of concrete structures. Part 1-1: General rules and rules for buildings.
- Bond of reinforcement in concrete. State-of-art report by Task group Bond models. FIB bulletin 10 (August 2000).
- FRP reinforcement in RC structures. Technical report prepared by a working party of Task group 9.3. FIB bulletin 40 (September 2007).
- Jansson A., Lofgren I., Lundgren K., Gylltoft K. Bond of reinforcement in self-compacting steel-fiber-reinforced concrete // *Magazine of Concrete Research*. 2012. Vol. 64(7). Pp. 617–630.
- Tepfers R.A. Theory of bond applied to overlapped tensile reinforcement splices for deformed bars. PhD thesis, Chalmers University of Technology. Goteborg, Sweden. 1973.
- Tepfers R., Karlsson M. Pull-out and tensile reinforcement splice tests using FRP C-BARs. Chalmers University of Technology, Division of Building Technology. Work No. 13.

11. Tepfers R., Karlsson M. *Pull-out and tensile reinforcement splice tests using FRP C-BARS*. Chalmers University of Technology, Division of Building Technology. Work No: 13. Publication No: 97:2. Göteborg, Sweden. 1997.
12. Tepfers R., Hedlund G., Rosinski B. Pull-out and tensile reinforcement splice tests with GFRP bars. *Proceedings of the ICCI' 98, Second International Conference on Composites in Infrastructure*. 1998. Vol. II. Pp. 37–51.
13. Bedarev V.V. Bazovaya dlina ankerovki armatury periodicheskogo profilya s uchetom otnositel'noi ploschadki smyatiya i haraktera razrusheniya betona [The basic length of anchoring of the reinforcement of the periodic profile, taking into account the relative area of the crushing and the nature of the destruction of concrete]. *Concrete and reinforced concrete*. 2013. No.1. Pp. 18–23. (rus)
14. Skorobogatov S.M., Edwards A.D. Vliyaniye vida periodicheskogo profilya stergnevoi armatury na sscepleniye s betonom [Influence of the form of the periodic profile of the rod reinforcement on the adhesion to concrete]. *Concrete and reinforced concrete*. 1979. No. 9. Pp. 20–21. (rus)
15. Benin A.W. Matematicheskoye modelirovaniye processov deformirovaniya i razrusheniya pri vityagivaniy armaturnogo stergzhnya iz betonnoy bloka [Mathematical modeling of the processes of deformation and fracture when pulling out the reinforcing bar from a concrete block]. *News of PGUPS*. 2010. No. 1. Pp. 129–141. (rus)
16. Krasnoshchekov Y.V. Vliyaniye treschin na ankerovku armatury periodicheskogo profilya [Influence of cracks on anchoring of reinforcement of periodic profile]. *Herald of SibADI*. 2008. No. 3. Pp. 39–45. (rus)
17. Zandi Hanjari K., Coronelli D. *Anchorage Capacity of Corroded Reinforcement. Eccentric Pull-out Tests*. CHALMERS, Civil and Environmental Engineering, Report 2010:6. 82 p.
18. Veselov A.A. *Teoriya sscpleniya armatury s betonom i ee primeneniye*. СПб, 2000. 169 с.
19. Shima H., Chou L.-L., Okamura H. Micro and Macro Models for Bond in Reinforced Concrete. *Journal of the Faculty of Engineering: University of Tokyo*. 1987. Vol. XXXIX. No. 2. Pp. 133–194.
20. Eligehausen R., Popov E.P., Bertero V.V. *Local Bond Stress-Slip Relationship of Deformed Bars under Generalized Excitations*. EERC Report 83-23. Earthquake Engineering Research Center, University of California, Berkeley, California, 1983. 169 p.
21. Benin A.V., Semenov A.S., Semenov S.G., Melnikov B.E. Matematicheskoye modelirovaniye protsessa razrusheniya sscpleniya armatury s betonom. Chast 2. Modeli bez ucheta nesploshnosti soyedineniya [The simulation of bond fracture between reinforcing bars and concrete. Part 2. Models without taking the bond discontinuity into account]. *Magazine of Civil Engineering*. 2014. No. 1(45). Pp. 23–40. (rus)
22. Benin A.V., Semenov A.S., Semenov S.G., Melnikov B.E. Matematicheskoye modelirovaniye protsessa razrusheniya sscpleniya armatury s betonom. Chast 1. Modeli s uchetom nesploshnosti soyedineniya [Simulation of degradation of bond between reinforcing bar and concrete. Part 1. Models with account of the discontinuity]. *Magazine of Civil Engineering*. 2013. No. 5(40). Pp. 86–99. (rus)
23. Krasnoshchekov Y.V. Modelirovaniye raskalivaniya betna v zone ankerovki nenapryagaemoy armatury [Modeling of concrete splitting in the anchoring zone of non-tensioning reinforcement]. *Herald of SibADI*. 2017. No. 2. Pp. 64–69. (rus)
24. Madatyanyan S.A. *Armatura zhelezobetonnykh konstruktsiy* [Reinforcement of reinforced concrete structures]. Moscow: Voentehlit, 2000. 256 p. (rus)
25. Bedarev V.V. *Obshchaya teoriya sscpleniya i ankerovki armatury periodicheskogo profilya v betone*. Novokuznetsk: SibGIU, 2014. 159 с.
26. ГОСТ 10180-2012. Бетоны. Методы определения прочности по контрольным образцам. М.: Стандартинформ, 2013. 30 с.
27. Тимошенко С.П. *Теория упругости*. М.: Наука, 1975. 576 с.
28. Краснощечков Ю.В. Моделирование анкеровки арматуры в бетоне // *Вестник СибАДИ*. 2015. № 4. С. 64–69.
29. Тихонов И.Н. О нормировании анкеровки стержневой арматуры // *Бетон и железобетон*. 2006. № 3. С. 2–7.
30. Beliaev M., Semenov A., Semenov S., Benin A. Simulation of pulling the reinforcing bar from concrete block with account of friction and concrete damage // XV international conference «Topical problem of architecture, civil engineering, energy efficiency and ecology – 2016». Tyumen. 2016. Pp. 04010.
31. Benin A., Semenov S., Semenov A., Bogdanova G. Publication No. 97 : 2, Göteborg, Sweden, 1997.
12. Tepfers R., Hedlund G., Rosinski B. Pull-out and tensile reinforcement splice tests with GFRP bars. *Proceedings of the ICCI' 98, Second International Conference on Composites in Infrastructure*. 1998. Vol. II. Pp. 37–51.
13. Бедарев В.В. Базовая длина анкеровки арматуры периодического профиля с учетом относительной площади смятия и характера разрушения бетона // *Бетон и железобетон*. 2013. № 1. С. 18–23.
14. Skorobogatov S.M., Edwards A.D. Влияние вида периодического профиля стержневой арматуры на сцепление с бетоном // *Бетон и железобетон*. 1979. № 9. С. 20–21.
15. Бенин А.В. Математическое моделирование процессов деформирования и разрушения при вытягивании арматурного стержня из бетонного блока // *Известия ПГУПС*. 2011. № 1. С. 129–141.
16. Краснощечков Ю.В. Влияние трещин на анкеровку арматуры периодического профиля // *Вестник СибАДИ*. 2008. № 3. С. 39–45.
17. Zandi Hanjari K., Coronelli D. Anchorage capacity of corroded reinforcement. *Eccentric Pull-out Tests*. CHALMERS, Civil and Environmental Engineering, Report 2010:6. 82 p.
18. Веселов А.А. Теория сцепления арматуры с бетоном и её применение. СПб, 2000. 169 с.
19. Shima H., Chou L.-L., Okamura H. Micro and Macro Models for Bond in Reinforced Concrete // *Journal of the Faculty of Engineering: University of Tokyo*. 1987. Vol. XXXIX. No. 2. Pp. 133–194.
20. Eligehausen R., Popov E.P., Bertero V.V. Local Bond Stress-Slip Relationship of Deformed Bars under Generalized Excitations // EERC Report 83-23, Earthquake Engineering Research Center, University of California, Berkeley, California, 1983. 169 p.
21. Бенин А.В., Семенов А.С., Семенов С.Г., Мельников Б.Е. Математическое моделирование процесса разрушения сцепления арматуры с бетоном. Часть 2. Модели без учета несплошности соединения // *Инженерно-строительный журнал*. 2014. № 1. С. 23–40.
22. Бенин А.В. Семенов А.С., Семенов С.Г., Мельников Б.Е. Математическое моделирование процесса разрушения сцепления арматуры с бетоном. Часть 1. Модели с учетом несплошности соединения // *Инженерно-строительный журнал*. 2013. № 5. С. 86–99.
23. Краснощечков Ю.В. Моделирование раскалывания бетона в зоне анкеровки ненапрягаемой арматуры // *Вестник СибАДИ*. 2017. № 2. С. 64–69.
24. Мадатян С.А. Арматура железобетонных конструкций. М.: Воентехлит, 2000. 256 с.
25. Бедарев В.В. Общая теория сцепления и анкеровки арматуры периодического профиля в бетоне. Новокузнецк: СибГИУ, 2014. 159 с.
26. ГОСТ 10180-2012. Бетоны. Методы определения прочности по контрольным образцам. М.: Стандартинформ, 2013. 30 с.
27. Тимошенко С.П. Теория упругости. М.: Наука, 1975. 576 с.
28. Краснощечков Ю.В. Моделирование анкеровки арматуры в бетоне // *Вестник СибАДИ*. 2015. № 4. С. 64–69.
29. Тихонов И.Н. О нормировании анкеровки стержневой арматуры // *Бетон и железобетон*. 2006. № 3. С. 2–7.
30. Beliaev M., Semenov A., Semenov S., Benin A. Simulation of pulling the reinforcing bar from concrete block with account of friction and concrete damage // XV international conference «Topical problem of architecture, civil engineering, energy efficiency and ecology – 2016». Tyumen. 2016. Pp. 04010.
31. Benin A., Semenov S., Semenov A., Bogdanova G.

Krasnoshchekov Y.V., Krasotina L.V., Pulido-Delgado J.L. Models of direct anchoring of reinforcement in concrete. *Magazine of Civil Engineering*. 2018. No. 3. Pp. 3–13. doi: 10.18720/MCE.79.1.

- armature periodicheskogo profilya v betone* [The general theory of coupling and anchoring of reinforcement of periodic profile in concrete]. Novokuznetsk: SibGIU, 2014. 159 p. (rus)
26. *Russian Standard. GOST 10180-2012. Betoni. Metodi opredeleniya prochnosti po control'nim obrazcam* [Concretes. Methods for determining the strength of control samples]. Moscow: Standardinform, 2013. 30 p. (rus)
27. Timoshenko S.P. *Teoriya uprugosti* [Theory of Elasticity]. Moscow: Science, 1975. 576 p. (rus)
28. Krasnoshchekov Y.V. Modelirovanie ankerovki armatury v betone [Modeling of anchoring of reinforcement in concrete]. *Herald of SibADI*. 2015. No. 4. Pp. 64–69. (rus)
29. Tikhonov I.N. O normirovanii ankerovki sterzhnevoi armatury [On the normalization of anchoring of rod reinforcement]. *Concrete and reinforced concrete*. 2006. No. 3. Pp. 2–7. (rus)
30. Beliaev M., Semenov A., Semenov S., Benin A. Simulation of pulling the reinforcing bar from concrete block with account of friction and concrete damage. *XV international conference «Topical problem of architecture, civil engineering, energy efficiency and ecology – 2016»*. Tyumen. 2016. Pp. 04010.
31. Benin A., Semenov S., Semenov A., Bogdanova G. Parameter identification for coupled elasto-plasto-damage model for overheated concrete. *Conference "Dynamics of civil engineering and transport structures and wind engineering - dinwind 2017"*. Trstena, Slovak Republic, 2017. Pp. 00042.

Yurii Krasnoshchekov,
+7(913)622-53-29; uv1942@mail.ru

Larisa Krasotina,
+7(913)973-79-80; krasotina.larisa@gmail.com

Jose Luis Pulido-Delgado,
+52(444)826-23-00; jpulido@uaslp.mx

Юрий Васильевич Краснощечков,
+7(913)622-53-29; эл. почта: uv1942@mail.ru

Лариса Владимировна Красотина,
+7(913)973-79-80;
эл. почта:
krasotina.larisa@gmail.com

Хосе Луиз Пулидо-Делегадо,
+52(444)826-23-00; эл. почта: jpulido@uaslp.mx

© Krasnoshchekov Y.V., Krasotina L.V., Pulido-Delgado J.L., 2018

doi: 10.18720/MCE.79.2

Characteristics of the droplet motion of a liquid antifreeze reagent

Характеристики движения капель жидкого противогололедного реагента

**K.P. Mandrovskiy,
Y.S. Sadovnikova,**
Moscow State Automobile and Road Technical
University, Moscow, Russia

**Канд.техн.наук, доцент К.П. Мандровский,
инженер Я.С. Садовникова,**
Московский автомобильно-дорожный
государственный технический
университет, Москва, Россия

Key words: anti-icing reagents (AR); airfield and road surfaces; distribution disk; nozzle; mathematical model of the motion of a drop of AR; a drop of AR; air environment; monitoring system of the process of distribution of reagents

Ключевые слова: противогололёдные реагенты (ПГР); аэродромные и дорожные покрытия; распределительный диск; форсунка; математическая модель движения капли ПГР; капля ПГР; воздушная среда; система мониторинга процесса распределения реагентов

Abstract. The object of investigation is the process of spraying of the anti-icing reagent. As an object of research, external forces are selected that affect on each drop of the reagent: counteraction forces, gravity forces, Coriolis force and centrifugal inertial forces, lifting force, frictional forces of the reagent on the surface of the working equipment: disk and blades. It is assumed that the liquid reactant is fed under pressure to the hydraulic nozzles installed in the disk casing, and then falls onto the distribution disk. The tasks solved within the framework of the article: the identification of external forces acting on each drop of the reagent from the moment of flow from the nozzle to the moment when it reaches the coating, the study of the effect of external forces on the characteristics of droplet motion, the mathematical description of the process of formation of the sputtering zone. To refine the droplet motion characteristics under the action of external forces using the already available mathematical description of the droplet motion along a distribution disk, a mathematical model of their motion in the air environment has been developed. The equation of motion of the drops of the reagent, the dependences of the droplet's flight range on the mode and parameters of the working equipment are obtained. Meteorological factors such as wind speed and direction, as well as air environment properties (dynamic and kinematic viscosity, depending on the temperature of the medium) are considered in the simulation. This model will provide an opportunity to the reasonably assignation of the parameters of the distribution equipment during their design and operation and will also serve as a base for mathematical and software systems for the continuous monitoring of the process of applying liquid reagents for road and airfield pavements. Its operation will allow to provide a high-quality treatment of coatings ensuring the preservation of their operational properties and to make a reagent savings.

Аннотация. Цель статьи – формирование комплексной математической модели, описывающей движение капель жидкого реагента при обработке покрытий. Объект исследования – процесс распыления противогололедного реагента. В качестве предмета исследований выбраны внешние силы, воздействующие на каждую, отдельно рассматриваемую, каплю реагента: силы сопротивления среды, сила тяжести, кориолисова и центробежная силы инерции, подъёмная сила, силы трения реагента о поверхность рабочего оборудования: диска и лопаток. Предполагается, что жидкий реагент подаётся под давлением к гидравлическим форсункам, установленным в кожухе диска, а затем попадает на распределительный диск. Задачи, решаемые в рамках статьи: выявление внешних сил, действующих на каждую каплю реагента с момента истечения из форсунки до момента достижения ею покрытия, изучение влияния внешних сил на характеристики движения капель, математическое описание процесса формирования зоны распыления. Для уточнения характеристик движения капель под действием внешних сил с использованием уже имеющегося математического описания движения капель по распределительному диску разработана математическая модель их движения в воздушной среде. Получены уравнения движения капель реагента, выявлены зависимости дальности полета капель от режима (частота вращения диска и давление подачи реагента) и параметров рабочего оборудования (диаметр распределительного диска, радиус его ступицы, наклон лопаток (ребер) диска и его высота над поверхностью покрытия, высота расположения форсунок относительно

Мандровский К.П., Садовникова Я.С. Характеристики движения капель жидкого противогололедного реагента // Инженерно-строительный журнал. 2018. № 3(79). С. 14–26.

плоскости диска). При моделировании учтены метеорологические факторы, такие как скорость и направление ветра, а также свойства воздушной среды (динамическая и кинематическая вязкость, зависящие от температуры среды). Данная модель предоставит возможность обоснованно назначать параметры распределительного оборудования при их конструировании и эксплуатации, а также будет являться базой для математического и программного обеспечения системы непрерывного контроля над процессом нанесения жидких реагентов на дорожные и аэродромные покрытия. Её функционирование позволит обеспечить качественную обработку покрытий, обеспечивая при этом сохранение их эксплуатационных свойств и экономию реагента.

1. Introduction

Most of the territory of Russia is situated in the temperate continental climatic zones, the northern regions are situated in the Arctic and subarctic areas. The climate of Central Russia is continental, characterized by the presence of hot summer and a prolonged cold winter. Similar climatic conditions are typical for Canada, Mongolia, countries of the Scandinavian Peninsula. With the peculiarity of the geographical location of the country, many problems are related to maintenance and operation of roads and airfields in winter.

The most important is the prevention of the appearance and removal of ice, sleet and snow-ice formations on the covers.

To prevent the icing on roads and airfields, two types of anti-icing reagents (AR) are used: liquid and solid.

There are the distinct designs of aerodrome dispensers of reagents which working organs provide for the use of one type of AR (or both) depending on the task (removal of ice or the adoption of preventive measures for its formation) [1, 2].

The following versions of the design of the distribution equipment (DE) are known: nozzles (injector, fan, side fan), mounted on bars (beams) and distribution disks, treating coatings with both liquid and solid reagents.

The main advantages of the nozzles are the uniformity of the AR application on the surface and the compactness of the workpiece design. Disadvantages are the complexity of adjusting of the height of the arrangement of several nozzles above the coating, the insufficient range of distribution of the AR which poses to complicate the design of the outrigger rods. In addition, such design of the DE imposes the restrictions on the type of AR applied to the surface.

The technology of disk distribution involves the treatment of coatings with both liquid and solid reagents. It is possible to vary the width of the processing strip by changing the speed of rotation of the disks and their height above the surface. Disk distributors allow the high-speed processing of aerodrome coverings (with a speed of up to 40 km/h) with a distribution width up to 40 m. However, when operating this type of DE it is important to take into account the presence of factors and conditions that adversely affect on the uniformity of the AR application. To assess them, it is necessary to consider the design features of the disk DE and to get the conception of the movement of the reagent jet relative to the coating. Automatic monitoring systems for reagent feeds have been developed to monitor the position of remote rods with disks/nozzles [3], the system for monitoring the speed of disks and the flow rate metering AR [4, 5, 6], automated control systems for actuators using the GNSS system [7]. The purpose of such systems is to maintain the consistency of the width and density of the coating regardless of the speed of the machine. However, the algorithm of their functioning does not provide the influence of the external environment on the process of distribution of the AR. The effect of the wind force and the direction on the range and uniformity of processing, the influence of the physical properties of the medium on the nature of the flow of the reagents are not considered. By considering these factors we will be able to continue the adjustment of operating modes and parameters of DE ensuring the uniformity and width of the AR application to the coating. In addition to the existing model for the movement of the reagent over the disk, it is necessary to develop a mathematical model of the flow of liquid AR in the air, which can be used to create a system for monitoring the distribution process of the AR, analogous to the systems considered in [8–10]. It will be part of a comprehensive automated system for monitoring and managing the distribution of the reagent. The development of information technologies and software systems [11–13] allows to work on the formation of mathematical and software for such technical means. The urgency of the developed model is also in the scientific justification given to it for the choice of location and modes of operation of the DE at various meteorological conditions (wind speed and direction). Judging by the published literature, in this direction such works were not earlier performed. At the moment, hydrodynamic processes active in viscous fluid flows and contact of a single drop with the

liquid surface are widely studied [14, 15]. The displacement of a liquid in a gaseous medium is considered in [16, 17, 18]. The jet flow from the nozzle is described in detail in [19, 20, 21, 22]. The mentioned studies, which are the closest to the analyzed processes can be used as a basis for the development of models. However, they require the adaptation to the characteristic design features of the distribution equipment and operational factors associated with the operating mode of the DE and the influence of the external environment on the movement of AR drops. Similar research in the field of agricultural machinery was carried out in [23, 24].

2. Methods

2.1. Mathematical model of the motion of a drop of AR on the disk

Since the initial conditions of motion and the medium in which the sputtering take place, and the types of acting forces for each drop from the set that make up the stream (jet) of the reagent are the same, the solution of the problem can be reduced to studying the process of motion by the example of one drop of AR. After this, it is necessary to proceed to a more complex problem of considering the moving flow of the reagent. The obtained data should be used to form the process of distribution of AR in different conditions, with different density of air and reagent, with different parameters of DE to determine the most favorable combination of these conditions, factors and parameters from the viewpoint of the quality of coating treatment.

Let us consider the trajectory of the motion of a drop of liquid AR relative to the surface of an airfield cover to determine the influence of the type and parameters of the distribution equipment, its location and operating modes on it.

The mode of operation determines the rotational speed of the distribution disk and the pressure created by the injectors. The main parameters of the distribution equipment are the diameter of the distribution disk, the radius of its hub, the inclination of the blades (ribs) of the disk and its height above the surface of the coating, the height of the nozzles relative to the plane of the disk.

The study of the displacement of a drop of reagent in the air will allow to determine the methods and ways for improving the quality of the distribution of reagents and accordingly the achieved value of the coefficient of adhesion.

In further calculations, the following assumptions are made as follows:

- the drop has the shape of a sphere;
- physical properties of the air environment: temperature $T, ^\circ\text{C}$, a density $\rho_1, \text{kg/m}^3$, the coefficient Dynamic Viscosity $\eta, \text{kg/m}\cdot\text{s}$;
- density of the liquid reagent ρ_2 is selected based on of Temperatures The surrounding environment and objectives of ongoing works (prevention or deleting the ice);
- type working equipment – distributing disk diameter d, m ;
- reagent is sprayed by built in the blade guard nozzles under pressure $P_0 \text{ MPa}$, and then discarded by the shoulder of disk blades;
- blade's angle φ_0 ;
- the calculation takes into account the friction of the PGR on the surface of the blades, the wind speed and direction, the time of motion, the disk height above the coating;
- angle between the direction of the wind and the axis which the velocity vector of the drop of the AR is projected to varies at bounds from 0° to 360° .

The study should begin with a consideration of a drop of AR moving along the disk with the initial flow rate from the nozzle.

To study the motion of the droplet two coordinate systems will be used – xy , to move the drop along the disk and XYZ -to describe its motion relative to the surface of the coating.

When the droplet moves from the nozzle to the periphery of the disk centrifugal forces act on it, the frictional forces on the blade surface of the disk, and the Coriolis force (Figure 1).

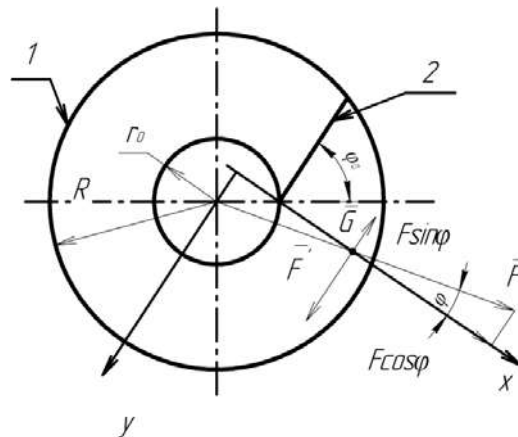


Figure 1. The scheme of the forces acting on a drop of AR on the disk surface

The diagram shows: 1 – distribution disk, 2 – blade (edge) of the disk, R – the radius of the disk, r_0 – radius of the disk hub, φ_0 – tilt angle of disk rib.

The differential equation of motion of a drop of a reagent along with a disk edge located at an angle to the radial position has the form:

$$m \frac{d^2 x}{dt^2} = F \cos \varphi (F' - F \sin \varphi) f - G \cdot f,$$

where F is the centrifugal force of inertia, H ;

F' is the Coriolis inertia force H ;

G is the weight of the drop, H ;

f is the friction coefficient of the AR on steel.

In turn, these forces are equal:

$$F = m \cdot r \cdot \omega^2,$$

$$F' = 2m \cdot \omega \frac{dx}{dt},$$

$$G = m \cdot g,$$

where ω is the angular velocity of rotation of the disk;

g – acceleration of gravity, m/s^2 .

The solutions of this equation are as follows:

$$x = \frac{K_1 + r_0 \cos \varphi_0}{2K} \left((K + f) e^{\omega(K-f)t} + (K - f) e^{-\omega(K-f)t} \right) - K_1,$$

$$K = \sqrt{f^2 + 1},$$

$$K_1 = r_0 \cdot f \cdot \sin \varphi_0 + g \cdot f \frac{1}{\omega^2}.$$

The velocity of the AR drops in the projection onto the x-axis (m/s) can be found by the equation:

$$V_x = \frac{dx}{dt} = \frac{K_1 + r_0 \cos \varphi_0}{2K} (K^2 - f^2) \omega (e^{\omega(K-f)t} - e^{-\omega(K-f)t}).$$

The process of motion and the nature of the acting forces are described in detail in [25].

Leaving the nozzle, the flow of liquid formed by individual drops is discarded by the blades of the disk, acquiring additional kinetic energy, and flies off the disk. Then it starts to move in the air.

The velocity of the liquid outflow from the nozzle (the speed of motion in the projection on the y axis) [26, 27]:

$$V_y = \sqrt{\frac{2(P_0 + \rho_2 g h)}{\rho_2}},$$

where h is the height of the nozzle relative to the disk, m;

P_0 – AR feed pressure, MPa.

Using the vector addition of velocities, the initial velocity of the droplet is determined at the time of flight from the disk:

$$V = \sqrt{V_x^2 + V_y^2}.$$

According to the XYZ coordinate system, the rotational motion of the disk is portable, and the motion of the AR drop over the disk is a relative motion. Therefore, the droplet velocity at the moment of separation from the disk is calculated according to the classical law of addition of velocities by vector addition of the initial velocity and the linear speed of rotation of the distribution disk:

$$V_1 = \sqrt{V^2 + V_d^2}, \quad (1)$$

where V_d – linear disk rotation speed, m/s.

$$V_d = \omega R,$$

where R is the radius of the disk, m.

Once being left from the distribution disk, the drop in the relation to the coating will have a speed:

$$\bar{V}_2 = \bar{V}_1 + \bar{V}_m, \quad (2)$$

where V_m – machine speed.

The velocity values V_2 in the projection on the axis will be the initial conditions for further consideration of the droplet moving in the XYZ coordinate system. The X axis is perpendicular to the machine's axis of motion, the Z axis is parallel to it. The Y axis is parallel to the axis of rotation of the distribution disk.

This analysis is necessary for specifying the initial conditions for the equations of motion of drops of reagent in the air.

2.2. Mathematical model of the motion of a drop of AR in the air

At the time of gathering the disk (Figure 2), and on further movement droplet in air on it are: gravity \bar{G} , since there is a drop near the ground, the force of the air resistance of the medium \bar{F}_V [28] and the lift force \bar{R} directed opposite to the force of gravity [29]. In scheme arbitrarily, specified wind speed vector \bar{V}_V acting in the XZ plane and directed at an angle α to the X axis.

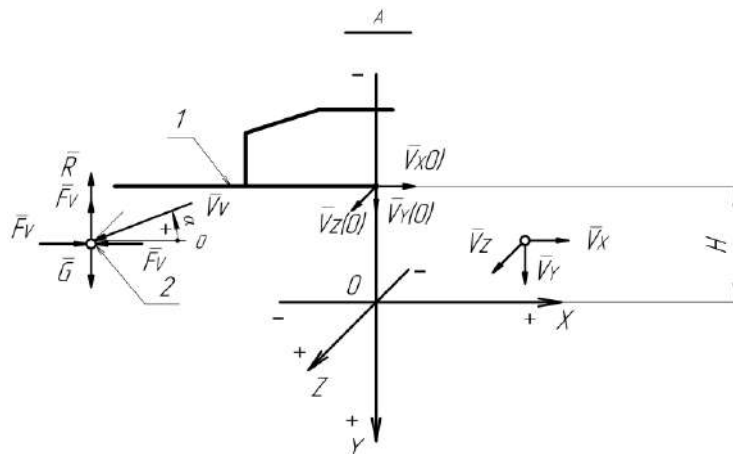


Figure 2. Scheme of the direction of velocity vectors and forces acting on a drop of AR in the process of its movement

In the diagram shown: 1 – the distribution disk 2 – a drop PGR (shown in phantom), \bar{V}_V – wind velocity vector, H – disk height above coated (0), $\bar{V}_x(0)$ – vector initial drop velocity at the time of the

gathering from the disk at an angle of 0° to the X axis, $\overline{V}_z(0)$ – initial velocity vector of droplets at the time of a meeting with the disk at an angle of 0° to Z axis, $\overline{V}_y(0)$ – vector initial drop velocity at the time of the gathering from the disk at an angle of 0° to Y axis, $\overline{V}_x, \overline{V}_y, \overline{V}_z$ – the vectors drop rate at arbitrary moment of time.

The force of gravity is determined by the formula $G = m \cdot g$, the lifting force, which is a part of the total aerodynamic force is determined by the formula

$$R = \rho_1 \cdot V_k \cdot g,$$

where V_k – drop's amount m^3 ;

ρ_1 is the density of air in kg/m^3 .

The strength of the air environment resistance characterizes its viscous properties and is calculated by the formula $F_v = k \cdot v$ [30, 31],

where $v = V_2$ – PRT speed drops when gathering from the disk, m/s;

k is the coefficient of medium resistance, kg/s.

k depends on the dynamic viscosity of the medium and the geometric shape of the body moving inside. For bodies of spherical shape $k = 6\pi \cdot R \cdot \eta$ [32, 33],

where R is the radius of the drop, m;

η is the coefficient of dynamic viscosity of the medium, kg/m·s. This value is a reference and calculated depending on the temperature of the medium [34].

According to Newton's Second Law, the change in the momentum of a body is equal to the sum of the forces acting on it. Then the equation of motion of the drop in the projection onto the Y axis takes the form:

$$m \cdot \overline{a}_y = m \cdot \overline{g} - \rho_1 \cdot v_k \cdot \overline{g} - k \cdot \overline{v}, \tag{3}$$

where m is the mass of a drop of liquid PGR, kg;

\overline{a}_y – drop's acceleration, m/s^2 ;

ρ_1 is the density of air, kg/m^3 ;

At the final moment of the considered time interval (when the drop reaches the coating), the value of the Y coordinate must be zero (Figure 2).

At different times, the droplets will leave the disk, flying off from it at some angle β , analogous to the angle of unloading when the solid particles move on the rotating disk [35]. Using this angle and applying the basic theorem of the vector algebra on the decomposition of a vector along an orthogonal basis [36], we can obtain the projections of the initial velocity vector of the drop on the X, Y, Z axis (Figure 3).

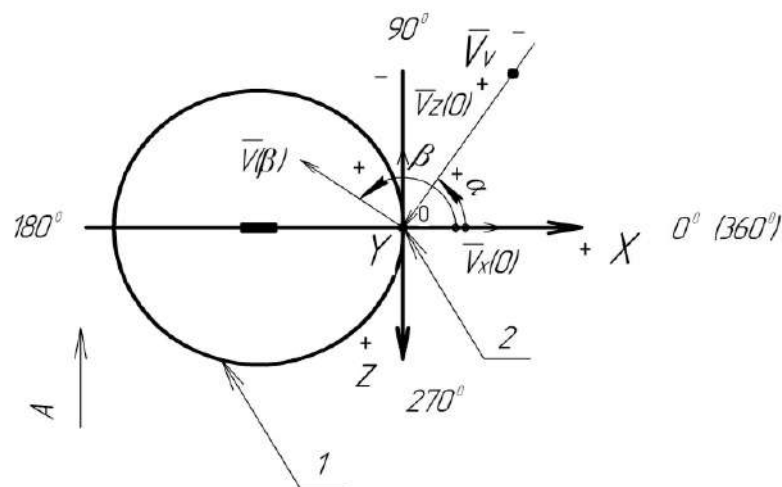


Figure 3. Scheme of the direction of the initial velocity vector of the drop of the PGR at flight from the disk surface

The diagram shows: 1 – the distribution disk, 2 – the drop of the PGR, β – the angle of the drop of the PGR drop from the disk, $\vec{V}(\beta)$ – the vector of the initial velocity of the droplet upon the flight from the disk at the angle, \vec{V}_V – wind velocity vector directed at an angle to the X axis, $\vec{V}_X(0)$ – initial vector of drop's velocity at the time of the gathering from the disc at an angle of 0° to the X axis, $\vec{V}_Z(0)$ – initial vector of drop's velocity at the time of gathering from the disc at an angle of 0° to the Z axis, $\vec{V}_Y(0)$ – initial vector of drop's velocity at the time of the gathering from the disc at an angle of 0° to the axis Y.

The angle β is measured from the X axis in the XZ plane counterclockwise. If we change its value with an arbitrarily chosen step, we obtain the projections of the initial velocity vector $V(\beta)$ on the X and Z axes. The projection of the vector on the Y axis which lies in the perpendicular plane will be zero.

When studying the drop's behavior in the air traffic, it can be divided into four computational cases:

case I – the angle $\beta = 0^\circ \dots 90^\circ$ and $\beta = 270^\circ \dots 360^\circ$, II – value of the angle $\beta = 90^\circ \dots 270^\circ$, III – the angle $\beta = 0^\circ \dots 180^\circ$, IV – the angle $\beta = 180^\circ \dots 360^\circ$.

When the angle β is between 0° and 360° the values of the initial velocity of the reagent droplets in the expansion axis in the chosen coordinate system change and therefore change the value of drop's displacements along the axes X, Y, Z.

The data on these displacements makes it possible to determine the initial and final coordinates of the drop in the XYZ system, visualize the trajectories of the flow of liquid reagents, and calculate the maximum width of the coating strip for the liquid reagent.

In order to take into account the effect of wind on a moving drop, we use the calculation schemes shown in Figures 2 and 3. Figure 2 shows the positions of the reagent drop in the planes XY and ZY, indicating the droplet velocity vectors \vec{V}_X and \vec{V}_Z . Let us consider the displacement of a drop relative to the X axis. In this case, there are two possible variants: movement toward the positive direction of the X axis and toward the negative direction. In both cases, the forces of resistance of the air environment are acting. The wind flow, conventionally designated by the vector \vec{V}_V and determined by the strength and direction of the wind, will decrease the velocity of the drop if it moves in the windward zone and increase it if the drop is in the leeward zone [37].

The leeward zone is the zone in which the wind does not exert any influence, that is $\vec{V}_V = 0$.

The strength of the air resistance of the medium $F_v = k \cdot V_x$ is directed opposite to the vector of drop's velocity and is effective equally in all directions. Projecting all the forces on the X-axis, we get:

For the first design case:

$$m \cdot \bar{a}_x = k(\vec{V}_x - \vec{V}_v \cos \alpha), \quad (4)$$

For the second design case:

$$m \cdot \bar{a}_x = k(\vec{V}_x - \vec{V}_v \cos \alpha) \quad (5)$$

If the drop moves in the leeward zone, the equation of motion takes the form:

$$m \cdot \bar{a}_x = k \cdot \vec{V}_x \quad (6)$$

Similarly, there will be movement in the plane ZY.

A drop from the AR stream can move either in the positive direction along the Z axis (case 3), or in the opposite direction (case IV).

The equation of motion in the projection on the Z axis takes the form:

For the III design case:

$$m \cdot \bar{a}_z = k(\vec{V}_z - \vec{V}_v \sin \alpha), \quad (7)$$

For IV settlement case:

$$m \cdot \bar{a}_z = k(\vec{V}_z - \vec{V}_v \sin \alpha), \quad (8)$$

In the case of movement in the leeward zone:

$$m \cdot \bar{a}_z = k \cdot \vec{V}_z, \quad (9)$$

The obtained equations and dependencies are introduced into the monitoring system software provide an opportunity to accurately estimate the most important quality parameters of the reagent spraying – the width of the processing strip and the uniformity of the AR application under different conditions. If the distributor is equipped with measuring sensors that determine the strength and direction of the wind, as well as the height of the disk above the coating, then by means of the hydraulic drive of the distribution disks, flow regulators and pressure of the reagent feed, it is possible to purposefully change the operating modes and arrangement of the working equipment.

Data on the state of the environment and the performance of the equipment will flow into the control unit of the monitoring system of the reagent dispenser. After their processing and automatic calculations on the above formulas, the system will determine the optimal mode of operation of the equipment (the frequency of disk's rotation, the installation height above the coating, pressure and the value of the AR feed). Data from the sensors will be continuously fed into the control unit in real time. Thus, both external factors related to the environment and internal ones that depend on the working equipment will be considered, and the efficiency and quality of the process of anti-icing processing are ensured.

3. Results and Discussion

1. For the resulting droplet motion equations (3–5, 7, 8), we formulate the initial conditions: the time of motion of the droplet relative to the coating begins in the moment of the droplet's fly off the disk, the maximum time of investigation is the time when the drop reaches the coating. The value of the velocity and acceleration of the drop relative to the Y axis at the initial instant of time is zero. The angle of departure of the β drop from the disk is assumed to be equal zero.

Under the initial conditions for solving the differential equation 3: $Y(0) = H$, $Y'(0) = 0$, t the solution of the equation takes the form:

$$Y = \frac{(g(m - \rho_1 \cdot v_k) \cdot (m - m \cdot e^{k \cdot t/m} + k \cdot t \cdot e^{k \cdot t/m}))}{(k^2 \cdot e^{k \cdot t/m})}, \quad (10)$$

$$Y' = \frac{(g(m - \rho_1 \cdot v_k) \cdot (e^{k \cdot t/m} - 1))}{(k \cdot e^{k \cdot t/m})}, \quad (11)$$

$$Y'' = \frac{(g(m - \rho_1 \cdot v_k))}{(m \cdot e^{k \cdot t/m})}, \quad (12)$$

where Y is the coordinate of the drop in the projection onto the Y axis, m. At the initial instant of time t, it is assumed to be equal zero;

Y' is the first derivative of the time coordinate Y, i.e. droplet speed, m/s;

Y'' is the second derivative of the time coordinate Y, i.e. droplet acceleration, m/s²;

t is the time of motion of the drop, sec;

v_k is the volume of the drop, m³.

At the final moment of the considered time interval (when the drop reaches the coating), the value of the Y coordinate must be zero (Figure 2). At the initial moment, $Y = H$.

2. The solution of the differential equations 4,5 with the initial conditions $V_x(0) = V_2 \cos(\alpha)$, is the velocity of the drop at the initial instant of time, and $X(0) = 0$ is the coordinate of the drop along the X axis at the initial instant of time,

$$X = \frac{(m(V_v \cdot \cos \alpha - V_2))}{k} + V_v \cdot t \cdot \cos \alpha - \frac{(m \cdot e^{k \cdot t/m}(V_v \cdot \cos \alpha - V_2))}{k}, \quad (13)$$

$$X' = V_v \cdot \cos \alpha - e^{k \cdot t/m} (V_v \cdot \cos \alpha - V_2), \quad (14)$$

$$X'' = \frac{-(k \cdot e^{k \cdot t/m}(V_v \cdot \cos \alpha - V_2))}{m}, \quad (15)$$

where X' is the first derivative of the time for X coordinate, i.e. droplet speed, m/s;

X'' is the second derivative of the time for X coordinate, i.e. acceleration of the drop, m/s^2 .

3. Under the initial conditions, $V_z(0) = -V_2 \cdot \sin(0)$, $Z(0) = 0$.

The solution of equations 7, 8 takes the form:

$$Z = \frac{(m(V_v \sin \alpha - V_z(0)))}{k} + V_v \cdot t \cdot \sin \alpha - \frac{(m \cdot e^{k \cdot t/m}(V_v \sin \alpha - V_z(0)))}{k}, \quad (16)$$

$$Z' = V_v \sin \alpha - e^{k \cdot t/m} (V_v \sin \alpha - V_z(0)), \quad (17)$$

$$Z'' = \frac{-(k \cdot e^{k \cdot t/m}(V_v \sin \alpha - V_z(0)))}{m}, \quad (18)$$

where Z' is the first derivative of the time for Z coordinate, i.e. droplet speed, m/s ; Z'' is the second derivative of the time for Z coordinate, i.e. acceleration of the drop, m/s^2 . These equations are derived and based on similar studies [28, 30, 33].

4. The resulting differential equations (3–9) of the AR droplet motion in the air environment in the projections on the X, Y, Z axes allow us to conclude that the acceleration value with which the PGD droplet moves in the air environment is determined by the values of the viscosity coefficient of the medium, mass droplet, travel time and the speed of the AR drop, wind direction and machine speed (equations 12, 15, 18). This confirms and develops the already available results of the study [38–40], since it provides an opportunity to describe the entire process of droplet's motion, starting to fly off the disk and ending with the reaching the coating.

5. The value of the droplet's velocity of a liquid reagent is determined by the droplet's mass, viscosity, travel time, and the departure angle of the droplet from the disk, and by the direction and force of the wind (11, 14, 17). With the change of wind's speed, the deviation of the trajectory of the PGR drop will be observed, the magnitude and direction of which is affected by the force of the wind and its direction relative to the axis of motion of the machine.

6. When wind influences on the flow of reagents, the deviation of the trajectories of the droplets are moving on different sides relative to the rotation axis of the disk will differ in magnitude (equations 4–9).

7. With increasing the wind's strength, it is necessary to reduce the height of the distribution equipment to maintain the range of the AR drop and the required width of the processed strip.

8. As the altitude of the disk increases, the value of the range of the flight of the AR drop increases and consequently the overlapping areas of the coating treatment areas with the liquid reagent in the case of two disks (equations 3, 10, 13, 16). Related results are described in [41], but with reference to the agricultural engineering.

9. The value of the initial velocity of the AR drop at the time of flight from the distribution disk depends on the exhaust velocity of the AR from the injector, that is, not only on the reagent feed pressure, but also on the height of the spray nozzle relative to the distributing disk (formulas 1, 2).

10. The flight range and the width of the processing strip are determined by such parameters of the environment as:

- a) the viscosity of the air;
- b) direction and speed of the wind.

4. Conclusion

1. A mathematical model of describing the motion of drops of a liquid reagent in the process of treatment with roadside reagents of road and airfield coatings is developed.

2. An analytical solution of the differential equations of AR droplets moving in the air is obtained.

3. Dependences of the trajectory, speed and acceleration of motion on the parameters of the working equipment (the geometrical dimensions of the distribution disk, the mode of operation of the disk and the spray nozzle) and the characteristics of the external environment (viscosity of the air medium, direction and air flow velocity) are determined.

4. Some factors that will allow to maintain the given range continuously and the uniformity of treatment of coatings with liquid reagents are determined. The developed model is recommended to be used in an automatic monitoring system for the distribution of liquid AR.

5. The system should ensure the continuous collection, processing and analysis of environmental data and the distribution equipment in real time. The obtained information will be used to calculate the effectiveness of the coating application process (i.e, the best combination of range, density and uniformity of the AR feed). In the article, the basis of the mathematical support of the work of this system is proposed.

References

1. Glushko A.N., Chelnokov V.V., Bessarabov A.M. Sistema komp'yuternogo menedzhmenta kachestva dlya otsenki ekologicheskogo vozdeystviya protivogolodnykh reagentov na vkhode [Computer quality management system for assessing the environmental impact of anti-ice reagents on the environment]. *Mathematical methods in engineering and technology - MMTT*. 2016. No. 10(92). Pp. 176–177. (rus)
2. Vasilyev R.Yu. Protivogolodnoye i meteorologicheskoye obespecheniye zimnego soderzhaniya avtomobil'nykh dorog [Anti-ice and meteorological support of winter maintenance of highways]. *Transport and transport-technological systems*. 2017. Pp. 83–86. (rus)
3. Lemchuzhnikov V.E., Masyagin A.V., Novikov V.A., Filatov Yu.V. Mashina dorozhnaya s raspredelitelem protivogolodnykh materialov, avtomaticheskim upravleniyem i kontrolem tekhnologicheskogo protsesssa, s privodom transportera ot planetarnogo gidromotora, osnashchennogo preobrazovatelem okruzhnoy skorosti gidromotora v chastotu [Road machine with a distributor of de-icing materials, automatic control and monitoring of the technological process, with the drive of the conveyor from the planetary hydraulic motor equipped with a converter of the circumferential speed of the motor to the frequency]. *Patent Russia no. 22263739*, 2005. (rus)
4. Sistema upravleniya mobil'nym raspredelitelem protivogolodnykh materialov [Mobile dispenser control system for de-icing materials][Electronic resource] URL: <http://russianpatents.com/patent/239/2398929.html> (reference date: July 14, 2017). (rus)
5. Belotserkovsky G.M., Ahrameev E.V., Karjakin S.B. Sposob obespecheniya raboty sistem upravleniya rabochim protsessom mobil'nogo raspredelitelya materialov dlya obrabotki dorozhnykh pokrytiy ustroystvo upravleniya rabochim protsessom mobil'nogo raspredelitelya materialov [A way to ensure the operation of the workflow control system of a mobile material distributor for the treatment of road surfaces and the device for controlling the workflow of a mobile material distributor]. *Patent Russia no. 2398929*, 2013. (rus)
6. Lukanov N.I. Ustroystvo avtomaticheskogo dozirovaniya khimicheskikh reagentov pri nanesenii ikh na poverkhnost' iskusstvennogo pokrytiya [The device of automatic dosing of chemical reagents when applied to the surface of an artificial coating]. *Patent Russia no. 2487971*, 2013. (rus)
7. *Avtomatizirovannaya sistema upravleniya kommunal'noy dorozhnoy mashinoy. Raspredeleniye zhidkikh protivogolodnykh reagentov* [Automated control system for a public road vehicle. Distribution of liquid anti-ice reagents] [Electronic resource]. URL: www.kbkoloss.ru/products/avtomatika-dlya-kommunalnoy-dorozhnoy-mashiny/avtomatika-dlya-peskorazbrasyvatelya-asu2c (reference date: July 19, 2017). (rus)
8. Mandrovskiy K.P. Sistemy upravleniya v upravlenii effektivnost'yu i tekhnicheskim audite dorozhnykh mashin [Control systems in efficiency management and technical audit of road machines]. *Tekhnicheskyye nauki v Rossi i za rubezhom. Materialy V Mezhdunarodnaya konferentsiya konferentsii*. Brynsk. 2016. Pp. 75–78. (rus)
9. Mandrovskiy K.P. Sistemy monitoringa dorozhno-stroitel'nykh, transportnykh mashin i dorozhnykh pokrytiy

Литература

1. Глушко А.Н., Челноков В.В., Бессарабов А.М. Система компьютерного менеджмента качества для оценки экологического воздействия противогололедных реагентов на окружающую среду // Математические методы в технике и технологиях – ММТТ. 2016. № 10 (92). С. 176–177.
2. Васильев Р.Ю. Противогололедное и метеорологическое обеспечение зимнего содержания автомобильных дорог // Транспортные и транспортно-технологические системы. 2017. С. 83–86.
3. Патент РФ № 22263739, 10.11.2005. Машина дорожная с распределителем противогололедных материалов, автоматическим управлением и контролем технологического процесса, с приводом транспортера от планетарного гидромотора, оснащенного преобразователем окружной скорости гидромотора в частоту / Лемчужников В.Е., Масыгин А.В., Новиков В.А., Филатов Ю.В. // Патент России № 2263739. 2003. Бюл. № 31.
4. Система управления мобильным распределителем противогололедных материалов [Электронный ресурс] URL: <http://russianpatents.com/patent/239/2398929.html> (дата обращения: 14.07.2017).
5. Патент РФ № 2398929, 20.07.2013. Способ обеспечения работы системы управления рабочим процессом мобильного распределителя материалов для обработки дорожных покрытий и устройство управления рабочим процессом мобильного распределителя материалов / Белоцерковский Г.М., Ахрамеев Э.В., Карякин С.Б. // Патент России № 2398929. 2009. Бюл. № 25.
6. Патент РФ № 2487971, 20.07.2013. Устройство автоматического дозирования химических реагентов при нанесении их на поверхность искусственного покрытия / Луканов Н.И. // Патент России № 2487971. 2012. Бюл. № 20.
7. Автоматизированная система управления коммунальной дорожной машиной. Распределение жидких противогололедных реагентов [Электронный ресурс]. URL: www.kbkoloss.ru/products/avtomatika-dlya-kommunalnoy-dorozhnoy-mashiny/avtomatika-dlya-peskorazbrasyvatelya-asu2c (дата обращения: 19.07.2017).
8. Мандровский К.П. Системы мониторинга в управлении эффективностью и техническом аудите дорожных машин // Технические науки в России и за рубежом. Материалы V Международной научной конференции. 2016. С. 75–78.
9. Мандровский К.П. Системы мониторинга дорожно-строительных, транспортных машин и дорожных покрытий // ИНТЕРСТРОЙМЕХ – 2015. Материалы международной научно-технической конференции. 2015. С. 310–315.
10. Мандровский К.П. Оценка динамической устойчивости в мониторинговой системе управления технико-экономической эффективностью дорожных машин // Вестник Донского государственного технического университета. 2016. Т. 16. № 2(85). С. 69–76.
11. Kulkarni A., Mohsenin T., Pino Y., French M. Real-time anomaly detection framework for many-core router through

- [Monitoring systems in the sphere of road construction, transportation and road surfaces]. *INTERSTROYMEKH - 2015. Materialy mezhdunarodnoy nauchno-tekhnicheskoy konferentsii*. Kazan. 2015. Pp. 310–315. (rus)
10. Mandrovskiy K.P. Otsenka dinamicheskoy ustoychivosti v monitoringovoy sisteme upravleniya tekhniko-ekonomicheskoy effektivnost'yu dorozhnykh mashin [Evaluation of dynamic stability in the monitoring system of management of technical and economic efficiency of road vehicles]. *Vestnik Donskogo gosudarstvennogo tekhnicheskogo universiteta*. 2016. Vol. 16. No. 2(85). Pp. 69–76. (rus)
 11. Kulkarni A., Mohsenin T., Pino Y., French M. Real-time anomaly detection framework for many-core router through machine-learning techniques. *ACM Journal on Emerging Technologies in Computing Systems*. 2016. Vol. 13. Pp. 10.
 12. Öörni R., Meilikhov E., Korhonen T.O. Interoperability of ecall and era-glonass in-vehicle emergency call systems // *IET Intelligent Transport Systems*. 2015. Vol. 9 No. 6. Pp. 582–590.
 13. Lara-Molina F.A., Rosário J.M., Dumur D., Wenger P. Robust, generalized predictive control of the orthoglide robot // *Industrial Robot*. 2014. Vol. 41.No. 3. Pp. 275–285.
 14. Ye Y., Li G. Modeling of hydrodynamic cavitating flows considering the bubble-bubble interaction // *International Journal of Multiphase Flow*. 2016. Vol. 84. Pp. 155–164.
 15. Ilyinikh A.Yu., Chashechkin Yu.D. Gidrodinamika kontakta padayushchey kapli so svobodnoy poverkhnost'yu zhidkosti [Hydrodynamics of contact of a falling drop with a free surface of a liquid]. *Izvestiya Rossiiskoi Akademii Nauk. Mekhanikazhidkosti i gaza*. 2016. No. 2. Pp. 3–12. (rus)
 16. Ibrahim A., Girimaji S.S., Suman S. On air-chemistry reduction for hypersonic external flow applications. *International Journal of Heat and Fluid Flow*. 2015. Vol. 51. Pp. 298–308.
 17. Kim M.-K., Song J., Hwang J., Yoon Y. Effects of canted injection angles on the spray characteristics of liquid jets in subsonic crossflows. *Atomization and Sprays*. 2010. Vol. 20. No. 9. Pp. 749–762.
 18. Eggers J., Villermaux E. Physics of liquid jets. *Reports on Progress in Physics*. 2008. Vol. 71. No. 036601. Pp. 1–79.
 19. Salehi-Shabestari A., Raisee M., Sadeghy K., Ahmadvour A. Flow and displacement of waxy crude oils in a homogenous porous medium: a numerical study. *Journal of Non-newtonian Fluid Mechanics*. 2016. Vol. 235. Pp. 47–63.
 20. Dumouchel C. The experimental investigation on primary atomization of liquid streams. *Experiment in Fluid*. 2008. Vol. 45. Pp. 371–422.
 21. Santangelo P.E. Characterization of high-pressure water-mist sprays: Experimental analysis of droplet size and dispersion // *Experimental thermal and fluid science*. 2010. Vol. 34. Pp. 1353–1366.
 22. Er D.Z., Liew C.V., Heng P.W. Layered growth with bottom-spray granulation for spray deposition of drug // *International Journal of Pharmaceutics*. 2009. No. 377. Pp. 16–24.
 23. Onishchenko V.B., Lyubchenko I.S. Review of theoretical studies of process of liquid mineral fertilizers. *Науковий Вісник Нубіп України. Серія: Техніка та Енергетика АПК*. 2016. No. 251. Pp. 26.
 24. Polishchuk V.N. Irregular movement air-mix for fluids in dispensing system sprayers. *Swordjournal*. 2016. Vol. 1110. No. 11. Pp. 221–224.
 25. Balovnev V.I. *Mashiny dlya obsluzhivaniya i remonta gorodskikh i avtomobil'nykh dorog* [Machines for maintenance and repair of urban and highways]. Moscow–Omsk: OMSK HOUSE OF PRESS, 2005. 768 p. (rus)
 26. Bondarev A., Galaktionov V. *Sovremennyye napravleniya razvitiya vizualizatsii dannykh v vychislitel'noy mekhanike* // *ACM Journal on Emerging Technologies in Computing Systems*. 2016. Vol. 13. Pp. 10.
 27. Öörni R., Meilikhov E., Korhonen T.O. Interoperability of ecall and era-glonass in-vehicle emergency call systems // *IET Intelligent Transport Systems*. 2015. Vol. 9 No. 6. Pp. 582–590.
 28. Lara-Molina F.A., Rosário J.M., Dumur D., Wenger P. Robust generalized predictive control of the orthoglide robot // *Industrial Robot*. 2014. Vol. 41. No. 3. Pp. 275–285.
 29. Ye Y., Li G. Modeling of hydrodynamic cavitating flows considering the bubble-bubble interaction // *International journal of multiphase flow*. 2016. Vol. 84. Pp. 155–164.
 30. Ильиных А.Ю., Чашечкин Ю.Д. Гидродинамика контакта падающей капли со свободной поверхностью жидкости // *Известия Российской академии наук. Механика жидкости и газа*. 2016. № 2. С. 3–12.
 31. Ibrahim A., Girimaji S.S., Suman S. On air-chemistry reduction for hypersonic external flow applications // *International journal of heat and fluid flow*. 2015. Vol. 51. Pp. 298–308.
 32. Kim M.-K., Song J., Hwang J., Yoon Y. Effects of canted injection angles on the spray characteristics of liquid jets in subsonic crossflows // *Atomization and sprays*. 2010. Vol. 20. No. 9. Pp. 749–762.
 33. Eggers J., Villermaux E. Physics of liquid jets // *Reports on progress in physics*. 2008. Vol. 71. No. 036601. Pp. 1–79.
 34. Salehi-Shabestari A., Raisee M., Sadeghy K., Ahmadvour A. Flow and displacement of waxy crude oils in a homogenous porous medium: a numerical study // *Journal of non-newtonian fluid mechanics*. 2016. Vol. 235. Pp. 47–63.
 35. Dumouchel C. The experimental investigation on primary atomization of liquid streams // *Experiment in fluid*. 2008. Vol. 45. Pp. 371–422.
 36. Santangelo P.E. Characterization of high-pressure water-mist sprays: Experimental analysis of droplet size and dispersion // *Experimental thermal and fluid science*. 2010. Vol. 34. Pp. 1353–1366.
 37. Er D.Z., Liew C.V., Heng P.W. Layered growth with bottom-spray granulation for spray deposition of drug // *International Journal of Pharmaceutics*. 2009. No. 377. Pp. 16–24.
 38. Onishchenko V.B., Lyubchenko I.S. Review of theoretical studies of process of liquid mineral fertilizers // *Науковий вісник нубіпукраїни. Серія: техніка та енергетика АПК*. 2016. № 251. С. 26.
 39. Polishchuk V.N. Irregular movement air-mix for fluids in dispensing system sprayers // *SWORLDJOURNAL*. 2016. Vol. 1110. № 11. Pp. 221–224.
 40. Баловнев В.И. *Машины для содержания и ремонта городских и автомобильных дорог*. М. - Омск: ОМСКИЙ ДОМ ПЕЧАТИ, 2005. 768 с.
 41. Бондарев А., Галактионов В. *Современные направления развития визуализации данных в вычислительной механике жидкости и газа* // *Научная визуализация*. 2013. Т. 5. № 4. С. 18–30.
 42. Вараксин А.Ю. *Гидрогазодинамика и теплофизика двухфазных потоков: проблемы и достижения (обзор)* // *Теплофизика высоких температур*. 2013. Т. 51. № 3. С. 377–407.
 43. Шварц К.Г., Шварц Ю.А., Шкляев В.А. *Двумерная модель мезомасштабных процессов в нижнем слое атмосферы с учетом неоднородности температуры и влажности воздуха* // *Вычислительная механика сплошных сред*. 2015. Т. 8. № 1. С. 5–15.
 44. Kalnay E. *Atmospheric modeling, data assimilation and predictability*. Cambridge University Press. 2003. Pp. 369
 45. Гуськов О.Б. *О вращении сферического тела в вязкой суспензии* // *Физико-химическая кинетика в газовой*

- zhidkost i igaza [Current trends in the development of data visualization in the computational mechanics of fluid and gas]. *Scientific visualization*. 2013. Vol. 5. No. 4. Pp. 18–30. (rus)
27. Varaksin A.Yu. Hidrogazodinamika i teplofizika dvukhfaznykh potokov: problemy i dostizheniya (obzor)[Hydrodynamics and thermophysics of two-phase flows: problems and achievements (review)]. *Thermophysics of high temperatures*. 2013. Vol. 51. No. 3. Pp. 377–407. (rus)
 28. Shvarts K.G., Shvarts Yu.A., Shklyaev V.A. Two-dimensional model of mesoscale processes in the lower atmosphere with allowance for the inhomogeneity of air temperature and humidity. *Computational Mechanics of Continuous Media*. 2015. Vol. 8. No. 1. Pp. 5–15.
 29. Kalnay E. *Atmospheric modeling, data assimilation and predictability*. Cambridge University Press. 2003. 369 p.
 30. Guskov O.B. O vrashchenii sfericheskogo tela v vyazkoy suspenzii [On the rotation of a spherical body in a viscous suspension]. *Fiziko-khimicheskayakinetika v gazovoydinamike*. 2015. Vol. 16. No. 2. Pp. 7.(rus)
 31. Kartushinsky A.I., Mihaelides E.E., Rudy Yu.A., Tisler S.V., Scheglov I.N. Chislennoye modelirovaniye dvumernoy vertikal'noy dvukhfaznoy strui [Numerical simulation of a two-dimensional vertical two-phase jet]. *Izvestiya Rossiiskoi Akademii Nauk. Mechanics of fluid and gas*. 2012. No. 6. Pp. 99–108.(rus)
 32. Goncharova O.N. Konvektivnoye dvizheniye zhidkostey pod deystviyem soputstvuyushchikh gazovykh potokov: matematicheskoyemodelirovaniye, chislennyyeissledovaniya [Convective motion of liquids under the action of concomitant gas flows: mathematical modeling, numerical research]. *Omsk Scientific Herald*. 2013. No. 1(117). Pp. 21–24.(rus)
 33. Yushkov V.P. Energiyai dissipatsiya turbulentnykh kolebaniy skorosti i temperatury vetra v pogranichnom sloye atmosfery [Energy and dissipation of turbulent fluctuations in wind speed and temperature in the boundary layer of the atmosphere]. *Bulletin of Moscow University. Series 3: Physics. Astronomy. Moscow*. No. 3. Pp. 100–109.(rus)
 34. Mukhtorov L.T., Abdumannonov A.A. Opredeleniye koeffitsiyenta vyazkosti sredy metodomkom p'yuternogo modelirovaniya [Determination of the viscosity coefficient of the medium by the method of computer simulation]. *Bulletin of the Tajik National University. Series of Natural Sciences*. 2016. No. 1-2(196). Pp. 121–127.(rus)
 35. Zemdikhanov M.M. Gabdullin T.R. Obosnovaniye skhemyi parametrovt sentrobezhnogo razbrasyvatelya peska i reagentov [Justification of the scheme and parameters of the centrifugal sand spreader and reagents]. *Izvestiya KGASU*. 2014. No. 4(30). Pp. 484–489.(rus)
 36. Qin Z., Buehler M.J. Computational and theoretical modeling of intermediate filament networks: structure, mechanics and disease. *Acta Mechanica Sinica*. 2012. Vol. 28. No. 4. Pp. 941–950.
 37. Simio E., Scanlan R.H. Wind Effects on Structures: An Introduction to Wind Engineering. By John Wiley & Sons, Inc. 1978. 360 p.
 38. Bogdanov V.S, Logachev I.N., Dmitrienko V.G., Zhidkov V.V. Zakonomernosti segregatsii chastits navrashchayushchemsya diske klassifikatora tsentrobezhnogo tipa [Patterns of segregation of particles on a rotary disc of a centrifugal classifier]. *Vestnik Belgorod Technological University V.G. Shukhov*. 2012. No. 1. Pp. 73–78. (rus)
 39. Vinogradov A.G. Vrauvannya aerodinamichnogo koeffitsiynta matematicheskuyu moduluvanni ruhu krapel voda v pavitriro *News of the National Technical University of Ukraine "Kyiv Polytechnic Institute"*. 2011. No. 63. Pp. 264–267.
 40. Pshennikova G.V, Mitrakov M.V, Khripin V.A. Vneseniye dinamike. 2015. T. 16. № 2. С. 7
 31. Картушинский А.И., Михаелидес Э.Э., Руди Ю.А., Тислер С.В., Щеглов И.Н. Численное моделирование двумерной вертикальной двухфазной струи // Известия Российской академии наук. Механика жидкости и газа. 2012. № 6. С. 99–108.
 32. Гончарова О.Н. Конвективные движения жидкостей под действием сопутствующих потоков газа: математическое моделирование, численные исследования // Омский Научный Вестник. 2013. № 1(117). С. 21–24.
 33. Юшков В.П., Энергия и диссипация турбулентных флуктуаций скорости ветра и температуры в пограничном слое атмосферы // Вестник Московского Университета. Серия 3: Физика. Астрономия. 2011. № 3. С. 100–109.
 34. Мухторов Л.Т., Абдуманнонов А.А. Определение коэффициента вязкости среды методом компьютерного моделирования // Вестник Таджикского Национального Университета. Серия Естественных Наук. 2016. № 1–2(196). С. 121–127.
 35. Земдикханов М.М., Габдуллин Т.Р. Обоснование схемы и параметров центробежного разбрасывателя песка и реагентов // Известия КГАСУ. 2014. № 4(30). С. 484–489.
 36. Qin Z., Buehler M.J. Computational and theoretical modeling of intermediate filament networks: structure, mechanics and disease // Acta Mechanica Sinica. 2012. Vol. 28. No. 4. Pp. 941–950.
 37. Simio E., Scanlan R.H. Wind Effects on Structures: An Introduction to Wind Engineering. By John Wiley & Sons, Inc, 1978. 360 p.
 38. Богданов В.С., Логачев И.Н., Дмитриенко В.Г., Жидков В.В. Закономерности сегрегации частиц на вращающемся диске классификатора центробежного типа // Вестник Белгородского технологического университета им. В.Г. Шухова. 2012. № 1. С. 73–78.
 39. Виноградов А.Г. Врахування аеродинамічного коефіцієнта при математичному моделюванні руху крапель води в повітрі // Вісник Національного технічного університету України «Київський політехнічний інститут». Серія Машинобудування. 2011. № 63. С. 264–267.
 40. Пшенникова Г.В., Митраков М.В., Хрипин В.А. Внесение минеральных удобрений центробежными разбрасывателями// Проблемы механизации агрохимического обеспечения сельского хозяйства. 2010. № 2010. С. 68–71.
 41. Подшиваленко И.Л., Кузюр В.М. Обоснование рабочей ширины захвата штанги машины для внесения жидких органических удобрений // Конструирование, использование и надежность машин сельскохозяйственного назначения. 2013. № 1(12). С. 18–23.

emineral'nykh udobreniy tsentrobezhnymi razbrasyvatel'nyimi [Introduction of mineral fertilizers by centrifugal spreaders]. *Problems of Mechanization of Agrochemical Provision of Agriculture*. 2010. No. 2010. Pp. 68–71. (rus)

41. Podshivalenko I.L., Kuzyur V.M. Obosnovaniye rabochey shiriny zakhvata shtangi mashiny dlya vneseniya zhidkikh organicheskikh udobreniy [Justification of the working width of the rod of the machine for introducing liquid organic fertilizers]. *Designing, Use and Reliability of Agricultural Machines*. 2013. No. 1(12). Pp. 18–23. (rus)

Konstantin Mandrovskiy,
+7(926)275-05-52; *effectmash@mail.ru*

Константин Петрович Мандровский,
+7(926)275-05-52; эл. почта: *effectmash@mail.ru*

Yana Sadovnikova,
+7(903)533-50-68; *jana.sadovnikova@yandex.ru*

Яна Сергеевна Садовникова,
+7(903)533-50-68;
эл. почта: *jana.sadovnikova@yandex.ru*

© Mandrovskiy K.P., Sadovnikova Y.S., 2018

doi: 10.18720/MCE.79.3

Micro-turbulence of the stream and its connection with the roughness of the pipeline inner surface

Микротурбулентность потока и ее связь с рельефом внутренней поверхности трубопроводов

*V.A. Orlov,
I.S. Dezhina,
E.V. Orlov,
National Research Moscow State Civil
Engineering University, Moscow, Russia*

*Д-р техн. наук, заведующий кафедрой
В.А. Орлов,
аспирант И.С. Дежина,
канд. техн. наук, доцент Е.В. Орлов,
Национальный исследовательский
Московский государственный
строительный университет, Москва,
Россия*

Key words: gravity pipelines; the surface shape; artificial obstacles; local micro-turbulence; flow rate

Ключевые слова: самотечные трубопроводы; рельеф поверхности; искусственные преграды; местная микротурбулентность; скорость течения

Abstract. This study has been aimed at investigating the problems of a fluid stream flowing in an open chute, which imitates a small-diameter gravity pipeline (up to 150 mm) at low rates of sewage. The works on a specially developed hydraulic bench have enabled determination of the conditions of the flow vortex formation (micro-turbulence) by changing the geometric shape of the internal surface of the pipe by placing artificial protrusions (obstacles) on it, which can help to prevent deposition of suspended particles on the pipeline surface and facilitate their efficient removal. The technique of carrying out hydraulic experiments on the bench has been developed. Several types of artificial obstacles have been studied to investigate their activity in creation of micro-turbulence phenomena on the inner surface of the chute near the frontal surface of streamlined obstacles that can contribute to the stable transport capacity of suspended solids in the flow of a moving fluid. As obstacles, provision has been made of single and grouped bars made of metal and polymeric materials in the form of a parallelepiped and a cylinder, a polyhedron in the form of a prism and screw-nuts, as well as obstacles in the form of an inverted spherical segment, etc. Based on the results of study of the fluid stream flow in an open chute, as well as the location of obstacles, the nature of the vortex formation before and after them was revealed, the optimal geometric dimensions of the obstacles have been got and the areas of disturbance zones at low water flow rates (less than 0.4 m/s) have been determined.

Аннотация. Исследованы вопросы течения потока жидкости в открытом желобе, имитирующем самотечный трубопровод малого диаметра (до 150 мм) при низких скоростях течения сточной воды. На специально разработанном гидравлическом стенде выявлены условия, обеспечивающие вихреобразование (микротурбулентность) потока за счет изменения геометрической формы внутренней поверхности трубы путем расположения на ней искусственных выступов (препятствий), что может способствовать предотвращению осаждения взвешенных частиц на поверхности трубопровода и способствовать их эффективному перемещению. Разработана методика проведения гидравлических экспериментов на стенде. Изучено несколько типов искусственных препятствий, создающих явления микротурбулентности на внутренней поверхности желоба вблизи лобовой поверхности обтекаемых препятствий, которые могут способствовать стабильной транспортирующей способности взвешенных веществ в потоке движущейся жидкости. В качестве препятствий рассматривались единичные и групповые выполненные из металла и полимерных материалов бруски в виде параллелепипеда и цилиндра, многогранника в виде призмы и гаек, а также препятствия в форме перевернутого шарового сегмента и другие. По результатам исследования течения жидкости по открытому желобу и расположения препятствий выявлен характер вихреобразования до и после них, установлены оптимальные геометрические размеры препятствий и определены площади зон возмущения при малых скоростях течения воды (менее 0,4 м/с).

Орлов В.А., Дежина И.С., Орлов Е.В. Микротурбулентность потока и ее связь с рельефом внутренней поверхности трубопроводов // Инженерно-строительный журнал. 2018. № 3(79). С. 27–35.

1. Introduction

Increase of the transport capacity of small diameter water discharge gravity pipelines, which contain in the water flow a significant amount of suspended sandy particles, is an urgent task of all city services bearing responsibility of an effective operation of water discharge networks. This problem is the most acute one due to the general tendency of decrease in water consumption in modern cities. At low flow rates, formation of stagnant zones (siltation) is possible due to the accumulation of suspended solids in the chute portion of gravity pipelines. As an exit from this situation provision may be made of creation of the micro-turbulence conditions on the inner surface of the pipeline chute by formation of a special shape of its relief. The above-mentioned issues have been the subject of these investigations. The purpose of the research was to perform a visual description of the emerging vortex structure with a certain arrangement of obstacles, as well as to fix the character of the perturbation zone geometric parameters in front of the obstacles and behind them. When having these results, researchers are able to select the optimal type of structure and location of obstacles in the chute part of the pipeline to ensure the maximum effect of the local micro turbulence. The works on the study of the micro-turbulence, which arises when the stream is flowing over the obstacles (protrusions), have been performed on a hydraulic bench developed by the authors [1]. As obstructions, use has been made of point and linearly stretched obstacles of equal and different size, which can be considered as an artificial roughness, which does not create large hydraulic resistances.

One of the decisive factors that ensure an effective transport capacity of both operating pipelines and those, that have been repaired by applying internal protective coatings, is the condition of the inner surface of their walls [2, 3]. For a long period of time the researchers have had the opinion, that the inner surface of the pipes should be as smooth as possible, because this ensures the absence or minimal amount of precipitating and accumulating components of contaminants of various origins (for example, sand) in the continuously operating water discharge gravity network [4]. The intensity of precipitation of suspended particles in the bottom of a pipeline is related to the flow rate of the waste fluid [5, 6]. If the flow rate remains below the critical (self-cleaning) one within a long period of time, the impurities do not rest in the suspension state and precipitate, forming deposits. Some sediments, mostly the upper layers, can be taken out by the stream during the hours of maximum water consumption in the city, and the caked (as a rule, the core) ones stay in the chute part of the pipe, which ultimately requires periodic cleaning of the pipeline by various methods [7, 8].

The most common are the General sewage systems are the most commonly subject to a high variability of the flow rate. At the night hours, when the water consumption is minimum and there is no rain, the pipelines work at a low filling, i.e. the live section of the pipeline is only partly filled, which leads to a greater amount of deposits [9]. The presence of deposits in sewerage pipelines and even in water supply systems in the form of a variety of sediments and deposits (suspended matter, bio-fouling, metal oxides, etc.) may decrease the efficiency of the pipeline system or need additional costs of overcoming frictional forces due to narrowing of the living section of pipelines.

The accumulated knowledge in creation of self-cleaning surfaces and provision of self-cleaning rates made it possible to forward the idea of working out such a structure of the pipeline inner surface, which would reduce to a minimum the amount of deposited sediments regardless of the velocities and the filling matters in the pipeline [10, 11]. This purposeful work aimed at the efficient transportation of liquid and solid substances through pipelines has been based on the examples of the wildlife, such as the structure of blood vessels of the insects' wings and the system of transportation of water and nutrient solutions of mineral salts from roots to leaves in the tissues of higher plants, i.e. in the so-called xylem [12-14]. Some researchers have shown, that the effective stirring of the flow and the movement of suspended particles, which have deposited in the chute portion of the pipelines, is observed in the pipes with corrugated internal surfaces made in the form of rectangular needle lips (obstacles) such as a herringbone [15]. With such a structural surface of the chute, the time required for detaching sand deposits from its bottom part due to local turbulence of the water flow in the near-wall area between the obstacles, sediment lifting and their transportation by water should shorten. As shown by investigations on special benches, the effect of the conveying capacity of pipelines can be enhanced by using hydrophobic surfaces that shall be applied to their inner surface by modern trenchless methods [16, 17].

The results of the performed experiments [18] served a scientifically grounded basis for the development of self-cleaning pipeline systems (for example, Self Cleaning Systems), which were implemented into the practice of trenchless renovation using the Trolining method, where internal polymer protective coatings with external and internal corrugated profiles are applied.

However, today there is no general understanding of the surface relief structure, as well as specific technical information on geometric parameters of the corrugated surfaces, in particular the distances

between the obstacles, the angles of their location with respect to the axis of the tray and other circumstances.

The aim of these studies is to obtain and complement knowledge on the study of a wide range of obstacles in the form of corrugated pipe surfaces or their internal protective coatings, which are widely used in the practice of the trenchless rehabilitation of technical utility networks [19, 20]. The tasks of the research include: analysis of the different types of obstacles emerging vortex structure, development of the special testing bench, experimental studies with different types of obstacles [21–22].

2. Methods

The research was based on performing hydraulic experiments on an installation, which has been specially installed in the laboratory, and represented a container rigidly coupled to a polypropylene open chute (trench), of 130 mm diameter (Figure 1), which housed various types of protective coatings with structural features in the form of obstacles to the flow of liquid. Retention of the corresponding obstacles on the tray was made by gluing them on the inner surface of the tray or by using a powerful magnet placed under the tray. The slope of the tray was $1/130 = 0.077$.



Figure 1 Side view of a special stand in the form of an open inclined chute of 130 mm diameter for performing experiments

The works on the bench were performed according to a specially developed procedure. The method of carrying out experiments for investigation of the micro turbulence consisted in flowing of the design water stream from a measuring container along the chute, fixing the water flow rates and the filled amount.

The experiments were accompanied by filming (Sony HDR-CX250 camera) and continuous multi-frame photography (Sony α 550 digital SLR camera, DT 1.8 / 50 SAM lens) using a light-shadow effect to reflect the vortex configurations and backwater in the frontal parts of obstacles. For these purposes, a light source in the form of a lamp with free rotation was mounted on the installation, and a measuring ruler was rigidly fixed in the tray to its upper edge from the inside.

The corresponding flow rate and the stream rate were provided by opening / closing a valve on the pipeline, which supplied water to the measuring vessel. The water consumption was monitored by a volumetric method using a calibration curve describing the dependence of the amount of water flowing out of the chute on time. The rate was determined by the "bobber method", i.e. using a stopwatch and a bobber, triggered into the flow at a certain length of the chute. The values of the wetted perimeter and hydraulic radius were to be calculated.

The final target of the experiments was to determine the optimal configuration of single linearly elongated objects (obstacles), as well as of a set of them, which differ by their location on the tray and dimensions; it allows to get the micro turbulence effect of the flow with small fillings and rates (up to 0.4 m/s). These parameters should provide a stable state of weighing of sediments, which are transported by water due to the created turbulence of the stream.

3. Results

The experiments' results, which have been got by different options (positions 1–9) of single and grouped obstacles on the inner surface of the chute, are given below. Two options are represented by illustrative photos (positions 1 and 2).

- 1) A single obstacle in the form of a rectangular bar, 1 cm long, 0.3 cm wide and 0.2 cm high

- position in the center at an angle of 45 degrees to the axis of the chute (Figure 2).

A distinct ripple (flow disturbance) is observed in front of the obstacle, nearly 1.4-1.6 cm long, with the perturbation area about 1.95 cm². The bed of the stream is not really displaced. Behind the obstacle, the disturbance zone covers the whole width of the stream along 2.5 cm due to the formed vortex and has an area about 2.25 cm². After the perturbation zone, the width of the stream narrows by nearly 1/3.



Figure 2. A single obstacle in the form of a rectangular bar (with a measuring ruler on the right)

- location with a displacement from the center at an angle of 45 degrees to the axis of the chute (Figure 3).

A distinct ripple is observed in front of the obstacle at a length about 2.9-3.1 cm with a perturbation area nearly 6.8 cm². The bed of the stream is displaced somewhat from the axis to the side opposite to the obstacle. The disturbance zone behind the obstacle covers the whole width of the stream due to the formed vortex and makes nearly the same area as in the case with the bar in the center, i.e. 2.25 cm². The width of the stream narrows by about 1/3 after the perturbation zone.



Figure 3. Single obstacle in the form of a rectangular bar with displacement

- 2) Single obstacle in the form of a lying metal cylinder

- location in the center of the chute.

The length of the cylinder is about 1 cm, the diameter is about 1.5 mm. The cylinder is located at the center of the axis of water stream flow, at an angle of 45 degrees. The ripple in front of the obstacle is observed for 1.5–1.7 cm, and after it the swirling of the flow is located at 1.4–1.8 cm.

- location with a small displacement from the center.

The nature of the vortex formation is identical to the position of the cylinder in the center. The areas of the perturbation zone are approximately equal and make about 6.25–6.5 cm².

- 3) A single obstacle in the form of a lying hexagonal prism with location in the center.

The length of the prism is about 2 cm, the maximum width is about 2 mm. It is located at the center of the axis of the water stream flow, at an angle of 45 degrees. Ripples before the obstacle are observed for 2.1–2.6 cm, and after the obstacle – at the length about 3 cm. In contrast to the experiments with cylinders, the area of the perturbation zone makes about 9 cm², which is explained by the greater length of the obstacle.

4) Single obstacle in the form of an inverted spherical segment with a displacement from the center.

The diameter at the base of the inverted ball segment is 0.9 cm. Ripples before the obstacle are observed for 2.5–2.9 cm, and after the obstacle the swirl of the stream is a kind of torch with the area of the disturbance zone about 5 cm², which distinguishes this obstacle from those previously considered.

5) Double obstacle in the form of inverted spherical segments with a displacement from the center.

The pattern of the ripple distribution and turbulence of the flow is almost identical, as in the case of single obstacles in the form of inverted spherical segments. The areas of the perturbation zones are approximately equal and make about 10 cm².

6) Grouped obstacles (Figure 4) in the form of identical polyhedral (screw -nut-type) figures, which are displaced from the axis of the chute.

The maximum obstacle size is 0.8 cm, the height is 0.3 cm, the distance between individual obstacles is about 2 cm. The stream twists have an intense turbulence and are observed from one obstacle to the other in the form of "Karman paths". The area of the disturbance zone is significant and practically covers the entire area of the free surface of the water flow in the chute.

7) Grouped obstacles in the form of identical round (checker-type) figures

The diameter of the obstacle is 0.8 cm, the height is 0.2 cm, the distance between individual obstacles is about 2 cm. Fluctuations of the flow are observed near the axis of the chute in the form of persistent perturbations.

8) Obstacles of different size in the form of round (checker-type) figures in the plan with a strictly perpendicular arrangement as to the axis of the chute.

The diameters of the obstacle are 0.8 and 0.6 cm, the height is 0.2 cm, the distance between individual obstacles is about 2 cm. the swirling of the stream is observed practically over all the entire free surface of the stream.

9) Obstacles of different size in the form of round (checker-type) figures in plan which are positioned at an angle to axis of the chute.

The diameter of the obstacles is 0.8 and 0.6 cm. In this case, a chaotic, practically continuous area of vortices is observed that surrounds the free surface of the water flow in the chute.



Figure 4. Grouped obstacles in the form of identical polyhedral figures displaced from the axis of the chute

4. Discussion

Table 1 (below) presents summary results and interpretation of the vortex formation nature and their geometric parameters, depending on the location of obstacles.

Table 1. Summary results of experiments to determine the nature of the disturbance zones at water flow rates less than 0.4 m/s

Location of obstacles	Vortex formation nature	Averaged geometric dimensions of disturbance zones	
		Lengths before / after obstacles, cm	Areas before / after obstacles, cm ²
1. A single obstacle in the form of a rectangular bar 1 cm long, 0.3 cm wide and 0.2 cm high. Center location at an angle of 45 degrees to the axis of the tray Location with displacement from the center at an angle of 45 degrees to the axis of the chute	Coherent Coherent	1.5 / 2.5 3.0 / 3.0	1.95 / 2.25 6.8 / 2.25
2. A single obstacle in the form of a lying metal cylinder 1 cm long, 1.5 mm in diameter Location with a small displacement from the center Location with a small displacement from the center	Coherent Coherent	1.6 / 1.6 1.6 / 1.6	6.25 / 6.25 6.25 / 6.25
3. A single obstacle in the form of a lying hexagonal prism with the placement in the center 2 cm long, 2 mm wide (at an angle of 45 degrees)	Coherent	2.4 / 3.0	5 / 9
4. Single obstacle in the form of an inverted spherical segment with a diameter of 0.9 cm with a displacement from the center	Coherent	2.8 / 2.5	7 / 5
5. Double obstacle in the form of inverted spherical segments with a displacement from the center	Coherent	2.8 / 2.5	10 / 10
6. Group obstacles in the form of identical polyhedral figures (nuts) displaced from the axis of the trough; the maximum obstacle size is 0.8 cm, the height is 0.3 cm, the distance between individual obstacles is about 2 cm.	Vortex	Vortex path at the whole length	- / 5
7. Grouped obstacles in the form of identical round figures in plan displaced from the axis of the chute; diameter of obstacle 0.8 cm, height 0.2 cm, distance between individual obstacles about 2 cm	Vortex	Vortex path from obstacle to obstacle	- / 3.5
8. Multiple obstacles of different size in the form of round figures in plan with a strictly perpendicular location to the axis of the chute; the diameter of the obstacle is 0.8 and 0.6 cm, the height is 0.2 cm, the distance between individual obstacles is about 2 cm.	Coherent	Vortex path at the whole length along the chute axis	8 / 8
9. Multiple obstacles in the form of round figures in plan located at an angle to the axis of the chute; the diameter of the obstacles is 0.8 and 0.6 cm.	Coherent	Vortex path at the whole length along the chute axis	8 / 8

Based on the results of the analysis of the vortex formation nature behind individual (items 1–5 in Table 1) and grouped obstacles (items 6–9) and the size of the perturbation zones, additional experiments were carried out with 6 variants of grouped obstacles with such geometric distances between them that provide a stable flow turbulence at relatively low water flow rates (within 0.2–0.4 m/s).

The study was performed for configurations of grouped obstacles in the form of rectangular cross section bars with a height of about 2–3 mm and the length of about 2–3 cm, as well as round objects (diameter in plan about 1 cm) located at the chute:

- 1) at an angle of 90 degrees to each other

- 2) crosswise,
- 3) at an angle of more than 90 degrees ("herringbone"),
- 4) at an angle of 120 degrees;
- 5) along the axis of the chute (round obstacles),
- 6) displaced from the axis of the chute (round obstacles).

In Figure 5, as an example, a typical view of one of the investigated variants of the location of obstacles is presented (item e), illustrating the flow turbulence at the water flow rate of 0.4 m/s.



Figure 5 Grouped obstacles in the form of bars of rectangular cross-section, located at an angle of 120 degrees

Below is the interpretation of the results of experiments according to the got photos and film materials.

Variant 1: at the rate of 0.4–0.6 m/s, there is an active disturbance of the flow, thus it can be assumed that the transport capacity of the liquid flow will be increased. At the rate of less than 0.4 m/s, the vortex is weaker, so it can be concluded that this relief of the inner surface of the pipeline will work efficiently at the rates of 0.4–0.6 m/s.

Variant 2: when the rate is less than 0.4 m/s, the formation of vortices is coherent. The active disturbance of the flow began with the rate increase. However, it shall be assumed that the substances precipitating as sediments will not stop in front of the obstacle itself.

Variant 3: the nature of the vortices is stable along the entire flow of the fluid, including in front of the obstacle.

Variant 4: the liquid stagnation is clearly observed when there is a low filling.

Variant 5: at the rate of 0.4 m/s the liquid stagnation is observed in front of the obstacles, so this can entail the accumulation of suspended substances, but after the obstacle in the form of a screw-nut the disturbance of the flow becomes coherent.

Variant 6: the active disturbance of the flow occurs at low rates (0.4 m/s) and remains stable throughout the disposed obstacles even with the rate increase.

For comparison with the results of other authors, other testing benches with similar working models can be mentioned. However, similar experiments with a creation of the micro-turbulence flow with a study of a different type of the obstacles and the interpretation of the vortex formation nature (coherent or vortex) during the transportation of the thin layers of water have been never carried out by other researches.

The closest patent of the known analogs is a device that allows to investigate the hydrophobicity of materials by examining the flow and detachment of droplets from the plane with a change of a slope [23]. This testing bench includes a fixed frame with a movable sliding surface fixed to it, a slope changing system, photo camera for a frontal shooting of drops, dispenser for a dosing of droplets on a surface, which can be one of a various range of materials with hydrophobic properties, and container for droplets collecting.

Also known a device for determining (in the static and dynamic modes) interfacial tension of liquids surface, as well as for determining the angle of wetting of solid surfaces. The device includes an

adjustable surface under the sample, dispensers and video devices for checking the position of droplets and the liquid surface tension [24]. The fundamental difference in this case is the lack of slope changing devices, as well as imperfection of the video units.

5. Conclusions

1. On a special hydraulic bench in the form of an open chute with various surface relief, complex studies were conducted to identify the effect of the micro turbulence.

2. Provision has been made for determination of the parameters describing the nature of the vortices and their dimensions both before and after single, double and grouped obstacles of rectangular, cylindrical, prismatic, spherical and circular shapes with their different locations in relation to the axis of the flow (perpendicular to or at an angle).

3. On the basis of the got results, it was ascertained that practically all obstacles to some extent provoke the micro-turbulence of the flow at flow rates less than self-cleaning ones: there were no obvious advantages of any of the obstacle categories.

4. Based on the experimental data, it is suggested to carry out further experiments on revealing the micro-turbulence effect on the basis of the surface relief in the form of grouped obstacles of a rectangular shape, which are located at an angle to the axis of the chute on both sides of it and a free cross-section about 0.2 cm along the axis of the chute.

5. In future, the experiments are planned to be performed for studying the transfer of the sand particles in order to identify the optimal surface relief for the effective movement of suspended solids by the flow of water at low flow rates.

References

1. Orlov V.A., Dezhina I.S., Pelipenko A.A., Orlov E.V. Ispytatelnyy stand po issledovaniyu turbulentnosti i transportiruyushoi sposobnosti potoka zhidkosti opticheskimi sredstvami v otkrytykh lotkakh pri razlichnom relefe ih vnutrenney poverhnosti [Testing stand for investigation of turbulence and carrying capacity of flow of fluid by optical means in open pipe at different topography of their internal surfaces]. *Utility model patent Russia no. 176330*. (rus).
2. Ariaratnam S.T., Sihabuddin S. Comparison of emitted emissions between trenchless pipe replacement and open cut utility construction. *Journal of Green Building*. 2009. Vol. 4. No. 2. Pp. 126–140.
3. Manneville P. Transition to turbulence in wall-bounded flows: Where do we stand? *Mechanical Engineering Reviews* 3.2. 2016. 15-00684.
4. Barkley D. Theoretical perspective on the route to turbulence in a pipe. *Journal of Fluid Mechanics*. 2016. Vol. 803.
5. Song B., Barkley D., Hof B., Avila M. Speed and structure of turbulent fronts in pipe flow. *Journal of Fluid Mechanics*. 2017. Vol. 813. Pp. 1045–1059.
6. Girgidov A.D. Changing of energy dissipation in the transition of laminar flow to turbulence. *Magazine of Civil Engineering*. 2011. No. 5. Pp. 49–52. (rus)
7. Geem Z.W. Particle-swarm harmony search for water network design. *Engineering Optimization*. 2009. Vol. 41(4). Pp. 297–311.
8. Feldman M. Aspects of energy efficiency in water supply systems. *Proceedings of the 5th IWA water loss reduction specialist conference*. South Africa. 2009. Pp. 85–89.
9. Coelho B., Andrade A. Campos Efficiency achievement in water supply systems—A review. *Renewable and Sustainable Energy Reviews*. 2014. Vol. 30. Pp. 59–84.
10. Kuliczowski A., Kuliczowska E., Zwierzchowska A. *Technologie beswykopowe w inzynierii srodowiska*. Wydawnictwo Seidel-Przywecki Sp, 2010. 735 p.
11. Bryanskaya Y.V. Utochneniye kinematicheskikh kharakteristik turbulentnogo techeniya [Refinement of turbulent flow velocity characteristics]. *Magazine of Civil Engineering*. 2013. No. 6(41). Pp. 31–38

Литература

1. Патент РФ № 176330 на полезную модель. Испытательный стенд по исследованию турбулентности и транспортирующей способности потока жидкости оптическими средствами в открытых лотках при различном рельефе их внутренней поверхности / Орлов В.А., Дежина И.С., Пелипенко А.А., Орлов Е.В.
2. Ariaratnam S.T., Sihabuddin S. Comparison of emitted emissions between trenchless pipe replacement and open cut utility construction // *Journal of Green Building*. 2009. Vol. 4. No. 2. College Publishing. Pp. 126–140.
3. Manneville P. Transition to turbulence in wall-bounded flows: Where do we stand? // *Mechanical Engineering Reviews* 3.2. 2016. № 15-00684.
4. Barkley D. Theoretical perspective on the route to turbulence in a pipe // *Journal of Fluid Mechanics*. 2016. Vol. 803.
5. Song B., Barkley D., Hof B., Avila M. Speed and structure of turbulent fronts in pipe flow // *Journal of Fluid Mechanics*. 2017. Vol. 813. Pp. 1045–1059.
6. Гиргидов А.Д. Изменение диссипации энергии при переходе от ламинарного режима к турбулентному // *Инженерно-строительный журнал*. 2011. № 5(23). С. 49–52.
7. Geem Z.W. Particle-swarm harmony search for water network design // *Engineering Optimization*. 2009. Vol. 41(4). Pp. 297–311.
8. Feldman M. Aspects of energy efficiency in water supply systems // *Proceedings of the 5th IWA water loss reduction specialist conference*. South Africa. 2009. Pp. 85–89.
9. Coelho B., Andrade A. Campos Efficiency achievement in water supply systems—A review // *Renewable and Sustainable Energy Reviews*. 2014. Vol. 30. Pp. 59–84.
10. Kuliczowski A., Kuliczowska E., Zwierzchowska A. *Technologie beswykopowe w inzynierii srodowiska*. Wydawnictwo Seidel-Przywecki Sp, 2010. 735 p.
11. Брянская Ю.В. Уточнение кинематических характеристик турбулентного течения // *Инженерно-строительный журнал*. 2013. № 6(41). С. 31–38.
12. Niu S., Li B., Mu Z., Yang M., Zhang J., Han Z., Ren L.

Orlov V.A., Dezhina I.S., Orlov E.V. Micro-turbulence of the stream and its connection with the roughness of the pipeline inner surface. *Magazine of Civil Engineering*. 2018. No. 3. Pp. 27–35. doi: 10.18720/MCE.79.3.

12. Niu S., Li B., Mu Z., Yang M., Zhang J., Han Z., Ren L. Excellent structure-based multifunction of Morpho butterfly wings: a review. *Journal of Bionic Engineering*. 2015. Vol. 12(2). Pp. 170–189.
13. Dorrer C., Ruhe J. Condensation and wetting transitions on microstructured ultrahydrophobic surfaces. *Langmuir*. 2007. No. 23, Pp. 3820–3824.
14. Wang G., Guo Z., Liu W. Interfacial effects of superhydrophobic plant surfaces: a review. *Journal of Bionic Engineering*. 2014. Vol. 11(3). Pp. 325–345.
15. Yang Z.L., Ladam Y., Laux H., Danielson T.J., Leporcher E. Dynamic simulation of sand transport in a pipeline. *5th North American Conference on Multiphase Technology*. 2006.
16. Orlov V.A., Dezhina I.S., Orlov E.V., Averkeev I.A. Испытательный стенд по определению степени гидрофобности материалов для изготовления труб и ремонта трубопроводов [Testing stand for determine the hydrophobic properties of materials, used for a pipelines fabrication]. *Utility model patent Russia no. 157695*. 2015. (rus).
17. Boynovich L.B., Emelyanenko A.M. Hydrofobnye materialy i pokrytia: principy sozdania, svoystva i primeneniye [Hydrophobic materials, creation, properties and usability]. *Uspekhi khimii*. 2008. No. 77(7). Pp. 621–638. (rus).
18. Abel T. Laboratory tests of pipelines reinforced with close-fit Trolining liner. *Archives of Civil and Mechanical Engineering*. 2015. Vol. 15(2). Pp. 427–435.
19. Rabmer-Koller U. No-dig technologies – innovative solution for efficient and fast pipe rehabilitation. *29 NO-DIG International Conference and Exhibition*. NO-DIG Berlin, 2011. Paper 2C-1. Pp. 1–10.
20. Grossmann S., Lohse D. Curvature effects on the velocity profile in turbulent pipe flow. *Eur. Phys. J. E*. 2017. No. 40. Pp. 16–19.
21. Orlov V.A., Zotkin S.P., Dezhina I.S., Zotkina I.P. Calculation of the hydraulic characteristics of the protective coating used in trenchless technologies for the construction and renovation of pipelines to extend their service life. *MATEC Web of Conferences*. 2017. Vol. 117. 00185.
22. Scholtmeijer K., Janssen, M.I., Gerssen B., de Vocht M.L., van Leeuwen B.M., van Kooten T.G., Wosten H.A.B., Wessels J.G.H. Surface Modifications Created by Using Engineered Hydrophobins. *Appl. Environ. Microbiol.* 2002. Vol. 68(3). 1367.
23. Sikarwar B., Khandekar S., Muralidhar K. Coalescence of pendant droplets on an inclined super-hydrophobic substrate. *7th International Symposium on Multiphase Flow. Heat Mass Transfer and Conversion*. Xi, an. China, 2012. Paper № MF-38. Pp. 1–7.
24. Boynovich L.B., Emelyanenko A.M. Portativnoe ustroystvo dlya izmereniya uglov smachivaniya poverhnostey i poverhnostnogo natyazheniya zhidkostey [A portative device for measuring the wetting angles of the surface and tension of the liquids]. *Utility model patent Russia no. 92860 IPC S08J 7/00*. (rus).
- Excellent structure-based multifunction of Morpho butterfly wings: a review // *Journal of Bionic Engineering*. 2015. Vol. 12(2). Pp. 170–189.
13. Dorrer C., Ruhe J., Condensation and Wetting Transitions on Microstructured Ultrahydrophobic Surfaces // *Langmuir*. 2007. Vol. 23(1). Pp. 3820–3824.
14. Wang G., Guo Z., Liu W. Interfacial effects of superhydrophobic plant surfaces: a review // *Journal of Bionic Engineering*. 2014. Vol. 11(3). Pp. 325–345.
15. Yang Z.L., Ladam Y., Laux H., Danielson T.J., Leporcher E. Dynamic simulation of sand transport in a pipeline // *5th North American Conference on Multiphase Technology*. 2006.
16. Патент на полезную модель РФ № 157695. Испытательный стенд по определению степени гидрофобности материалов для изготовления труб и ремонта трубопроводов / Орлов В.А., Дежина И.С., Орлов Е.В., Аверкеев И.А.
17. Бойнович Л.Б., Емельяненко А.М. Гидрофобные материалы и покрытия: принципы создания, свойства и применение // *Успехи химии*. 2008. № 77(7). С. 621–638.
18. Abel T. Laboratory tests of pipelines reinforced with close-fit Trolining liner // *Archives of Civil and Mechanical Engineering*. 2015. Vol. 15(2). Pp. 427–435.
19. Rabmer-Koller U. No-dig technologies – innovative solution for efficient and fast pipe rehabilitation // *29 NO-DIG International Conference and Exhibition*. NO-DIG Berlin 2011. Paper 2C-1. 2011. Pp. 1–10.
20. Grossmann S., Lohse D. Curvature effects on the velocity profile in turbulent pipe flow // *Eur. Phys. J. E*. 2017. № 40. Pp. 16–19.
21. Orlov V.A., Zotkin S.P., Dezhina I.S., Zotkina I.P. Calculation of the hydraulic characteristics of the protective coating used in trenchless technologies for the construction and renovation of pipelines to extend their service life // *MATEC Web of Conferences*. 2017. Vol. 117. 00185.
22. Scholtmeijer K., Janssen, M.I., Gerssen B., de Vocht M.L., van Leeuwen B.M., van Kooten T.G., Wosten H.A.B., Wessels J.G.H. Surface Modifications Created by Using Engineered Hydrophobins // *Appl. Environ. Microbiol.* 2002. Vol. 68(3). 1367.
23. Sikarwar B., Khandekar S., Muralidhar K. Coalescence of pendant droplets on an inclined super-hydrophobic substrate // *7th International Symposium on Multiphase Flow. Heat Mass Transfer and Conversion*. Xi, an. China, 2012. Paper № MF-38. Pp. 1–7.
24. Патент РФ № 92860 на полезную модель МПК С08J 7/00. Портативное устройство для измерения углов смачивания поверхностей и поверхностного натяжения жидкостей // Бойнович Л.Б., Емельяненко А.М.

Vladimir Orlov,
8-917-538-43-16; orlov950@yandex.ru

Irina Dezhina,
8-905-562-43-55; dejina07@mail.ru

Evgeniy Orlov,
8-965-326-80-21; jeks-2003@yandex.ru

Владимир Александрович Орлов,
8-917-538-43-16; эл. почта: orlov950@yandex.ru

Ирина Сергеевна Дежина,
8-905-562-43-55; эл. почта: dejina07@mail.ru

Евгений Владимирович Орлов,
8-965-326-80-21;
эл. почта: jeks-2003@yandex.ru

© Orlov V.A., Dezhina I.S., Orlov E.V., 2018

doi: 10.18720/MCE.79.4

Strength of composite steel and concrete beams of high-performance concrete

Прочность железобетонных балок с жесткой арматурой из высокопрочного бетона

V.I. Travush,
GORPROJECT, Moscow, Russia

D.V. Konin,

A.S. Krylov,

JSC Research Center of Construction, Moscow,
Russia

**Д-р техн. наук, профессор главный
конструктор, заместитель
генерального директора по научной
работе В.И. Травуш,
ЗАО «ГОРПРОЕКТ», г. Москва, Россия
канд. техн. наук, заведующий сектором
Д.В. Конин,
научный сотрудник А.С. Крылов,
АО «Научно-исследовательский центр
«Строительство», г. Москва, Россия**

Key words: reinforced concrete; composite steel and concrete structures; crack width; stresses; strain; standard-based calculation; crack resistance; numerical simulation; verification

Ключевые слова: сталежелезобетон; жесткая арматура; ширина раскрытия трещин; напряжения; относительные деформации; расчет по нормам; трещиностойкость; численное моделирование; верификация

Abstract. A brief review of the use of high-performance concrete in monolithic structures in Russia in recent years is made; the last experimental work for the study of high-performance concrete in composite steel and concrete structures is observed. Strength assessment of composite steel and concrete beams has been carried out by a pure-bending test. The models destruction pattern has been described. Vertical displacement and crack width measurement results have been conducted; comparison with the standardized values has been carried out. The models steel core and concrete stress-strain diagrams have been presented, their features have been pointed out. The existing methods of calculating composite steel and concrete structures have been estimated by the ultimate and service limit state. The results necessary to carry out numerical studies in the sphere of contact interaction have been obtained.

Аннотация. Выполнен краткий обзор применения высокопрочных бетонов в монолитном строительстве в РФ за последние годы; отмечены последние экспериментальные работы по изучению особенностей высокопрочных бетонов в составе комбинированных конструкций. Выполнена оценка прочности сталежелезобетонных балок из высокопрочных бетонов при испытании на чистый изгиб. Описан характер разрушения моделей. Приведены результаты измерений вертикальных перемещений и ширины раскрытия трещин; выполнено сравнение с нормируемыми величинами. Представлены графики напряжений и деформаций в стальном сердечнике и бетоне моделей, отмечены их особенности. Дана оценка существующих методик расчета изгибаемых сталежелезобетонных конструкций по первой и второй группе предельных состояний. Получены необходимые результаты для проведения численных исследований в области контактного взаимодействия.

1. Introduction

Against the background of the rapid development of the construction industry, increasing pace of construction, increasing buildings height, the need for new load-bearing structures materials and their production technologies has arisen. Most of the existing site-cast concrete buildings are made of compression breaking strength class concrete B25...B30. However, there is a tendency in these days to increase the strength class of concrete used especially for high-rise and long-span construction (for example, concrete of B40...B90 compression breaking strength class is used for the buildings of the City

of Moscow [1]). At the moment technologies of B80...B100 compression breaking strength class concrete mixture industrial scale production have been developed and successfully tested.

Currently a number of experimental works devoted to studying of composite steel and concrete structures made of high-performance concrete under eccentric compression has been carried out [2, 3]; specific features of the "steel-concrete" contact surface operation [4] have been studied. Use of high-performance concrete in bending structures, especially in a composite cross-section, has not been adequately studied. This shows the actuality of the issues under consideration and of the tests conducted. A series of experiments has been prepared and carried out in order to study the stress-strain state of composite steel and concrete beams. In preparation for the experiment, publications on the improvement of the theoretical foundations of reinforced concrete structures [5–9] and fiber-reinforced concrete [10, 11] were studied. Special attention was paid to research in the field of contact interaction of steel and concrete [12–15], including numerical investigations [16–18]. Issues of numerical modeling of reinforced concrete structures [19] and cracking [20–23] were considered. Examples of the use of high-performance concrete is considered [24, 25].

The aim of the study is to obtain experimental data that will form a basis for numerical studies using of ANSYS models in strength calculation and in contact interaction tasks.

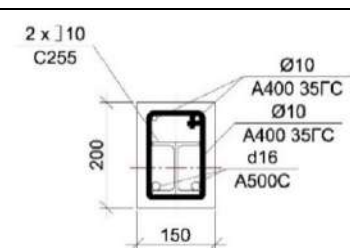
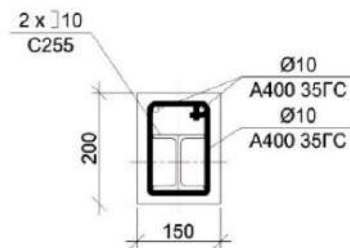
Objectives of the study:

- perform tests of 9 models of beams made of high-performance concrete;
- to evaluate the existing methods of calculation of reinforced concrete structures at the ultimate limit state (ULS) and the service limit state (SLS) for high-performance concrete;
- to identify the characteristics of fracture, the nature of the formation and cracks propagation;
- to assess the stress-strain state of the models.

The results of this experiment will be used as the basis for numerical studies of composite steel and concrete beams in a nonlinear setting contact interaction simulation. The obtained experimental data are the necessary stage of work for further verification of calculation methods.

Within the research 9 models of composite steel and concrete beams with rectangular cross-section 200 x 150 mm and a length 1.5 m have been tested. A detailed description of the models is stated in paper [26]. The models characteristics (cross-section type, construction materials) are stated in Table 1.

Table 1. The Models Characteristics

Group of models	Number of models in the group	Concrete compression breaking strength class	μ , % reinforcement ratio	Cross-section
1 (B4)	3	B90	9.13	 <p>Figure 1. Cross-section for models group 1,2</p>
2 (B5)	3	B75	9.13	
3 (B6)	3	B90	7.79	 <p>Figure 2. Cross-section for models group 3</p>

2. Methods

Preparation of the beams models for the experiment has been carried out in the following sequence: steel cores have been manufactured and frame reinforcement has been tied (Figure 3); resistive-strain sensors have been installed on the pretreated steel surface and protected by epoxy resin (Figure 4); concrete has been poured and resistive-strain sensors have been attached to the concrete surface. The sensors location schemes are shown in Figure 5.

All models have been tested in pure-bending test (Figure 6). Models supports were hinge. Uniform distribution of forces between two points was ensured by steel I-shaped cross arm mounted on the rollers, transferring the load to the beam through steel plates (Figure 7).



Figure 3. Frame reinforcement tying



Figure 4. Cleaning of resistive-strain sensors installation places; fixing wires and measuring points protection with epoxy resin

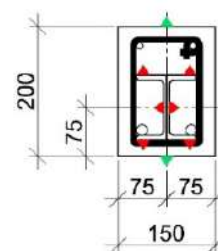


Figure 5a. Diagram of resistive-strain sensors installation on group 1, 2 model

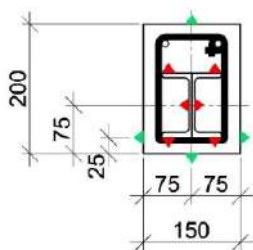


Figure 5b. Diagram of resistive-strain sensors installation on group 3 model

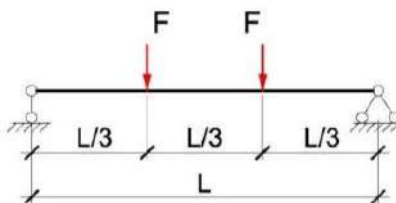


Figure 6. Diagram of load application to the models



Figure 7. Diagram of load transfer to the models

3. Results and Discussion

In order to determine strength properties of concrete 3 test cubes with 10 cm side were prepared for each group of models. The cubes according with Russian State Standard GOST 10180-90 "Concretes. Methods for determining the strength of control samples" test results are stated in Table 2.

Table 2. Test results of the test cubes

Group of models	Concrete cube crushing strength at the age of 28 days, MPa	Concrete cube crushing strength during beams model testing, MPa
1 (B4)	105.3	115.7
2 (B5)	86.7	96.4
3 (B6)	103.8	117.5

All models have been tested in accordance with the provisions of Russian State Standard GOST 8829-94 "Product construction of concrete and reinforced concrete prefabrication. Test methods the loading. Rules for the evaluation of strength, stiffness and crack resistance". The sequence of the operations performed is described in paper [26].

Before the tests, theoretical calculations was carried out: the ultimate bending moment values were calculated that can be perceived by the models according to Construction Rules SP 266.1325800.2016

Травуш В.И., Конин Д.В., Крылов А.С. Прочность железобетонных балок с жесткой арматурой из высокопрочного бетона // Инженерно-строительный журнал. 2018. № 3(79). С. 36–44.

“Composite steel and concrete structures. Design rules” in accordance with the formulas (6.52), (6.53). The actual concrete strength were used in the calculations. Theoretical calculation results and experimental ultimate moments are stated in Table 3.

Table 3. Ultimate bending moment

Group of models	$M_{theor}^{ultimate}$, kNm	$M_{experimental}^{ultimate}$ (average for models group), kNm	Average deviation for models group, %
1 (B4)	91.89	90.94	-1.0
2 (B5)	86.62	88.66	2.3
3 (B6)	71.02	77.03	7.8

Table 3 shows that theoretical calculations have a fairly good convergence with the test results (the maximum deviation is 7.8 %), which indicates the possibility to apply for the high-performance concrete the approach stated in Russian Construction Rules SP 266.1325800.2016 “Composite steel and concrete structures. Design rules”.

In the course of the experiment, the crack width and crack propagation mode were registered. The crack width (experimental and theoretical) and the loads under which it has been tested are shown in Table 4.

According to the Manual for design of reinforced concrete structures with rigid reinforcement [27], calculations of crack formation normal to the longitudinal axis of the bending elements are made on the following condition:

$$M \leq M_T \quad (1)$$

where M_T is the moment perceived by the cross-section normal to the element's longitudinal axis during cracks formation.

The theoretical crack width normal to the longitudinal axis of the bending element is determined according to empirical formula (43) [27]:

$$a_{crc} = c_l \frac{\sigma_a}{E_a} 25(3.5 - 100\mu) \sqrt[3]{d_{red}} \quad (2)$$

where c_l is the coefficient depending from the duration of load application, $c_l = 1.5$;

σ_a is the stress in the bars of the edge tensioned reinforcement;

E_a is the reinforcement steel elasticity modulus;

μ is the cross-section reinforcement ratio equals to the ration between the area of the entire tensioned reinforcement to concrete area, but not more than 0.02;

d_{red} is the equivalent diameter of steel core and beam reinforcement located in the tensioned cross-section area.

Table 4. Crack width

Group of models	Test load, kN	Crack Width, $m \times 10^{-3}$		Deviation, %
		Theoretical in accordance with [27]	Experimental *	
1 (B4)	248.29	0.229	0.283	19.2
2 (B5)	242.06	0.224	0.230	2.6
3 (B6)	211.45	0.231	0.344	32.8

The values given in Table 4 (both theoretical and experimental) do not exceed the maximum allowable crack width from the condition of the reinforcement safety $a_{crc,ult} = 0.4 \text{ mm}$ as specified in Russian Construction Rules SP 63.13330.2012 “Concrete and reinforced concrete structures” with short-term crack opening. However, significant deviations between the theoretical values obtained according to [27] and the actual crack width have been found out. The difference in values is up to 33 %, which indicates the necessity to make changes in the methodology used to calculate the crack resistance set forth in the Manual [27].

Destruction of all model groups was similar and was characterized by the appearance of a large number of vertical and inclined cracks as well as horizontal cracks along the upper and lower sides of the beam, which led to partial spall of the protective layer concrete and exposure of the reinforcement cage and steel cores fragments in the extreme thirds of the beam – between the bearing point and the load application point at the last stages (Figure 8). Crack formation due to the high-performance concrete fragility began at the early stages of loading. Thin cracks (visible without optical instruments) were noted at the first loading stage for almost all models (the first loading stage corresponded to less than 10 % of the ultimate breaking load).



Figure 8. Representative beam destruction

Based on the test results, graphs of the models vertical displacements under load (Figure 9) and diagrams illustrating the crack width at each loading stage (Figure 10) have been made.

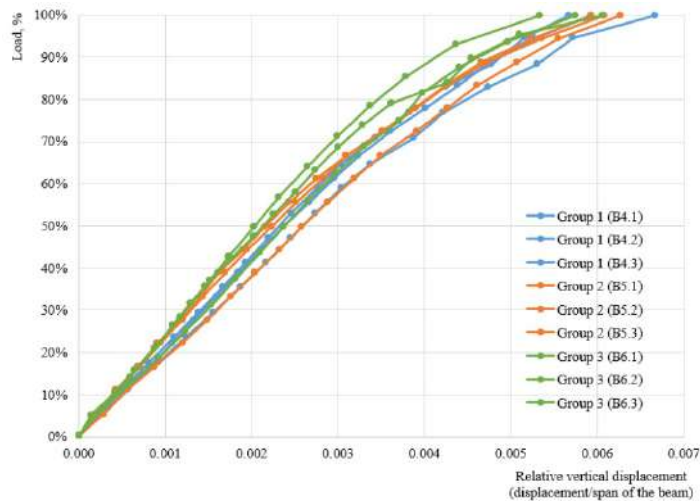


Figure 9. Vertical models displacements by loading steps

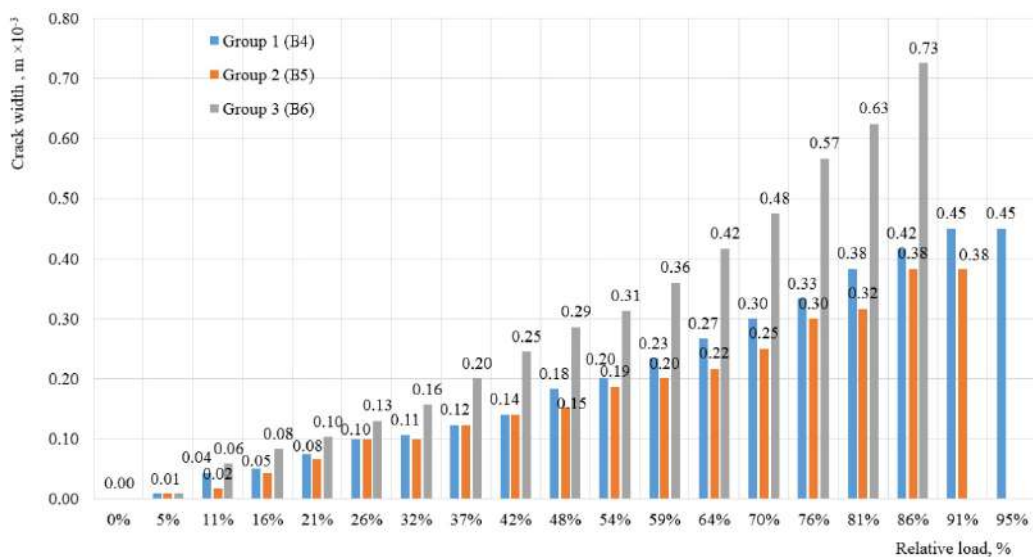


Figure 10. Crack width in the models by loading steps

In general, vertical displacements of all models before destruction do not exceed 9 mm, which is 1/155 of the beam span value (according to the test diagram). Herewith, the maximum crack width for groups 1, 2, 3 was 0.47 mm, 0.40 mm and 0.68 mm respectively. The greatest crack width was registered for the beams with a smaller reinforcement percentage (group 3 (B6)).

As a result of the resistive-strain sensors readings processing stress and strain diagrams for the concrete and steel parts of the models were made. The graphs are of similar nature for different groups of models. Figures 11–14 show the dependencies for models group 1.

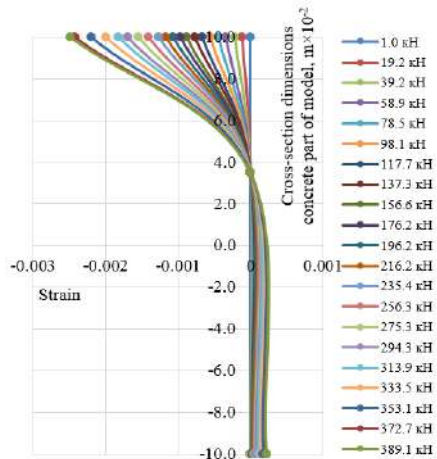


Figure 11. Strains in the concrete part of model by loading steps

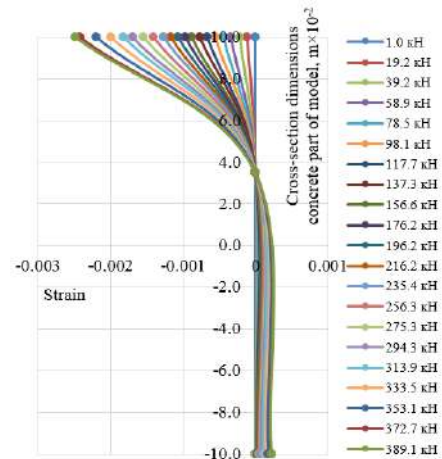


Figure 12. Strains in the rigid reinforcement of model by loading steps

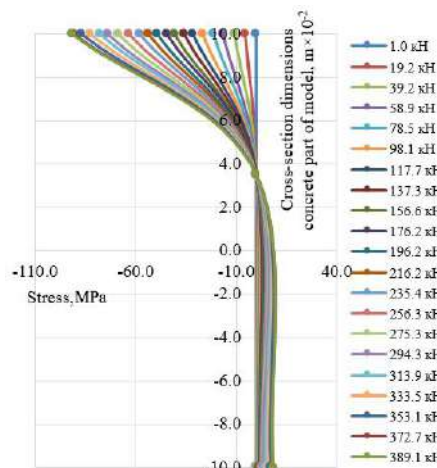


Figure 13. Stress in the concrete part of model by loading steps

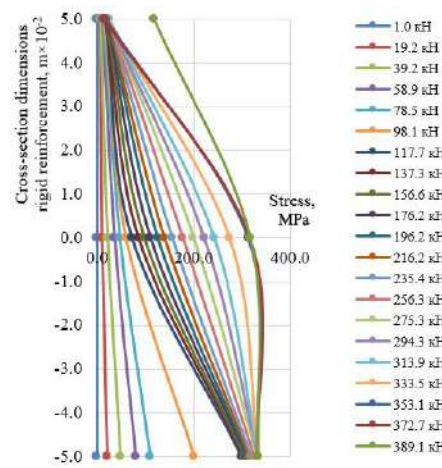


Figure 14. Stress in the rigid reinforcement of model by loading steps

The cross-section neutral axis near the top flanges of the U-profiles can be traced clearly in the graphs. The plane section hypothesis is observed up to the total load on the model of 235 kN (Figure 14), 203 kN and 213 kN, which constitutes 60 %, 53 % and 64 % of the ultimate breaking load for groups 1, 2 and 3 respectively. Apparently, further loading caused the influence of the progressive cracks.

Detailed studies of the characteristics of the high-performance concrete used are given in [28], where the ultimate unit strains (the maximum strains at the moment before the test sample destruction during bending tests) of the compressed concrete are fixed at 0.00254 value. The experimental values of the unit compression strains before destruction of individual models obtained within the framework of the present study made up 0.002975, which is 17 % higher than the values given in [27], but almost completely coincides with the values in Russian Construction Rules SP 63.13330.2012 "Concrete and reinforced concrete structures". This result is probably achieved due to the fact that concrete works as part of a composite construction. The excess ultimate tensile strains (obtained experimentally) have been noted as compared with Russian Construction Rules SP 63.13330.2012. This can be explained by the formation and opening of a large number of cracks in the tensioned part of the cross-section, some of which fell within the resistive-strain sensor gauge length, which increased its readings. Comparison of the obtained unit

strain values at the time of the models destruction and the values indicated in [28] and Construction Rules SP 63.13330.2012 is given in Table 5.

Table 5. Ultimate strains of concrete models

Group of models	Experiment		Construction Rules SP 63.13330.2012		According to [28]		Eurocode 2	Average deviation from SP 63.13330.2012, %	Average deviation from [28], %
	Compression	Tension	Compression	Tension	Compression	Tension		Compression	Compression
1 (B4)	0.00249	0.00022	0.00297	0.00015	0.00254	0.00048	0.0026	19.5	5.9
	0.00234	0.00381							
	0.00234	0.00381							
2 (B5)	0.00274	0.00025	0.00322	0.00015	0.00254	0.00048	0.0026	14.7	-8.2
	0.00285	0.00381							
	0.00266	0.00028							
3 (B6)	0.00290	0.00381	0.00297	0.00015	0.00254	0.00048	0.0026	4.3	-11.9
	0.00298	0.00381							
	0.00265	0.00036							

4. Conclusions

1. A set of works of composite steel and concrete structures models bending test has been carried out. Nine models made of high-performance concrete of B75 ... B90 compression breaking strength class have been tested.

2. Behavior of composite steel and concrete structures with the use of high-performance concrete in the calculations for the ultimate limit state (ULS) is well described by the calculation methods presented in Russian Construction Rules SP 266.1325800.2016 "Composite steel and concrete structures. Design rules" – deviation between the theoretical and experimental values does not exceed 8%.

3. The results of the calculations performed for the service limit state (SLS) according with "Manual for design of steel and concrete structures" have significant deviations from the experimental data. The formulas given in Manual for determining crack width give the erroneously low result in relation to the experimental data. The difference in values is up to 33%, which indicates the necessity to make changes in the methodology used to calculate the crack resistance set forth in Manual.

4. The process of destruction of all tested models was similar and characterized by abundant crack formation (vertical and inclined cracks along the lateral sides of the models and horizontal ones along the lower and upper sides). Cracks were formed at the early stages of loading, which confirms high-performance concrete fragility. Thin cracks have been noted at the first loading stage (less than 10% of the ultimate breaking load) for almost all models.

5. In general, the measured strains of the compressed concrete part of the cross-section before destruction do not exceed the limit values given in design rules Construction Rules SP 63.13330.2012 "Concrete and reinforced concrete structures", but are somewhat overestimated as compared with the experimental data given in scientific work Romkin D.S. "The Influence of age high-strength concrete on the physical, mechanical and rheological properties" and the data given in the Eurocode 2. Such a discrepancy (up to 17 %) was probably due to the casing effect achieved by composite cross-section formation from rigid reinforcement, clamps and longitudinal reinforcement bars.

6. The measured strains of the tensioned concrete part of the cross-section before destruction significantly exceed the corresponding values regulated by Russian Construction Rules SP 63.13330.2012 "Concrete and reinforced concrete structures". This can be explained by the formation and opening of a large number of cracks in the tensioned part of the cross-section, some of which fell within the resistive-strain sensor gauge length, which increased its readings.

7. It can be concluded from the strain graphs that the plane section hypothesis is observed to a value that constitutes on the average 60 % of the ultimate load.

8. The analysis of the model's displacements under load and cracks opening by loading stages demonstrated absence of abrupt changes and drops (even at the moment before destruction), which is

Травуш В.И., Конин Д.В., Крылов А.С. Прочность железобетонных балок с жесткой арматурой из высокопрочного бетона // Инженерно-строительный журнал. 2018. № 3(79). С. 36–44.

illustrative of smooth development of plastic strains and cracks. The composite steel and concrete cross-section destruction is not sudden, which is of great importance for design of real structures of buildings and constructions including unique ones, where brittle destruction prevention is required and stricter requirements are applied to the structures reliability.

References

1. Kapriyev S.S., Travush V.I., Sheynfeld A.V., Karpenko N.I., Kardumyan G.S., Kiseleva Yu.A., Prigozhenko O.V. Modifitsirovannyye betony novogo pokoleniya v sooruzheniyakh MMDЦ «Moskva-Siti». [Modified concretes of new generation in the construction of MIBC "Moscow-city"]. *Building materials*. 2006. No. 10. Pp. 8–12. (rus)
2. Travush V.I., Konin D.V., Rozhkova L.S., Krylov A.S., Kapriyev S.S., Chilin I.A., Martirosyan A.S., Fimkin A.I. Eksperimentalnyye issledovaniya stalezhelezobetonnykh konstruktсий, rabotayushchikh na vnetsentrennoye szhatiye [Experimental study of composite structures, working for eccentric compression]. *Academia. Architecture and Construction*. 2016. No. 3. Pp. 127–135. (rus)
3. Travush V.I., Konin D.V., Rozhkova L.S., Krylov A.S. Otechestvennyy i zarubezhnyy opyt issledovaniy raboty stalezhelezobetonnykh konstruktсий na vnetsentrennoye szhatiye [Domestic and foreign experience in research of composite structures for eccentric compression]. *Building and Reconstruction*. 2016. No. 5(67). Pp. 31–44. (rus)
4. Travush V.I., Kapriyev S.S., Konin D.V., Krylov A.S., Kashevarova G.G., Chilin I.A. Opredeleniye nesushchey sposobnosti na sdvig kontaktnoy poverkhnosti «stal-beton» v stalezhelezobetonnykh konstruktсийakh dlya betonov razlichnoy prochnosti na szhatiye i fibrobetona [Determination of the bearing capacity in shear on the contact surface "steel-concrete" of steel-concrete structures for concretes of different compressive strength and fiber reinforced concrete]. *Building and Reconstruction*. 2016. No. 4(66). Pp. 45–55. (rus)
5. Krylov S.B., Arlenin P.D. Inzhenernyy podkhod k resheniyu zadachi ob izgibe uprugopolzuchego sterzhnya [The engineering approach to solving the problem of bending of elastic-creeping rod]. *Structural Mechanics and Analysis of Constructions*. 2013. No. 2(247). Pp. 6–9. (rus)
6. Krylov S.B., Arlenin P.D. Uravneniye izgiba sterzhnya pri kusochno-lineynom zakone deformirovaniya polzuchego materiala [The equation of bending of a rod with a piecewise-linear law of deformation of the creeping material]. *Structural Mechanics and Analysis of Constructions*. 2013. No. 3(248). Pp. 9–11. (rus)
7. Lubliner J., Oliver J., Oller S., Onate E. A. Plastic-damage model for concrete. *International Journal of Solids and Structures*. 1989. Vol. 25. No. 3. Pp. 229–326.
8. Mazars J. A description of micro- and macro-scale damage of concrete structures. *Engineering Fracture Mechanics*. 1986. Vol. 25. No. 5/6. Pp. 729–737.
9. Willam K.J., Warnke E.D. Constitutive model for the triaxial behavior of concrete. *Proceedings, International Association for Bridge and Structural Engineering*. Zurich, 1975. Report 19. Section III. 30 p.
10. Gribniak V., Kaklauskas G., Hung Kwan A.K., Bacinskis D., Ulbinas D. Deriving stress-strain relationships for steel fibre concrete in tension from tests of beams with ordinary reinforcement. *Engineering Structures*. 2012. Vol. 42. Pp. 387–395.
11. Yuguang Y., Walraven J.C., den Uijl J.A. Combined effect of fibers and steel rebars in high performance concrete. *Heron*. 2009. Vol. 54. No. 2/3. Pp. 205–221.
12. Torre-Casanova A., Jason L., Davenne L., Pinelli X. Confinement effects on the steel-concrete bond strength and pull-out failure. *Engineering Fracture Mechanics*. 2013. Vol. 97. Pp. 92–104.
13. Shima H., Chou L.-L., Okamura H. Micro and Macro models for bond in reinforced concrete. *Journal of the Faculty of Engineering: University of Tokyo*. 1987. Vol. XXXIX. No. 2. Pp. 133–194.

Литература

1. Каприелов С.С., Травуш В.И., Шейнфельд А.В., Карпенко Н.И., Кардумян Г.С., Киселева Ю.А., Пригоженко О.В. Модифицированные бетоны нового поколения в сооружениях ММДЦ «Москва-Сити» // *Строительные материалы*. 2006. № 10. С. 8–12.
2. Травуш В.И., Конин Д.В., Рожкова Л.С., Крылов А.С., Каприелов С.С., Чилин И.А., Мартиросян А.С., Фимкин А.И. Экспериментальные исследования сталежелезобетонных конструкций, работающих на внецентренное сжатие // *Academia. Архитектура и строительство*. 2016. № 3. С. 127–135.
3. Травуш В.И., Конин Д.В., Рожкова Л.С., Крылов А.С. Отечественный и зарубежный опыт исследований работы сталежелезобетонных конструкций на внецентренное сжатие // *Строительство и реконструкция*. 2016. № 5(67). С. 31–44.
4. Травуш В.И., Каприелов С.С., Конин Д.В., Крылов А.С., Кашеварова Г.Г., Чилин И.А. Определение несущей способности на сдвиг контактной поверхности «сталь-бетон» в сталежелезобетонных конструкциях для бетонов различной прочности на сжатие и фибробетона // *Строительство и реконструкция*. 2016. № 4(66). С. 45–55.
5. Крылов С.Б., Арленинов П.Д. Инженерный подход к решению задачи об изгибе упруго-ползучего стержня // *Строительная механика и расчет сооружений*. 2013. № 2(247). С. 6–9.
6. Крылов С.Б., Арленинов П.Д. Уравнение изгиба стержня при кусочно-линейном законе деформирования ползучего материала // *Строительная механика и расчет сооружений*. 2013. № 3(248). С. 9–11.
7. Lubliner J., Oliver J., Oller S., Onate E.A. Plastic-damage model for concrete // *International Journal of Solids and Structures*. 1989. Vol. 25. No. 3. Pp. 229–326.
8. Mazars J. A description of micro- and macro-scale damage of concrete structures // *Engineering Fracture Mechanics*. 1986. Vol. 25. No. 5/6. Pp. 729–737.
9. Willam K.J., Warnke E.D. Constitutive model for the triaxial behavior of concrete // *Proceedings, International Association for Bridge and Structural Engineering*. Zurich, 1975. Report 19. Section III. 30 p.
10. Gribniak V., Kaklauskas G., Hung Kwan A.K., Bacinskis D., Ulbinas D. Deriving stress-strain relationships for steel fibre concrete in tension from tests of beams with ordinary reinforcement // *Engineering Structures*. 2012. Vol. 42. Pp. 387–395.
11. Yuguang Y., Walraven J.C., den Uijl J.A. Combined effect of fibers and steel rebars in high performance concrete // *Heron*. 2009. Vol. 54. No. 2/3. Pp. 205–221.
12. Torre-Casanova A., Jason L., Davenne L., Pinelli X. Confinement effects on the steel-concrete bond strength and pull-out failure // *Engineering Fracture Mechanics*. 2013. Vol. 97. Pp. 92–104.
13. Shima H., Chou L.-L., Okamura H. Micro and Macro models for bond in reinforced concrete // *Journal of the Faculty of Engineering: University of Tokyo*. 1987. Vol. XXXIX. No. 2. Pp. 133–194.

14. Smith F., Brown R. The Shearing Strength of Concrete. *Bull. Univ. of Washington*. 2001. No. 106. Pp. 205
 15. Balazs G.L. Connecting reinforcement to concrete by Bond. *Beton- und Stahlbetonbau*. 2007. No. 102. Pp. 46–50.
 16. Brisotto D.E., Bittencourt. V. Simulating bond failure in reinforced concrete by a plasticity model. *Computers and Structures*. 2012. Vol. 106–107. Pp. 81–90.
 17. Kashevarova G.G., Martirosyan A.S. Computational and experimental research of the contact debonding process when rigid reinforcement is pressed into concrete. *PNRPU Mechanics Bulletin*. 2016. No. 3. Pp. 62–75.
 18. Sajedi S., Grassemzaden F., Shekarchi M., Faraji F., Solemani M. Numerical investigation on the effect of concrete-FRP bond on the flexural behavior of RC beams. *Concrete Repair, Rehabilitation and Retrofitting III: 3rd International Conference on Concrete Repair, Rehabilitation and Retrofitting ICCRRR-3*. Cape Town, South Africa, 2012. Pp. 417–418.
 19. Schnobrich W.C., Suidan M. Finite element analysis of reinforced concrete. *ASCE Journal of the Structural Division*. 1973. October. ST10. Pp. 2109–2122.
 20. Broms B.B. Stress distribution in reinforced concrete members with tension cracks. *JACI*. 1965. Vol. 62. No. 9.
 21. Goto Y. Cracks formed in concrete around deformed tension bars. *Journal of the American Concrete Institute*. 1971. Vol. 68. No. 4. Pp. 244–251.
 22. Coronado C.A., Lopez M.M. Numerical modeling of concrete-FRP debonding using a crack band approach. *Journal of Composites for Construction*. 2010. Vol. 14. No. 1. Pp. 11–20.
 23. Kwon S-H., Ferron R.P., Akkaya Y., Shah S.P. Cracking of fiber-reinforced self-compacting concrete due to restrained shrinkage. *International Journal of Concrete Structures and Materials*. 2007. Vol. I. Pp. 3–9.
 24. Almansour H., Lounis Z. Innovative precast bridge superstructure using ultra high performance concrete girders. *Proceedings of the PCI National Bridge Conference*. Phoenix, Arizona, 2007. Pp. 1–21.
 25. Graybel B. *Ultra-high performance concrete*. Federal Highway Administration. Publication number FHWA-HRT-11-038. [Electronic resource]. System requirements: AdobeAcrobatReader. URL: <http://www.fhwa.dot.gov/publications/research/infrastructure/structures/1038/index.cfm> (date of application: 14.11.2013).
 26. Travush V.I., Konin D.V., Krylov A.S., Kapriyelov S.S., Chilin I.A. Eksperimentalnyye issledovaniya stalezhelezobetonnykh konstruksiy, rabotayushchikh na izgib [Experimental study of composite structures for bending elements]. *Building and Reconstruction*. 2017. No. 4(72). Pp. 63-71.
 27. *Rukovodstvo po proyektirovaniyu zhelezobetonnykh konstruksiy s zhestkoy armaturoy* [Manual for design of steel and concrete structures]. Moscow: Stroiizdat, 1978. 55 p. (rus)
 28. Romkin D.S. *The Influence of age high-strength concrete on the physical, mechanical and rheological properties*. Cand. Diss. (Engineering). Moscow. 2007. 139 p. (rus)
- when rigid reinforcement is pressed into concrete // PNRPU Mechanics Bulletin. 2016. No. 3. Pp. 62–75.
18. Sajedi S., Grassemzaden F., Shekarchi M., Faraji F., Solemani M. Numerical investigation on the effect of concrete-FRP bond on the flexural behavior of RC beams // *Concrete Repair, Rehabilitation and Retrofitting III: 3rd International Conference on Concrete Repair, Rehabilitation and Retrofitting ICCRRR-3*. Cape Town, South Africa, 2012. Pp. 417–418.
 19. Schnobrich W.C., Suidan M. Finite element analysis of reinforced concrete // *ASCE Journal of the Structural Division*. 1973. ST10. Pp. 2109–2122.
 20. Broms B.B. Stress distribution in reinforced concrete members with tension cracks // *JACI*. 1965. Vol. 62. No. 9.
 21. Goto Y. Cracks formed in concrete around deformed tension bars // *Journal of the American Concrete Institute*. 1971. Vol. 68. No. 4. Pp. 244–251.
 22. Coronado C.A., Lopez M.M. Numerical modeling of concrete-FRP debonding using a crack band approach // *Journal of Composites for Construction*. 2010. Vol. 14. No. 1. Pp. 11–20.
 23. Kwon S-H., Ferron R.P., Akkaya Y., Shah S.P. Cracking of fiber-reinforced self-compacting concrete due to restrained shrinkage // *International Journal of Concrete Structures and Materials*. 2007. Vol. I. Pp. 3–9.
 24. Almansour H., Lounis Z. Innovative precast bridge superstructure using ultra high performance concrete girders // *Proceedings of the PCI National Bridge Conference*. Phoenix, Arizona, 2007. Pp. 1–21.
 25. Graybel B. Ultra-high performance concrete. Federal Highway Administration. Publication number FHWA-HRT-11-038. [Electronic resource]. System requirements: AdobeAcrobatReader. URL: <http://www.fhwa.dot.gov/publications/research/infrastructure/structures/1038/index.cfm> (дата обращения 14.11.2013).
 26. Травуш В.И., Конин Д.В., Крылов А.С., Каприелов С.С., Чилин И.А. Экспериментальные исследования сталежелезобетонных конструкций, работающих на изгиб // *Строительство и реконструкция*. 2017. № 4(72). С. 63–71.
 27. Руководство по проектированию железобетонных конструкций с жесткой арматурой. М.: Стройиздат, 1978. 55 с.
 28. Ромкин Д.С. Влияние возраста высокопрочного бетона на его физико-механические и реологические свойства : дис.... канд. техн. наук : 05.23.01. Москва, 2007. 140 с.

Vladimir Travush,
+7(495)775-75-65; travush@mail.ru

Denis Konin,
+7(926)853-99-73; konden@inbox.ru

Alexey Krylov,
+7(919)723-05-71; kryl07@mail.ru

Владимир Ильич Травуш,
+7(495)775-75-65; эл. почта: travush@mail.ru

Денис Владимирович Конин,
+7(926)853-99-73; эл. почта: konden@inbox.ru

Алексей Сергеевич Крылов,
+7(919)723-05-71; эл. почта: kryl07@mail.ru

© Travush V.I., Konin D.V., Krylov A.S., 2018

doi: 10.18720/MCE.79.5

Thermal cracking resistance in massive steel-reinforced concrete structures

Термическая трещиностойкость массивных сталежелезобетонных конструкций

*A.V. Bushmanova,
D.K. Kharchenko,
K.S. Semenov,
Yu.G. Barabanshchikov,
V.K. Korovina,
A.V. Dernakova,
Peter the Great St. Petersburg Polytechnic
University, St. Petersburg, Russia*

*Студент А.В. Бушманова,
студент Д.К. Харченко,
канд. техн. наук, доцент К.В. Семенов,
д-р техн. наук, профессор
Ю.Г. Барабанщиков,
студент В.К. Коровина,
студент А.В. Дернакова,
Санкт-Петербургский политехнический
университет Петра Великого, Санкт-
Петербург, Россия*

Key words: steel-reinforced concrete; stressed state; cracking resistance; analytic model; construction period

Ключевые слова: сталежелезобетонные конструкции; термонапряженное состояние; термическая трещиностойкость; расчетная схема; строительный период

Abstract. The work is dedicated to research of the thermal crack resistance in massive steel-reinforced concrete structures in construction period. The article examines the results of the analysis of the thermal stress state, which occurs in massive steel-reinforced concrete column. The steel part of the column is represented by a system of cross UC-beams. The study was conducted with using analytical models, which include the factor of steel profiles availability in comparison with simplified methods. Authors established that calculations of thermal stresses state of massive steel-reinforced concrete structures in construction period should be carried out with using analytical models, which assumed accounting of the availability steel profiles in cross-section of the column. Structure heating and tension stresses are significantly lower in this case. With all characteristics averaged, maximum tension stresses are less than real by 50.9% and thickness of the thermal insulation is less than required 5 times. Was defined, that calculations of thermal crack resistance in construction period of steel-reinforced concrete structures by simplified analytical model (which assume absence of steel profiles in cross-section of the column) lead to significant errors.

Аннотация. Работа посвящена исследованию термической трещиностойкости массивных сталежелезобетонных конструкций в строительный период. В статье рассматриваются результаты анализа термонапряженного состояния массивной сталежелезобетонной колонны, стальная часть которой представлена системой перекрестных двутавров. Исследование проводилось с использованием расчетной схемы, предполагающей учет наличия в поперечном сечении стальных профилей, а также по упрощенным методикам. Авторами установлено, что расчеты термонапряженного состояния массивных сталежелезобетонных конструкций в строительный период следует проводить с использованием расчетных схем, предполагающих учет наличия в поперечном сечении стальных профилей: разогрев конструкции и растягивающие напряжения существенно меньше. Показано, что при осреднении всех характеристик максимальные растягивающие напряжения меньше реальных на 50.9 %, а толщина теплоизоляции меньше реально требуемой в 5 раз. Определено, что упрощенная расчетная схема (предполагающая отсутствие стальных профилей в поперечном сечении) также приводит к существенным погрешностям.

Бушманова А.В., Харченко Д.К., Семенов К.В., Барабанщиков Ю.Г., Коровина В.К., Дернакова А.В. Термическая трещиностойкость массивных сталежелезобетонных конструкций // Инженерно-строительный журнал. 2018. № 3(79). С. 45–53.

1. Introduction

Most of massive steel-reinforced concrete structures are made of rigid steel profiles placed inside of reinforced concrete part of the structure [1–3]. Such kinds of structures are usually used for designing massive beam system, columns, and pillars. During the construction period, massive concrete and reinforced concrete structures may suffer from hard cracking [4–10]. In general, the cause of this phenomenon should be called irregular temperature fields at the body of the structure [11–17]. These fields generate significant tensile surface thermal stresses [18–26].

Many researches are devoted to the analysis of possible methods of steel and concrete calculations: definition of the analytical model [27–31]; estimation of different affects, such as concreting conditions, characteristics of materials, application of various technologies [32–36]; etc.

According to the paper [27], material modeling plays a major role in how reinforced concrete beams and frames react to temperature variation. Hence, the nonlinear temperature gradient, which is the realistic profile, is important to implement in the analysis.

In the paper [29], the ultimate strength behavior of the RC beams under different low temperatures is investigated by the methods of experiment, analysis and evaluation. The accuracies of the analytical models and FEM simulations were checked through validations of the predictions by different models against the test results.

In the article [35], a fibre beam element is perceived as a degenerated solid element, and for the last an unified concrete constitutive model is proposed. Beam/column members with a wide range of shear span-to-depth ratios can be simulated with the degenerated solid element considering normal-shear interaction.

Structural calculation methods involve usage of structural models made with certain simplifications that greatly facilitate the calculation. Calculation with a wrong structural model cannot be valid qualitative.

For the foregoing reasons, the vital task is to estimate the necessity of steel elements' presence in structure's cross-section model for the construction period. Since the presence or absence of steel elements in calculation of thermal crack resistance may cause a significant distortion of the real thermal stresses diagram while calculation with an incorrectly chosen structural model cannot be valid qualitative, even when using the most accurate methods.

The purpose of article is to estimate the necessity of steel elements' presence in structure's cross-section calculations of thermal crack resistance in massive steel-reinforced concrete structures for the construction period. These calculations are partly carried out by simplified method. It is important to identify possible mistakes in this approach to calculation.

As initial data (thermophysical and stress-related characteristics of concrete, cement heat radiation) the results of research, obtained in laboratory "Polytech-SKiM-Test" in CUBS department by Professor Y.G. Barabanschikov were accepted.

2. Methods and Materials

This paper demonstrates calculation of stressed state with the help of TERM software developed by the Institute of Civil Engineering at the Peter the Great St.Petersburg Polytechnic University [23]. This software calculates nonstationary fields of temperature and thermal stresses in slabs.

In order to estimate the cracking resistance of the concrete column, we would use the deformation criterion suggested by P.I. Vasiliev [26]. According to this criterion, concrete elongation deformations, determined in view of the concrete creep factor and variable deformation modulus, should not exceed the ultimate concrete elongation.

The article examines the results of the analysis of the thermal stress state in construction period, which occurs in massive steel-reinforced concrete column (Figure 1) with dimension in cross-section 1500 x 1500mm. The steel part of the column is represented by a system of cross-UC beams.

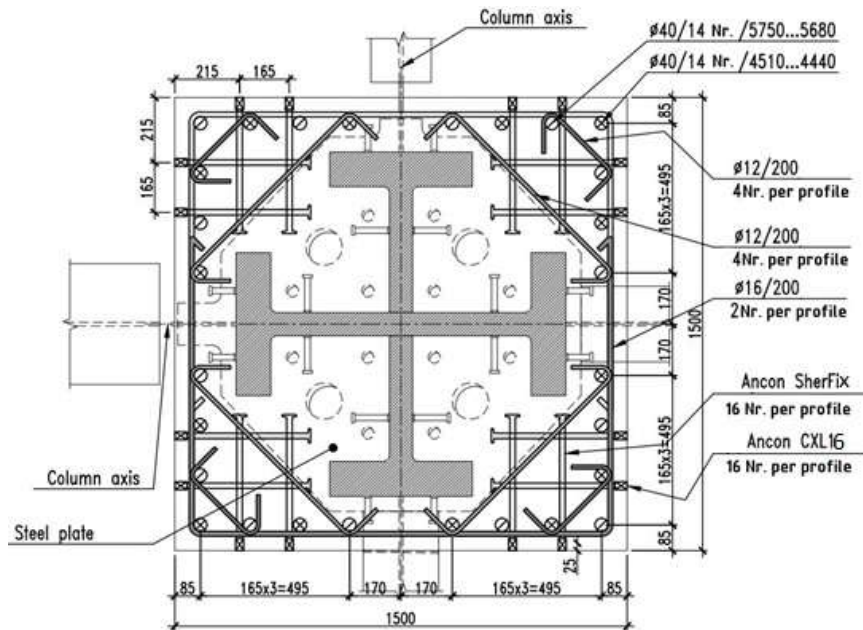


Figure 1. The steel-reinforced concrete column

The research was carried out in three principal analytical models:

- The first analytical model implied a simplified approach, which means it did not take into account the presence of metal profiles in cross-section of the column. The entire cross-section of the column should be considered to consist of concrete. The calculations are made for the cross-section quarter (the symmetry of the section along the horizontal and vertical axes is used).
- The second analytical model implied accurate estimation of the availability of the steel profiles – UC-beams. The calculations are made for the cross-section quarter (Figure 2) (the symmetry of the section along the horizontal and vertical axes is used).

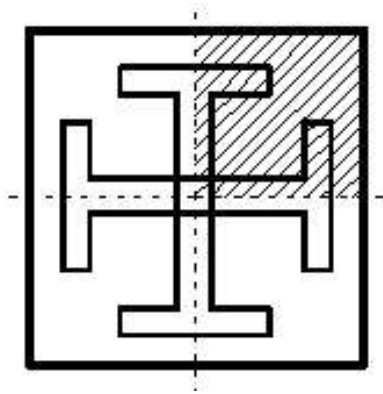


Figure 2. Analytical model

- The third analytical model implied averaging of material characteristics within the limits of the column cross-section and subsequent use of simplified model with homogeneous medium.

Consider B80 steel-reinforced concrete column the cement consumption of 450 kg/m^3 constructed in summer. Thermal and physical characteristics of the concrete B80 are defined by the concrete thermal conductivity $\lambda = 2.67 \text{ W/(m}\cdot^\circ\text{C)}$ and thermal capacity $c = 1.0 \text{ kJ/(kg}\cdot^\circ\text{C)}$. For modulus of concrete deformation $E_{\text{max}} = 45000 \text{ kg/cm}^2$, $\alpha = -0.37$, $\gamma = 0.72$ [22]. Thermal and physical characteristics of the steel are defined by the steel thermal conductivity $\lambda = 45 \text{ W/(m}\cdot^\circ\text{C)}$ and thermal capacity $c = 0.48 \text{ kJ/(kg}\cdot^\circ\text{C)}$. The reinforcing steel is assumed to be elastic-perfectly plastic material in both tension and compression with elasticity modulus $E = 2 \times 10^5 \text{ MPa}$ and Poisson's ratio equal to 0.2.

The heat dissipation process follows the I.D. Zaporozhets equation [12].

Бушманова А.В., Харченко Д.К., Семенов К.В., Барабанщиков Ю.Г., Коровина В.К., Дернакова А.В. Термическая трещиностойкость массивных сталежелезобетонных конструкций // Инженерно-строительный журнал. 2018. № 3(79). С. 45–53.

$$Q_T(\tau) = Q_{max} \left\{ 1 - \left[1 + A_{20} \int_0^t F_Q[T(\tau)d\tau] \right]^{-\frac{1}{m-1}} \right\} \quad (1)$$

The equation parameters I.D. Zaporozhets gets from experimental evidence on concrete heat dissipation [20] $Q_{max} = 157500 \text{ kJ/m}^3$, $A_{20} = 1.97 \times 10^{-6} \text{ C}^{-1}$.

The following technological specifications of concrete pouring were taken into account: the concrete mix temperature is $15 \text{ }^\circ\text{C}$ and air temperature is $15 \text{ }^\circ\text{C}$. Primary there was no thermal insulation on the surface of the column. Then the required thickness of thermal insulation was selected to provide crack resistance.

3. Results and Discussion

3.1. Results of applying the first analytical model

Temperature fields and stress direction fields in cross-section of the column are mentioned below. Moreover, the analysis of possible cracking pattern for the most dangerous moments has been conducted. The maximum of the column tension surface stresses occurs at the first day after concreting. This stresses are equal 23.8 kg/cm^2 . Temperature maximum in the cross-section at the first day was $57.1 \text{ }^\circ\text{C}$.

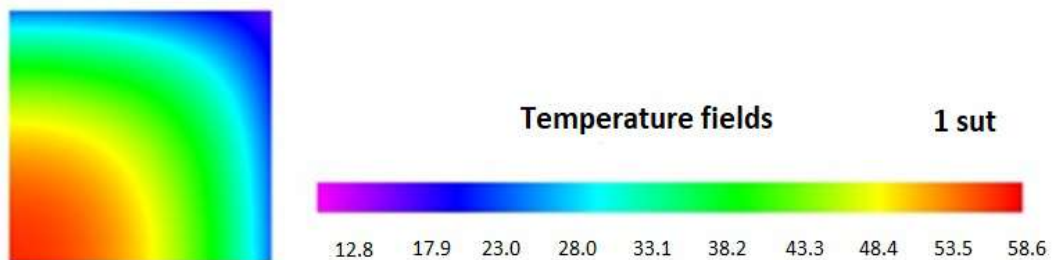


Figure 3. Thermal fields in section of the column at the first day

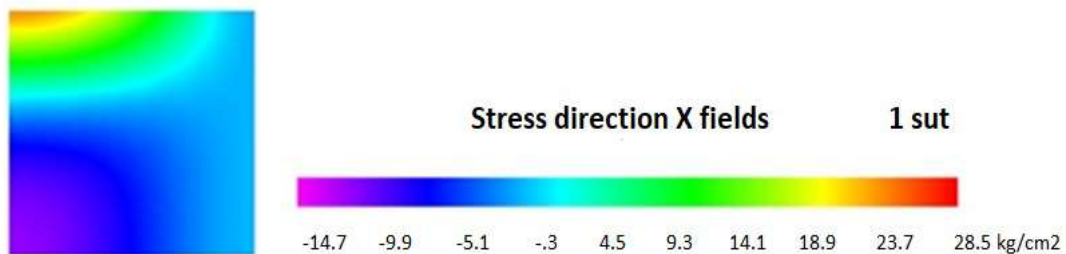


Figure 4. Stress direction fields in section of the column at the first day

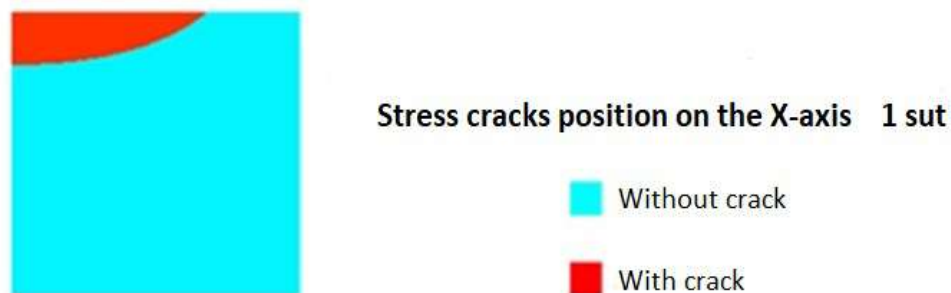


Figure 5. Stress cracks position at the first day

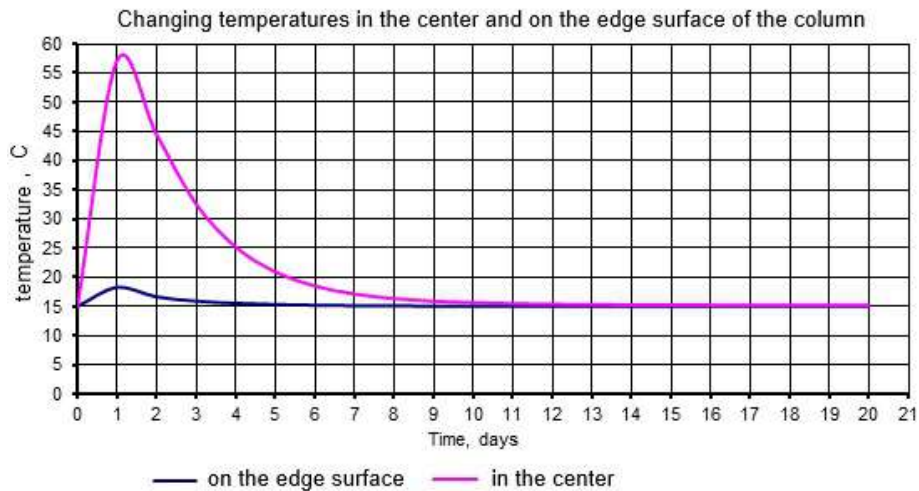


Figure 6. Graphs of changing temperatures in section of the column

To provide full crack resistance of the column during construction period a covering of surfaces with special thermal insulation requires $\beta_{red} = 3.24 \text{ W/m}^2 \cdot ^\circ\text{C}$ (β_{red} match to the thermal insulation thickness 8 mm, using thermal insulation with $\lambda = 0.03 \text{ W/m} \cdot ^\circ\text{C}$).

3.2. Results of applying the second analytical model

The maximum of the column tension surface stresses occurs at the first day after concreting. This stresses are equal $\sigma = 17.2 \text{ kg/cm}^2$. Temperature maximum in the cross-section at the first day was $40.2 \text{ }^\circ\text{C}$.

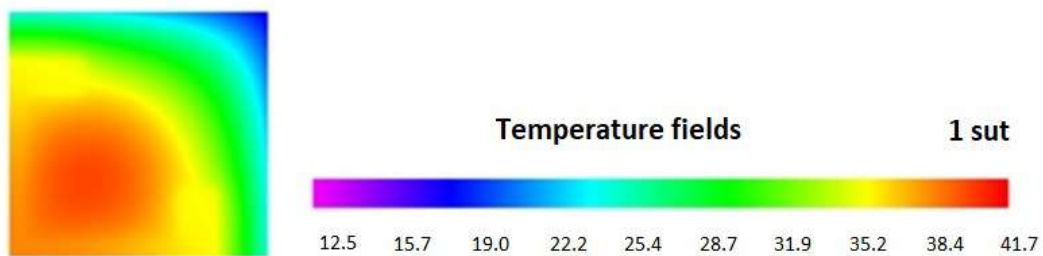


Figure 7. Thermal fields in section of the column at the first day

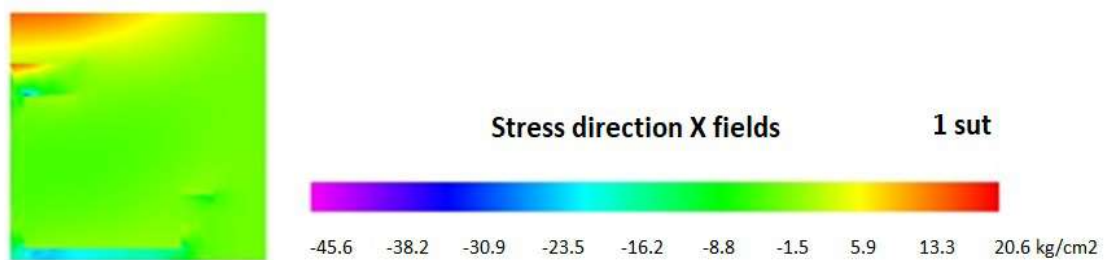


Figure 8. Stress direction fields in section of the column at the first day

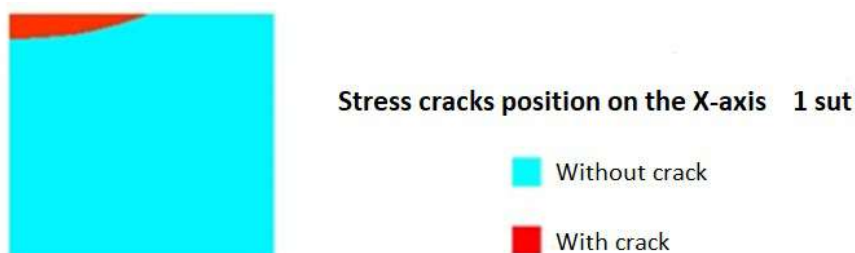


Figure 9. Stress cracks position at the first day

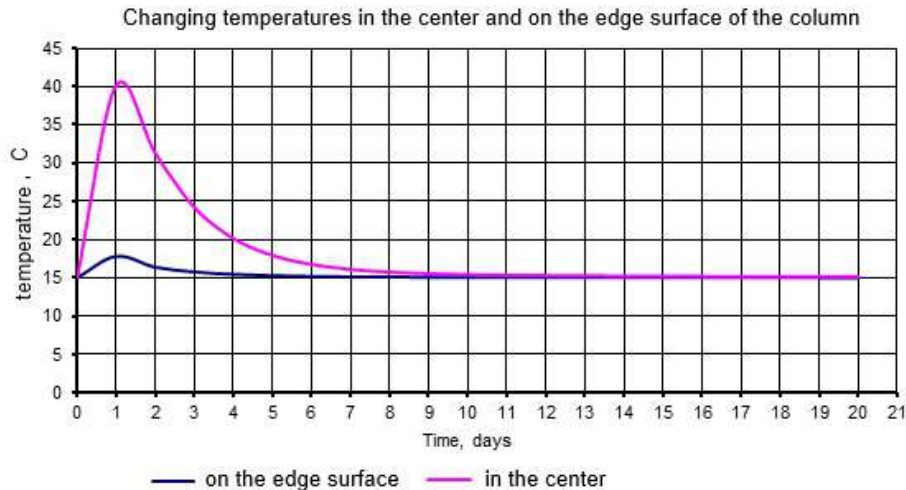


Figure 10. Graphs of changing temperatures in section of the column

To provide full crack resistance of the column in construction period, a covering of surfaces with special thermal insulation requires $\beta_{red} = 4.92 \text{ W/m}^2 \cdot ^\circ\text{C}$ (β_{red} match to the thermal insulation thickness 5 mm using thermal insulation with $\lambda = 0.03 \text{ W/m} \cdot ^\circ\text{C}$).

3.3. Results of applying the third analytical model

When all thermophysical characteristics of steel and concrete have been averaged, the maximum of the column tension surface stresses at the first day after concreting were equal $\sigma = 11.4 \text{ kg/cm}^2$. Temperature maximum in the cross-section at the first day was equal 41.5°C . Required thickness of the thermal insulation was 1 mm ($\beta_{red} = 13.2 \text{ W/m}^2 \cdot ^\circ\text{C}$).

If the characteristics of heat release of materials were averaged, then maximum tension surface stresses of the column would occur at the first day after concreting and would be equal $\sigma = 21.0 \text{ kg/cm}^2$. Maximum temperature in the cross-section at the first day was equal 53.7°C . Required thickness of the thermal insulation was 7 mm ($\beta_{red} = 3.7 \text{ W/m}^2 \cdot ^\circ\text{C}$).

3.4. Discussion

Thus, according to the paper [27, 28] it is important to possess knowledge of aspects having the greatest influence on data calculated while researching the thermal cracking resistance of massive concrete and reinforced structures. Calculation with an incorrectly chosen structural model or calculation implying a simplified approach could not be valid qualitative [30–32, 35, 36]. According to studies, those calculations of thermal stresses state of the massive steel-reinforced concrete structures in construction period by analytical models, which include the factor of steel profiles availability, are more appropriate and accurate in comparison with simplified methods.

4. Conclusion

The results of the experiments conducted lead us to the following conclusions:

1. The calculations of thermal crack resistance in construction period of steel-reinforced concrete structures by simplified analytical model (which assume absence of steel profiles in cross-section of the column) lead to significant errors. In comparison with the real situation (the second analytical model), maximum tension stresses from the simplified case more on 27.7 %. Required thickness of the thermal insulation is too high, which means that the first analytical model is economically unreasonable.

2. Averaging of thermophysical characteristics of steel and concrete in cross-section of the column also does not bring a satisfactory result. With all characteristics averaged, maximum tension stresses are less than real by 50.9% and thickness of the thermal insulation is less than required 5 times. Consequently, the calculation by this model may lead to the appointment of an incorrect stowage technique and cracking with subsequent full or partial destruction of the structure. When we are only averaging heat release characteristic, like in the first case, stresses rise and required thickness is too high.

3. The calculations of thermal stresses state of massive steel-reinforced concrete structures in construction period should be carried out with using analytical models, which assumed accounting of the

availability steel profiles in cross-section of the column. Structure heating and tension stresses are significantly lower in this case. This calculation should be called the most effective, economically feasible and structurally accurate.

References

1. Kashevarova G.G., Martirosjan A.S., Travush V.I. Raschetno-eksperimental'noe issledovanie processa razrusheniya svyazey scepneniya pri vdvavlianii sterzhnja zhestkoj armatury v beton [Computational and experimental study of the process of destruction of bonding bonds when pressing a rod of rigid reinforcement into concrete]. *Vestnik permskogo nacional'nogo issledovatel'skogo politehnicheskogo universiteta. Mehanika*. 2016. No. 3. Pp. 62–75.
2. Seryh I.R., Chernysheva E.V. Stalebeton v sovremennom stroitel'stve [Steel concrete in modern construction]. *Naukoemkie tehnologii i innovacii: sb. dokl. Jubilejnoj Mezhdunar. nauch.-prakt. konf., posvjashhennoj 60-letiju BGTU im. V.G.Shuhova*. Belgorod: Izd-vo BGTU, 2014. Vol. 2. Pp. 112–115.
3. Seryh I.R., Degtjar' A.N., Naumov A.E. Jeffect primeneniya stalebetonnyh kolonn [The effect of using steel-reinforced concrete columns]. *Vestnik BGTU im. V.G. Shuhova*. 2014. No. 5. Pp. 63–66.
4. Holt E., Leivo M. Cracking risks associated with early age shrinkage. *Cement and Concrete Composites*. 2004. No. 26(5). Pp. 521–530.
5. Larson M. *Thermal crack estimation in early age concrete-models and methods for practical application*. Division of Structural Engineering, Lulea University of Technology, Doctoral Thesis, 2003. 190 p.
6. Miyazawa S., Koibuchi K., Hiroshima A., Ohtomo T., Usui T. Control of thermal cracking in mass concrete with blast-furnace slag cement. *Concrete Under Severe Conditions*. 2010. No. 7-9. Pp. 1487–1495.
7. Se-Jin J. Advanced Assessment of Cracking due to Heat of Hydration and Internal Restraint. *ACI Materials Journal*. 2008. No. 105. Pp. 325–333.
8. Shengxing W., Donghui H. Estimation of cracking risk of concrete at early age based on thermal stress analysis. *Journal of Thermal Analysis and Calorimetry*. 2011. Vol. 105. No. 1. Pp. 171–186.
9. Zhang Z., Zhang X., Wang X., Zhang T. Merge concreting and crack control analysis of mass-concrete base slab of nuclear power plant. *Applied Mechanics and Materials*. 2011. No. 94-96. Pp. 2107–2110.
10. Lee Y., Kim J-K. Numerical analysis of the early age behavior of concrete structures with a hydration based microplane model. *Computers and Structures*. 2009. No. 7. Pp. 1085–1101.
11. Gorshkov A., Vatin N., Nemova D., Tarasova D. The brickwork joints effect on the thermotechnical uniformity of the exterior walls from gas-concrete blocks. *Applied Mechanics and Materials*. 2015. No. 725-726. Pp. 3–8.
12. Zaporozhets I.D., Okorokov S.D., Pariyskiy A.A., *Teplovydeleniye betona* [Heat Liberation by concrete]. Leningrad-Moscow: Stroyizdat, 1966. 316 p. (rus)
13. Ginzburg S.M., Sheynker N.Y., Dobretsova I.V., Voznesenskaya N.V., Issledovaniya po termike betonnykh sooruzheniy [Studies of thermal processes in concrete structures]. *Proc. of the VNIIG*. 2011. Vol. 263. Pp. 87–97. (rus)
14. Korsun V., Vatin N., Franchi A., Korsun A., Crespi P., Mashtaler S. The strength and strain of high-strength concrete elements with confinement and steel fiber reinforcement including the conditions of the effect of elevated temperatures. *Procedia Engineering*. 2015. Vol. 117. Pp. 970–979.
15. Jaafar M.S, et.al. Development of finite element computer code for thermal analysis of roller compacted concrete

Литература

1. Кашеварова Г.Г., Мартиросян А.С., Травуш В.И. Расчетно-экспериментальное исследование процесса разрушения связей сцепления при вдавливании стержня жесткой арматуры в бетон // Вестник пермского национального исследовательского политехнического университета. Механика. 2016. № 3. С. 62–75.
2. Серых И.Р., Чернышева Е.В. Сталебетон в современном строительстве // Научно-технические технологии и инновации: сб. докл. Юбилейной Международ. науч.-практ. конф., посвященной 60-летию БГТУ им. В.Г. Шухова. Белгород: Изд-во БГТУ, 2014. Ч. 2. С. 112–115.
3. Серых И.Р., Дегтярь А.Н., Наумов А.Е. Эффект применения сталебетонных колонн // Вестник БГТУ им. В.Г. Шухова. 2014. № 5. С. 63–66.
4. Holt E., Leivo M. Cracking risks associated with early age shrinkage // *Cement and Concrete Composites*. 2004. № 26(5). Pp. 521–530.
5. Larson M. Thermal crack estimation in early age concrete-models and methods for practical application. Division of Structural Engineering, Lulea University of Technology, Doctoral Thesis, 2003. 190 p.
6. Miyazawa S., Koibuchi K., Hiroshima A., Ohtomo T., Usui T. Control of thermal cracking in mass concrete with blast-furnace slag cement // *Concrete Under Severe Conditions*. 2010. № 7-9. Pp. 1487–1495
7. Se-Jin J. Advanced Assessment of Cracking due to Heat of Hydration and Internal Restraint // *ACI Materials Journal*. 2008. № 105. Pp. 325–333.
8. Shengxing W., Donghui H. Estimation of cracking risk of concrete at early age based on thermal stress analysis // *Journal of Thermal Analysis and Calorimetry*. 2011. Vol. 105. № 1. Pp. 171–186.
9. Zhang Z., Zhang X., Wang X., Zhang T. Merge concreting and crack control analysis of mass-concrete base slab of nuclear power plant // *Applied Mechanics and Materials*. 2011. № 94-96. Pp. 2107–2110.
10. Lee Y., Kim J-K. Numerical analysis of the early age behavior of concrete structures with a hydration based microplane model // *Computers and Structures*. 2009. № 7. Pp. 1085–1101.
11. Gorshkov A., Vatin N., Nemova D., Tarasova D. The Brickwork Joints Effect on the Thermotechnical Uniformity of the Exterior Walls from Gas-Concrete Blocks // *Applied Mechanics and Materials*. 2015. № 725-726. Pp. 3–8.
12. Запорожец И.Д., Окорок С.Д., Парийский А.А. Тепловыделение бетона. М.: Стройиздат, 1966. 316 с.
13. Гинзбург С.М., Шейнкер Н.Я., Добрецова И.В., Вознесенская Н.В. Исследования по термике бетонных сооружений // Известия ВНИИГ. 2011. Т. 263. С. 87–97.
14. Korsun V., Vatin N., Franchi A., Korsun A., Crespi P., Mashtaler S. The Strength and Strain of High-strength Concrete Elements with Confinement and Steel Fiber Reinforcement Including the Conditions of the Effect of Elevated Temperatures // *Procedia Engineering*. 2015. Vol. 117. Pp. 970–979.
15. Jaafar M.S, et.al. Development of finite element computer code for thermal analysis of roller compacted concrete dams // *Advances in Engineering Software*. 2007. № 38. Pp. 886–895.
16. Kim S.G. Effect of heat generation from cement hydration on mass concrete placement, Civil Engineering, Iowa State University, Master of Science Thesis, 2010. 126 p.
17. Пуляев И.С. Методы регулирования теплового режима бетона при ускоренном возведении железобетонных

Бушманова А.В., Харченко Д.К., Семенов К.В., Барабанщиков Ю.Г., Коровина В.К., Дернакова А.В. Термическая трещиностойкость массивных сталежелезобетонных конструкций // Инженерно-строительный журнал. 2018. № 3(79). С. 45–53.

- dams. *Advances in Engineering Software*. 2007. No. 38. Pp. 886–895.
16. Kim S.G. *Effect of heat generation from cement hydration on mass concrete placement*. Civil Engineering, Iowa State University, Master of Science Thesis, 2010. 126 p.
 17. Pulyayev I.S. *Metody regulirovaniya teplovogo rezhima betona pri uskorennom vozvedenii zhelezobetonnykh elementov pilonov vantovykh mostov*. Diss. na soisk. uchen. step. kand. teh. nauk: Spets 05.23.05 [Methods of concrete thermal regime regulation during accelerated construction of reinforced concrete pier elements in cable bridges. Cand. Tech. sci. diss.]. Moscow: 2010. 207 p. (rus)
 18. Korsun V.I., Korsun A.V. Vliyaniye masshtabnogo faktora i povyshennykh temperatur na prochnost' i deformatsii vysokoprochnogo modifi tsirovannogo betona [The Influence of the Scale Effect and high Temperatures on the Strength and Strains of High Performance Concrete]. *Vestnik MGSU*. 2014. No. 3. Pp. 179–188.
 19. Korsun V.I. *Napryazhenno-deformirovannoe sostoyaniye zhelezobetonnykh konstruksiy v usloviyakh temperaturnykh vozddeystviy* [Stress and Strain State of Reinforced Concrete Structures under Thermal Impacts]. Makeevka, DonGASA Publ., 2003, 153 p.
 20. Chekalkin A.V. *Termonapryazhennnoe sostoyaniye betona fundamenta turboagregata LAES-2 v stroitelnyi period*. Dis. na soisk. uchen. step. magistra: Spets. 270800.68.09 [Thermo-stressed state of concrete foundation of turbine unit of LNPP-2 in construction period. M. Sci. Eng. Tech], URL: <http://elib.spbstu.ru/dl/2/3330.pdf/view>, 2014 (rus)
 21. Yamkova E.V. *Treschinostoykost i termonapryazhennnoe sostoyaniye massivnoy fundamentnoy plity LAES-2*. Dis. na soisk. uchen. step. magistra: Spets. 08.04.01.09 [Thermal crack resistance and thermo-stressed state of massive fundamental slab of LNPP-2. M. Sci. Eng. Tech] URL: <http://elib.spbstu.ru/dl/2/v16-1267.pdf/view>, 2015 (rus)
 22. Malinin N.A. *Issledovaniye termonapryazhennogo sostoyaniya massivnykh betonnykh konstruksiy s peremennymi deformativnymi kharakteristikami*. Diss. na soisk. uchen. step. kan. teh. nauk: Spets 05.23.01. [Research of thermal stressed state of mass concrete structures with changing deformations characteristics. Cand. tech. sci. diss.]. Leningrad, 1977. 186 p. (rus)
 23. Semenov K.V. *Temperaturnoye i termonapryazhennnoe sostoyaniye blokov betonirovaniya korpusa vysokogo davleniya v stroitelnyy period*. Dis. na soisk. uchen. step. kan. teh. nauk: Spets 05.23.01 [Temperature and thermal stressed state of concreting blocks in a high pressure shell during the building period]. Leningrad, 1990. 156 p. (rus)
 24. Krat T.Y., Rukavishnikova T.N. Otsenka temperaturnogo rezhima i termonapryazhennogo sostoyaniya blokov vodosliva pri razlichnykh usloviyakh betonirovaniya [Assessment of temperature regime and thermo-stressed state of spillway units at different concreting conditions]. *Proc. of the VNIIG*. 2007. Vol. 248. Pp. 77–85. (rus)
 25. Tsybin A.M. Programma bystrogo rascheta termonapryazhennogo sostoyaniya sistemy narashchivayemykh betonnykh blokov [Program for rapid calculation routine for thermal stress state of a system of concrete blocks under construction]. *Proc. of the VNIIG*. Vol. 237. Pp. 69–76.
 26. Vasilyev P.I., Ivanov D.A., Kononov Yu.I., Semenov K.V., Starikov O.P. Raschetnoye obosnovaniye razmerov blokov i posledovatelnosti betonirovaniya korpusa reaktora VG-400 s proverkoj na modeli 1/5 naturalnoy velichiny [Calculation analysis of concreting blocks and VG-400 reactor shell concreting sequence using a 1/5 scale model]. *Problems of atomic science and technology*. 1988. No. 1. Pp. 62–68. (rus)
 27. El-Tayeb E.H., El-Metwally S.E., Askar H.S., Yousef A.M. Thermal analysis of reinforced concrete beams and frames. *HBRC Journal*. 2017. Vol. 13. No. 1. Pp. 8–24.
 - элементов пилонов вантовых мостов: дисс. на соиск. учен. степ. к. т. н.: Спец. 05.23.05. М., 2010. 207 с.
 18. Корсун В.И., Корсун А.В. Влияние масштабного фактора и повышенных температур на прочность и деформации высокопрочного модифицированного бетона // *Вестник МГСУ*. 2014. № 3. С. 179–188.
 19. Корсун В.И. Напряженно-деформированное состояние железобетонных конструкций в условиях температурных воздействий. *Макеевка: ДонГАСА*, 2003. 153 с.
 20. Чекалкин А.В. Термонапряженное состояние бетона фундамента турбоагрегата ЛАЭС-2 в строительный период: Дис. на соиск. учен. степ. магистра: Спец 08.04.01 [Электронный ресурс]: Систем. требования: Google Chrome. URL: <http://elib.spbstu.ru/dl/2/3330.pdf/view> (дата обращения: 5.09.2016)
 21. Ямкова Е.В. Трещиностойкость и термонапряженное состояние массивной фундаментной плиты ЛАЭС-2: Дис. на соиск. учен. степ. магистра: Спец 08.04.01 [Электронный ресурс]: Систем. требования: Google Chrome. URL: <http://elib.spbstu.ru/dl/2/v16-1267.pdf/view> (дата обращения 5.09.2016)
 22. Малинин Н.А. Исследование термонапряженного состояния массивных бетонных конструкций с переменными деформативными характеристиками: Дис. на соиск. учен. степ. к. т. н.: Спец. 05.23.01. Л., 1977. 186 с.
 23. Семенов К.В. Температурное и термонапряженное состояние блоков бетонирования корпуса высокого давления в строительный период: Дис. на соиск. учен. степ. к. т. н.: Спец. 05.23.01. Л., 1990. 156 с.
 24. Крат Т.Ю., Руквишников Т.Н. Оценка температурного режима и термонапряженного состояния блоков водослива при различных условиях бетонирования // *Известия ВНИИГ*. 2007. Т. 248. С. 77–85.
 25. Цыбин А.М. Программа быстрого расчета термонапряженного состояния системы наращиваемых бетонных блоков // *Известия ВНИИГ*. 2000. Т. 237. С. 69–76.
 26. Васильев П.И., Иванов Д.А., Кононов Ю.И., Семенов К.В., Стариков О.П. Расчетное обоснование размеров блоков и последовательности бетонирования корпуса реактора VG-400 с проверкой на модели 1/5 натуральной величины // *Вопросы атомной науки и техники*. 1988. № 1. С. 62–68.
 27. El-Tayeb E.H., El-Metwally S.E., Askar H.S., Yousef A.M. Thermal analysis of reinforced concrete beams and frames // *HBRC Journal* 2017. Vol. 13. № 1. Pp. 8–24.
 28. Васильев А.А. Оценка прочности бетона и ее прогнозирование для бетонных и железобетонных конструкций // *Вестник гомельского государственного технического университета им. П.О. Сухого*. 2005. № 4(23). С. 16–22.
 29. Плевков В.С., Малиновский А.П., Балдин И.В. Оценка прочности и трещиностойкости железобетонных конструкций по российским и зарубежным нормам // *Вестник томского государственного архитектурно-строительного университета*. 2013. № 2(39). С. 144–153.
 30. Yan J.-B., Xie J. Behaviours of reinforced concrete beams under low temperatures // *Construction and Building Materials*. 2017. Vol. 141. Pp. 410–415.
 31. Lantsoght E.O.L., de Boer A., der Veen C. Distribution of peak shear stress in finite element models of reinforced concrete slabs // *Engineering Structures*. 2017. Vol. 148. Pp. 571–583.
 32. Hu B., Wu Y.-F. Quantification of shear cracking in reinforced concrete beams // *Engineering Structures*. 2017. Vol. 147. Pp. 666–678.
 33. Moallemi S., Pietruszczak S. Analysis of localized fracture in 3D reinforced concrete structures using volume

28. Vasil'ev A.A. Ocenka prochnosti betona i ee prognozirovanie dlja betonnyh i zhelezobetonnyh konstrukcij [Evaluation of the strength of concrete and its prediction for concrete and reinforced concrete structures]. *Vestnik gomeľ'skogo gosudarstvennogo tehničeskogo universiteta im. P.O. Suhogo*. 2005. No. 4(23). Pp. 16–22. (rus)
29. Plevkov V.S., Malinovskij A.P., Baldin I.V. Ocenka prochnosti i treshhinostojkosti zhelezobetonnyh konstrukcij po rossijskim i zarubezhnym normam [Evaluation of strength and fracture toughness of reinforced concrete structures according to Russian and foreign norms]. *Vestnik tomskogo gosudarstvennogo arhitekturno-stroitel'nogo universiteta*. 2013. No. 2(39). Pp. 144–153. (rus)
30. Yan J.-B., Xie J. Behaviours of reinforced concrete beams under low temperatures. *Construction and Building Materials*. 2017. Vol. 141. Pp. 410–415.
31. Lantsoght E.O.L., de Boer A., der Veen C. Distribution of peak shear stress in finite element models of reinforced concrete slabs. *Engineering Structures*. 2017. Vol. 148. Pp. 571–583.
32. Hu B., Wu Y.-F. Quantification of shear cracking in reinforced concrete beams // *Engineering Structures*. 2017. Vol. 147. Pp. 666–678.
33. Moallemi S., Pietruszczak S. Analysis of localized fracture in 3D reinforced concrete structures using volume averaging technique. *Finite Elements in Analysis and Design*. 2017. Vol. 125. Pp. 41–52.
34. Chen W., Hao H., Chen S. Numerical analysis of prestressed reinforced concrete beam subjected to blast loading. *Materials and Design*. 2015. Vol. 65. Pp. 662–674.
35. Long X., Bao J.Q., Tan K.H., Lee C.K. Numerical simulation of reinforced concrete beam/column failure considering normal-shear stress interaction. *Engineering Structures*. 2014. Vol. 74. Pp. 32–43.
36. Dede T., Ayvaz Y. Nonlinear analysis of reinforced concrete beam with/without tension stiffening effect. *Materials and Design*. 2009. Vol. 30. No. 9. Pp. 3846–3851.
37. Rabczuk T., Akkermann J., Eibl J. A numerical model for reinforced concrete structures. *International Journal of Solids and Structures*. 2005. Vol. 42. No. 5–6. Pp. 1327–1354.
- averaging technique // *Finite Elements in Analysis and Design*. 2017. Vol. 125. Pp. 41–52.
34. Chen W., Hao H., Chen S. Numerical analysis of prestressed reinforced concrete beam subjected to blast loading // *Materials and Design*. 2015. Vol. 65. Pp. 662–674.
35. Long X., Bao J.Q., Tan K.H., Lee C.K. Numerical simulation of reinforced concrete beam/column failure considering normal-shear stress interaction // *Engineering Structures*. 2014. Vol. 74. Pp. 32–43.
36. Dede T., Ayvaz Y. Nonlinear analysis of reinforced concrete beam with/without tension stiffening effect // *Materials and Design*. 2009. Vol. 30. No. 9. Pp. 3846–3851.
37. Rabczuk T., Akkermann J., Eibl J. A numerical model for reinforced concrete structures // *International Journal of Solids and Structures*. 2005. Vol. 42. No. 5–6. Pp. 1327–1354.

Aleksandra Bushmanova,
+7(981)822-34-63; nicealexa@mail.ru

Daria Kharchenko,
+7(952)242-65-44; dashulity@gmail.com

Kirill Semenov,
+7(921)781-19-57; kvsemenov@bk.ru

Yuriy Barabanshchikov,
+7(812)534-12-86; ugb@mail.ru

Victoria Korovina,
+7(911)785-54-29; vika9696@inbox.ru

Aleksandra Dernakova,
+7(911)774-90-23; sasha231296@mail.ru

Александра Васильевна Бушманова,
+7(981)822-34-63; эл. почта: nicealexa@mail.ru

Дарья Константиновна Харченко,
+7(952)242-65-44;
эл. почта: dashulity@gmail.com

Кирилл Владимирович Семенов,
+7(921)781-19-57; эл. почта: kvsemenov@bk.ru

Юрий Германович Барабанщиков,
+7(812)534-12-86; эл. почта: ugb@mail.ru

Виктория Константиновна Коровина,
+7(911)785-54-29; эл. почта: vika9696@inbox.ru

Александра Вячеславовна Дернакова,
+7(911)774-90-23;
эл. почта: sasha231296@mail.ru

© Bushmanova A.V., Kharchenko D. K., Semenov K.S., Barabanshchikov Yu.G., Korovina V.K., Dernakova A. V., 2018

Бушманова А.В., Харченко Д.К., Семенов К.В., Барабанщиков Ю.Г., Коровина В.К., Дернакова А.В. Термическая трещиностойкость массивных сталежелезобетонных конструкций // Инженерно-строительный журнал. 2018. № 3(79). С. 45–53.

doi: 10.18720/MCE.79.6

Refined finite element of rods for stability calculation

Улучшенный стержневой конечный элемент для решения задач устойчивости

Yu. Ya. Tyukalov,
Vyatka State University, Kirov, Russia

Д-р техн. наук, профессор Ю.Я. Тюкалов,
Вятский государственный университет,
Киров, Россия

Key words: finite element; stability; rod; critical parameter

Ключевые слова: конечный элемент; устойчивость; стержень; критический параметр

Abstract. The article deals with the application of a rod finite element with five degrees of freedom in a node to solve problems of stability of planar rod systems. In the presented finite element, additional degrees of freedom are introduced in the nodes in the form of curvature and axial deformation. Additional degrees of freedom provide a higher degree of approximation of displacements and deformations along the length of the finite element, which can be useful for calculation of rods with variable rigidity, as well as for solving geometrically nonlinear problems and stability problems. In this paper the elements of stiffness matrix and the elements of geometric matrix of the finite element are obtained. The results of the calculation of straight rods and frames under various conditions of support and various loads are presented. A comparison is made with the results of calculations using a classic finite element with three degrees of freedom. It is shown that the introduction of additional degrees of freedom at the nodes, in the form of the curvature of the axis and longitudinal deformation, makes it possible in a few cases to more accurately determine the value of the critical load. In this case, the system has more degrees of freedom, so the approximation of the forms of stability loss is more accurate.

Аннотация. В статье рассматривается применение стержневого конечного элемента с пятью степенями свободы в узле для решения задач устойчивости плоских стержневых систем. В представленном конечном элементе в узлах введены дополнительные степени свободы в виде кривизны и осевой деформации. Дополнительные степени свободы обеспечивают более высокую степень аппроксимации перемещений и деформаций по длине конечного элемента, что может быть полезным для стержней переменной жесткости, а также при решении геометрически нелинейных задач и задач устойчивости. В работе получены элементы матрицы жесткости и геометрической матрицы конечного элемента. Представлены результаты расчетов прямых стержней и рам при различных условиях вариантах опор и нагрузок. Выполнено сравнение с результатами расчетов при использовании конечного элемента с тремя степенями свободы. Показано, что введение дополнительных степеней свободы в узлах, в виде кривизны оси и продольной деформации, позволяет в ряде случаев более точно определить величину критической нагрузки. В этом случае система имеет больше степеней свободы, поэтому аппроксимация форм потери устойчивости является более точной.

1. Introduction

Numerous fundamental studies, including papers [1–3], have been devoted to the calculation of various constructions by the finite element method. For rod systems, most attention is paid to the construction of functionals for solving stability problems of rods [4], as well as to the methods calculations constructions considering geometric and physical nonlinearities [5, 6]. In paper [7], an exact, analytical solution of the beam bending problem is constructed according to Euler-Bernoulli and Timoshenko theories. The work [8] is devoted to the determination of critical forces by the flexural-torsional form of the loss of stability of steel columns with allowance for physical nonlinearity. In [9, 10] we consider the computational efficiency of the proposed method of quadrature finite elements for calculating the stability of planar rod systems. In these articles the rods of constant and variable cross sections are considered and comparison of the proposed method of calculation with the finite element method in displacements is performed.

To analyze the stability of rods, models based on plane stress finite elements can be used. In [11] the steel I-beam is modeled by such plane finite elements and the influence of the compressive load

distribution law over cross section to the critical value of the load is studied. In [12, 13] we consider the calculation of the stability of perforated steel columns. In [12] the calculation of stability of perforated columns is based on the approximation of transverse and longitudinal displacements by trigonometric functions and the obtained solutions compares with the solutions by the finite element method.

In article [14] the influence of the position of the compressive load in the calculation of the stability of flat steel frames is studied. The load in the form of a concentrated force applied to the beam is considered and the influence of its position on the value of the critical load is determined. The solution is constructed by the finite element method.

The paper [15] presents numerical studies of possible scenarios for the loss of stability of flat arches using the NASTRAN program. Many papers are devoted to the calculation of thin-walled rod systems by the finite element method [16, 17] and to the study of various variational formulations of stability problems of planar systems and geometrically nonlinear deformation of rod systems [18–19]. Features of the calculation of the stability of bars in the exact formulation are considered in [20–22]. In this case, the solution reduces to a system of transcendental equations. This approach is highly accurate but can only be used for simple systems.

In [23, 24] the solutions of stability problems and free vibrations of rod systems are based on the functional of additional energy and the using approximations for the forces. It is shown that with this approach one can obtain the upper limits of the critical forces and of the frequencies of free oscillations.

In [25] a finite element with five degrees of freedom in a node is used to calculating planar rod systems with allowance for physical nonlinearity. Additional degrees of freedom provide better approximation of displacements and deformations along the length of the finite element, what can be useful for calculating the rods of variable rigidity, as well as for solving geometrically nonlinear problems and stability problems. Note, that in solving static problems of rods bending by the finite element method, a cubic polynomial function is used to approximate transverse displacements, which ensures the obtaining of exact values of internal forces. But under the action of distributed loads, the displacements along the length of the beam vary according to the polynomial of the fifth degree and so a cubic polynomial function can't provide the exact values of the displacements.

The aim of this paper is to construct a more accurate solution to the problem of stability of planar rod systems using the finite element with five degrees of freedom at nodes. The main tasks are: obtaining expressions for the elements of the stiffness matrix and the geometric matrix of the rod finite element with five degrees of freedom in the node; the development of an algorithm for calculating the stability of planar rod systems; comparison of the results of the determination of critical parameters for various rod systems, according to the proposed methodology, with the results obtained using the LIRA-SAPR program, which uses a finite element with three degrees of freedom.

2. Methods

In paper [23] the rod finite element with five degrees of freedom at a node (Figure 1) is used to solve the dynamic problems of reinforced concrete planar bar systems with allowance for physical nonlinearity. In this finite element additional degrees of freedom were introduced in the form of curvature and axial deformation. Note that the curvatures and axial deformations in the node are different for the finite elements adjacent to this node. Therefore, the total number of unknowns for the whole system is $n = 3k_n + 4k_e - s$. k_n – number of nodes; k_e – number of finite elements; s – the number of superimposed links. On the other hand, such the finite element provides an accurate calculation of deformations and stresses and ensures, if necessary, their continuity. As is known, when using a standard rod finite element, with three degrees of freedom, gaps of deformations and stresses may appear at the nodes, for example, at the start or end points of a distributed load. In addition, direct calculation of deformations and ensuring continuity of stresses makes it easier to obtain of solving physically nonlinear problem and can improve the accuracy of calculations. Also, when solving stability problems, increasing the number of degrees of freedom makes the system more flexible and, therefore, leads to smaller and more accurate values of the critical forces.

We use this finite element to solve the problem of determining the critical load for planar rod systems. At the first stage, it is necessary to determine the internal forces (longitudinal forces) in the rods from the action of the applied loads. In Figure 1 this finite element is represented and the following notations are introduced: w_1, w_2 – displacements of nodes along the Y_1 axis; φ_1, φ_2 – angles of rotation of sections; u_1, u_2 – displacements of nodes along the X_1 axis; k_1, k_2 – the curvatures of the axes at the nodes; $\varepsilon_1, \varepsilon_2$ – axial deformations at the nodes.

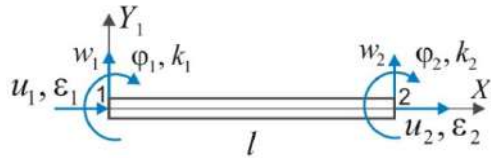


Figure 1. Finite element with five degrees of freedom in the node

The transverse displacement of the axis of the finite element is represented by the polynomial of the fifth degree in the following form:

$$w(x) = L_1(x)w_1 + L_2(x)\varphi_1 + L_3(x)k_1 + L_4(x)w_2 + L_5(x)\varphi_2 + L_6(x)k_2, \quad (1)$$

where:

$$\begin{aligned} L_1(x) &= 1 - 10\left(\frac{x}{l}\right)^3 + 15\left(\frac{x}{l}\right)^4 - 6\left(\frac{x}{l}\right)^5, \\ L_2(x) &= l\left[\frac{x}{l} - 6\left(\frac{x}{l}\right)^3 + 8\left(\frac{x}{l}\right)^4 - 3\left(\frac{x}{l}\right)^5\right], \\ L_3(x) &= \frac{l^2}{2}\left[\left(\frac{x}{l}\right)^2 - 3\left(\frac{x}{l}\right)^3 + 3\left(\frac{x}{l}\right)^4 - \left(\frac{x}{l}\right)^5\right], \\ L_4(x) &= 10\left(\frac{x}{l}\right)^3 - 15\left(\frac{x}{l}\right)^4 + 6\left(\frac{x}{l}\right)^5, \\ L_5(x) &= l\left[-4\left(\frac{x}{l}\right)^3 + 7\left(\frac{x}{l}\right)^4 - 3\left(\frac{x}{l}\right)^5\right], \\ L_6(x) &= \frac{l^2}{2}\left[\left(\frac{x}{l}\right)^3 - 2\left(\frac{x}{l}\right)^4 + \left(\frac{x}{l}\right)^5\right]. \end{aligned} \quad (2)$$

Longitudinal displacements are approximated by the polynomial of the third degree:

$$u(x) = L_7(x)u_1 + L_8(x)\varepsilon_1 + L_9(x)u_2 + L_{10}(x)\varepsilon_2, \quad (3)$$

$$\begin{aligned} L_7(x) &= 1 - 3\left(\frac{x}{l}\right)^2 + 2\left(\frac{x}{l}\right)^3, \\ L_8(x) &= l\left[\frac{x}{l} - 2\left(\frac{x}{l}\right)^2 + \left(\frac{x}{l}\right)^3\right], \\ L_9(x) &= 3\left(\frac{x}{l}\right)^2 - 2\left(\frac{x}{l}\right)^3, \\ L_{10}(x) &= l\left[-\left(\frac{x}{l}\right)^2 + \left(\frac{x}{l}\right)^3\right]. \end{aligned} \quad (4)$$

The unknowns and the form functions are combined into vectors:

$$\{w_e\} = \begin{Bmatrix} w_1 \\ \varphi_1 \\ k_1 \\ w_2 \\ \varphi_2 \\ k_2 \end{Bmatrix}, \quad \{L_w\} = \begin{Bmatrix} L_1(x) \\ L_2(x) \\ L_3(x) \\ L_4(x) \\ L_5(x) \\ L_6(x) \end{Bmatrix}, \quad \{u_e\} = \begin{Bmatrix} u_1 \\ \varepsilon_1 \\ u_2 \\ \varepsilon_2 \end{Bmatrix}, \quad \{L_u\} = \begin{Bmatrix} L_7(x) \\ L_8(x) \\ L_9(x) \\ L_{10}(x) \end{Bmatrix}. \quad (5)$$

When solving problems of stability, without considering the shear strains, deformations are expressed in the following form [1]:

$$\varepsilon_x = \frac{du}{dx} - z \frac{d^2w}{dx^2} + \frac{1}{2} \left(\frac{dw}{dx}\right)^2. \quad (6)$$

Then the strain energy of the finite element is expressed in the following form [1, 2]:

$$U^e = \frac{1}{2} \int_0^l [EI \left(\frac{d^2w}{dx^2}\right)^2 + EA \left(\frac{du}{dx}\right)^2 + N(x) \left(\frac{dw}{dx}\right)^2] dx. \quad (7)$$

where: EI, EA – flexural and longitudinal stiffness of cross-section of the element. The longitudinal force can vary along the length of the finite element, so we assume that

$$N(x) = N_1(1 - x/l) + N_2 x/l, \quad (8)$$

where: N_1, N_2 – longitudinal forces at the beginning and end of the finite element.

Using (1 5), we write expression (7) in the matrix form:

$$U^e = \frac{1}{2} (\{w_e\}^T [k_w] \{w_e\} + \{u_e\}^T [k_u] \{u_e\} + \{w_e\}^T [k_N] \{w_e\}), \quad (9)$$

$$[k_w] = \int_0^l EI \{L''_w\} \{L''_w\}^T dx, [k_u] = \int_0^l EA \{L'_u\} \{L'_u\}^T dx, [k_N] = \int_0^l N(x) \{L'_w\} \{L'_w\}^T dx. \quad (10)$$

We unite the nodal unknowns into one vector

$$\{y_e\} = \begin{Bmatrix} \{w_e\} \\ \{u_e\} \end{Bmatrix}. \quad (11)$$

The expression (8) can be written in the following form:

$$U^e = \frac{1}{2} \{y_e\}^T ([k_e] + [k_{Ne}]) \{y_e\}, \quad (12)$$

$$[k_e] = \begin{bmatrix} \frac{120 \cdot EI}{7 \cdot l^3} & \frac{60 \cdot EI}{7 \cdot l^2} & \frac{3 \cdot EI}{7 \cdot l} & -\frac{120 \cdot EI}{7 \cdot l^3} & \frac{60 \cdot EI}{7 \cdot l^2} & -\frac{3 \cdot EI}{7 \cdot l} & 0 & 0 & 0 & 0 \\ & \frac{192 \cdot EI}{35 \cdot l} & \frac{11 \cdot EI}{35} & -\frac{60 \cdot EI}{7 \cdot l^2} & \frac{108 \cdot EI}{35 \cdot l} & -\frac{4 \cdot EI}{35} & 0 & 0 & 0 & 0 \\ & & \frac{3 \cdot EI}{35} & \frac{7 \cdot EI}{35} & \frac{4 \cdot EI}{35} & \frac{EI \cdot l}{70} & 0 & 0 & 0 & 0 \\ & & & \frac{120 \cdot EI}{7 \cdot l^3} & -\frac{60 \cdot EI}{7 \cdot l^2} & \frac{3 \cdot EI}{7 \cdot l} & 0 & 0 & 0 & 0 \\ & & & & \frac{192 \cdot EI}{35 \cdot l} & -\frac{11 \cdot EI}{35} & 0 & 0 & 0 & 0 \\ & & & & & \frac{3 \cdot EI}{35} & 0 & 0 & 0 & 0 \\ & & & & & & \frac{6 \cdot EA}{5 \cdot l} & \frac{EA}{10} & -\frac{6 \cdot EA}{5 \cdot l} & \frac{EA}{10} \\ & & & & & & & \frac{2 \cdot l \cdot EA}{15} & -\frac{EA}{10} & -\frac{l \cdot EA}{30} \\ & & & & & & & & \frac{6 \cdot EA}{5 \cdot l} & -\frac{EA}{10} \\ & & & & & & & & & \frac{2 \cdot l \cdot EA}{15} \end{bmatrix}, \quad (13)$$

$$[k_{Ne}] = \begin{bmatrix} \frac{5(N_1+N_2)}{7 \cdot l} & \frac{5N_1+13N_2}{84} & \frac{N_2 l}{84} & -\frac{5(N_1+N_2)}{7 \cdot l} & \frac{13N_1+5N_2}{84} & -\frac{N_1 l}{84} & 0 & 0 & 0 & 0 \\ & \frac{N_1 l}{6} + \frac{13N_2 l}{210} & \frac{11N_1 l^2}{1008} + \frac{29N_2 l^2}{5040} & -\frac{5N_1-13N_2}{84} & -\frac{(N_1+N_2)l}{140} & \frac{(11N_1+13N_2)l^2}{5040} & 0 & 0 & 0 & 0 \\ & & \frac{N_1 l^3}{1008} + \frac{N_2 l^3}{1680} & -\frac{N_2 l}{84} & -\frac{(13N_1+11N_2)l^2}{5040} & \frac{(N_1+N_2)l^3}{2520} & 0 & 0 & 0 & 0 \\ & & & \frac{5(N_1+N_2)}{7 \cdot l} & -\frac{13N_1-5N_2}{84} & \frac{N_1 l}{84} & 0 & 0 & 0 & 0 \\ & & & & \frac{13N_1 l}{210} + \frac{N_2 l}{6} & -\frac{29N_1 l^2}{5040} - \frac{11N_2 l^2}{1008} & 0 & 0 & 0 & 0 \\ & & & & & \frac{N_1 l^3}{1680} + \frac{N_2 l^3}{1008} & 0 & 0 & 0 & 0 \\ & & & & & & 0 & 0 & 0 & 0 \\ & & & & & & & 0 & 0 & 0 \\ & & & & & & & & 0 & 0 \\ & & & & & & & & & 0 \end{bmatrix}. \quad (14)$$

The matrices (13) and (14) are symmetric, therefore the matrix elements above the main diagonal are shown.

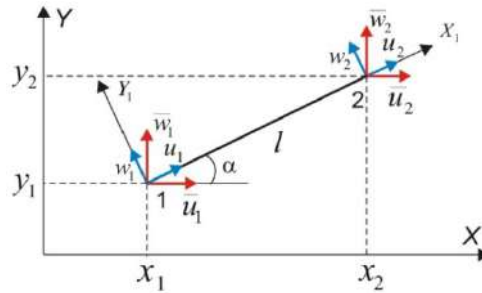


Figure 2. Global and local coordinate systems.

In Figure 2 shows the global and local coordinate systems. Nodal unknowns in the global coordinate system are indicated by an upper line. Vectors of nodal unknown finite elements in local $\{y_e\}$ and global coordinate systems $\{\bar{y}_e\}$ are connected by a matrix of directing cosines:

$$\{\bar{y}_e\} = [S]\{y_e\}, \quad (15)$$

$$[S] = \begin{bmatrix} \cos \alpha & 0 & 0 & 0 & 0 & 0 & \sin \alpha & 0 & 0 & 0 \\ 0 & 1 & 0 & 0 & 0 & 0 & 0 & 0 & 0 & 0 \\ 0 & 0 & 1 & 0 & 0 & 0 & 0 & 0 & 0 & 0 \\ 0 & 0 & 0 & \cos \alpha & 0 & 0 & 0 & 0 & \sin \alpha & 0 \\ 0 & 0 & 0 & 0 & 1 & 0 & 0 & 0 & 0 & 0 \\ 0 & 0 & 0 & 0 & 0 & 1 & 0 & 0 & 0 & 0 \\ -\sin \alpha & 0 & 0 & 0 & 0 & 0 & \cos \alpha & 0 & 0 & 0 \\ 0 & 0 & 0 & 0 & 0 & 0 & 0 & 1 & 0 & 0 \\ 0 & 0 & 0 & -\sin \alpha & 0 & 0 & 0 & 0 & \cos \alpha & 0 \\ 0 & 0 & 0 & 0 & 0 & 0 & 0 & 0 & 0 & 1 \end{bmatrix}. \quad (16)$$

Using the vector of nodal unknowns in the global coordinate system, we get:

$$U^e = \frac{1}{2} \{\bar{y}_e\}^T ([\bar{k}_e] + [\bar{k}_{Ne}]) \{\bar{y}_e\}, \quad (17)$$

$$[\bar{k}_e] = [S][k_e][S]^T, \quad [\bar{k}_{Ne}] = [S][k_{Ne}][S]^T. \quad (18)$$

$[\bar{k}_e]$ is the finite element stiffness matrix in the global coordinate system; $[\bar{k}_{Ne}]$ is the geometric matrix of the finite element in the global coordinate system. From the matrices $[\bar{k}_e]$ and $[\bar{k}_{Ne}]$ of all finite elements of the system, in accordance with the numbering of nodes and elements, the corresponding global matrices – $[K]$ and $[K_N]$ are formed, and the unknowns for the whole system are represented by the vector $\{Y\}$. Then the energy of deformation of all finite elements

$$U = \frac{1}{2} \{Y\}^T ([K] + [K_N]) \{Y\}. \quad (19)$$

To obtain a solution, it is necessary to write down the expression for the potential of external concentrated and distributed forces V . For the loads distributed over the length of the finite element, the potential is expressed as the integral

$$V^e = - \int_0^l (q_{y_1} w(x) + q_{x_1} u(x)) dx, \quad (20)$$

where:

$$q_{y_1} = q_y \cos \alpha - q_x \sin \alpha, \quad q_{x_1} = q_y \sin \alpha + q_x \cos \alpha. \quad (21)$$

q_y, q_x – values of the loads distributed along the length of the finite element, directed along the global axes Y and X, respectively. For evenly distributed loads:

$$V^e = \{y_e\}^T \{F_e\}, \quad (22)$$

$$\{F_e\}^T = \left(\frac{q_{y_1} L}{2}, \frac{q_{y_1} L^2}{10}, \frac{q_{y_1} L^3}{120}, \frac{q_{y_1} L}{2}, \frac{-q_{y_1} L^2}{10}, \frac{q_{y_1} L^3}{120}, \frac{q_{x_1} L}{2}, \frac{q_{x_1} L^2}{12}, \frac{q_{x_1} L}{2}, \frac{-q_{x_1} L^2}{12} \right). \quad (23)$$

Using the vector of nodal unknowns in the global coordinate system, we get:

$$V^e = \{\bar{y}_e\}^T \{\bar{F}_e\}, \quad (24)$$

$$\{\bar{F}_e\} = [S]\{F_e\}. \quad (25)$$

From vectors $\{\bar{F}_e\}$ for all finite elements the global vector $\{F\}$ is formed for the whole system. The forces P_x, P_y , concentrated in the nodes, which directed along the global axes, and the concentrated in the nodes moments M are added to the corresponding elements of the global vector $\{F\}$.

Using the notation introduced above, we write the total potential energy of the system in the following form:

$$\Pi = U + V = \frac{1}{2}\{Y\}^T ([K] + [K_N])\{Y\} + \{Y\}^T \{F\} \rightarrow \min. \quad (26)$$

Equating the derivatives of the total potential energy of the system with along the vector of nodal unknowns to zero, we obtain a system of resolving equations:

$$([K] + [K_N])\{Y\} + \{F\} = 0. \quad (27)$$

In the classical approach, the matrix $[K_N]$ is not considered when solving the system of equations (27), therefore the values of displacements and internal forces are determined without considering the effect of longitudinal forces on bending. In a more precise variant, the iterative solution of the system (27) is performed and the elements of the matrix $[K_N]$ are calculated using the longitudinal forces obtained in the previous step. For some constructions, solutions for the two options may differ materially.

Solving the system of linear equations (27), we find the displacement vector $\{Y\}_0$ and, further, calculate the longitudinal forces in finite elements. The critical load parameter λ_{cr} can be found by the well-known method of reverse iterations. The algorithm consists of the following steps:

$$\left\{ \begin{array}{l} i = 1, 2, \dots, m; \\ \{Y\}_i = [K]^{-1}[K_N]\{Y\}_{i-1}, \\ y_{max} = \max_{j=1..n} |\{Y\}_i|, \\ \lambda_{cr,i} = \frac{1}{|y_{max}|}, \\ \{Y\}_i = \lambda_{cr,i}\{Y\}_i. \end{array} \right. \quad (28)$$

In (28) y_{max} is the maximum modulo element of the vector $\{Y\}_i$. The iterative procedure ends when the necessary accuracy is getting for $|\lambda_{cr,i} - \lambda_{cr,i-1}| < \varepsilon$. The vector $\{Y\}_i$ is the vector of the shape of the loss of stability.

3. Results and Discussion

As a first example, according to a program compiled in Mathcad 14.0, calculations of the critical forces for straight rods were performed under various conditions of supporting the ends (Figure 3). To simplify the analysis of the results, all the parameters of the rods were equal as single ones. The rod was modeled by only one finite element. Table 1 shows the results of calculations using the proposed finite element and the results of calculations using the LIRA-SAPR program, as well as the exact, analytically obtained values [26].

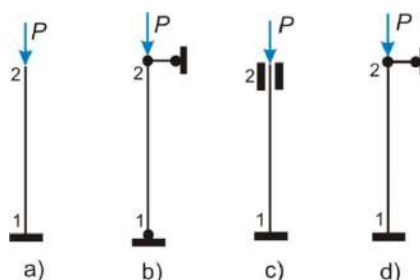


Figure 3. Variants of support of straight rods. $l = 1 \text{ m.}, EI = 1 \text{ kN} \cdot \text{m}^2$

Table 1. Critical forces for straight rods (Figure 3)

Rod	Finite element with five degrees of freedom			Finite element with three degrees of freedom, LIRA-SAPR			Exact decision, P_{cr}, kN
	P_{cr}, kN	Error, %	Quantity of unknowns	P_{cr}, kN	Error, %	Quantity of unknowns	
a) Console rod	2.4674	0	7	2.486	0.75	4	2.4674
b) Hinged supports	9.882	0.125	7	12.0	21.6	3	9.8696
c) Clamped ends	39.480	0.004	5	-	-	1	39.4784
d) Clamped and hinged support	20.347	0.77	6	30	48.6	2	20.1906

The obtained solutions show that when using the finite element with five degrees of freedom, the calculated values of the critical forces are very close to the exact values under any conditions of support of the rod ends. The greatest error in the calculation of the critical force of only 0.77 % was obtained for a rod with one pinched and one hinged support end.

When using the classical finite element with three degrees of freedom in a node, for a rod with clamped supports (Figure 3c), a solution can't be obtained, since the calculation scheme with one finite element has only one degree of freedom associated with the longitudinal displacement of the upper node. For this finite element, the exact solution is obtained only for the console rod (Figure 3a), in other cases the errors of the solutions are significant. To obtain more precise solutions, it is obviously necessary to divide the rod into two finite elements, thereby increasing the total number of degrees of freedom.

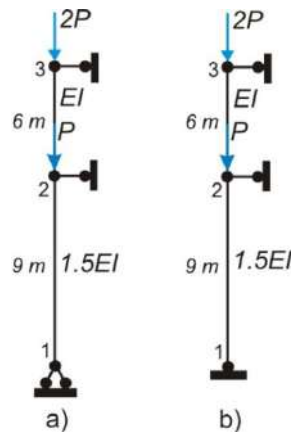


Figure 4. Straight rods with intermediate support. Flexural stiffness varies stepwise

In Figure 4 shows straight rods with intermediate supports and with different bending stiffness, varying stepwise. A well-known "forces method" can be used to determine the exact value of the critical load. In this case, the coefficients of the canonical equations are determined based on the exact solution of the differential equation of a compressed-bent rod. We introduce the following notation:

$$\lambda_1 = l_{2-3} \sqrt{\frac{N_{2-3}}{EI}} = 6 \sqrt{\frac{2P}{EI}}, \quad \lambda_2 = l_{1-2} \sqrt{\frac{N_{1-2}}{EI}} = 9 \sqrt{\frac{3P}{1.5EI}} = 1.5\lambda_1. \quad (29)$$

Then the equation of the "forces method" for determining the critical load for the rod in Fig. 4a will be as follows:

$$\frac{3}{\lambda_1} \left(\frac{1}{\lambda_1} - \frac{1}{\tan \lambda_1} \right) + \frac{3}{\lambda_2} \left(\frac{1}{\lambda_2} - \frac{1}{\tan \lambda_2} \right) = \frac{3}{\lambda_1} \left(\frac{1}{\lambda_1} - \frac{1}{\tan \lambda_1} \right) + \frac{2}{\lambda_1} \left(\frac{1}{1.5\lambda_1} - \frac{1}{\tan 1.5\lambda_1} \right) = 0. \quad (30)$$

Solving equation (30) in Mathcad 14, we obtain that $\lambda_{1,cr} = 2.355779$. We will take $EI = 1 \text{ kN/m}^2$, then $P_{cr} = \frac{1}{2.36} \lambda_{1,cr}^2 = 0.077079 \text{ kN}$. The equation of the "forces method" for the rod in Figure 4b has the form:

$$\frac{18}{\lambda_1} \left(\frac{1}{\lambda_1} - \frac{1}{\tan \lambda_1} \right) + \frac{36 \tan \lambda_2}{\lambda_2 (\tan \lambda_2 - \lambda_2)} \left(\tan \frac{\lambda_2}{2} - \frac{\lambda_2}{2} \right) = 0. \tag{31}$$

Solving equation (31), we obtain $\lambda_{1,cr} = 3.053638$, $P_{cr} = \frac{1}{2.36} \lambda_{1,cr}^2 = 0.1295098 \text{ kN}$.

In Table 2, in addition to the exact values, the values of the critical load are given, which are determined using a finite element with 5 degrees of freedom and the results of calculations using the LIRA-SAPR program for the rods in Figure 4.

Table 2. Critical forces for straight rods with an intermediate support (Figure 4)

Rod	Finite element with five degrees of freedom		Finite element with three degrees of freedom, LIRA-SAPR		Exact decision, P_{cr}, kN
	P_{cr}, kN	Error, %	P_{cr}, kN	Error, %	
Figure 4a	0.077158	0.10	0.097055	25.9	0.0770790
Figure 4b	0.129967	0.35	0.175336	35.4	0.1295098

The obtained results confirm the high accuracy of determining the critical forces when using the finite element with five degrees of freedom. Since the proposed finite element quite accurately simulates the stress-strain state of compressed-bent rods with different types of supports, it can be confidently asserted that for arbitrary rod systems, this finite element will allow us to determine the values of the critical forces with sufficiently high accuracy.

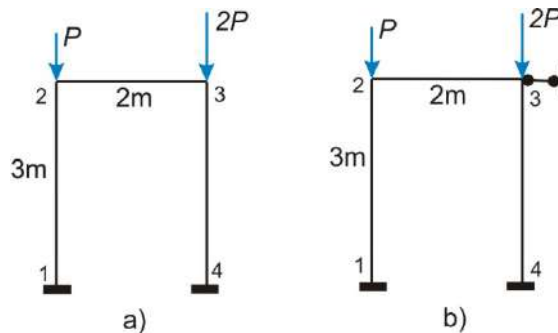


Figure 5. Single-span frame with clamped ends

Calculations have also been performed to determine the critical load for a single-span frame shown in Figure 5. The lengths of the rods are shown in the figure. The flexural rigidity of the rods is $EI = 10 \text{ kH/m}^2$, longitudinal stiffness $EA = 100 \text{ kH}$, $P = 10 \text{ kH}$. The critical load parameter was determined by using from 1 to 8 finite elements for modeling each rod (Table 3).

Table 3. Critical loading parameter λ_{cr} for frames (Figure 5)

Crushing of rods into finite elements	The frame in Figure 5a			The frame in Figure 5b		
	Finite element with three degrees of freedom, LIRA-SAPR	Finite element with five degrees of freedom	Difference of the results, %	Finite element with three degrees of freedom, LIRA-SAPR	Finite element with five degrees of freedom	Difference of the results, %
1	0.5171	0.51200	0.99	3.2898	1.66299	97.8
2	0.5135	0.51199	0.27	1.6711	1.63717	2.07
4	0.5121	0.51199	0.02	1.6421	1.63712	0.3
8	0.5120	0.51199	0.02	1.6375	1.63712	0.02

For the frame in Figure 5a, the critical load parameter, calculated using a finite element with five degrees of freedom in the node, practically does not change when the rods are crushed. If we use a classical finite element with three degrees of freedom, then λ_{cr} with an increase in crushing of the rods to

8 finite elements decreases by approximately 1 % and becomes equal to the critical parameter calculated using a finite element with five degrees of freedom without crushing the rods.

For a frame with an additional support (Figure 5b), which excludes horizontal displacement, the change in the critical parameter during crushing of rods for finite elements with three degrees of freedom is more significant (Table 3). If you don't divide the rods into few finite elements, then the critical parameter is almost twice as large as the parameter obtained by using one element with five degrees of freedom. When dividing each rod into 2 finite elements, the difference of solutions is only 2 %. With further crushing of the rods, the results become practically equal.

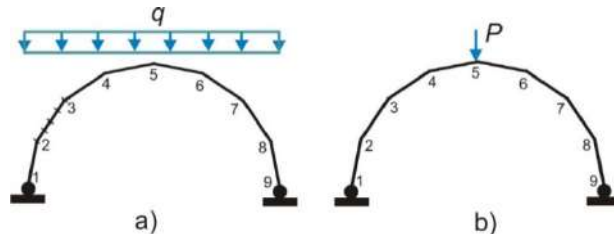


Figure 6. Frame from eight rods inscribed in a circle, with hinged supports

Figure 6 shows a frame, which inscribed in a circle of radius $R = 6\text{ m}$. The frame consists of eight straight rods. The flexural rigidity of the rods is $EI = 10\text{ kH/m}^2$, longitudinal stiffness $EA = 100\text{ kH}$. We considered loading in a form uniformly distributed load and in a form single concentrated force. The critical load parameter was determined for the additional dividing all the rods by 1, 2, 4, 8, and 16 finite elements (Table 4). In Fig. 6a shows an example of dividing the rod (2-3) into 4 finite elements.

Table 4. Critical loading parameter λ_{cr} for the frame (Figure 6)

Crushing of rods into finite elements	The frame in Figure 6a			The frame in Figure 6b	
	Finite element with three degrees of freedom, LIRA-SAPR	Finite element with five degrees of freedom	Difference of the results, %	Finite element with three degrees of freedom, LIRA-SAPR	Finite element with five degrees of freedom
1	0.1109	0.12341	10.1	1.7212	1.7212
2	0.1164	0.12341	5.7	1.7212	1.7212
4	0.1197	0.12341	3.0	1.7212	1.7212
8	0.1215	0.12341	1.5	1.7212	1.7212
16	0.1224	0.12341	0.8	1.7212	1.7212

The results of calculations for the frame in Figure 6 show, that with additional crushing of the rods into finite elements (from 1 to 16):

1. for a finite element with five degrees of freedom – critical load parameter λ_{cr} does not change for both loading schemes;
2. for a finite element with three degrees of freedom – value of the critical load parameter λ_{cr} , for the action of the distributed load (Figure 6a), increases by approximately 10 % and approaches the value obtained for a finite element with five degrees of freedom (Figure 7);
3. for a finite element with three degrees of freedom – value of the critical load parameter λ_{cr} , for the action of a concentrated load (Figure 6b), does not change and is equal to the value obtained for a finite element with five degrees of freedom.

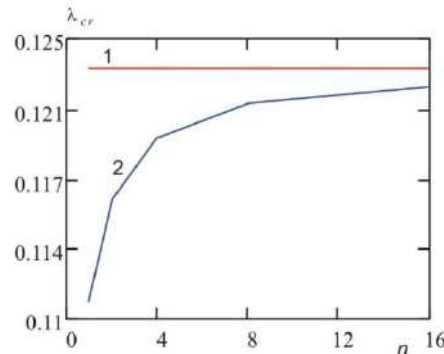


Figure 7. Changing the parameter λ_{cr} for the frame in Figure 6a, depending on the division of the rods into finite elements.

1 – for finite element with 5 degrees of freedom; 2 – for finite element with 3 degrees of freedom.

Figure 8 and Table 5 show the results of calculating the critical load parameter for a three-story frame, depending on the number of finite elements into which each rod of the frame is divided. The flexural rigidity of the rods is $EI = 10 \text{ kH/m}^2$, longitudinal stiffness $EA = 100 \text{ kH}$. The columns of the frame are rigidly clamped, and the crossbars have hinged fixed supports.

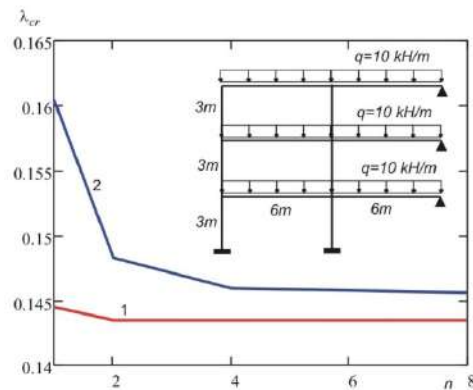


Figure 8. Changing the parameter λ_{cr} for the three-story frame, depending on the division of the rods into finite elements.

1 – for finite element with 5 degrees of freedom; 2 – for finite element with 3 degrees of freedom.

Table 5. Critical loading parameter λ_{cr} for the frame (Figure 8)

Crushing of rods into finite elements	Finite element with three degrees of freedom, LIRA-SAPR	Finite element with five degrees of freedom
1	0.1605	0.1445
2	0.1482	0.1434
4	0.1459	0.1434
8	0.1456	0.1434

The results of calculations for the frame in Figure 8 show, that with additional crushing of the rods into finite elements (from 1 to 8):

1. for finite elements with five degrees of freedom, the critical load parameter λ_{cr} decreases by 0.8 %, when rods divided by two finite elements, and does not change with further crushing of the rods;
2. for finite elements with three degrees of freedom, the value of the critical load parameter λ_{cr} decreases by approximately 9 % and approaches the value obtained for finite element with five degrees of freedom.

4. Conclusion

1. The introduction of additional degrees of freedom at the nodes, in the form of the curvature of the axis and longitudinal deformation, makes it possible in many cases to more accurately determine the

magnitude of the critical load. In this case, the system has more degrees of freedom, so the approximation of the forms of stability loss is more accurate.

2. For some calculation schemes, for example, shown in Figures 3–5, when using a classical finite element with three degrees of freedom, the critical parameter is determined with a significant error of 20 % to 100 %. To increase the accuracy of determining the critical load, it is necessary to divide the rods into several finite elements. When using a finite element with five degrees of freedom, the error in calculating the critical parameter is no more than 10.1 % without additional crushing of the rods.

3. For computational schemes, in which there are no distributed loads and in which there are enough degrees of freedom in the form of displacements of nodes along the coordinate axes, the solutions for the two finite elements under consideration coincide.

4. For the frame in Figure 6, for finite element with three degrees of freedom, with additional division of the rods into finite elements, the value of the critical load parameter increases and approaches the value obtained for the finite element with five degrees of freedom.

5. For the frame in Figure 8, for finite element with three degrees of freedom, with additional division of the rods into finite elements, the value of the critical load parameter decreases by approximately 9 %, and approaches the value, obtained for the finite element with five degrees of freedom.

6. The use of the finite element with five degrees of freedom will avoid possible large errors in the determination of critical forces for design schemes in which no additional crushing of the rods into finite elements is used.

References

- Zenkevich O. *Metod konechnykh elementov v tekhnike* [Finite element method in engineering]. Moscow: Mir, 1975. 541 p.(rus)
- Zenkevich O., Morgan K. *Konechnyye elementy i approksimatsiya* [Finite Elements and Approximation]. Moscow: Mir, 1986. 318 p.(rus)
- Gallager R. *Metod konechnykh elementov. Osnovy* [Finite element method. Basics]. Moscow: Mir, 1984. 428 p.(rus)
- Yevzerov I.D. Stability problems for rods and plates]. *Magazine of Civil Engineering*. 2014. No. 1(45). Pp. 6–11. (rus)
- Noor A.K., Green W.H., Hartley S.J. Nonlinear finite element analysis of curved beams. *Comput. Meth. Appl. Mech. and Eng.* 1977. Vol. 12. No. 3. Pp. 289–307.
- Schmidt W.F. Nonlinear bending of beams using the finite element method. *Comput. and Struct.* 1978. Vol. 8. No. 1. Pp. 153–158.
- Tuna M., Kirca M. Exact solution of Eringen's nonlocal integral model for bending of Euler–Bernoulli and Timoshenko beams. *International Journal of Engineering Science*. 2016. Vol. 105. Pp. 80–92.
- Kucukler M., Gardner L., Macorini L. Flexural–torsional buckling assessment of steel beam–columns through a stiffness reduction method. *Engineering Structures*. 2015. Vol. 101. Pp. 662–676.
- Zhong H., Zhang R., Yu H. Buckling analysis of planar frameworks using the quadrature element method. *International Journal of Structural Stability and Dynamics*. 2011. Vol. 11. No. 2. Pp. 363–378.
- Xiao N., Zhong H. Non-linear quadrature element analysis of plane frames based on geometrically exact beam theory. *Int. J. Non-linear Mech.* 2012. Vol. 47. Pp. 481–488.
- Javidinejad A. Buckling of beams and columns under combined axial and horizontal loading with various axial loading application location. *Journal of Theoretical and Applied Mechanics*. 2012. Vol. 42. No. 4. Pp. 19–30.
- Yuan W.B., Kim B., Li L. Y. Buckling of axially loaded castellated steel columns. *J. Construct. Steel Res.* 2014. No. 92. Pp. 40–45.
- Soltani M.R., Bouchaïr A., Mimoune M. Nonlinear FE analysis of the ultimate behaviour of steel castellated

Литература

- Зенкевич О. *Метод конечных элементов в технике*. М.: Мир, 1975. 541 с.
- Зенкевич О., Морган К. *Конечные элементы и аппроксимация*. М.: Мир, 1986. 318 с.
- Галлагер Р. *Метод конечных элементов. Основы*. М.: Мир, 1984. 428 с.
- Евзеров И.Д. Задачи устойчивости для стержней и пластин// *Инженерно-строительный журнал*. 2014. № 1(45). С. 6–11.
- Noor A.K., Green W.H., Hartley S.J. Nonlinear finite element analysis of curved beams // *Comput. Meth. Appl. Mech. and Eng.* 1977. Vol. 12. № 3. Pp. 289–307.
- Schmidt W.F. Nonlinear bending of beams using the finite element method // *Comput. and Struct.* 1978. Vol. 8. № 1. Pp. 153–158.
- Tuna M., Kirca M. Exact solution of Eringen's nonlocal integral model for bending of Euler–Bernoulli and Timoshenko beams // *International Journal of Engineering Science*. 2016. Vol. 105. Pp. 80–92.
- Kucukler M., Gardner L., Macorini L. Flexural–torsional buckling assessment of steel beam–columns through a stiffness reduction method // *Engineering Structures*. 2015. Vol. 101. Pp. 662–676.
- Zhong H., Zhang R., Yu H. Buckling analysis of planar frameworks using the quadrature element method // *International Journal of Structural Stability and Dynamics*. 2011. Vol. 11. № 2. Pp. 363–378.
- Xiao N., Zhong H. Non-linear quadrature element analysis of plane frames based on geometrically exact beam theory // *Int. J. Non-linear Mech.* 2012. Vol. 47. Pp. 481–488.
- Javidinejad A. Buckling of beams and columns under combined axial and horizontal loading with various axial loading application location // *Journal of Theoretical and Applied Mechanics*. 2012. Vol. 42. № 4. Pp. 19–30.
- Yuan W.B., Kim B., Li L.Y. Buckling of axially loaded castellated steel columns // *J. Construct. Steel Res.* 2014. № 92. Pp. 40–45.
- Soltani M.R., Bouchaïr A., Mimoune M. Nonlinear FE analysis of the ultimate behaviour of steel castellated beams // *J. Constr. Steel Res.* 2012. Vol. 70. Pp. 101–114.
- Salem A.H., El Dib F.F., El Aghoury M., Hanna M.T.

Тюкалов Ю.Я. Улучшенный стержневой конечный элемент для решения задач устойчивости // *Инженерно-строительный журнал*. 2018. № 3(79). С. 54–65.

- beams. *J. Constr. Steel Res.* 2012. Vol. 70. Pp. 101–114.
14. Salem A.H., El Dib F.F., El Aghoury M., Hanna M.T. Elastic stability of planar steel frames with unsymmetrical beam loading. *Journal of structural engineering.* 2004. Vol. 130. No. 11. Pp. 1852–1859.
 15. Manuylov G.A., Kositsyn S.B., Begichev M.M. Chislennoye issledovaniye prostranstvennoy ustoychivosti uprugikh krugovykh zashchemlennykh arok [Numerical study of the spatial stability of elastic circular pinched arches]. *International Journal for Computational Civil and Structural Engineering.* 2013. Vol. 9. No. 1. Pp. 78–84.(rus)
 16. Senjanović I., Vladimir N., Cho D.-S. A simplified geometric stiffness in stability analysis of thin-walled structures by the finite element method. *Inter J. Nav. Archit. Oc. Engng.* 2012. Vol. 4. Pp. 313–321.
 17. Lalin V., Rybakov V., Alexander S. The finite elements for design of frame of thin-walled beams. *Applied Mechanics and Materials.* 2014. Vol. 578-579. Pp. 858–863.
 18. Lalin V.V., Rozin L.A., Kushova D.A. Variatsionnaya postanovka ploskoy zadachi geometricheski nelineynogo deformirovaniya i ustoychivosti uprugikh sterzhney [Variational formulation of the plane problem of geometrically nonlinear deformation and stability of elastic rods]. *Magazine of Civil Engineering.* 2013. No. 1(36). Pp. 87–96.(rus)
 19. Qiu W., Demkowicz L. Mixed hp-finite element method for linear elasticity with weakly imposed symmetry: stability analysis. *SIAM J. Numer. Anal.* 2011. Vol. 49. No. 2. Pp. 619–641.
 20. Kim B., Li L., Edmonds A. Analytical solutions of lateral-torsional buckling of castellated beams. *International Journal of Structural Stability and Dynamics.* 2016. Vol. 16. No. 8. Pp. 443–455.
 21. Blyumin S.L., Zverev V.V., Sotnikova I.V., Sysoyev A.S. Resheniye zadachi ustoychivosti szhato-izgibayemykh zhestko opertykh sterzhney peremennoy zhestkosti [The solution of the problem of the stability of squeezed-bent rigidly supported rods of variable rigidity]// *Vestnik MGSU.* 2015. No. 5. Pp. 18–26.(rus)
 22. Dubrovin V.M., Butina T.A. Modelirovaniye ustoychivosti szhatogo i skruchennogo sterzhnya v tochnoy postanovke zadachi [Simulation of the stability of a compressed and twisted rod in the exact formulation of the problem]. *Matematicheskoye modelirovaniye i chislennyye metody.* 2015. No. 3. Pp. 3–16.(rus)
 23. Kuo Y.-L. Stress-based finite element analysis of sliding beams. *Appl. Math. Inf. Sci.* 2015. Vol. 9. No. 2. Pp. 609–616.
 24. Tyukalov Yu.Ya. The functional of additional energy for the analysis of the stability of spatial rod systems. *Magazine of Civil Engineering.* 2017. No. 2(70). Pp. 18–32. (rus)
 25. Tyukalov Yu.Ya. *Raschet zhelezobetonnykh ploskikh sterzhnevyykh sistem na kratkovremennyye dinamicheskiye vozdeystviya s uchetom fizicheskoy nelineynosti* [Calculation of reinforced concrete flat rod systems on short-term dynamic influences taking into account physical nonlinearity]. PhD dissertation. Kirov, 1990. 140 p.(rus)
 26. Timoshenko S. P. Ustoychivost sterzhney, plastin i obolochek [Stability of rods, plates and shells]. Moscow: Nauka, 1971. 808 p.(rus)
- Elastic stability of planar steel frames with unsymmetrical beam loading // *Journal of structural engineering.* 2004. Vol. 130. № 11. Pp. 1852–1859.
15. Мануйлов Г.А., Косицын С.Б., Бегичев М. М. Численное исследование пространственной устойчивости упругих круговых защемленных арок// *International Journal for Computational Civil and Structural Engineering.* 2013. Vol. 9. № 1. Pp. 78–84.
 16. Senjanović I., Vladimir N., Cho D.-S. A simplified geometric stiffness in stability analysis of thin-walled structures by the finite element method // *Inter J. Nav. Archit. Oc. Engng.* 2012. Vol. 4. Pp. 313–321.
 17. Lalin V., Rybakov V., Alexander S. The finite elements for design of frame of thin-walled beams// *Applied Mechanics and Materials.* 2014. Vol. 578–579. Pp. 858–863.
 18. Лалин В.В., Розин Л.А., Кушова Д.А. Вариационная постановка плоской задачи геометрически нелинейного деформирования и устойчивости упругих стержней // *Инженерно-строительный журнал.* 2013. № 1(36). С. 87–96.
 19. Qiu W., Demkowicz L. Mixed hp-finite element method for linear elasticity with weakly imposed symmetry: stability analysis // *SIAM J. Numer. Anal.* 2011. Vol. 49. № 2. Pp. 619–641.
 20. Kim B., Li L., Edmonds A. Analytical solutions of lateral-torsional buckling of castellated beams // *International Journal of Structural Stability and Dynamics.* 2016. Vol. 16. № 8. Pp. 443–455.
 21. Блюмин С.Л., Зверев В.В., Сотникова И.В., Сысоев А.С. Решение задачи устойчивости сжато-изгибаемых жестко опертых стержней переменной жесткости // *Вестник МГСУ.* 2015. № 5. С. 18–26.
 22. Дубровин В.М., Бутина Т.А. Моделирование устойчивости сжатого и скрученного стержня в точной постановке задачи // *Математическое моделирование и численные методы.* 2015. № 3. С. 3–16.
 23. Kuo Y.-L. Stress-based finite element analysis of sliding beams // *Appl. Math. Inf. Sci.* 2015. Vol. 9. № 2. Pp. 609–616.
 24. Тюкалов Ю.Я. Функционал дополнительной энергии для анализа устойчивости пространственных стержневых систем // *Инженерно-строительный журнал.* 2017. № 2(70). С. 18–32.
 25. Тюкалов Ю.Я. Расчет железобетонных плоских стержневых систем на кратковременные динамические воздействия с учетом физической нелинейности : диссертация ... кандидата технических наук : 05.23.17. - Киров, 1990. 140 с.
 26. Тимошенко С.П. Устойчивость стержней, пластин и оболочек. М.: Наука, 1971. 808 с.

Yury Tyukalov,
+7(912)8218977; yutvgu@mail.ru

Юрий Яковлевич Тюкалов,
+7(912)8218977; эл. почта: yutvgu@mail.ru

© Tyukalov Yu. Ya., 2018

doi: 10.18720/MCE.79.7

Self-compacting concrete using pretreated rice husk ash

Самоуплотняющийся бетон с использованием
предварительно подготовленной золы рисовой шелухи**R.S. Fediuk,***Far Eastern Federal University, Vladivostok, Russia***V.S. Lesovik,***V.G. Shukhov Belgorod State Technological University, Belgorod, Russia***A.P. Svintsov,***Peoples' Friendship University of Russia, Moscow, Russia***A.V. Mochalov,****S.V. Kulichkov,****N.Y. Stoyushko,****N.A. Gladkova,****R.A. Timokhin,***Far Eastern Federal University, Vladivostok, Russia***Канд. техн. наук, доцент Р.С. Федюк,***Дальневосточный Федеральный Университет, г. Владивосток, Россия***д-р техн. наук, заведующий кафедрой****В.С. Лесовик,***Белгородский государственный технологический университет**им. В.Г. Шухова, г. Белгород, Россия***д-р техн. наук, заведующий кафедрой****А.П. Свинцов,***Российский университет дружбы народов, Москва, Россия***заместитель начальника учебного****военного центра А.В. Мочалов,****канд. техн. наук, доцент С.В. Куличков,****канд. экон. наук, заместитель директора****филиала Н.Ю. Стоюшко,****канд. экон. наук, доцент Н.А. Гладкова,****студент Р.А. Тимохин,***Дальневосточный Федеральный**Университет, г. Владивосток, Россия***Key words:** self-compacting concrete; rice husk ash; pozzolanic materials; heat treatment; fresh properties; mechanical properties**Ключевые слова:** самоуплотняющийся бетон; зола рисовой шелухи; пуццолановые материалы; тепловая обработка; свойства бетонной смеси; механические свойства

Abstract. Self-compacting concrete was obtained by partially replacing Portland cement with a previously prepared rice husk ash. Preliminary preparation included the thermal treatment of the ash under various conditions. The optimum technology of preparation, allowing to receive a homogeneous concrete mix is revealed. All concrete mixtures were designed in such a way as to have a slump flow of 680 ± 30 mm in diameter, which was achieved by using different dosages of a superplasticizer based on polycarboxylate ether. All mixtures with the replacement of cement by ash to 25 % meet the requirements for rheological characteristics and resistance to segregation. The bulk density for the samples with 10 %, 15 %, 20 % and 25 % of the rice husk ash was reduced by 3.19 %, 5.18 %, 5.58 and 6.37 % respectively, compared to the samples without ash. An increase in the rice husk ash content led to a decrease in the early mechanical properties, while the final strength of self-compacting concrete containing ash was comparable to conventional samples. This was achieved due to the pozzolanic activity of the ash. Inclusion of rice husk ash reduced the amount of portlandite in the system by obtaining an additional C-S-H gel, which led to matrix compacting and blocking of networks with open porosity.

Аннотация. Самоуплотняющийся бетон получен путем частичной замены портландцемента предварительно подготовленной золой рисовой шелухи. Предварительная подготовка включала в себя термическую обработку золы при различных условиях. Выявлена оптимальная технология приготовления, позволяющая получить однородную бетонную смесь. Все бетонные смеси были спроектированы таким образом, чтобы иметь осадку конуса диаметром 680 ± 30 мм, что было достигнуто за счет использования различных дозировок суперпластификатора на основе поликарбоксилатного эфира. Все смеси с заменой цемента золой до 25 % отвечают требованиям к реологическим характеристикам и сопротивлению расслоению. Объемная плотность для образцов

Федюк Р.С., Лесовик В.С., Свинцов А.П., Мочалов А.В., Куличков С.В., Стоюшко Н.Ю., Гладкова Н.А., Тимохин Р.А. Самоуплотняющийся бетон с использованием предварительно подготовленной золы рисовой шелухи // Инженерно-строительный журнал. 2018. № 3(79). С. 66–76.

с 10 %, 15 %, 20 % и 25 % золы рисовой шелухи была снижена на 3,19 %, 5,18 %, 5,58 и 6,37 % соответственно по сравнению с образцами без золы. Увеличение содержания золы рисовой шелухи привело к снижению ранних механических свойств, тогда как конечная прочность самоуплотняющегося бетона, содержащего золу, была сопоставима с обычными образцами. Это было достигнуто за счет пуццолановой активности золы. Включение золы рисовой шелухи уменьшило количество портландита в системе за счет получения дополнительного геля C-S-H, что привело к уплотнению матрицы и блокированию сетей с открытой пористостью.

1. Introduction

Self-compacting concrete (SCC) is characterized by the fact that under its own weight a dispersed-reinforced concrete mix completely fills the formwork without the need for an external seal. Delamination resistance and adaptability allow the SCC remain homogeneous and to maintain stable characteristics. SCC is mainly characterized by excellent workability of the concrete mix. Reducing labor and construction time, improving the quality of the finished surface make self-compacting concrete better than ordinary concrete. Nevertheless, the production of self-compacting concrete with high workability and the required strength requires more cement and the addition of expensive chemical impurities to reduce the amount of water-binding ratio, which leads to an increase in the cost of self-compacting concrete. Furthermore, the SCC production occurs more carbon dioxide emissions than ordinary concrete production. And also, a higher consumption of Portland cement in SCC mixture leads to an increase in hydration energy and high autogenous shrinkage [1].

Addition of pozzolanic materials leads to energy savings and materials costs, economic efficiency, durability, increased productivity of workplaces [2]. In addition, the best performance characteristics of concrete are achieved by reducing of energy of hydration and autogenous shrinkage [3]. In addition, in terms of environmental considerations, reducing cement consumption results in energy and resource savings, as well as a significant reduction in greenhouse gas emissions [4].

Nearly one hundred million tons of ordinary rice husks are produced every year, which is an excellent raw material – cheap, renewable, with a chemical composition that is constant for a given region and plant variety, suitable for obtaining about 15 million tons of pure amorphous silica. In particular, according to prof. L. Zemnuhova et al [5], from 1 ton of rice husks it is possible to obtain from 120 to 200 kg of silica with a SiO₂ content of 90 to 99.999 %. In addition, from the standpoint of environmental protection, waste utilization is one of priority tasks [6]. A successful implementation of this task can be rice husk ash (RHA) using as an alternative material in the production of concrete.

The use of crop waste for the production of building materials was investigated in a number of papers by the world leading experts. In these works, the possibility of using rice husk ash in cementitious materials based on Portland cement has been proved [7–10].

Therefore, the abundance of RHA, coupled with a high content of SiO₂ in them, opens the way for its use as a partial replacement of Portland cement and the development of concrete with high mechanical characteristics [10]. In particular, the additive RHA improves the strength of concrete, due to the increase in the amount of CSH gel during the hydration process over time. However, to our knowledge, the use of RHA as pozzolanic materials as partial replacements of Portland cement has not been widely investigated in the self-compacting concrete. Considering the agglomeration of particles and their inherent high requirements for water consumption for the addition of RHA, it is expected that its inclusion in Portland cement based self-compacting concrete will reduce the rigidity of the mixture and, therefore, will adversely affect the properties of the matrix of setting concrete.

Thus, the purpose of the research is to study the effect of partial replacement of RHA in self-compacting Portland cement based concrete by 10, 15, 20, 25 and 30 wt. % of a binder in a concrete mixture and as well as in a concrete when applying a compression load.

To achieve this purpose, accomplished tasks include the following:

- research of the physical properties and chemical composition, and the structure of the raw materials;
- pretreatment of rice husk ash for increase its activity;
- determination of fresh properties the self-compacting concrete;
- research of concrete strength characteristics

2. Materials and Methods

2.1. Materials

The Spassky Portland cement type CEM I 42.5 N was applied for concrete samples. Parts of the rice plants of the Khankaisky district (Primorsky Krai) were burned to get ash for the RHA production. This RHA contained large particles and impurities. In addition, since the RHA was stored in an open area after production with an unknown moisture condition, it was dried at 105 °C for 24 hours before use in the composite binder. Then the dried RHA was sieved through a 300 µm sieve to remove coarse particles and impurities. Then the ash was ground in a vario-planetary mill to increase the specific surface area (550 m²/kg) and, accordingly, the reactivity. Physical characteristics and chemical composition of the starting materials are presented in Table 1 and Table 2.

Table 1. Physical characteristics of raw materials

Characteristic	Coarse aggregate	Fine aggregate	Portland cement	RHA
Maximum size, mm	12.4	4.65		
Water absorption, %	0.42	1.14		
Size module	6.2	2.93		
Passage through a 45-µm sieve (No. 325), %			92	97
Average particle size, µm			14.5	11
Specific gravity, kg/m ³	2.61	2.57	3.14	1.82

Table 2. The chemical composition of Portland cement and RHA

Content of elements in terms of oxides, %	RHA	Portland cement
SiO ₂	84.3	20.2-20.9
Al ₂ O ₃	1.1	6.0-6.7
Fe ₂ O ₃	0.3	3.5-4.0
CaO	0.5	66.2-67
MgO	0.9	1.4-2.0
K ₂ O	3.7	-
Na ₂ O	1.0	-
SO ₃	0.1	-
LOI	8.1	0.18

Both Portland cement and RHA are in the form of agglomerated particles, but RHA has a more porous structure than Portland cement. As shown in Figure 1, the particle size distribution of the materials after preparation of the rice husk ash becomes smaller than that of the Portland cement.

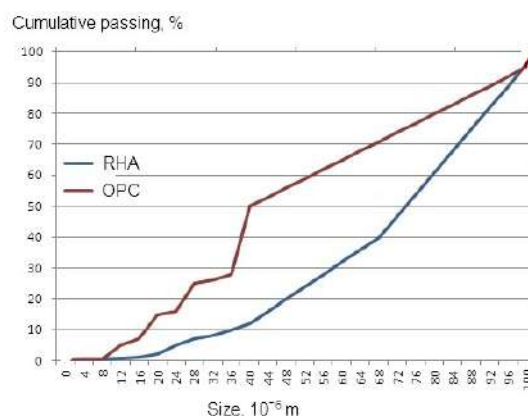


Figure 1. Particle size distribution for ground ash and Ordinary Portland cement (OPC)

Федюк Р.С., Лесовик В.С., Свинцов А.П., Мочалов А.В., Куличков С.В., Стоюшко Н.Ю., Гладкова Н.А., Тимохин Р.А. Самоуплотняющийся бетон с использованием предварительно подготовленной золы рисовой шелухи // Инженерно-строительный журнал. 2018. № 3(79). С. 66–76.

Various types of pretreatment of ash were used to increase the reactivity, as shown in Table 3.

Table 3. Pretreatment of ash used in the study

Heat treatment methods	Processing sequence			
	Pre-drying at 105 °C	Moistening	Heat treatment at 800 °C	Cooling in cold water
1. PD – Pre-drying (reference sample)	X		X	
2. US – Unprepared sample			X	
3. MD – Moistening / drying		X	X	
4. Moistening / drying / cooling		X	X	X

The reference sample of the ash is preliminarily held at 105 °C for 24 hours, then heated to 800 °C at a heating rate of 10 °C/min and cooled at room temperature.

The second set of samples, marked as unprepared, was heated directly to 800 °C using a heating rate of 10 °C/min and cooled at room temperature without preliminary and subsequent treatment.

The following samples, called MD, were preliminarily held under water for 24 hours to fill all the pores with water. The ash was then removed from the water and placed in a preheated oven at a temperature of 800 °C for 60 minutes and gradually cooled.

The last set of samples designated as MDC was treated similarly to the MD, but after heat treatment at 800 °C for 60 minutes, they were immediately cooled in cold water. It was found that shock cooling leads to the formation of cracks in the ash particles. The powder was then dried at 300 °C for 30 minutes.

Thus, the surface area of the RHA was increased using furnaces. This increase in particle size is caused by the formation of cracks, because the captured porous water can not be removed as quickly as it evaporates. This causes internal stress, which leads to the formation of cracks. When the RHA powder is heated to 800 °C, the sintering of the particles leads to deformation. In addition, as was revealed in [1], during the preheating reactivation of the RHA occurs. Both effects in combination result in a reduced setting time and an increase in compressive strength at the beginning.

As a fine aggregate, the local mountain sand was used with a modulus of fineness 2.93, specific gravity 2.57 kg/m³ and water absorption 1.14 %. As a coarse aggregate, limestone crushed stone was used with a maximum size of 12.4 mm, specific gravity 2.61 kg/m³ and water absorption 0.42 %. The test procedures and data obtained were in accordance with ASTM C33 [11], GOST 8736-2014 [12] and GOST 8269.0-97 [13] for compliance.

2.2. The proportions of the mixtures

The ground RHA was used as a partial replacement for Type I Portland cement in the proportions of 10 %, 15 %, 20 %, 25 % and 30 % by weight of the binder content. The composition of the mixtures of self-compacting concrete included 475 kg/m³ of binder and a water-binder ratio of 0.34 for all samples, as shown in Table 4. Superplasticizer "HIDETAL-GP-9" alpha "A" (SKT-Standard, Russia) was used in SCC to reduce the water-cement ratio. "HYDETAL-GP-9" alpha "A" promotes maximum water reduction, which meets the requirements of superplasticizers in accordance with ASTM C494 [14] and GOST 24211-2008 [15]. Due to the agglomerated shape of the RHA particles, a higher superplasticizer was used to obtain a similar workability of the samples.

Table 4. Design of sample compositions

Mixture number	Water-binder ratio	OPC, kg/m ³	RHA, kg/m ³	Fine aggregate, kg/m ³	Coarse aggregate, kg/m ³	Water, kg/m ³	Superplasticizer, % of binder			
0-PD*	0.34	475	0	930	749	151.5	1.1			
0-US**										
0-MD***										
0-DC****										
10-PD		427.5	47.5							1.2
10-US										
10-MD										
10-MDC										
15-PD		403.75					71.25			1.3
15-US							71.25			
15-MD							71.25			
15-MDC							71.25			
20-PD		380					95			1.4
20-US							95			
20-MD							95			
20-MDC							95			
25-PD		356.25					118.75			1.5
25-US							118.75			
25-MD							118.75			
25-MDC							118.75			
30-PD	332.5		142.5			1.6				
30-US			142.5							
30-MD			142.5							
30-MDC			142.5							

* – PD – Pre-drying

** – US – Unprepared sample

*** – MD – Moistening / drying

**** – MDC – Moistening / drying / cooling

2.3. Methods for preparing and testing samples

2.3.1. Fresh properties

Coarse and fine aggregates were mixed first. Then 10 % water was added. Then, cement and RHA were added to the mixture, followed by the addition of 50 % water. The remaining proportion of water was added to the mixture with the superplasticizer, so that homogeneous mixtures could be obtained. Usually the process of mixing self-compacting concrete mixes requires more time than ordinary concrete mixes. It should be noted that the inclusion of RHA leads to a further level of complexity in meeting the test requirements for SCC, so the maximum RHA content selected in this study was limited to 30 % due to the higher water demand for ash. The properties of the concrete mix have been tested in accordance with [16–18] for workability and resistance to delamination after mixing. Initially, the mixtures were examined for the slump flow and slump flow for 50 seconds.

2.3.2. Research of concrete strength characteristics

Fresh properties of the concrete mixture were determined immediately after mixing. Then, cubes with an edge of 100 mm and prisms 100 x 100 x 500 mm in two layers of 5 cm each were molded from the concrete mix. The concrete mixture filled the molds under its own weight, without additional compaction. Then, the upper surface of the samples was smoothed and aligned by hand. After pouring,

Федюк Р.С., Лесовик В.С., Свинцов А.П., Мочалов А.В., Куличков С.В., Стоюшко Н.Ю., Гладкова Н.А., Тимохин Р.А. Самоуплотняющийся бетон с использованием предварительно подготовленной золы рисовой шелухи // Инженерно-строительный журнал. 2018. № 3(79). С. 66–76.

all samples were held for 24 hours under ambient conditions. The samples were then taken out of the mold and kept in water at 25 ± 3 °C until the day of testing.

The bulk density of the final samples was measured using the Archimedes method. To observe the effect of RHA content on the microstructure of self-compacting concrete, electron microscopy images (FESEM MIRA 3 TESCAN) were obtained. The compressive strength of the samples was obtained on 100 mm cubes at the age of 7 and 28 days. All mechanical tests were completed using a Servo-hydraulic Fatigue and Endurance Tester Shimadzu Servopulser U-type with capacity of 200 kN according to BS EN 12390-3:2002.

The error in the results of the experiments is no more than 5 %, so the results can be considered adequate.

3. Results and Discussions

3.1. Fresh properties of concrete mixes

The test results for fresh SCC properties were determined by performing filling tests (slump flow, $T_{50\text{cm}}$ slump flow and V-funnel spread time), passing tests (U-box and L-box flow) and the segregation resistance test of various SCC mixtures. The results of studies of the properties of the concrete mixes are given in Figure 2.

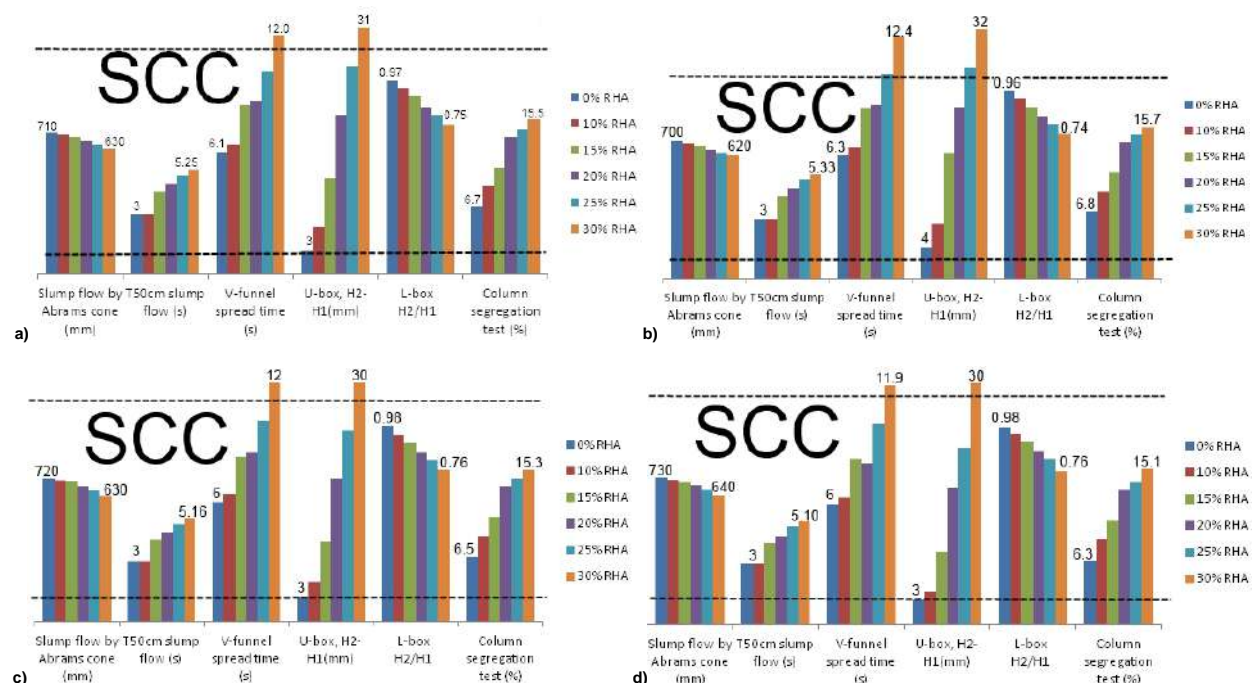


Figure 2. Fresh properties of concrete mixes: a) Pre-drying; b) Unprepared sample; c) Moistening / drying; d) Moistening / drying / cooling

For the study of unconfined flowability, all concrete mixtures were designed in such a way as to have a slump flow of an average diameter of 680 ± 30 mm, which was achieved by using different superplasticizer values. However, for a number of samples this was not achieved. In particular, this is observed for an unprepared sample with 25 % ash and for all samples with the replacement of 30 % ash. Thus, an increase in the ash content of the mixtures led to a reduction in workability due to a higher specific surface area of the ash particles, which led to a greater consumption of water to facilitate movement and rolling of particles over each other. Nevertheless, in the RHA there are still some unmilled or insufficiently ground particles. This can be found in previous studies [1, 21–25], from which it can be concluded that the particles of the grounded and unmilled RHA are extremely porous and agglomerated, while the Portland cement particles were denser even than the RHA with a reduced form. As the water content increases, the porosity increases too, this can lead to unfavorable effects on the properties of the concrete mix. The results of V-funnel and $T_{50\text{cm}}$ flow times for RHA mixtures were close to the control mixture and ranged between 6.0–12.4 s and 3–5.33 s, respectively, as shown in Figure 2. In addition, the data obtained showed that all mixtures with ash replacement by up to 25 % of ash meet the requirements of segregation resistance according to [18]. A higher content of RHA showed an increase in the viscosity

of the concrete, which led to a decrease in slump flow, U-box and L-box, while it increased the flow time of the $T_{50\text{ cm}}$, V-funnel and the segregation index. Summarizing, it can be concluded that up to 25 % of cement can be replaced by rice husk ash without adversely affecting the properties of the concrete mix. The results of the study of the properties of concrete mixtures are in good agreement with previous studies published by [1, 19, 20, 27].

3.2. Mechanical properties of concrete

The bulk density of the samples was reduced by increasing the percentage of RHA in SCC, as shown in Figure 3.

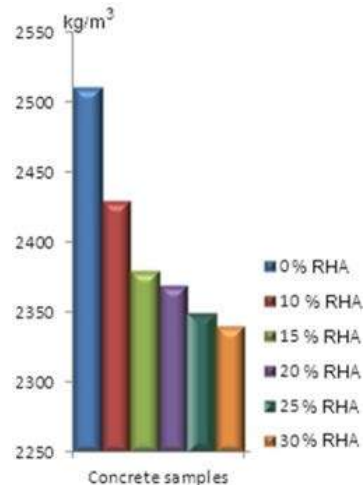


Figure 3. Bulk density of the concrete samples

The greatest decrease in bulk density was 6.77 % due to the inclusion of 30 % RHA in SCC. The bulk density for samples with 10 %, 15 %, 20 % and 25 % RHA was reduced by 3.19 %, 5.18 %, 5.58 % and 6.37 % respectively, compared to samples without RHA. The decrease in the density of concrete samples can be explained by several reasons. The main reason may be that the RHA has a lower specific gravity than cement. In Figure 4 microphotographs of cement stone without additives and cement stone with replacing 25 % of cement with rice husk ash are presented. It can be concluded from Figure 4 that the sample without RHA content is denser than the sample with 25 % RHA.

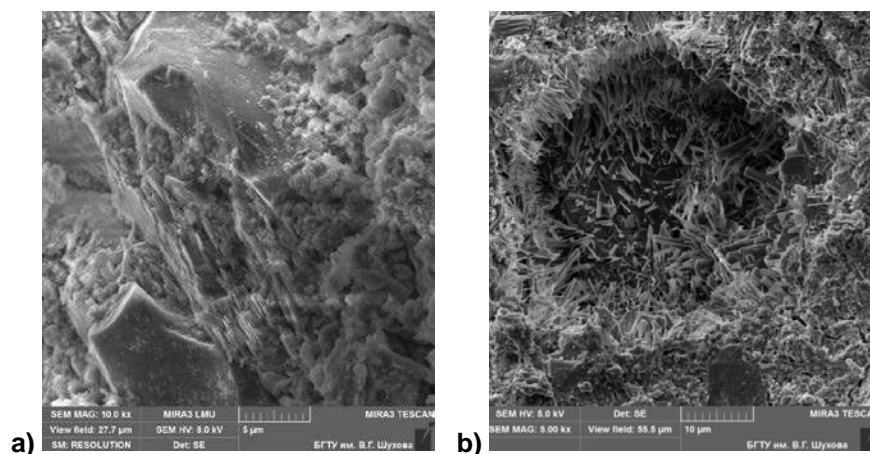


Figure 4. Microphotographs of cement stone without additives (a) and cement stone with replacing 25 % of cement by rice husk ash (b)

The initial study showed that preheat treatment of RHA not only affects the particle size distribution, but also causes dehydroxylation [1]. It is expected that both effects will be useful for the mechanical properties of concrete.

The tests in this paper were focused on the activity of the optimized composite binder, and, accordingly, the strength characteristics of self-compacting concrete. It was found that after 28 days, the maximum compressive strength and prismatic strength measure for the MDC samples, then the MD, then

the unprepared samples, and the lowest strength for the reference samples when heated to 800 °C. The mechanical properties of self-compacting concrete, in which the introduced RHA are preliminarily prepared, are shown in Figure 5.

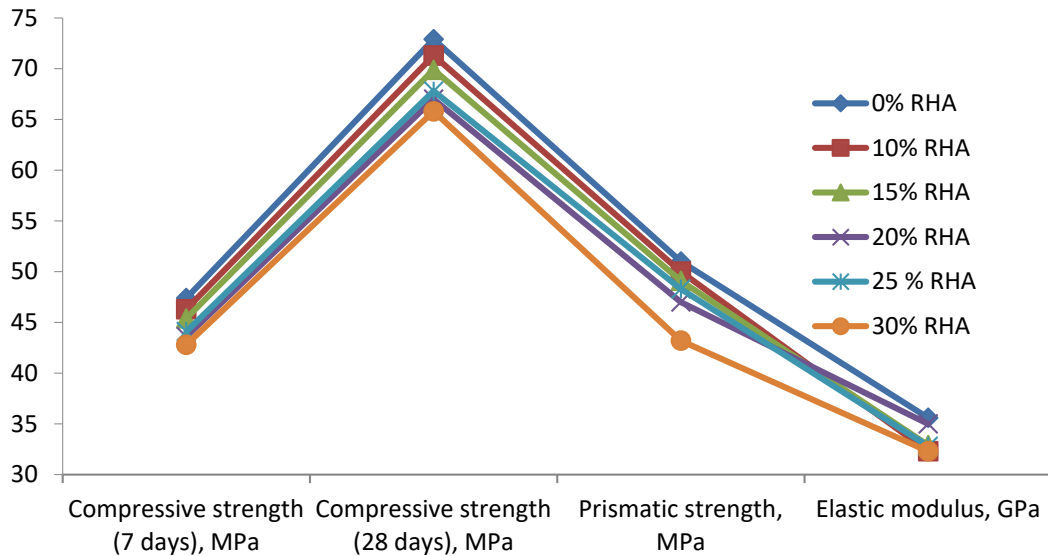


Figure 5. Strength characteristics of self-compacting concrete

According to the spread of the elastic modulus of the samples, no dependence is observed either on the amount of the introduced RHA, or on its method of preliminary preparation. It is obvious that elastic modulus of self-compacting concrete primarily depends on the amount of coarse aggregate what was revealed earlier [21, 22].

If we monitor the dependence of the 28-day strength on the amount of ash introduced, the following is noted. Samples containing RHA have slightly lower compressive strengths than conventional SCCs without RHA.

As a rule, the process of hydration of a composite binder can be divided into two main stages. The first stage is mainly related to the reaction of cement and water; the second stage is associated with the pozzolanic activity of ash with portlandite neoplasms from cement hydration. As a result of the reaction of alite and water, a C-S-H gel and portlandite are formed. Since hardening of the C-S-H gel is the main factor in enhancing the strength of concrete, a decrease in the content of Portland cement has led to a decrease in the strength of concrete. Meanwhile, the content of silicon dioxide in the RHA is able to react with portlandite and generates a secondary C-S-H gel. Therefore, the hardening of concrete occurs at a later stage in comparison with cement concrete. On the other hand, the pozzolanic reaction mainly contributes to the increase in compressive strength of concrete at a later age by improving the interfacial bond between the cement paste and the aggregate. In addition, the smallest particles of ash improve the strength of concrete, filling the gaps between the cement particles.

3.3. Place of rice husk ash among other mineral additives

Several composites with various mineral additives were compared. In particular, fine-grained concretes developed by the authors [21–22], as well as self-compacting concretes with the use of palm oil fuel ash [1] were considered.

The first concrete shows higher mechanical characteristics, in particular a compressive strength of about 80 MPa. This is achieved through the mechanochemical activation of the binder. However, the developed concretes with the use of fly ash do not provide the necessary rheological characteristics of self-compacting concrete. In addition, the fly ash of thermal power plants is potentially radioactive material, therefore, spectroscopic studies of the radioactive background of the raw materials are mandatory. On the contrary, the ash of the rice husks does not show a radioactive background.

The second composite, with the inclusion of palm oil fuel ash, is able to meet the requirements for self-compacting concrete mixtures (slump flow – 660–690 mm, depending on the percentage of the introduced ash, T_{50cm} spread time 3–4.57 s). The compressive strength at the age of 28 days is 50–55 MPa. However, these additives are not available for Russia, on the contrary, there are many ashes of rice husk in Russia, so it can be used as a mineral additive in concrete.

4. Conclusion

Thus, in the course of studying the mechanical properties of self-compacting concrete with partial replacement of Portland cement with rice husk ash, the following was revealed. As a rule, RHA as a secondary material has a great potential for use as a replacement for Portland cement in self-compacting concrete, which preserves the fresh and mechanical characteristics of the concrete mix and ready-mix concrete in an acceptable range. The surface area of the RHA was increased using furnaces. The particle size can even be increased by soaking the RHA in water and after quenching.

The inclusion of RHA led to a decrease in the workability of concrete, but with the help of an additional superplasticizer, these SCC properties for all samples were almost identical. An increase in the content of the RHA resulted in a decrease in the early mechanical properties, whereas the final strength of the SCC containing the RHA was comparable to that of the conventional samples. This was achieved due to the pozzolanic activity of the RHA. The inclusion of the RHA reduced the amount of portlandite in the system by obtaining an additional gel C-S-H, which led to matrix tightening and blocking of networks with open porosity. These results confirm the well-known patterns (for example, [3, 4, 27], which can be extended to pozzolanic additives of other species.

References

1. Ranjbar N., Behnia A., Alsubari B., Birgani P.M., Jumaat M.Z. Durability and mechanical properties of self-compacting concrete incorporating palm oil fuel ash. *Journal of Cleaner Production*. 2016. No. 112. Pp. 723–730.
2. Fediuk R.S., Yevdokimova Y.G., Smoliakov A.K., Stoyushko N.Y., Lesovik V.S. Use of geonics scientific positions for designing of building composites for protective (fortification) structures (Conference paper). *IOP Conference Series: Materials Science and Engineering*. 2017. Vol. 221(1). Pp. 012011.
3. Lesovik V.S., Urkhanova L.A., Gridchin A.M., Lkhasaranov S.A. Composite binders on the basis of pearlite raw material of Transbaikalia. *Research Journal of Applied Sciences*. 2014. No. 9(12). Pp. 1016–1020.
4. Ranjbar N., Kuenzel C. Influence of preheating of fly ash precursors to produce geopolymers. *J Am Ceram Soc*. 2017. No. 00. Pp. 1–10.
5. Zemnukhova L.A., Panasenko A.E., Artemyanov A.P., Tsoy E.A. Dependence of porosity of amorphous silicon dioxide prepared from rice straw on plant variety. *BioResources*. 2015. No. 10(2). Pp. 3713–3723.
6. Pelin G., Pelin C.-E., Ștefan A., Dincă I., Andronescu E., Ficai A. Mechanical and tribological properties of nanofilled phenolic-matrix laminated composites. *Materiali in Tehnologije*. 2017. No. 51(4). Pp. 569–575.
7. Shi C., Wu Z., Cao Z., Ling T.C., Zheng J. Performance of mortar prepared with recycled concrete aggregate enhanced by CO₂ and pozzolan slurry. *Cement and Concrete Composites*. 2018. No. 86. Pp. 130–138.
8. Chandra S. *Waste materials used in concrete manufacturing*. Westwood: Noyes Publication, 1997.
9. Siddique R. *Supplementary Cementing Materials*. Heidelberg: Springer, 2011.
10. Nesvetaev G.V., Ta Van Fan. Vliyanie beloj sazhi i metakaolina na prochnost' i deformatsionnye svoystva cementnogo kamnya [Effect of white carbon and metakaolin on the strength and deformation properties of cement stone]. *Engineering Journal of Don*. 2012. Vol. 4-1. P. 139.
11. *American Standard ASTM C33 / C33M-16e1*. Standard Specification for Concrete Aggregates, ASTM International, West Conshohocken, PA, 2016.
12. *Russian State Standard GOST 8736-2014*. Sand for construction works. Specifications. (rus)
13. *Russian State Standard GOST 8269.0-97*. Mountainous rock road-metal and gravel, industrial waste products for construction works. Methods of physical and mechanical

Литература

1. Ranjbar N., Behnia A., Alsubari B., Birgani P.M., Jumaat M.Z. Durability and mechanical properties of self-compacting concrete incorporating palm oil fuel ash // *Journal of Cleaner Production*. 2016. № 112. Pp. 723–730.
2. Fediuk R.S., Yevdokimova Y.G., Smoliakov A.K., Stoyushko N.Y., Lesovik V.S. Use of geonics scientific positions for designing of building composites for protective (fortification) structures (Conference paper) // *IOP Conference Series: Materials Science and Engineering*. 2017. Vol. 221(1). Pp. 012011.
3. Lesovik V.S., Urkhanova L.A., Gridchin A.M., Lkhasaranov S.A. Composite binders on the basis of pearlite raw material of Transbaikalia // *Research Journal of Applied Sciences*. 2014. No. 9(12), Pp. 1016–1020.
4. Ranjbar N., Kuenzel C. Influence of preheating of fly ash precursors to produce geopolymers // *J Am Ceram Soc*. 2017. № 00. Pp. 1–10.
5. Zemnukhova L.A., Panasenko A.E., Artemyanov A.P., Tsoy E.A. Dependence of porosity of amorphous silicon dioxide prepared from rice straw on plant variety // *BioResources*. 2015. № 10(2). Pp. 3713–3723.
6. Pelin G., Pelin C.-E., Ștefan A., Dincă I., Andronescu E., Ficai A. Mechanical and tribological properties of nanofilled phenolic-matrix laminated composites // *Materiali in Tehnologije*. 2017. № 51(4). Pp. 569–575.
7. Shi C., Wu Z., Cao Z., Ling T.C., Zheng J. Performance of mortar prepared with recycled concrete aggregate enhanced by CO₂ and pozzolan slurry // *Cement and Concrete Composites*. 2018. № 86. Pp. 130–138.
8. Богданов Р.Р., Ибрагимов Р.А. Процессы гидратации и структурообразования модифицированного самоуплотняющегося бетона // *Инженерно-строительный журнал*. 2017. № 5(73). С. 14–24.
9. Siddique R. *Supplementary Cementing Materials*. Heidelberg: Springer, 2011.
10. Несветаев Г.В., Та Ван Фан. Влияние белой сажи и метаксаолина на прочность и деформационные свойства цементного камня // *Инженерный вестник Дона*. 2012. № 4-1(22). С. 139.
11. *American Standard ASTM C33 / C33M-16e1*, Standard Specification for Concrete Aggregates, ASTM International, West Conshohocken, PA, 2016.
12. ГОСТ 8736-2014. Песок для строительных работ. Технические условия.
13. ГОСТ 8269.0-97. Щебень и гравий из плотных горных пород и отходов промышленного производства для строительных работ. Методы физико-механических

Федюк Р.С., Лесовик В.С., Свинцов А.П., Мочалов А.В., Куличков С.В., Стоюшко Н.Ю., Гладкова Н.А., Тимохин Р.А. Самоуплотняющийся бетон с использованием предварительно подготовленной золы рисовой шелухи // *Инженерно-строительный журнал*. 2018. № 3(79). С. 66–76.

- tests. (rus)
14. *American Standard ASTM C494 / C494M-17*. Standard Specification for Chemical Admixtures for Concrete, ASTM International, West Conshohocken, PA, 2017.
 15. *Russian State Standard GOST 24211-2008*. Admixtures for concretes and mortars. General specifications.
 16. *Self-compacting concrete: Test methods for SCC*. Nordic Innovation Centre. 2005.
 17. *Inspection manual for self-consolidating concrete in precast members*. The University of Texas at Austin. 2007.
 18. *Specification and Guidelines for Self-Compacting Concrete*. EFNARC. 2002.
 19. Sata V., Jaturapitakkul C., Kiattikomol K. Influence of pozzolan from various by-product materials on mechanical properties of high-strength concrete. *Constr. Build. Mater.* 2007. No. 21. Pp. 1589–1598.
 20. Ibragimov R.A., Bogdanov R.R. The influence of a complex modifying agent on the hydration and structure formation of self-compacting concrete. *ZKG International*. 2017. No. 70(4). Pp. 44–49.
 21. Fediuk R., Pak A., Kuzmin D. Fine-Grained Concrete of Composite Binder. *IOP Conference Series: Materials Science and Engineering (Conference paper)*. 2017. Vol. 262(1). Pp. 012025.
 22. Fediuk R., Smoliakov A., Muraviov A. Mechanical properties of fiber-reinforced concrete using composite binders. *Advances in Materials Science and Engineering*. 2017. Pp. 2316347.
 23. Ibragimov R.A., Pimenov S.I. Influence of mechanochemical activation on the cement hydration features. *Magazine of Civil Engineering*. 2016. No. 2. Pp. 3–12.
 24. Fediuk R.S., Smoliakov A.K., Timokhin R.A., Batarshin V.O., Yevdokimova Y.G. Using thermal power plants waste for building materials. *IOP Conference Series: Earth and Environmental Science (Conference paper)*. 2017. Vol. 87(9). Pp. 092010.
 25. Slavcheva G.S. *Struktura vysokotekhnologichnyh betonov i zakonmernosti proyavleniya ih svoystv pri ehkspluatacionnyh i vlazhnostnyh vozdeystviyah* [Structure of high-technological concrete and the regularities of the appearance of their properties with operating humidity exposure]. Abstract of the dissertation ... Dr. Tech.Sc. 2009. Voronezh. 44 p. (rus)
 26. Bogdanov R.R., Ibragimov R.A. Process of hydration and structure formation of the modified self-compacting concrete. *Magazine of Civil Engineering*. 2017. No. 5. Pp. 14–24.
 27. Lukutsova N., Pashayan A., Khomyakova E., Suleymanova L., Kleymenicheva Y. The use of additives based on industrial wastes for concrete. *International Journal of Applied Engineering Research*. 2016. Vol. 11(11). Pp. 7566–7570.
- испытаний.
14. ASTM C494 / C494M-17, Standard Specification for Chemical Admixtures for Concrete, ASTM International, West Conshohocken, PA, 2017.
 15. ГОСТ 24211-2008. Добавки для бетонов и строительных растворов. Общие технические условия.
 16. Self-compacting concrete: Test methods for SCC. Nordic Innovation Centre. 2005.
 17. Inspection manual for self-consolidating concrete in precast members. The University of Texas at Austin. 2007.
 18. Specification and Guidelines for Self-Compacting Concrete. EFNARC. 2002.
 19. Sata V., Jaturapitakkul C., Kiattikomol K. Influence of pozzolan from various by-product materials on mechanical properties of high-strength concrete // *Constr. Build. Mater.* 2007. № 21. Pp. 1589–1598.
 20. Ibragimov R.A., Bogdanov R.R. The influence of a complex modifying agent on the hydration and structure formation of self-compacting concrete // *ZKG International*. 2017. № 70(4). Pp. 44–49.
 21. Fediuk R., Pak A., Kuzmin D. Fine-Grained Concrete of Composite Binder // *IOP Conference Series: Materials Science and Engineering*. 2017. № 262(1). Pp. 012025.
 22. Fediuk R., Smoliakov A., Muraviov A. Mechanical properties of fiber-reinforced concrete using composite binders // *Advances in Materials Science and Engineering*. 2017. Pp. 2316347.
 23. Ибрагимов Р.А., Пименов С.И. Влияние механохимической активации на особенности процессов гидратации цемента // *Инженерно-строительный журнал*. 2016. № 2(62) С. 3–12.
 24. Fediuk R.S., Smoliakov A.K., Timokhin R.A., Batarshin V.O., Yevdokimova Y.G. Using thermal power plants waste for building materials // *IOP Conference Series: Earth and Environmental Science*. 2017. № 87(9). Pp. 092010.
 25. Славчева Г.С. Структура высокотехнологичных бетонов и закономерности проявления их свойств при эксплуатационных и влажностных воздействиях. Автореферат дисс. ... д.т.н.- Воронеж, 44 с.
 26. Chandra S. Waste materials used in concrete manufacturing. – Westwood: Noyes Publication, 1997.
 27. Lukutsova N., Pashayan A., Khomyakova E., Suleymanova L., Kleymenicheva Y. The use of additives based on industrial wastes for concrete // *International Journal of Applied Engineering Research*. 2016. Vol. 11(11). Pp. 7566–7570.

Roman Fediuk,
+7(950)281-79-45; roman44@yandex.ru

Valeriy Lesovik,
+7(910)361-32-63; naukavs@mail.ru

Alexandr Svintsov,
+7(905)582-69-10; svintsovap@rambler.ru

Aleksandr Mochalov,
+7(950)281-79-45; captainvmf@yandex.ru

Sergey Kulichkov,
+7(984)194-61-63; seku@yandex.ru

Natalia Stoyushko,
+7(984)194-61-63; opiv@yandex.ru

Natalia Gladkova,
+7(984)194-61-63; roman442012@gmail.com

Roman Timokhin,
+7(950)281-79-45; gera210307@yandex.ru

Роман Сергеевич Федюк,
+7(950)281-79-45;
эл. почта: roman44@yandex.ru

Валерий Станиславович Лесовик,
+7(910)361-32-63; эл. почта: naukavs@mail.ru

Александр Петрович Свинцов,
+7(905)582-69-10;
эл. почта: svintsovap@rambler.ru

Александр Викторович Мочалов,
+7(950)281-79-45; эл. почта:
captainvmf@yandex.ru

Сергей Владимирович Куличков,
+7(984)194-61-63; эл. почта: seku@yandex.ru

Наталья Юрьевна Стоюшко,
+7(984)194-61-63; эл. почта: opiv@yandex.ru

Наталья Александровна Гладкова,
+7(984)194-61-63;
эл. почта: roman442012@gmail.com

Роман Андреевич Тимохин,
+7(950)281-79-45;
эл. почта: gera210307@yandex.ru

© Fediuk R.S., Lesovik V.S., Svintsov A.P., Mochalov A.V., Kulichkov S.V., Stoyushko N.Y., Gladkova N.A., Timokhin R.A., 2018

doi: 10.18720/MCE.79.8

Serviceability of rockfill dam with reinforced concrete face and grout curtain

Работоспособность каменно-набросной плотины с железобетонным экраном и инъекционной завесой

**M.P. Sainov,
F.V. Kotov,
N.V. Nazarov,**
*National Research Moscow State Civil
Engineering University, Moscow, Russia*

**Канд. техн. наук, доцент М.П. Саинов,
аспирант Ф.В. Котов,
студент Н.В. Назаров,**
*Национальный исследовательский
Московский государственный
строительный университет, Москва,
Россия*

Key words: rockfill dam; reinforced concrete face; grout curtain; stress-strain state; numerical modeling

Ключевые слова: каменно-набросная плотина; железобетонный экран; инъекционная завеса; напряжённо-деформированное состояние; численное моделирование

Abstract. The article deals with design validation of a new structural design of an embankment dam, i.e. rockfill dam with seepage-control element of composite design. It consists of a reinforced concrete face (in the dam upper part) and a wide grout curtain (in the dam lower part). Analyses of the dam stress-strain state (SSS) were conducted on the example of a 235 m high dam. Numerical modeling of the dam was performed with consideration of its construction and loading sequence, as well as non-linear deformation of rockfill. Impact of rockfill deformation and grout curtain material on the dam SSS was studied. It was revealed that conditions of the reinforced concrete face operation in the considered dam structural design differ from conditions of its operation in the dam of classical design; it is subject to not tensile but compressive longitudinal force. This effect decreases the risk of cracking in the face. However, it should be taken into account that under certain conditions the compressive longitudinal stresses in the face may exceed the concrete compressive strength, therefore, the face thickness (in the lower part) is recommended to be taken equal more than 2 m. The least safe assembly of the considered dam structural design is interface of two seepage-control elements. It is arranged with the aid of a concrete gallery located under the grout curtain. SSS of the reinforced concrete face lower part greatly depends on the grout curtain deformations. To provide the face safety the deformation modulus of the grout curtain material should be not less than that of rockfill. The grout curtain strength and SSS are mainly determined by the material deformation. At high rigidity of the curtain material there is a danger of appearance in it of tensile stresses and separation of the curtain from the rock foundation. It is recommended to arrange the grout curtain of clay-cement grouts so that deformation modulus of the curtain material does not exceed 500 МПа.

Аннотация. Статья посвящена расчётному обоснованию новой конструкции грунтовой плотины – каменно-набросной плотины с противофильтрационным элементом составной конструкции. Он состоит из железобетонного экрана (в верхней части плотины) и широкой инъекционной завесы (в нижней части плотины). Расчёты напряжённо-деформированного состояния (НДС) плотины проводились на примере плотины высотой 235 м. Численное моделирование плотины проводилось с учётом последовательности её возведения и нагружения, а также с учётом нелинейности деформируемости каменной наброски. Было исследовано влияние на НДС плотины деформируемости каменной наброски и материала инъекционной завесы. Было получено, что условия работы железобетонного экрана в рассмотренной конструкции плотины отличаются от условий его работы в плотине классической конструкции – экран испытывает не растягивающее, а сжимающее продольное усилие. Этот эффект снижает риск образования трещин в экране. Однако следует иметь в виду, что при определённых условиях сжимающие продольные напряжения в экране могут превышать прочность бетона на сжатие, поэтому толщину экрана (понизу) рекомендуется принимать больше 2 м. Наименее надёжным узлом рассмотренной

Саинов М.П., Котов Ф.В., Назаров Н.В. Работоспособность сверхвысокой каменно-набросной плотины с противофильтрационным элементом в виде комбинации железобетонного экрана и инъекционной завесы // Инженерно-строительный журнал. 2018. № 3(79). С. 77–85.

конструкции плотины является сопряжение двух противофильтрационных элементов. Оно выполнено с помощью бетонной галереи, которая расположена над инъекционной завесой. НДС нижней части железобетонного экрана сильно зависит от деформаций инъекционной завесы. Для обеспечения прочности экрана необходимо, что модуль деформации материала инъекционной завесы был не меньше, чем у каменной наброски. Прочность и НДС инъекционной завесы в основном определяется деформируемостью её материала. При высокой жёсткости материала завесы возникает опасность появления в ней растягивающих напряжений и отрыва завесы от скального основания. Рекомендуется выполнять инъекционную завесу из глинисто-цементных растворов с тем, чтобы модуль деформации её материала не превышал 500 МПа. По результатам исследования можно сделать вывод, что рассмотренная конструкция каменно-набросной плотины с составным негрунтовым противофильтрационным элементом является хорошей альтернативой для классической конструкции грунтовой плотины с железобетонным экраном.

1. Introduction

At present at construction of ultrahigh dams (more than 200 m high) 2 types of embankment dams are used: a rockfill dam with a central core and a rockfill dam with a reinforced concrete face (CFRD). The highest rockfill dam is Nurek dam (Tajikistan) 300 m high [1], and the height of the highest Shuibuya CFRD in China is 233 m [2].

As construction and operation of a rockfill dam in severe climatic conditions is complicated at elaboration of designs for construction of ultrahigh embankment dams, only one structural design alternative was considered – CFRD [3–6]. However, it is known that CFRDs are insufficiently safe: cracks appeared in reinforced concrete faces of several ultrahigh dams [7–9]. In order to provide safety of CFRDs and to extend the area of their application the studies are conducted of their stress-strain state (SSS) [4, 10–12]. Based on studies there are improved structural designs of ultrahigh dams and measures are worked out on enhancing their safety. Namely, it is proposed to arrange transversal joints in the reinforced concrete faces, optimize the dam construction sequence [10, 12] and even make the under-face zone of soil-cement-concrete [11].

However, according to our studies [11, 12], these improvements of classical structural designs of CFRD does not allow guaranteeing their safety. This is connected with peculiar feature of such dam performance: at dam deformations in the lower part of the reinforced concrete face there appears a longitudinal tensile force, which results in formation of joints in the face. Therefore, it is necessary to search for other ways of improving structural designs of ultrahigh CFRD. Namely, one of such ways is use of a seepage-control element of composite (combined) design.

One of the alternatives of rockfill dam with a combined seepage-control element is design where a reinforced concrete face (in the dam upper part) is combined with the grout curtain (in the dam lower part) (Figure 1).

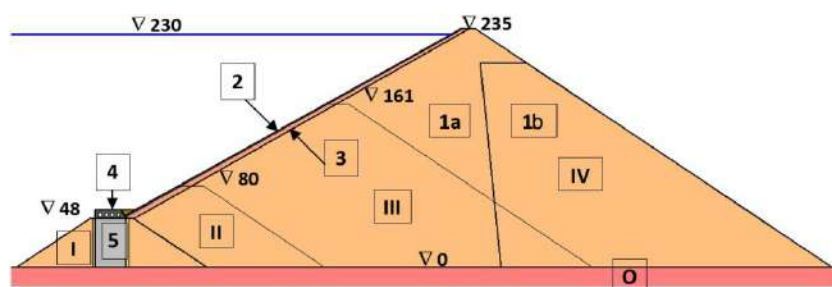


Figure 1. Dam design with combination of seepage-control elements: a reinforced concrete face and a grout curtain. 1a, 1b – rockfill, 2 – reinforced concrete face, 3 – under-face zone, 4 – concrete gallery, 5 – grout curtain, I, II, III, IV – dam construction stages

This structural design was proposed by VNIIG as an alternative for construction of ultrahigh (235 m) dam of Kankun HPP in South Yakutia [13]. The advantage of this structural design is possible increase of dam construction rates due to refusal from pit excavation for construction of a seepage-control element. It is envisaged that the 1st stage dam is filled as a rock-earthfill dam with a wide central core of sand-gravel soil. Then this core is injected with cement mortar (or cement-clay) and is turned into a grout curtain. The 1st stage dam 48 m high can take up the head required for passing water through a bypass along the closed river channel. The dam main part is arranged with a seepage-control element (SCE) in the form of a reinforced concrete face. The reinforced concrete face is interfaced with the grout curtain by arrangement

of a concrete gallery in the 1st stage dam upper part. The movement joint is arranged between the reinforced concrete face and the gallery.

The thickness of the reinforced concrete face in the lower part was taken equal 2 m, and in the upper part 1 m. The thickness of the grout curtain was taken equal 30 m.

The purpose of our study is assessment of workability, safety of this structural design alternative of an ultrahigh embankment dam.

2. Methods

The study was conducted with the aid of numerical modeling of the dam stress-strain state (SSS) with use of the computer program developed by Ph.Dr.(Tech.Sc) M.P. Sainov [14]. Analyses were conducted with consideration of the schedule of dam construction sequence and external forces applied to it. Besides, it was taken into account that the grout curtain in the 1st stage dam appears only after completion of its construction.

The structure finite element model included 1074 finite elements with cubic approximation of displacements inside the element. Contact finite elements were used for modeling non-linear effects of rigid structures contacts behavior among each other, as well as with soils. The total number of degrees of freedom in finite element model comprised 9979.

At analyses consideration was taken of non-linear character of rockfill deformation. For this purpose the used soil model was proposed by Dr. L.N. Rasskazov [15]. At determining parameters of the non-linear model the use was made of the data of experimental studies conducted by Marsal, Marachi and Gupta [16–18]. As the data analysis of field observations over construction settlements of real dams entails large studies of rockfill deformation properties [19-20], our investigations were carried out for a wide range of rockfill deformability. Three alternatives of rockfill deformation properties were considered in the dam upper part: A, B, C. In alternative B the rockfill deformation was adopted to be 2 times as less as in alternative A, and in alternative C – 4 times as less. The averaged rockfill deformation modulus in each alternative was approximately 45, 90 and 180 MPa. At the completion construction stage averaged values of rockfill deformation modulus of the upstream shell reached the following values: for alternative A – 90 MPa, for alternative B – 200 MPa and 300 MPa for alternative C. From the downstream part of the dam body the rockfill deformation in all calculations was taken as in alternative A.

For the grout curtain the elastic material was taken, because deformation and strength properties of soils strengthened by injecting cement-containing grouts, actually have not been studied. Evidently, they may vary in wide ranges, because injection may be accomplished with grouts of different composition and properties. Pure cement or cement-clay grouts may be used [21]. For tentative assessment of the grouted soil properties we used the data on properties of clay-cement-concretes, which greatly vary depending on the content of cement and bentonite.

Our analyses were conducted for three alternatives of grouted soil properties. In alternative 1 the grouted soil deformation modulus was taken equal 5000 MPa, in alternative 2 – 1000 MPa, in alternative 3–200 MPa.

Accordingly, 9 alternatives were analyzed. They are designated by a combination of figures and letters, for example, 3B. The figure indicates the alternative of the grouted soil properties and a letter indicated the alternative of rockfill properties.

3. Results and Discussion

The results of analyses are given in Figures 2–8 and in Table 1, 2 for the most critical moment of time – the moment of the reservoir impoundment to FSL 230 m. Let us see how the selected factors affect the workability of each component of the dam seepage control element.

SSS of the grout curtain is characterized by bend deformations occurring due to the dam body displacement towards the downstream side. Maximum displacement of the curtain towards the downstream side for alternatives A is equal from 47 to 64 cm, for alternatives B – from 33 to 39 cm, for alternatives C – 20 cm (Table 1). The curtain bend is accompanied by decrease of compression on its upstream face and increase of compression on the downstream face.

Table 1. Typical parameters of the grout curtain SSS for different alternatives

SSS parameter	alternatives								
	1A	1B	1C	2A	2B	2C	3A	3B	3C
max u_x , cm	47	33	20	55	37	20	64	39	20
max u_y , cm	14	11	10	29	21	16	56	37	28
max σ_y , MPa	1.7	1.3	1.0	1.2	0.8	0.6	1.0	0.6	0.2
min σ_y , MPa	-31.1	-23.1	-16.8	-15.3	-11.0	-7.4	-4.9	-3.4	-2.6
L, m	18.9	15.7	4.8	11.5	5.7	0.6	1.2	1.2	0.6
P, mm	63.6	58.2	18.9	93.6	57.7	14.0	95.0	80.0	32.3

Designations:

L, P – the length of opening and maximum opening of the contact between the curtain and the foundation respectively,

u_x , u_y – horizontal displacement and settlement of the grout curtain downstream face respectively.

At grout curtain bending there is a danger of crack formation on its upstream face, especially in the near-contact zone. This evidences about the existing zone of tensile vertical normal stresses σ_y (Figure 2, Table 1), as well as about opening of the grout contact with rock foundation (Table 1). These manifestations are typical for all the considered alternatives in different degrees.

If the grout material is comparable by its deformability with rockfill (alternatives of series 3, Figures 2a, b, c), the zone of tension is small by dimensions, and the values of tensile stresses σ_y are not large. The length of the curtain opening contact with rock does not exceed 2 m (Figure 4).

If the grout material is rigid (alternatives of series 1, Figures 2g, h, i), tensile stresses σ_y cover large volume and will inevitably result in formation of cracks in the grout curtain. At that, on the curtain downstream face (Figures 2 g, h, i) high compressive stresses σ_y are concentrated (from 17 to 30 MPa), therefore, compressive strength failure may be expected. Besides, the length of the curtain opening contact with rock will amount from 15 to 60 % of its width (Figure 4).

Judging by Figures 3a, b, the grout curtain may have the acceptable level of compressive and tensile stresses σ_y only in case when the deformation modulus of the curtain material does not exceed 500 MPa, and averaged value of deformation modulus of rockfill (at perception of hydrostatic forces) is not less than 200 MPa. We came to the similar conclusion earlier for the case of the dam with massive grout curtain [22].

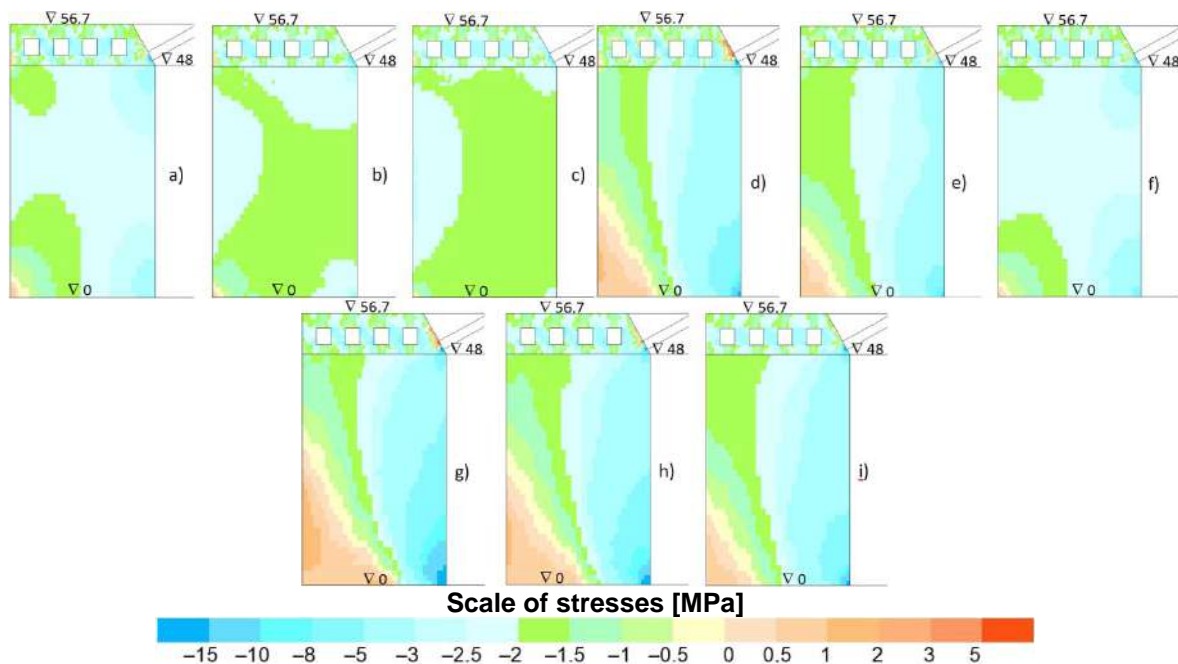


Figure 2. Distribution of stresses σ_y in grout curtain for different alternatives
 a – 3A, b – 3B, c – 3C, d – 2A, e – 2B, f – 2C, g – 1A, h – 1B, i – 1C

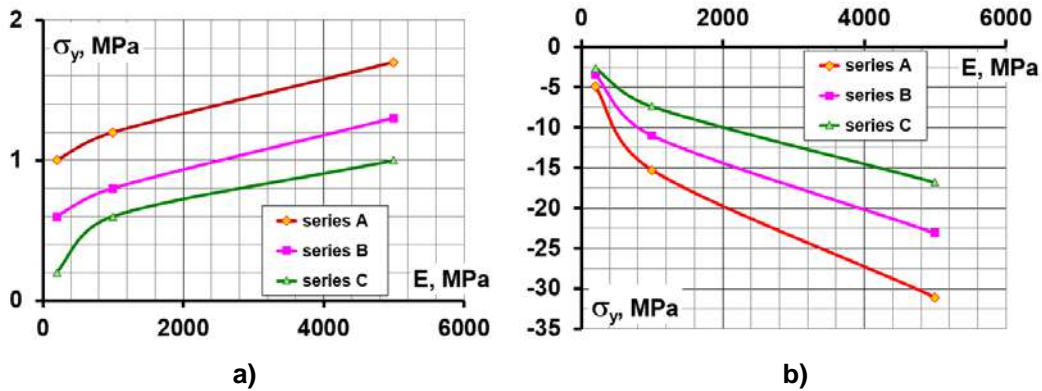


Figure 3. Variation of maximum stresses σ_y in the grout curtain depending on deformation modulus of its material a – tensile, b – compressive

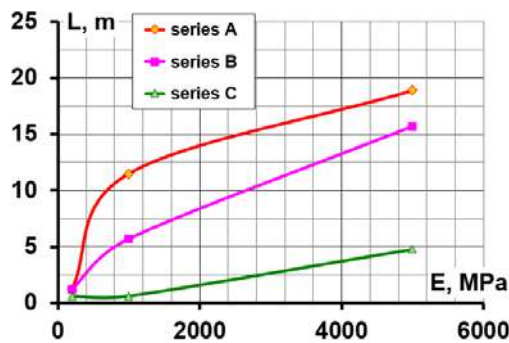


Figure 4. Variation of length of the contact “curtain-rock” depending on deformation modulus of the grout curtain material

Now let us consider SSS of the reinforced concrete face shown in Figures 5–7 and Table 2. Maximum displacement of the reinforced concrete face in direction across the slope is observed on the 2nd stage dam crest. Accordingly the reinforced concrete face is subject to bend deformations towards the downstream side (Figure 5).

But in spite of bend deformations the most part of the reinforced concrete face is subject to compression along the slope (Figures 6, 7). By this the SSS of the reinforced concrete face in the considered dam principally differs from that of rockfill dam classical design for which according to our studies [12] the characteristic feature is longitudinal tensile force existing in the reinforced concrete face. The same effect is characteristic for the dam alternative where the reinforced concrete face is combined with clay-cement-concrete diaphragm [23].

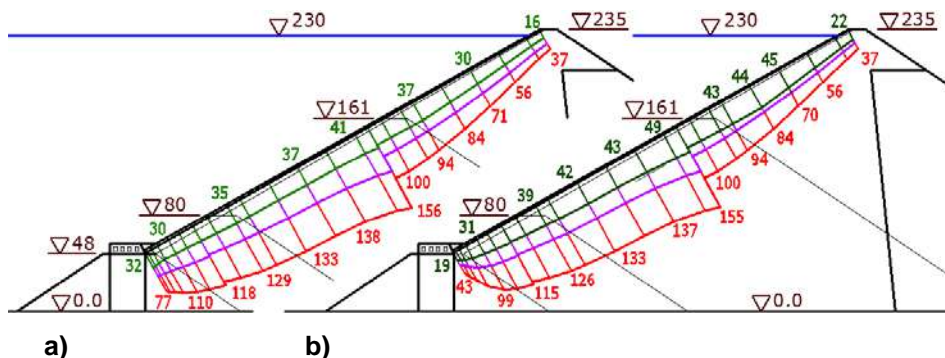


Figure 5. Deflections of the reinforced concrete face (cm) in various alternatives. a – alternatives of series 3, b – alternatives of series 1. Red color indicates the curve corresponding to alternatives of group A, violet color– group B, green – group C.

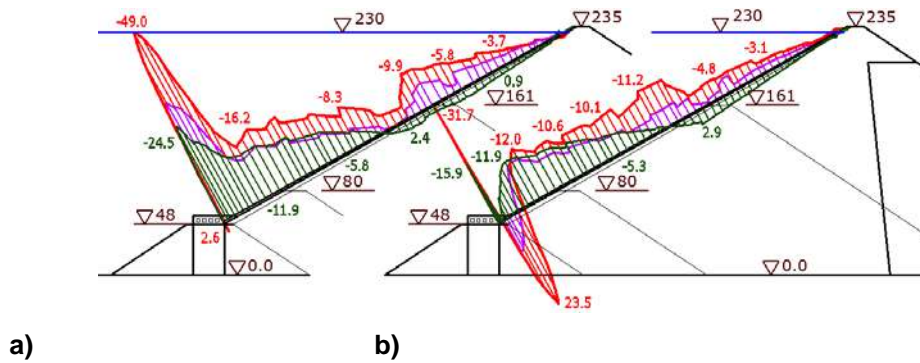


Figure 6. Longitudinal stresses in the reinforced concrete face (MPa) in alternatives of group 1. a – on the upstream face, b – on the downstream face. Red color indicates the curve corresponding to alternative 1A, violet color– 1B, green – 1C.

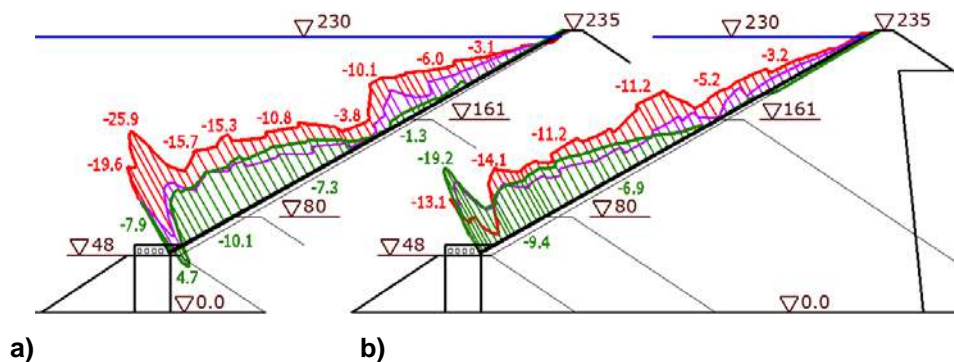


Figure 7. Longitudinal stresses in the reinforced concrete face (MPa) in alternatives of group 3. a – on the upstream face, b – on the downstream face. Red color indicates the curve corresponding to alternative 3A, violet color– 3B, green – 3C.

SSS of the reinforced concrete face upper part is different for all the alternatives and is determined by rockfill deformability. At high rockfill deformability (alternatives of series A) concrete strength of the reinforced concrete face upper part is not provided. Compressive longitudinal stresses σ_E in the reinforced concrete face exceed concrete design compressive strength of class B25 which according to Building code¹ amounts to 14.5 MPa.

SSS of the reinforced concrete face lower part is to a greater extent determined by the grout curtain deformation. If the grout curtain is made of rigid material (alternatives of series 1), the reinforced concrete face lower part is subject to great bend deformations towards the downstream side (Figure 5b). At that on the reinforced concrete face upstream part the compressive stresses are concentrated (Figure 6a), and the downstream part – tensile stresses (Figure 6a). In all the alternatives of series 1 the reinforced concrete compressive strength is not provided (Figure 8).

The reinforced concrete face lower part has more favorable SSS in the alternatives of series 2 and 3.

In alternatives of series 3, when the grout curtain material has low deformation modulus (200 MPa), the reinforced concrete face lower part is subject to bend towards the downstream side (Figure 5a). This results in increase of compression on the face downstream part (Figure 7a) and its decrease on the upstream part (Figure 7b). In alternative 3C SSS of the reinforced concrete face is unfavorable. On the upstream face the longitudinal stress σ_E is tensile. It reaches 4.7 MPa and cannot be perceived by reinforcement. Maximum value of compressive strength σ_E on the downstream face reaches 19.2 MPa and exceeds concrete compressive strength. Thus, deformability of the grout curtain material should not be lower than rockfill deformability.

Thus, effect of deformability of rockfill and the grout curtain material on SSS is of complicated character and they are interconnected. The most favorable SSS of the reinforced concrete face is in alternatives 2C and 3B. These are alternatives where the grout curtain material is close by deformability to that of rockfill, but is slightly more rigid as compared to it. However, even in these alternatives the maximum

¹ Building Code SP 41.13330.2012. Concrete and reinforced concrete constructions of hydraulic structures. Updated version of SNiP 2.06.08-87.

value of compressive stresses σ_E in the reinforced concrete face slightly exceeds concrete design strength of class B25 (Table 2). It is necessary either to use concrete with higher strength or increase the reinforced concrete face thickness.

Table 2. Typical parameters of the reinforced concrete face SSS for various alternatives

parameter	alternatives								
	1A	1B	1C	2A	2B	2C	3A	3B	3C
U_{max} , cm	155	87	49	156	87	42	156	87	41
U_1 , cm	43	27	19	53	36	24	77	49	32
min σ_E , MPa	-49.2	-31.0	-25.0	-42.6	-21.8	-16.4	-25.8	-15.6	-19.2
max σ_E , MPa	23.6	8.5	0.4	14.4	-	-	-	-	4.7

Symbols: U_{max} – maximum deflection of the reinforced concrete face,

U_1 – deflection of the reinforced concrete face at the contact with the concrete gallery,

min σ_E – most significant by value longitudinal compressive stresses,

max σ_E – most significant by value longitudinal tensile stresses.

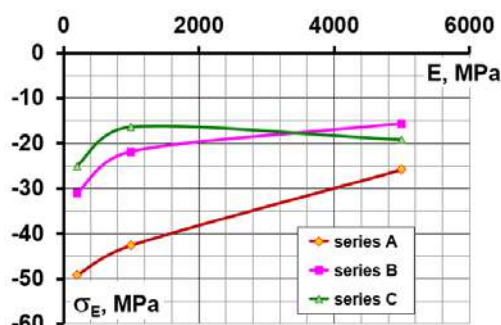


Figure 8. Variation of maximum values of reinforced concrete face depending on deformation modulus of the grout curtain material

4. Conclusions

1. The structural alternative of a rockfill dam where the seepage-control element is composed of a reinforced concrete face and a grout curtain is a good alternative to a classical structural design of a rockfill dam with a reinforced concrete face. The considered dam structural design is potentially efficient: at meeting certain conditions it may operate safely.

2. In the considered dam structural design the reinforced concrete face operates in more favorable conditions than in classical structural design of a rockfill dam with reinforced concrete face (CFRD). The face is subject to not tensile but compressive longitudinal force. To provide compressive strength of the reinforced concrete face it is necessary either to decrease rockfill deformability (rockfill deformation modulus should be tentatively at least 150 MPa), or increase its thickness. It is recommended to adopt the reinforced concrete face thickness in the lower part to be no less than 2 m.

3. To prevent crack formation in the grout curtain body and at the contact "curtain-rock" it is necessary that deformation modulus of the injected soil should not exceed 500 MPa. For grouting it is recommended to use bentonite-cement but not cement mortars.

4. SSS of the reinforced concrete face lower part greatly depends on deformations of the grout curtain located under the face, because the curtain high rigidity constricts the face movements and leads to its bending. To avoid considerable bend deformations of the reinforced concrete face lower part the deformation modulus of the grout curtain material should be not lower than that of rockfill.

5. Complexity in predicting workability of the considered dam structural design is attributed to insufficient knowledge of deformability of rockfill and soils strengthened by injecting grouts containing cement. Due to non-linearity of these material deformations the character of the reinforced concrete face deformations may change in the nature during dam construction and operation causing alternately compressive and tensile stresses.

6. To provide safe operation of combined seepage-control element it is necessary to think through the design of the contact between the reinforced concrete face and the concrete gallery located under the

grout curtain. Structural design of this interface should provide possibility of compensation of the reinforced concrete face displacements in direction along the slope, but considerable displacements in the perimeter joint are not allowed.

References

1. Sokolov I.B., Marchuk A.N., Tsarev A.I., Alipov V.V., Kuzmin K.K., Kuznecov V.C., Aleksandrovskaya E.K., Pavlov V.L. Stress state of dams during staged start-up of the Sayano-Shushenskoe and Nurek hydroelectric stations. *Hydrotechnical Construction*. 1986. No. 20(1). Pp. 14–19.
2. Luo D., Luo L. Study and engineering practice on cracks control measures for concrete face slab of high CFRD. *Advanced Materials Research*. 2012. Vol. 455-456. Pp. 1606–1611.
3. Li N.-H. Performance of high concrete face rockfill dams in China and its inspiration. *Yantu Gongcheng Xuebao / Chinese Journal of Geotechnical Engineering*. 2011. No. 33(2). Pp. 165–173.
4. Sun D., Zhang G., Wang K., Yao H. 3D finite element analysis on a 270m rockfill dam based on Duncan-Chang E-B model. *Advanced Materials Research*. 2011. Pp. 287–290, 1213–1216.
5. Zhang Z. Development of super-high concrete face rockfill dams in China. *14th Asian Regional Conference on Soil Mechanics and Geotechnical Engineering*. 2011.
6. Zhang Z.-L. Design and technical innovation of rockfill dam projects. *Yantu Gongcheng Xuebao / Chinese Journal of Geotechnical Engineering*. 2007. No. 29(8). Pp. 1184–1193.
7. Marques Filo P., Pinto N. de S. Karakteristiki kamennonabrosnykh plotin s betonnyim ekranom, poluchennyye opytным путем [Characteristics of rock casting dams with a concrete screen, obtained experimentally]. *Mezhdunarodnyy daydzhest po gidroenergetike i plotinam*. 2007. Pp. 69–74. (rus)
8. Freitas M.S.Jr. Concepts on CFRDs leakage control – cases and current experiences. *ISSMGE Bulletin*. 2009. Vol. 3. No. 4. Pp. 11–18.
9. Xavier L.V., Albertoni S.C., Pereira R.F., Antunes J. Campos Novos dam during second impounding. *The International Journal on Hydropower & Dams*. 2008. No. 15. Pp. 53–58.
10. Li N.-H., Sun D.-W., Li D.-H., Deng Y.-G., Yang J. Deformation behavior of 300 m high-concrete face rockfill dams. *Yantu Gongcheng Xuebao / Chinese Journal of Geotechnical Engineering*. 2009. No. 31(2). Pp. 155–160.
11. Rasskazov L.N., Sainov M.P. Numerical investigation of reliability of a high earthen dam with a reinforced-concrete shield and sub-shield zone formed from soil-cement concrete. *Power Technology and Engineering*. 2012. Vol. 46. No. 2. Pp. 116–120.
12. Sainov M.P. Impact of dam site configuration on 3D stress-strain state of concrete faced rockfill dam. *Magazine of Civil Engineering*. 2016. No. 3. Pp. 16–39.
13. Zairova V.A., Filippova Ye.A., Orishchuk R.N., Sozinov A.D., Radchenko S.V. Vybór protivofiltratsionnogo ustroystva v variantakh plotin Kankunskogo gidrouzla [The choice of the anti-filtration device in the variants of the dams of the Cancun hydropower center]. *Gidrotekhnicheskoye stroitelstvo*. 2010. No. 2. Pp. 8–13. (rus)
14. Sainov M.P. Vychislitel'naya programma po raschetu napryazhenno-deformirovannogo sostoyaniya gruntovykh plotin: opyt sozdaniya, metodiki i algoritmy [Computing program for calculating the stress-strain state of ground dams: creation experience, methods and algorithms]. *International Journal for Computational Civil and Structural Engineering*. 2013. Vol. 9. No. 4. Pp. 208–225. (rus)
15. Rasskazov L.N., Dzhkhа Dzh. Deformiruyemost i prochnost grunta pri raschete vysokikh gruntovykh plotin [Deformability and strength of soil in the calculation of high ground dams].

Литература

1. Sokolov I.B., Marchuk A.N., Tsarev A.I., Alipov V.V., Kuzmin K.K., Kuznecov V.C., Aleksandrovskaya E.K., Pavlov V.L. Stress state of dams during staged start-up of the Sayano-Shushenskoe and Nurek hydroelectric stations // *Hydrotechnical Construction*. 1986. № 20(1). Pp. 14–19.
2. Luo D., Luo L. Study and engineering practice on cracks control measures for concrete face slab of high CFRD // *Advanced Materials Research*. 2012. Vol. 455-456. Pp. 1606–1611.
3. Li N.-H. Performance of high concrete face rockfill dams in China and its inspiration // *Yantu Gongcheng Xuebao / Chinese Journal of Geotechnical Engineering*. 2011. № 33(2). Pp. 165–173.
4. Sun D., Zhang G., Wang K., Yao H. 3D finite element analysis on a 270m rockfill dam based on Duncan-Chang E-B model // *Advanced Materials Research*. 2011. Pp. 287–290, 1213–1216.
5. Zhang Z. Development of super-high concrete face rockfill dams in China // *14th Asian Regional Conference on Soil Mechanics and Geotechnical Engineering*. 2011.
6. Zhang Z.-L. Design and technical innovation of rockfill dam projects // *Yantu Gongcheng Xuebao / Chinese Journal of Geotechnical Engineering*. 2007. № 29(8). Pp. 1184–1193.
7. Маркес Фильо П., Пинто Н. де С. Характеристики каменно-набросных плотин с бетонным экраном, полученные опытным путем // *Международный дайджест по гидроэнергетике и плотинам*. 2007. С. 69–74.
8. Freitas M.S.Jr. Concepts on CFRDs Leakage Control – Cases and Current Experiences // *ISSMGE Bulletin*. 2009. Vol. 3. № 4. Pp. 11–18.
9. Xavier L.V., Albertoni S.C., Pereira R.F., Antunes J. Campos Novos dam during second impounding // *The International Journal on Hydropower & Dams*. 2008. № 15. Pp. 53–58.
10. Li N.-H., Sun D.-W., Li D.-H., Deng Y.-G., Yang J. Deformation behavior of 300 m high-concrete face rockfill dams // *Yantu Gongcheng Xuebao / Chinese Journal of Geotechnical Engineering*. 2009. № 31(2). Pp. 155–160.
11. Rasskazov L.N., Sainov M.P. Numerical investigation of reliability of a high earthen dam with a reinforced-concrete shield and sub-shield zone formed from soil-cement concrete // *Power Technology and Engineering*. 2012. Vol. 46. No. 2. Pp. 116–120.
12. Саинов М.П. Влияние формы створа на напряженное состояние железобетонного экрана каменно-насыпной плотины // *Инженерно-строительный журнал*. 2016. № 3(63). С. 16–39.
13. Заирова В.А., Филиппова Е.А., Орищук Р.Н., Созинов А.Д., Радченко С.В. Выбор противофильтрационного устройства в вариантах плотин Канкунского гидроузла // *Гидротехническое строительство*. 2010. № 2. С. 8–13.
14. Саинов М.П. Вычислительная программа по расчету напряженно-деформированного состояния грунтовых плотин: опыт создания, методики и алгоритмы // *International Journal for Computational Civil and Structural Engineering*. 2013. Vol. 9. № 4. С. 208–225.
15. Рассказов Л.Н., Джха Дж. Деформируемость и прочность грунта при расчете высоких грунтовых плотин // *Гидротехническое строительство*. 1987. № 7. С. 31–36.
16. Gupta A.K. Triaxial behaviour of rockfill materials // *Electronic Journal of Geotechnical Engineering - Ejge.com*. Bund J. 2009. Vol. 14.

Sainov M.P., Kotov F.V., Nazarov N.V. Serviceability of ultrahigh rockfill dam with seepage-control element presented by combination of a reinforced concrete face and a grout curtain. *Magazine of Civil Engineering*. 2018. No. 3. Pp. 77–85. doi: 10.18720/MCE.79.8.

- Gidrotekhnicheskoye stroitelstvo*. 1987. No. 7. Pp. 31–36. (rus)
16. Gupta A.K. Triaxial behaviour of rockfill materials. *Electronic Journal of Geotechnical Engineering - Ejge.com*. Bund J. 2009. Vol. 14.
 17. Marachi N.D., Chan C.K., Seed H.B. Evaluation of properties of rockfill materials. *Journal of Soil Mechanics and Foundation Engineering*. ASCE. 1972. No. 98(1). Pp. 95–114.
 18. Marsal R.J. Large scale testing of rockfill materials. *Journal of Soil Mechaics and Foundations Division*. ASCE. 1967. No. 93(2). Pp. 27–43.
 19. Park H.G., Kim Y.-S., Seo M.-W., Lim H.-D. Settlement behavior characteristics of CFRD in construction period. Case of Daegok Dam // *Journal of the KGS*. September 2005. Vol. 21. № 7. Pp. 91–105.
 20. Саинов М.П. Полуэмпирическая формула для оценки осадок однородных грунтовых плотин // Приволжский научный журнал. 2014. № 3(31). С. 108–115.
 21. Журкина Н.Н. Инъекционная завеса в основании грунтовой плотины Майнской ГЭС // Гидротехническое строительство. 1987. № 11. С. 39–42. (rus)
 22. Sainov M.P., Kotov F.V. Stress-strain state and performance of a high rockfill dam with a grout curtain. *Magazine of Civil Engineering*. 2017. No.1. Pp. 44–55.
 23. Sainov M.P. Analysis of normal operation of a rockfill dam with combination of seepage-control elements: reinforced concrete face and a clay-cement-concrete wall. *Magazine of Civil Engineering*. 2016. No. 4. Pp. 3–9.
 17. Marachi N.D., Chan C.K., Seed H.B. Evaluation of properties of rockfill materials // *Journal of Soil Mechanics and Foundation Engineering*. ASCE. 1972. № 98(1). Pp. 95–114.
 18. Marsal R.J. Large Scale Testing of Rockfill Materials // *Journal of Soil Mechaics and Foundations Division*. ASCE. 1967. № 93(2). Pp. 27–43.
 19. Park H.G., Kim Y.-S., Seo M.-W., Lim H.-D. Settlement behavior characteristics of CFRD in construction period. Case of Daegok Dam // *Journal of the KGS*. September 2005. Vol. 21. № 7. Pp. 91–105.
 20. Саинов М.П. Полуэмпирическая формула для оценки осадок однородных грунтовых плотин // Приволжский научный журнал. 2014. № 3(31). С. 108–115.
 21. Журкина Н.Н. Инъекционная завеса в основании грунтовой плотины Майнской ГЭС // Гидротехническое строительство. 1987. № 11. С. 39–42.
 22. Саинов М.П., Котов Ф.В. Напряжённо-деформированное состояние и работоспособность высокой грунтовой плотины с инъекционной завесой // Инженерно-строительный журнал. 2017. № 1(69). С. 44–55.
 23. Саинов М.П. Анализ работоспособности каменной плотины с комбинацией противифльтрационных элементов – железобетонного экрана и глиноцементобетонной стены // Инженерно-строительный журнал. 2016. № 4(64). С. 3–9.

Mikhail Sainov,
+7(926)607-89-31; mp_sainov@mail.ru

Filipp Kotov,
+7(926)652-58-81; filipp_net@mail.ru

Nikita Nazarov,
+7(968)779-07-69; g-i905@rambler.ru

Михаил Петрович Саинов,
+7(926)607-89-31; эл. почта:
mp_sainov@mail.ru

Филипп Викторович Котов,
+7(926)652-58-81; эл. почта: filipp_net@mail.ru

Никита Владимирович Назаров,
+7(968)779-07-69; эл. почта: g-i905@rambler.ru

© Sainov M.P.,Kotov F.V.,Nazarov N.V.,2018

doi: 10.18720/MCE.79.9

Fire protective dry plaster composition for structures in hydrocarbon fire

Огнезащитный штукатурный состав для конструкций в условиях углеводородного горения

**M.V. Gravit,
E.V. Golub,**

Peter the Great St. Petersburg Polytechnic University, St. Petersburg, Russia

S.P. Antonov,

LLC Prozask, Moscow, Russia

**Канд. техн. наук, доцент М.В. Гравит,
студент Е.В. Голуб,**

Санкт-Петербургский политехнический университет Петра Великого,

Санкт-Петербург, Россия

**генеральный директор С.П. Антонов,
ООО «Прозаск», Москва, Россия**

Key words: oil and gas facilities; steel structures; fire resistance limit; passive fire protection; fire protection means; hydrocarbon fire

Ключевые слова: сооружения нефтегазового комплекса; стальные конструкции; предел огнестойкости; пассивная огнезащита; средства огнезащиты; углеводородный пожар

Abstract. The result of the combustion of fire hazardous materials at the facilities of the oil and gas complex is extensive fires, characterizing the rapid temperature rise, and as a result the destruction of load-bearing structures occurs. The dynamics of the development of such fire type requires a different approach to test the structures in order to determine the limit of fire resistance. The article presents European and American normative documents that contain methods for testing structures taking into account the requirements for the hydrocarbon temperature regime of a fire. I-steel cross-sections with flame retardant coating "Fendolite MII" are tested, and the fire resistance of these structures is defined. Conclusions on the need to conduct numerous fire tests with different types of fire protection under a hydrocarbon fire regime in Russia were made in order to obtain the necessary experimental database sufficient to create a unified methodology for calculating and introducing it into national standards.

Аннотация. Результатом сгорания пожароопасных веществ на объектах нефтегазового комплекса являются обширные пожары, характеризующиеся стремительным ростом температуры, и как следствие разрушение несущих конструкций. Динамика развития такого пожара требует иной подход к проведению испытаний конструкций с целью определения предела огнестойкости. В статье приведены европейские и американские нормативные документы, содержащие методы испытаний конструкций с учетом требований к углеводородному температурному режиму пожара. Проведены испытания стальных колонн двутаврового сечения с огнезащитным покрытием «Fendolite MII», и определен предел огнестойкости данных конструкций. Сделаны выводы о необходимости проведения в России многочисленных огневых испытаний конструкций с различными типами огнезащиты в условиях углеводородного режима пожара с целью получения необходимой экспериментальной базы данных, достаточной для создания единой методики расчета и внедрения ее в национальные стандарты.

1. Introduction

Explosive combustion of fire hazardous substances at oil and gas facilities is the main cause of destruction of buildings and structures, as well as tanks, equipment, tankers and offshore platforms. The subsequent extensive fires resulting from the burning of petroleum products, as a rule, can be attributed to the so-called hydrocarbon fire.

In the articles [1, 2] the necessity of introduction and subsequent use for fire tests of building structures for fire resistance of a new temperature regime of a fire taking into account the real fire conditions is substantiated [3].

Hydrocarbon fire is characterized by a rapid temperature rise: the average surface temperature of the flame during the combustion of petroleum products reaches 1000 °C, which is much higher than the temperature of a conventional (cellulose) fire.

Гравит М.В., Голуб Е.В., Антонов С.П. Огнезащитный штукатурный состав для конструкций в условиях углеводородного горения // Инженерно-строительный журнал. 2018. № 3(79). С. 86–94.

Similar to the standard fire regime, in which not only cellulose can be a combustible material [4], combustion of a whole group of substances similar in ease of ignition and type of combustion is a hydrocarbon fire. This group of substances consists from not only pure hydrocarbons (petrol and natural gases – methane, ethane, propane, butane, etc.), but also from their organic derivative (alcohols, phenols, ketones), virtually all petroleum products, lubricants, paint and varnish materials, many plastics with a low oxygen index.

The dynamics of the development of hydrocarbon fire requires a different approach to ensuring fire resistance of building structures. Most fire-retardant and fire-resistant building structures have proved their effectiveness under the conditions of a standard fire [5-7]. In foreign publications, many studies are devoted to fire protection of steel structures. One of the papers is devoted to the calculation of the operation of a steel plate under high-temperature conditions [8]. However, the structures studied under these conditions can not provide the same characteristics under conditions of a hydrocarbon fire [9].

An important approach for ensuring the safety of petrochemical production is the use of the risk analysis method, which allows to determine the places of the most probable occurrence of an accident, and assess their consequences. This makes it possible to adequately protect the structures from special loads caused by hydrocarbon combustion. The method of risk analysis enables the development of safer and at the same time cost-effective design solutions, including for the protection of structures. This method was adopted in Russia, Great Britain, USA, Norway, Australia, France [10-15].

Recently, modeling of hydrocarbon fires in software complexes has been used to determine the duration of fires in different areas [16], and empirical relationships connecting the values of the fire resistance limits of structures in the hydrocarbon and standard temperature regimes of a fire [17], which makes it possible to approximately estimate the fire resistance limits of structures under the hydrocarbon fire condition, when the fire resistance limits are known at the standard fire regime, and thereby facilitate the testing of the structure.

Traditionally, researches in the field of fire safety is focused on providing the required degree of fire resistance of buildings, and a little attention has been paid to the construction of bridges. The works [18, 19] are aimed to develop knowledge about the behavior of steel bridges under the influence of the hydrocarbon fire regime, which occurs, for example, in the collapse or fire of a gasoline tanker.

On the international scale, the Technical Committee 92 "Fire Safety" of the International Organization of Standardization (ISO) is engaged in the improvement and unification of the methodology for testing structures for fire resistance. Within the framework of this committee and on the basis of international cooperation, a standard of ISO 834-75 "Fire resistance tests. Elements of building constructions" (in the updated version – ISO 834-1: 1999) has been developed for the method of testing the building structures for fire resistance, which is the methodological basis for conducting such tests, including in Russia.

In determining the fire resistance of structures under the conditions of the hydrocarbon fire regime, standards such as UL 1709 (USA) [20], ASTM E 1529-14A "Standard test methods for determining effects of large hydrocarbon pool fires on structural members and assemblies" (USA) and European EN 1363-2: 1999* "Fire resistance tests – Part 2: Alternative and additional procedures", DIN 4102-2-1977 "Fire tests on building materials and structures. Methods for determination of the fire resistance of load bearing elements of construction" (Germany), BS 476-20: 1987 "Fire tests on building materials and structures. Method for determination of the fire resistance of elements of construction (general principles)" (Great Britain) [21]. In most cases, these standards are used to assess the stability and fire resistance of load-bearing structures of railway and automobile tunnels, as well as to evaluate the efficiency of external technological installations for the extraction, processing and transportation of gas, oil and petroleum products on offshore oil platforms. They determine the criteria for the resistance of fireproof coatings in a hydrocarbon fire. Especially for evaluating the effectiveness of fire protection of pipelines, the method of "direct impact" of the jet flame is additionally applied. The criterion for the effectiveness of the fireproof composition is the time from the beginning of the test to the onset of the limit state.

It should be noted that, according to the research of the American insurance and engineering company Global Asset Protection Services LLC (GAPS), the values of the consumption and thickness of coatings for fire-retardant products for structures according to methods of ASTM E-119 "Fire tests of building construction and materials" and UL 1709 under the hydrocarbon fire regime had a significant difference and the data obtained by these methods, respectively, required correlation between themselves [22].

Up to date, Russia has not developed a regulatory framework for fire protection of load-bearing steel structures in conditions of hydrocarbon combustion. In 2015, the normative documentation introduced the concept of a "hydrocarbon curve" [23]. This standard is identical to the European regional standard EN 1363-2: 1999.

According to [23] the hydrocarbon temperature regime is an alternative to the standard temperature regime and takes into account the real fire conditions for burning hydrocarbon fuels.

Graphical representation of the hydrocarbon fire curve and other temperature regimes is shown in the figure:

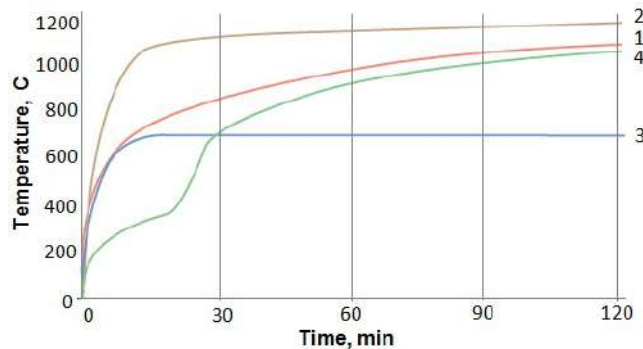


Figure 1. Fire curves. 1 – standard time-temperature curve; 2 – hydrocarbon curve; 3 – external fire exposure curve; 4 – slow heating curve

The curve for cellulose combustion is also called the standard combustion curve. As can be seen from the figure, the hydrocarbon scenario of the fire development is fundamentally different from the cellulose fire: the temperature jump is much sharper and the temperature effect is higher. In such conditions, traditional fire-retardant materials do not provide the necessary level of fire-protective efficiency.

Despite of the urgency of the problem of protection in the conditions of hydrocarbon combustion for Russia, this normative document of the Russian Federation became the first official standard in this field. However, it only establishes a temperature regime, and the test methods for various types of products under the conditions of hydrocarbon combustion are only to be developed. Despite the absence of requirements and norms in the Russian Federation for the limits of fire resistance of structures under the conditions of a hydrocarbon fire, Russian manufacturers voluntarily conduct tests of the available fire protection means according to the procedures given in various foreign regulatory documents, which is an additional competitive advantage, but because of the high costs applied only for a specific security object.

One way to protect structures is passive fire protection - solutions used to prevent the occurrence and spread of fire. The most common means of passive fire protection include special refractory compounds, paints, impregnations, varnishes and fireproofing plasters [24], which can significantly reduce the likelihood of fire and spread of fire. As a passive protection against a hydrocarbon fire, 2 types of materials are used [25]:

- Lightweight cement coatings (usually based on portland cement and lightweight aggregates)
- Intumescent paints and varnish coatings

Lightweight cement coating is a relatively inexpensive material, but the application works in several stages, which ultimately increases the cost of using this type of fire protection. It is not used in rooms with a high humidity level.

Intumescent coating protects the structure by forming a heat-insulating protective layer at high temperatures. This coating is easier to apply, and to increase the protection time of steel it can be applied in several layers.

In order to increase the operational characteristics of intumescent coatings, such as durability, elasticity, homogeneity of the foam layer being formed, additional additives are applied to the standard formulations of intumescent coatings [26].

Intumescent coatings are used for protection against hydrocarbon fires, mainly on an epoxy basis. Since the epoxy has a very high resistance to almost any chemical attack, this type of product adds to its

fire-retardant characteristics an even higher level of anti-corrosion protection. In the article [27] the influence of external factors such as ultraviolet radiation, humidity, temperature changes, seawater, on the flame retardant properties of epoxy coatings examines. It is determined to what extent the protective properties of coatings in aggressive environments are reduced. Among the epoxy fireproof materials, the most common are "Jotachar 1709", "Chartek 7", "Chartek 8", "Interchar 212", "Firetex M90".

Another type of intumescent coating is a silicone-based coating. In work [28], the effect of clay as a filler on the fire resistance of a coating as a whole is considered. In [29], a new test method was developed to determine the strength of intumescent coating in a fire test and tests were conducted for epoxy and silicone based coatings.

The purpose of this paper is to examine the behavior of the "Fendolite MII" coating in the hydrocarbon combustion regime. "Fendolite MII" is a dry plaster composition based on expanded vermiculite and portland cement, used to increase the fire resistance of bearing steel and reinforced concrete structures, equipment, tanks, pipelines, etc. in civil and industrial construction, at chemical and petrochemical facilities, fuel and energy complex and in tunnels [30].

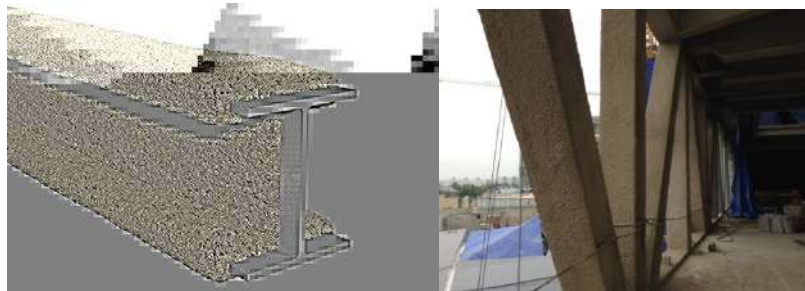


Figure 2. Coating "Fendolite MII" on an I-beam and on steel elements

Table 1. Properties and performances of "Fendolite MII"

Color and finish	Off-white, monolithic, spray texture. May be floated or roller finished
Minimum practical thickness	8 mm when unreinforced, 15 mm when reinforced
Theoretical coverage	62 m ² /tonne at 25 mm thickness
Cure	By hydraulic set
Initial set	2 to 6 hours at 20°C and 50% RH
Density (nominal)	775 kg/m ³ ±15% (when dry and in place)
Combustibility	Non-combustible to BS476:Part 4
Smoke generation	Does not contribute to smoke generation
Thermal conductivity	0.19 W/mK at 20°C
Corrosion resistance	Does not promote corrosion of steel. However, a primed substrate is recommended for long term corrosion resistance, particularly when the structure is to be fully exposed to the elements
pH value	12.0-12.5
Sound absorption	Noise reduction coefficient (NRC) 0.35

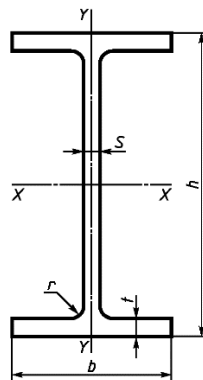


Figure 3. Sample cross-section

The object of the further test was 2 samples of steel columns with fireproof coating "Fendolite MII", which are rolled I-beams. The reduced thickness of the column metal is 6.3 mm.

Table 2. Characteristics of rolled I-beam profile

Profile characteristic	Dimension, mm
h	298
b	299
S	9
t	14
r	18

Material of the rolled I-beam is steel grade S345. Mechanical characteristics for the thickness $t=14$ mm are given in Table 3.

Table 3. Mechanical characteristics steel grade S345

Mechanical characteristic	Value
Yield strength, MPa	325
Tensile strength, MPa	470
Elongation, %	21

2. Methods

Tests of prototypes of steel columns with a flame retardant "Fendolite MII" on the fire impact in order to determine the fire resistance limit are performed in accordance with Russian State Standards GOST 30247.0-94 "Construction structures. Test methods for fire resistance. General requirements", GOST 30247.1-94 "Construction structures. Test methods for fire resistance, bearing and enclosing structures" provided that a hydrocarbon temperature regime is created in the fire chamber of the furnace.

According to the "Technological Regulations for the design and manufacture of works on the installation and operation of a coating based on a fire retardant mixture "Fendolite MII" to improve the fire resistance of metal structures", the application of a fire-protective coating is carried out on one layer of anticorrosion primer with a thickness of 0.05 mm, in two layers, fire retardant coating with steel plaster mesh. Thus, the average thickness of the dry coating layer for performing fire tests in a hydrocarbon fire is 30 mm for the 1st and 2nd prototype.

Experimental samples are installed in the fire chamber of the furnace and subjected to a four-sided thermal action. The furnace generates a hydrocarbon temperature regime, characterized by the dependence (1):

$$T = 1080 \cdot (1 - 0.325e^{-0.167t} - 0.675e^{-2.5t}) + 20 \quad (1)$$

where T – the temperature in the furnace, corresponding to the time t , °C;

t – time, calculated from the beginning of the test, min.

Tests of load-bearing elements must be carried out under load. In this paper, the effect of a static load equals to 294 kN (30 tons) was taken into account under the condition of vertical central compression with hinge support on one side and rigid fixing on the other side of the column. The load is established 60 minutes before the start of the test and is maintained constant (with an accuracy of not less than $\pm 5\%$) during the entire duration of the fire impact.

The temperature in the fire chamber of the furnace and on the test samples is measured with oven thermocouples, and the vertical deformations of the samples during the test are a deflectometer.

For load-bearing vertical bar structures, the limit state for a fire resistance test in accordance with 8.2 of Russian State Standard GOST 30247.1 is loss of bearing capacity (R) due to collapse of the structure or occurrence of ultimate deformations. According to Appendix A of Russian State Standard GOST 30247.1, the maximum vertical deformation for a given column is 30 mm, the rate of increase of vertical deformation is more than 10 mm/min.

3. Results and discussion

During the tests in the external state of the flame retardant coating "Fendolite MII", applied to the prototypes of the steel columns, no visible changes were recorded.



Figure 4. Appearance of the experimental image of a steel column with a flame retardant "Fendolite MII" after the fire impact (sample No. 1. view of the technological opening of the fire chamber)

The average temperatures in the fire chamber corresponded to the dependence (1). Curves of temperatures and vertical deformations changes of prototypes of steel columns with a flame retardant coating "Fendolite MII" are shown in Figure 4.

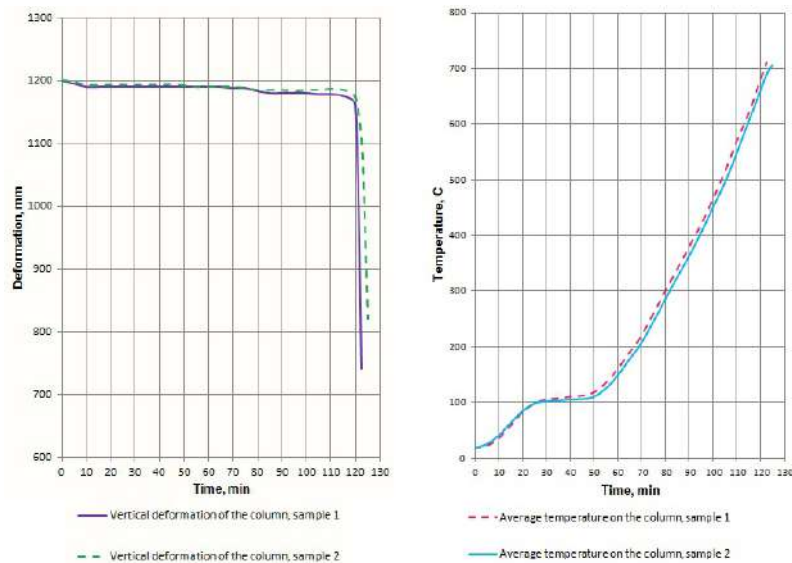


Figure 5. Curves of temperature changes and vertical deformations of prototypes of a steel column with a flame retardant coating "Fendolite MII" in the fire chamber of the furnace

On the 124th minute of the 1st and 126th tests of the 2nd test, the prototypes of steel columns passed to the limit state, characterized by a rapid increase in vertical deformation and not the ability of the design to accept a test load equal to 294 kN (30 tons).

At the time when the prototype limit state reached the loss of load capacity of the structure (R), the average temperature of the thermocouples (critical temperature) established on the metal of the test samples was 710 °C and 707 °C for the first and second samples.

Accordingly, the fire resistance limit according to the loss of bearing capacity (clause 8.1.1 and Annex A to Russian State Standard GOST 30247.1-94) of the construction of an I-steel column of height (3000 ± 10) mm with a reduced metal thickness of 6.3 mm with a flame retardant coating "Fendolite MII" at an average thickness of the dry coating layer of 30.0 mm, tested under the action of a static load equal to 294 kN (30 tons), provided the hydrocarbon temperature regime in the fire chamber of the furnace, was 125 minutes, which shows the significant ability of a fire-retardant coating "Fendolite MII" hydrocarbon type resists combustion, significantly exceeding the standard fire temperature regime.

For buildings and structures of the I degree of fire resistance according to Russian normative document SP 2.13130.2012 "Fire protection systems. Provision of fire resistance of protection facilities" the required fire resistance of load-bearing structures is 120 min, which means that the coating under investigation is capable of providing maximum regulatory requirements, but for a standard fire regime. At present, the standardization of fire resistance limits for the hydrocarbon fire regime is absent, the testing process goes randomly and leads to additional costs for manufacturers of fire protection means.

Plastered fire retardant compositions based on portland cement are the first in use as a flame retardant, the second is epoxy compositions [21].

According to the official websites of some companies that reported test results for fire retardant products for building structures tested for fire resistance under hydrocarbon fire, and UL 1709 certificates available in the open online database of Underwriters Laboratory [31] the reduced thickness of columns (column W10 x 49 according to the American classification) is about 6 mm. The thickness of the coating layer with a flame retardant efficiency of 120 minutes averages 30 mm. For example, for "Chartek 7", these data are 15 mm (epoxy base), for coating on the basis of portland cement "Pyrocrete 241" – 28.6 mm [27-29].

To use the correctly selected passive fire protection in conditions of hydrocarbon fire, and accordingly the most effective protection of objects at risk of this fire, there is a need to introduce a calculation procedure to determine the fire resistance of structures in the hydrocarbon combustion condition. To do this, it is necessary to collect and systematize the database for testing various types of load-bearing elements using different types of fire protection.

In the future, it is planned to test steel columns under different loads, with other reduced metal thicknesses to create an integral picture of the behavior of the fire-retardant coating under conditions of hydrocarbon combustion.

4. Conclusions

The results of experimental studies have shown that the fire resistance limit due to the loss of the load-carrying capacity of the I-section steel column with the "Fendolite MII" flame retardant coating, with an average dry film thickness of 30.0 mm, tested under a constant load of 294 kN (30 tons) the condition for creating a hydrocarbon temperature regime in the fire chamber of the furnace, was 125 minutes.

As a result of the work, conclusions on the need to create a national regulatory framework with a clear regulation of the test methods for designs and the relevance of research on passive fire protection in hydrocarbon combustion were made.

Reference

1. Golovanov V.I., Kuznetsova Y.V. Effektivnyye sredstva ognезashchity dlya stalnykh i zhelezobetonykh konstruktсий [Effective means of fire protection for steel and reinforced concrete structures]. *Promyshlennoye i grazhdanskoye stroitelstvo*. 2015. No. 9. Pp. 82–90. (rus)
2. Shvyrkov S.A., Yuryev Y.I. Temperaturnyy rezhim pozhara dlya opredeleniya predela ognestoykosti ograzhdayushchikh sten neftyanykh rezervuarov [Temperature mode of fire for determination of the fire resistance limit of wall walls of oil tanks]. *Tekhnologii tekhnosfernoy bezopasnosti*. 2016. No. 4. Pp. 50–56. (rus)
3. Khasanov I.R., Gravit M.V., Kosachev A.A., Pekhotikov A.V., Pavlov V.V. Garmonizatsiya yevropeyskikh i rossiyskikh normativnykh dokumentov, ustanavlivayushchikh obshchiye trebovaniya k metodam ispytaniy na ognestoykost stroitelnykh konstruktсий i primeneniyu temperaturnykh rezhimov, uchityvayushchikh realnyye usloviya pozhara [Harmonization of European and Russian regulatory documents that establish general requirements for fire test methods for building structures and the application of temperature regimes that take into account the real fire conditions]. *Pozharovzryvobezopasnost*. No. 3. 2014. Pp. 49–57. (rus)
4. Saknite T., Serdjuk D., Goremikins V., Pakrastins L., Vatin N.I. Fire design of arch-type timber roof. *Magazine of Civil Engineering*. 2016. No. 4(64). Pp. 26–39.
5. Schaumann P., Tabeling F., Weisheim W. Heating behaviour of intumescent coatings in steel constructions - Advanced numerical simulations taking the foaming process into account // *Stahlbau*. 2014. № 83(9). Pp. 646–651.

Литература

1. Голованов В.И., Кузнецова Е.В. Эффективные средства огнезащиты для стальных и железобетонных конструкций // *Промышленное и гражданское строительство*. 2015. № 9. С. 82–90.
2. Швырков С.А., Юрьев Я.И. Температурный режим пожара для определения предела огнестойкости ограждающих стен нефтяных резервуаров // *Технологии техносферной безопасности*. 2016. № 4. С. 50–56.
3. Хасанов И.Р., Гравит М.В., Косачев А.А., Пехотиков А.В., Павлов В.В. Гармонизация европейских и российских нормативных документов, устанавливающих общие требования к методам испытаний на огнестойкость строительных конструкций и применению температурных режимов, учитывающих реальные условия пожара // *Пожаровзрывобезопасность*. 2014. № 3. С. 49–57.
4. Сакните Т., Сердюк Д.О., Горемыкин В.В., Пакрастиньш Л., Ватин Н.И. Проектирование огнестойких арочных деревянных покрытий // *Инженерно-строительный журнал*. 2016. № 4(64). С. 26–39.
5. Schaumann P., Tabeling F., Weisheim W. Heating behaviour of intumescent coatings in steel constructions - Advanced numerical simulations taking the foaming process into account // *Stahlbau*. 2014. № 83(9). Pp. 646–651.
6. Schaumann P., Kirsch T. Protected steel and composite

Гравит М.В., Голуб Е.В., Антонов С.П. Огнезащитный штукатурный состав для конструкций в условиях углеродородного горения // *Инженерно-строительный журнал*. 2018. № 3(79). С. 86–94.

- Advanced numerical simulations taking the foaming process into account. *Stahlbau*. 2014. No. 83(9). Pp. 646–651.
6. Schaumann P., Kirsch T. Protected steel and composite connections: Simulation of the mechanical behaviour of steel and composite connections protected by intumescent coating in fire. *Journal of Structural Fire Engineering*. 2015. No. 6(1). Pp. 41–48.
 7. Kraus P., Mensinger M., Tabelaing F., Schaumann P. Experimental and numerical investigations of steel profiles with intumescent coating adjacent to space-enclosing elements in fire. *Journal of Structural Fire Engineering*. 2015. No. 6(4). Pp. 237–246.
 8. Salminen M., Heinisuo M. Numerical analysis of thin steel plates loaded in shear at non-uniform elevated temperatures. *Journal of Constructional Steel Research*. 2014. No. 97. Pp. 105–113.
 9. Shabalin S. Metody passivnoy ognезashchity [Methods of passive fire protection]. *Gazovaya promyshlennost*. 2017. No. 9. Pp. 122–125. (rus)
 10. Gimranov F.M. Prognozirovaniye stseneriyev razvitiya avariya na neftekhimicheskikh proizvodstvakh [Prediction accident scenarios in the petrochemical industry]. *Vestnik Kazanskogo tekhnologicheskogo universiteta*. 2010. No. 5. Pp. 301. (rus)
 11. Mordvinova A.V., Gordiyenko D.M., Shebeko Y.N., Lagozin A.Y., Nekrasov V.P. Metody upravleniya pozharным riskom morskikh stacionarnykh neftegazodobyvayushchikh platformakh. *Gazovaya promyshlennost* [Methods for managing fire risk for offshore stationary oil and gas production platforms. Gas industry]. *Promyshlennaya bezopasnost i protivopozharnaya zashchita obyektov gazovoy promyshlennosti*. 2014. Pp. 30–34. (rus)
 12. Lazarevska M., Cvetkovska M., Knezevic M., Trombeva Gavriloska A., Milanovic M., Murgul V., Vatin N. Neural network prognostic model for predicting the fire resistance of eccentrically loaded RC columns. *Applied Mechanics and Materials*. 2014. Vol. 627. Pp. 276–282.
 13. Paik J.K., Czujko J. Engineering and design disciplines associated with management of hydrocarbon explosion and fire risks in offshore oil and gas facilities. *Society of Naval Architects and Marine Engineers*. 2013. Vol. 120. Pp. 167–197.
 14. Paik J.K., Czujko J. Assessment of hydrocarbon explosion and fire risks in offshore installations: Recent advances and future trends. *IES Journal Part A: Civil and Structural Engineering*. 2016. Vol. 4. Pp. 167–179.
 15. Imran M., Liew M.S., Nasif M.S., Niazi U.M., Yasreen A. Hazard assessment studies on hydrocarbon fire and blast: An overview. *Advanced Science Letters*. 2017. Vol. 23. Pp. 1243–1247.
 16. Shebeko A.Y., Shebeko Y.N., Gordiyenko D.M. Raschetnaya otsenka ekvivalentnoy prodolzhitel'nosti pozhara dlya stalnykh konstruksiy tekhnologicheskoy estakady neftepererabatyvayushchego predpriyatiya [The estimated duration of the fire for the equivalent steel structure technology overpass refinery]. *Pozharnaya bezopasnost*. 2017. No. 1. Pp. 25–29. (rus)
 17. Shebeko A.Y., Shebeko Y.N. Vzaimosvyaz velichin temperatury stroitelnykh konstruksiy pri standartnom i uglevodorodnom temperaturnykh rezhimakh pozhara [Interrelation of temperature values of building structures under standard and hydrocarbon temperature conditions of a fire]. *Pozharnaya bezopasnost*. 2017. No. 2. Pp. 46–49. (rus)
 18. Payá-Zaforteza I., Garlock M.E.M. A 3D numerical analysis of a typical steel highway overpass bridge under a hydrocarbon fire. *Structures in Fire - Proceedings of the Sixth International Conference, SiF'10*. 2010. Pp. 11–18.
 19. Alos-Moya J., Paya-Zaforteza I., Garlock M.E.M., Loma-Ossorio E., Schiffner D., Hospitaler A. Analysis of a bridge failure due to fire using computational fluid dynamics and finite element models. *Engineering Structures*. 2014.
 - connections: Simulation of the mechanical behaviour of steel and composite connections protected by intumescent coating in fire // *Journal of Structural Fire Engineering*. 2015. No. 6(1). Pp. 41–48.
 7. Kraus P., Mensinger M., Tabelaing F., Schaumann P. Experimental and numerical investigations of steel profiles with intumescent coating adjacent to space-enclosing elements in fire // *Journal of Structural Fire Engineering*. 2015. No. 6(4). Pp. 237–246.
 8. Salminen M., Heinisuo M. Numerical analysis of thin steel plates loaded in shear at non-uniform elevated temperatures // *Journal of Constructional Steel Research*. 2014. № 97. Pp. 105–113.
 9. Шабалин С. Методы пассивной огнезащиты // *Газовая промышленность*. 2017. № 9. С. 122–125.
 10. Гимранов Ф.М. Прогнозирование сценариев развития аварий на нефтехимических производствах // *Вестник Казанского технологического университета*. 2010. № 5. С. 301.
 11. Мордвинова А.В., Гордиенко Д.М., Шебеко Ю.Н., Лагозин А.Ю., Некрасов В.П. Методы управления пожарным риском морских стационарных нефтегазодобывающих платформ. *Газовая промышленность // Промышленная безопасность и противопожарная защита объектов газовой промышленности*. 2014. С. 30–34.
 12. Lazarevska M., Cvetkovska M., Knezevic M., Trombeva Gavriloska A., Milanovic M., Murgul V., Vatin N. Neural network prognostic model for predicting the fire resistance of eccentrically loaded RC columns // *Applied Mechanics and Materials*. 2014. Vol. 627. Pp. 276–282.
 13. Paik J.K., Czujko J. Engineering and design disciplines associated with management of hydrocarbon explosion and fire risks in offshore oil and gas facilities // *Society of Naval Architects and Marine Engineers*. 2013. Vol. 120. Pp. 167–197.
 14. Paik J.K., Czujko J. Assessment of hydrocarbon explosion and fire risks in offshore installations: Recent advances and future trends // *IES Journal Part A: Civil and Structural Engineering*. 2016. Vol. 4. Pp. 167–179.
 15. Imran M., Liew M.S., Nasif M.S., Niazi U.M., Yasreen A. Hazard assessment studies on hydrocarbon fire and blast: An overview // *Advanced Science Letters*. 2017. Vol. 23. Pp. 1243–1247.
 16. Шебеко А.Ю., Шебеко Ю.Н., Гордиенко Д.М. Расчетная оценка эквивалентной продолжительности пожара для стальных конструкций технологической эстакады нефтеперерабатывающего предприятия // *Пожарная безопасность*. 2017. № 1. С. 25–29.
 17. Шебеко А.Ю., Шебеко Ю.Н. Взаимосвязь величин температуры строительных конструкций при стандартном и углеводородном температурных режимах пожара // *Пожарная безопасность*. 2017. № 2. С. 46–49.
 18. Payá-Zaforteza I., Garlock M.E.M. A 3D numerical analysis of a typical steel highway overpass bridge under a hydrocarbon fire // *Structures in Fire - Proceedings of the Sixth International Conference, SiF'10*. 2010. Pp. 11–18.
 19. Alos-Moya J., Paya-Zaforteza I., Garlock M.E.M., Loma-Ossorio E., Schiffner D., Hospitaler A. Analysis of a bridge failure due to fire using computational fluid dynamics and finite element models // *Engineering Structures*. 2014. Vol. 68. Pp. 96–110.
 20. UL 1709 «Standard for safety for rapid rise fire tests of protection materials for structural steel».
 21. Gravit M., Gumerova E., Bardin A., Lukinov V. Increase of fire resistance limits of building structures of oil-and-gas complex under hydrocarbon fire // Springer, Cham: International Scientific Conference Energy Management of Municipal Transportation Facilities and Transport. 2018. Vol. 692. Pp. 818–829.
 22. Fireproofing for hydrocarbon fire exposures. GAPS Guidelines. Publication of Global Asset Protection Services

- Vol. 68. Pp. 96–110.
20. UL 1709 «Standard for safety for rapid rise fire tests of protection materials for structural steel».
 21. Gravit M., Gumerova E., Bardin A., Lukinov V. Increase of fire resistance limits of building structures of oil-and-gas complex under hydrocarbon fire. *Springer, Cham: International Scientific Conference Energy Management of Municipal Transportation Facilities and Transport*. 2018. Vol. 692. Pp. 818–829.
 22. *Fireproofing for hydrocarbon fire exposures*. GAPS Guidelines. Publication of Global Asset Protection Services LLC.
 23. Russian State Standard GOST R EN 1363-2-2014 "Konstruktsii stroitelnyye. Ispytaniya na ognestoykost. Chast 2. Alternativnyye i dopolnitelnyye metody" [Fire resistance tests. Alternative and additional procedures]. (rus)
 24. Gravit M., Gumenyuk V., Sychoy M., Nedryshkin O. Estimation of the pores dimensions of intumescent coatings for increase the fire resistance of building structures. *Procedia Engeneering*. 2015. Vol. 117. Pp. 119–125.
 25. Dybal D.A., Shishilov O.N., Garustovich I.V. Passivnaya ognезashchita v usloviyakh uglevodorodnogo pozhara [Passive fire protection in a hydrocarbon fire]. *Lakokrasochnyye materialy i ikh primeneniye*. 2017. No. 6. Pp. 16–19. (rus)
 26. Zybina O., Gravit M., Stein Y. Influence of carbon additives on operational properties of the intumescent coatings for the fire protection of building construction. *IOP Conference Series: Earth and Environmental Science*. 2017. Vol. 90. Pp. 1–4.
 27. Jimenez M., Bellayer S., Revel B., Duquesne S., Bourbigot S. Comprehensive study of the influence of different aging scenarios on the fire protective behavior of an epoxy based intumescent coating. *Industrial and Engineering Chemistry Research*. 2013. Vol. 52. Pp. 729–743.
 28. Gardelle B., Duquesne S., Vandereecken P, Bellayer S., Bourbigot S. Resistance to fire of intumescent silicone based coating: The role of organoclay. *Progress in Organic Coatings*. 2013. Vol. 76. Pp. 1633–1641.
 29. Bourbigot S, Naik A.D., Bachelet P., Duquesne S. Novel dynamic method for evaluating the char strength of intumescent coatings. *Foreign Language Association of Maine, Annual Conference*. 2016
 30. Огнезащитная штукатурка FENDOLITE-MII [Электронный ресурс]. Систем. требования: Internet Explorer. URL: <https://www.promat.ru/ru-ru/ognezashchitnye-materialy/ognezashchitnyye-shtykatutki/promaspray-f5>. (дата обращения: 16.04.18)
 31. Database of Underwriters Laboratory [Электронный ресурс]. Систем. требования: Internet Explorer. URL: http://database.ul.com/cgi-bin/XYV/template/LISEXT/1FRAME/index.html?_ga=2.154590717.417029873.1502435981-973715613.1499071474 (дата обращения: 16.04.2018).

Marina Gravit,
+7(912)912-64-07; marina.gravit@mail.ru

Elena Golub,
+7(911)972-24-66; alen-go@bk.ru

Sergey Antonov,
+7(903)107-61-52; asp@prozask.ru

Марина Викторовна Гравит,
+7(912)912-64-07;
эл. почта: marina.gravit@mail.ru

Елена Владимировна Голуб,
+7(911)972-24-66; эл. почта: alen-go@bk.ru

Сергей Порфирьевич Антонов,
+7(903)107-61-52; эл. почта: asp@prozask.ru

© Gravit M.G., Golub E.V., Antonov S.P., 2018

doi: 10.18720/MCE.79.10

Granulated foam-glass ceramics for ground protection against freezing

Гранулированная пеностеклокерамика для защиты грунтов от сезонного промерзания и морозного пучения

K.S. Ivanov,
Earth Cryosphere Institute SB RAS, Tyumen,
Russia

**Канд. техн. наук, старший научный
сотрудник К.С. Иванов,**
Институт криосферы Земли ТюмНЦ СО
РАН, г.Тюмень, Россия

Key words: foam-glass ceramic; frost heaving;
seasonal freezing; thermal protection of soils

Ключевые слова: гранулированная
пеностеклокерамика; морозное пучение;
сезонное промерзание; теплозащита грунтов

Abstract. The problem of seasonal freezing and frost heaving of soils of the engineering structures foundations is considered. For the purpose of thermal protection of soils, a granular inorganic closed-porous material, named granulated foam-glass ceramic is proposed. In the laboratory modeling of seasonal freezing, the dynamics of temperature and deformation, as well as the distribution of moisture over the depth of the soil, were studied in three cases: a soil without thermal insulation, a soil with a layer of granulated foam glass ceramics and a soil with an extruded polystyrene layer. Simulation was carried out with ensuring the flow of water to the freezing front. Heat-insulating layers allow to reduce frost heaving of models to the same extent (in comparison with soil without insulation) due to the decreasing of the depth of soil freezing. As a result, the relationship of soil deformations with the distribution of temperature and humidity over the depth of the soil was established. The increased frost heaving deformation of the soil without a heat-insulating layer is explained by the significant migration of capillary water to the upper layer of soil at freezing. The data of the annual monitoring of the experimental road section with the thermal insulation layer of granular foam-glass ceramics placed in embankment is given. The suggested constructive measure was made it possible to substantially reduce the depth of seasonal freezing of the soil compared with the typical road section.

Аннотация. Рассмотрена проблема сезонного промерзания и морозного пучения грунтов оснований инженерных сооружений. С целью теплозащиты грунтов предложен зернистый неорганический закрыто-пористый материал – пеностеклокерамика в виде гранул. При лабораторном моделировании сезонного промерзания, исследованы динамика температуры и деформаций, а также распределение влажности по глубине грунта в трёх случаях: грунт без теплоизоляции, грунт с покрытием из гранулированной пеностеклокерамики и грунт с покрытием из экструзионного пенополистирола. Моделирование проводилось с обеспечением подтока воды к фронту промерзания. Теплоизоляционные слои позволяют в одинаковой мере уменьшить морозное пучение моделей (в сравнении с грунтом без изоляции) за счёт снижения глубины промерзания грунта. В результате была установлена взаимосвязь деформаций грунта с распределением температуры и влажности по глубине грунта. Повышенное морозное пучение грунта без теплоизоляционного слоя объясняется существенным потоком воды к верхнему слою при его промерзании. Приведены данные годичного мониторинга опытного участка автомобильной дороги с устройством в теле насыпи теплоизоляционного слоя из гранулированной пеностеклокерамики, в сравнении с типовым участком. Предложенная конструктивная мера позволяет существенно сократить глубину сезонного промерзания грунта.

1. Introduction

At construction of engineering structures in areas with seasonal freezing special measures to reduce the freezing depth of soils are required. As it known, one of such measures is the heat protection of soils, i.e. the creation of heat-insulation (frost-proof) layers at building of the foundations, pavements and embankments. The boards of extruded polystyrene (EPS) and crushed foamed glass are mainly used for this purpose in practice [1–5]. Due to these layers, the freezing depth of soil is reduced, which is

Иванов К.С. Гранулированная пеностеклокерамика для защиты грунтов от сезонного промерзания и морозного пучения // Инженерно-строительный журнал. 2018. № 3(79). С. 95–102.

especially important at the construction on highly frost-heaving soils and watered soils. In the latter case, the water migration from the warm subsoil to the freezing front can substantially increase the frost heaving deformation by the formation of ice lenses [6–9]. According to the evaluation of the Swedish Road Administration, the costs associated with the annual elimination of the effects of frost heaving of the roadbed are 25 % of the organization's budget [1]. The aforesaid can be attributed to the railways. Studies on the reducing of deformations of frost heave process on the railways of the USSR were carried out back in the early 1930s. The heat-insulation in the form of slag layers was recognized as one of the effective methods of reducing frost heaving deformations of the railway embankment at that time [10].

The experience with the application of EPS and crushed foam glass to protect the soil from frost heaving testifies to the essential effectiveness of these measures [2–5, 11–14]. However, there are difficulties in organizing the mechanized stacking of ESP boards in the roads and railways construction. Foam glass crushed stone is made from waste glass, which creates difficulties in their collection and transportation while ensuring the production of raw materials.

The thermal protection of soils is important technical task, therefore the appearance of new heat insulation materials is of practical interest. For example, granular foam-glass ceramic known as an inorganic heat insulation material, which is pelletized granules, whose thermal conductivity lies in the range 0.08–0.01 W/(m·K), can find use in thermal insulation of soils in addition to EPS and crushed foam glass [15]. The granular structure of the material creates the possibility of laying heat-insulating layers with the use of mechanized means, which is especially important in the construction of long engineering facilities (roads, railways, pipelines, etc.) [16–19]. In this connection, the aim of the work was to study the temperature and deformation changes in the soil with the use of a heat-insulating layer of granulated foam-glass ceramics (GC), under the conditions of laboratory modeling of seasonal freezing and under the conditions of a field test as well. The present work was supported by the Basic Research Program of RAS No. IX.135.2.3, project No. 77.2.5.

2. Methods

The freezing simulation was carried out in an experimental setup representing a thermally insulated cubic tray with soil, having the possibility to create a vertical temperature gradient and free the water migration from the bottom of the tray to the freezing front, Fig. 1a and 1b. The latter is due to the fact that frost heave process is understood as the deformation of soil not only due to the crystallization of pore water, but also due to capillary water migrating to the freezing front [7, 11, 12].

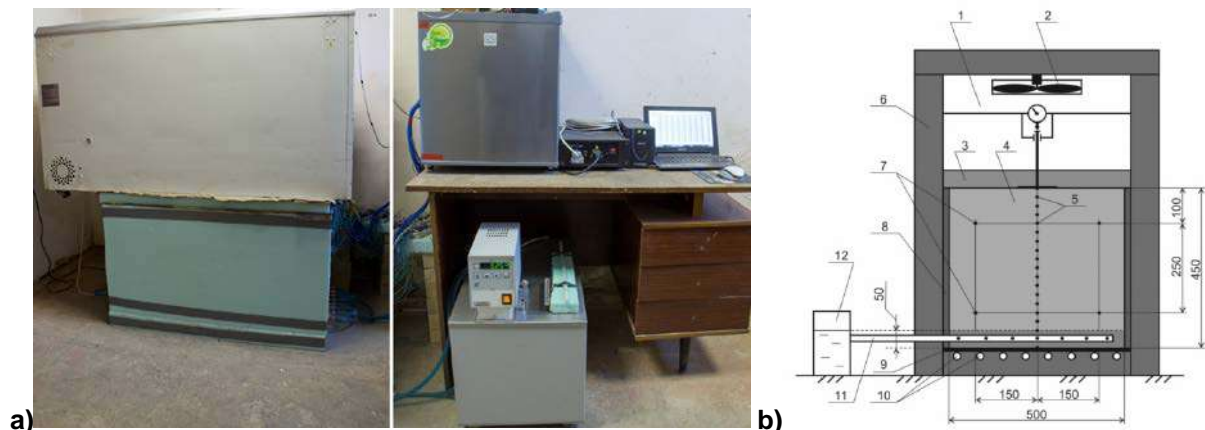


Figure 1. Experimental setup: a – General view and measuring system; b – Schematic view (dimensions given in mm): 1 – freezing chamber; 2 – fan; 3 – layer of heat-insulating material; 4 – soil; 5 – thermocouples; 6 – walls with thermal insulation; 7 – auxiliary thermocouples; 8 – plywood tray; 9 – steel sheet (3 mm thick); 10 – copper tubes of the system for maintaining the set temperature at the bottom of the tray; 11 – perforated tube; 12 – water tank

On the surface of the soil, a layer of the insulating material being inspected can be placed. A temperature gradient inside the tray, which promotes the freezing of soil, is created by setting the temperatures at the top and bottom of the tray, respectively, equal to -9 ± 0.2 and $+0.5 \pm 0.1$ °C. Perforated tube is mounted at the bottom of the tray and connected to a reservoir in which a constant water level of 5 cm is maintained. The perforated tube is laid in a layer of coarse sand of 5 cm thick (Figure 1b), which creates a natural migrating of capillary water upward to the freezing front.

With an interval of 2.5 cm along the vertical axis, temperature sensors are placed: type T (copper-constantan) thermocouples. On both sides of the axis auxiliary thermocouples are placed, which are

designed to measure the lateral temperature gradient. The deformations of the soil are measured with using a dial indicator at ± 0.01 mm accuracy (shown in Figure 1b). The dial indicator is fixed to the walls of the freezing chamber. The rod of the dial indicator touches the steel rod, which, having free vertical movement, transfers the deformations of the soil through the layer of thermal insulation, leaning on the plate.

The soil was represented by light loam, with the following physical characteristics: moisture content 15 %, soil density 1.69 g/cm^3 , plasticity index 8.4, soil salinity degree 0.4 % (with predominance of chloride sulfate salinity). According to X-ray phase analysis, the mineralogical composition of loam is represented by quartz (82 %), montmorillonite and illite (12 %) and albite (6 %). The soil which was stacked into the tray with layers 2.5 cm thick, with a compaction factor of 0.95 ± 0.01 . A heat-insulating layer was laid over the soil (Figure 1). The temperature was measured using an analog-to-digital converter. The error in measuring the temperature was ± 0.1 °C. The end of the measurements was corresponded to the formation of a stationary temperature field in the tray with the soil. In view of the fact that the difference in the readings between the main and auxiliary thermocouples at one depth did not exceed ± 0.2 °C, one can judge about the practically one-dimensional heat flux in the tray.

At the end of each experiment, the water content at a different depth of the soil was determined using a standard procedure. The initial water content of the soil when stacked in the tray was 15%. Before starting the freezing chamber of the experimental setup, the soil mass was held to stabilize the temperature within 20 ± 0.2 °C.

Thermal insulation layers made of EPS boards of 3 cm thick, with an average density of 35 kg/m^3 , and a layer of fraction 5–10 mm from GC with a bulk density of 300 kg/m^3 were used in the studies. The values of the thermal conductivity of the EPS and GC were established equal to 0.035 and $0.086 \text{ W/(m} \cdot \text{K)}$, respectively. Due to the fact that the thermal conductivity of the GC layer is almost twice high as the ESP boards, the thickness of the thermal insulation layer in the experiments was taken to be 6 and 3 cm for the GC and ESP, respectively. This provides approximately equal thermal resistance. Depending on the type of thermal insulation, laboratory experiments had the following marking: soil without thermal insulation – C, soil with ESP – E and soil with GC – G.

A field test of the GC layer to protect the foundation from seasonal freezing was carried out on the experimental section of the Beskozobovo-Evsino-Lamensky road (Golysmanovsky district, Tyumen region, Russia). The experimental and typical sections of the road were carried out during the repair work from 5.10 to 16.10.2016, km 47+540 – km 47+690. The GC of 5–10 mm fraction was laid in the experimental section as a heat-insulation layer, and the layer of sand instead of GC was laid in the typical section. Both sections had the following layers (from top to bottom): surface course – 12 cm, base course (gravel mixture for pavements) – 30 cm, geotextile, heat-insulation layer of GC or sand (in the first and the second section respectively) – 25 cm, geotextile, natural soil. The roadway and heat-insulation layer were 7.3 and 8.3 m width, respectively, the length of each section was 50 m.

The temperature sensors were placed into vertical wells located on the axis of the corresponding sections of the road (depth up to 3.5 m). Temperature monitoring was carried out from October 18, 2016 to October 27, 2017. The temperature of the ground was measured twice a day with a digital data logger (accuracy of ± 0.1 °C).

3. Results and Discussion

The process of the freezing of soil without the use of thermal insulation was investigated in the first stage. A fragment of the temperature dynamics at depths from 2.5 to 25 cm is shown on Figure 2a. After 90 hours all the temperature curves are aligned along the horizontal axis of the graph, which indicates the formation of a stationary temperature field in the soil. A sharp bend of the curve at a depth of 2.5 cm characterizes the heat release of the underlying layers of the soil during the water-ice phase transition and indicates that the soil freezing point is in the range from -0.2 to -0.4 °C. At depths of 7.5 to 20 cm, a more smooth and prolonged inflection is observed, corresponding to a slowing down of the freezing rate and transition to a stationary state. Extrapolating the data of Figure 2a near 0 °C, the freezing depth of 23 cm after 90 hours was established.

Dynamics of deformation of soil in experiment C is shown in Figure 3 (curve C). Up to 25 hours the shrinkage deformation of soil (up to -1.5 mm) is observed, despite the fact that by this time the soil was frozen to a depth of 5–6 cm (according to Figure 2a). Apparently, the deformation of the frost heave process and the shrinkage deformation are developed simultaneously as a result of the capillary water

migration and the compaction of soil particles. Similar shrinkage deformations were observed when the loam was frozen from above, under conditions of capillary water moving upward to the freezing front [20].

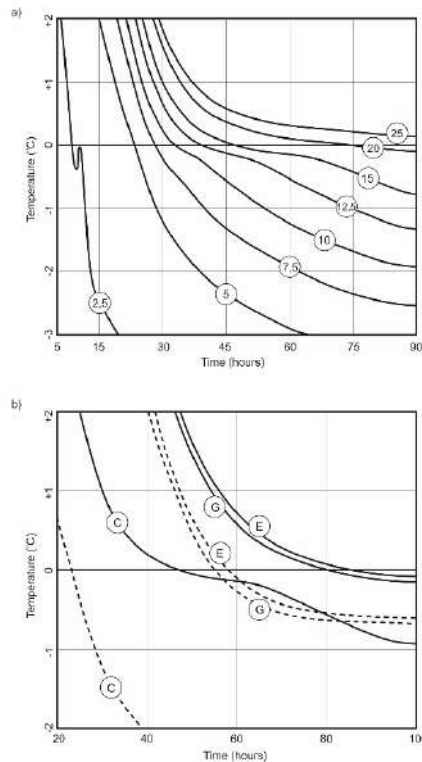


Figure 2. Temperature dynamics: a – experiment C (the numbers in the circles correspond to the depths, cm); b – experiments E and G compared to C (the dashed curves correspond to a depth of 5 cm, solid curves – 15 cm)

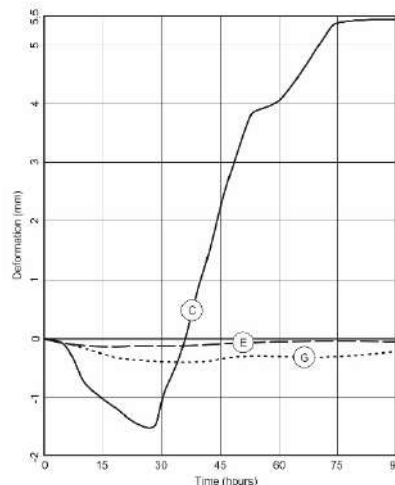


Figure 3. Deformation dynamics of soil

During the period from 25 to 37 hours the initial position of the soil level was reached due to the increase of development of frost heave process, which lasts up to 75 hours and practically stops to 90 hours, reaching a value of 5.45 mm. From the graphs in Figure 3 it is seen that the most intensive growth of deformations was occurred from 25 to 52 hours, corresponding to the freezing of the soil from 6 to 17.5 cm (Figure 2a). Corresponding value of deformation of the soil of 3.8 mm was reached. Freezing from 17.5 to 20 cm took place from 52 to 75 hours and corresponded to an increase in the deformation of the soil by 1.65 mm: from 3.8 to 5.45 mm. The inflection of curve C in the interval 45–60 hours is associated with a significant slowdown in the freezing rate of the soil (Figure 3). Thus, the freezing time of soil from 10 to 15 cm was about 15 hours, and from 15 to 20 cm – 28 hours (according to Figure 2a). During this period, the processes of shrinkage of the unfrozen part of the soil under the rising capillary water could begin to develop again.

The significant water content at the upper layers of soil is established according to the graph of water content distribution along the depth for experiment C, Figure 4 (dotted curve). With increasing the depth, a continuous increase in the water content of soil from 15 to 45 % is noted. Water content of a part of the soil at a depth from 10 to 20 cm, corresponding to the most intensive frost heave deformations in period from 37 to 75 hours (Figure 2a) is 26–28 %.

Subsequently, the soil was frozen using heat-insulating layers. The dynamics of soil freezing in experiments E and G is similar, as can be seen from the graphs in Figure 2b. In comparison with soil without insulation (curves C), cases E and G are characterized by a much later start of the freezing of the upper layer at a depth of 5 cm: 55–57 hours against 24 hours for the case C. The depth of freezing of 15 cm is reached through 83 (for E and G) and 47 hours (for C). Thus, the cooling rate of the soil is reduced by about half.

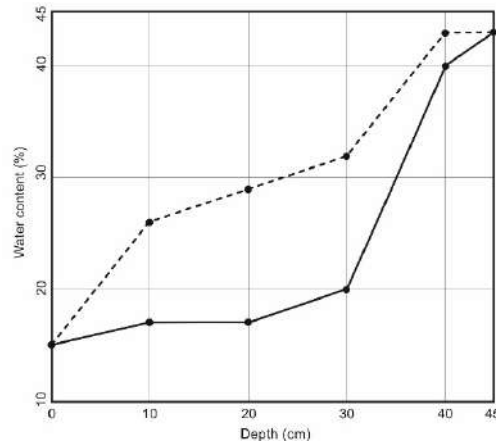


Figure 4. Distribution of water content over the depth of the soil (the dotted curve corresponds to experiment C, solid – E and G)

Extrapolating the E and G graphs at a depth of 15 cm (Figure 2b) and taking into account the error in measuring the soil temperature, it was established that the freezing depth in the cases E and G can be taken to be 16 ± 1 cm. However, in spite of this, frost heaving deformations of the soil, characteristic for the case of C, are absent. A slight shrinkage of the soil during freezing is proved by curves E and G in Figure 3. The peak of shrinkage deformation, characteristic for curve C, is smoothed, due to the later freezing of the upper layers in cases E and G (Figure 2b). After 40 hours, the deformations of the soil are close to the initial position, but their values are negative (Figure 3, curves E and G).

The water content distribution along the depth of the soil in Figure 4 for the cases E and G is presented on the same graph (solid curve), in view of the insignificant discrepancies in the measurements. As it is seen on Figure 4, the soil layer up to a depth of 20 cm has water content in the range of 15–17 %, which is almost twice less than in the case of C and close to initial water content. Consequently, the smoothing of the soil shrinkage and frost heaving deformations in cases E and G can be explained by an insignificant raise of capillary water to the freezing layer. Thus, due to the application of ESP and GC, a water-thermal regime in the soil is formed, therefore the development of shrinkage and frost heaving deformations are substantially reduced, despite the freezing of a part of the soil.

Decrease in the depth of seasonal freezing of soil with the use of GC is observed in the field test. The pattern of temperature distribution in the soil on the experimental section of the road is presented in Figure 5. Three types of the temperature distribution of the soil are shown on the graphs: the initial temperature distribution on 18.10.2016 (curves G1 and S1), the distribution corresponding to the maximum freezing depth of the soil in the sections by 24.03.2017 (curves G2 and S2) and the distribution at the maximum temperature at a depth of 0 cm in summer 03.08.2017 (curves G3 and S3). Construction of the experimental section with GC in October 2016 is shown on Figures 6a and 6b.

The graphs labeled G1 and S1 corresponding to the initial temperature distribution (section with GC and typical section, respectively) are shifted to the left as the ground cools in autumn and winter, after which they pass to curves G2 and S2 – when a maximum value of the depth of freezing is reached. The soil temperature at a depth of 0 cm at this moment is -3.8 and -6.1 °C, and the depth of freezing is 100 and 162 cm, respectively for section with GC and typical section (curves G2 and S2 on Figure 5).

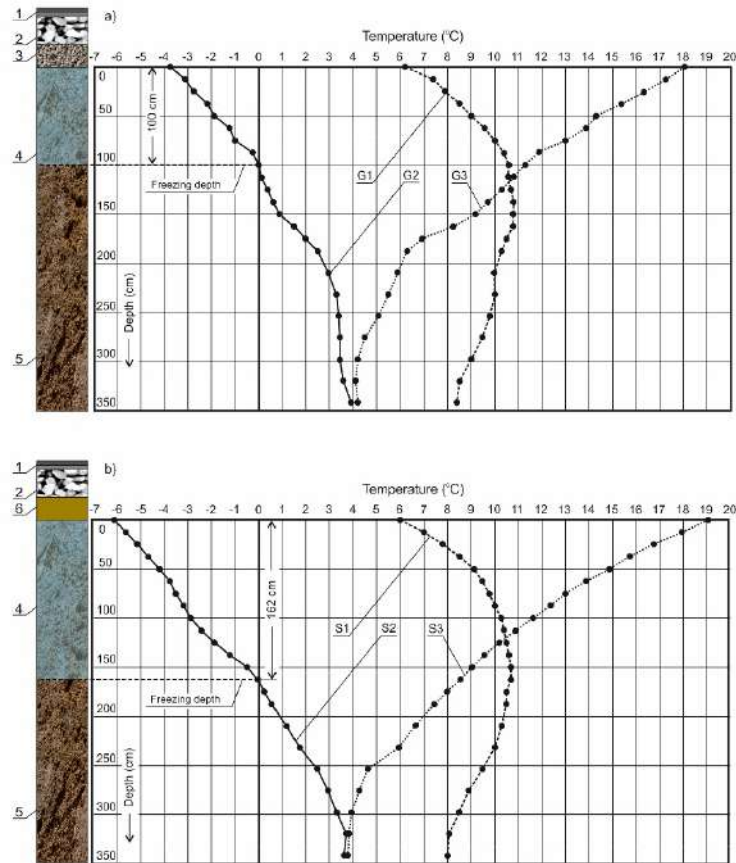


Figure 5. Distribution of temperature in the soil: a – road section with GC; b – typical road section. 1 – surface course 12 cm thick; 2 – base course 30 cm thick; 3 – GC 25 cm thick; 4 – frozen soil; 5 – soil with a positive temperature; 6 – layer of fine sand



Figure 6. Construction of the experimental section with GC: a – GC compaction by roller; b – geotextile laying above GC

The obtained results can be compared with the data of the authors who monitored the experimental section of the road with a heat-insulating layer of crushed foam glass stone of 35 cm thick (Norway) [2, 5]. After the first winter the authors observed a reduction of the freezing depth in the experimental section from 35 to 0 cm (in comparison with the typical section where granite crushed stone was used instead of crushed foam glass).

As the air temperature during the spring and summer is raised, the curves G2 and S2 are shifted to the right and took the form of G3 and S3 (Figure 5). At this point, the soil under the layer of GC at a depth of 0 cm has a temperature of 1 °C lower than the typical section: 18 and 19 °C correspondingly. In the future, the annual cycle of soil temperature change is repeated, beginning with the temperature distribution near the curves G1 and S1.

4. Conclusions

1. Frost heaving deformation of the soil without insulation equal to 5.45 mm was established, while in experiments with ESP and GC the shrinkage deformation of soil was observed. In the first case, a significant rise of capillary water to the upper layers is established, because the water content of the soil at a depth of 20 cm was changed from 15 to 28 %, and in the experiments with ESP and GC – up to 17 %.

2. The freezing depth of soil with the use of heat-insulating layers of ESP and GC with equal thermal resistance is approximately 16 cm, whereas without usage of thermal insulation the freezing depth of the soil is 23 cm. In the field test for the first year of operation of the experimental section of the motorway with heat insulating layer of GC the freezing depth of soil was decreased from 162 to 100 cm. According to the data of Swedish Road Administration, the elimination of the frost heaving due to the use of thermal insulation can save up to a quarter of the organization's budget spent on road repair [1, 5].

3. Apparently, the frost heaving deformations in experiments with ESP and GC are summarized with shrinkage deformations of the soil due to high water content at a depth below 20 cm (where a positive temperature persists), which explains the slight shrinkage.

4. Experiments clearly demonstrate not only the effectiveness of the application of GC and ESP to reduce the freezing depth, but also the importance of taking into account the interrelationship of the water-heat regime arising in this case with the nature of soil deformations.

References

1. Furuberg T., Watn A., Amundsgård K.O. Effects of Leca insulation in roads and railways. *Proceedings of the 9th International Symposium on Ground Freezing and Frost Action in Soil*. 2000. Pp. 203–207.
2. Øiseth E., Aabøe R., Hoff, I. Field test comparing frost insulation materials in road construction. *Proceedings of the 13th International Conference on Cold Region Engineering*. 2006. Pp. 662–673.
3. Øiseth E., Refsdal G. Lightweight aggregates as frost insulation in roads – Design chart. *Proceedings of the International Conference on Cold Regions Engineering*. 2007. Pp. 63.
4. Hoff I., Want A., Øiseth E., Emdal A., Amundsgård K.O. Light Weight Aggregate (LWA) Used in Road Pavements. *Proceedings of the 6th International Conference on the Bearing Capacity of Road and Airfields*. 2002. Pp. 1013–1022.
5. Frydenlund T.E., Aabøe R. Foamglass – A New Vision in Road Construction. *Proceedings of the 22th World Road Congress*. 2003. Pp. 96.
6. Haghi N.T., Hashemian L., Bayat A. Effects of seasonal variation on the load-bearing capacity of pavements composed of insulation layers. *Transportation Research Record*. 2016. No. 2579. Pp. 87–95.
7. Xu J., Niu F.-J., Li A.-M., Lin Z.-J. Analysis of the prevention effect of thermal-insulation method on frost heave of railway subgrade in seasonal frozen regions. *Journal of the China Railway Society*. 2010. No. 32(6). Pp. 124–131.
8. Yin Y., Zhang D., Feng C., Ji C., Yang H. Insulation and anti-freezing test research of channel lining project in Linhe district of Inner Mongolia. *Journal of Drainage and Irrigation Machinery Engineering*. 2016. No. 34(10) Pp. 867–871.
9. Tatarniuk C., Lewycky D. A case study on the performance of high load polystyrene as roadway insulation in Edmonton, Alberta, Canada. *Conference and Exhibition of the Transportation Association of Canada - Transportation Successes: Let's Build on Them*. 2011. Pp 121.
10. *Izucheniye puchin zheleznodorozhnogo polotna* [Study of the depths of the railroad tracks]. Moscow: Ogiz-Gostransizdat, 1932. 110 p. (rus)
11. Nurmikolu A., Kolisoja P. Extruded polystyrene (XPS) foam frost insulation boards in railway structures. *Proceedings of the 16th International Conference on Soil Mechanics and*

Литература

1. Furuberg T., Watn A., Amundsgård K.O. Effects of Leca insulation in roads and railways // *Proceedings of the 9th International Symposium on Ground Freezing and Frost Action in Soil*. 2000. Pp. 203–207.
2. Øiseth E., Aabøe R., Hoff, I. Field Test Comparing Frost Insulation Materials in Road Construction // *Proceedings of the 13th International Conference on Cold Region Engineering*. 2006. Pp. 662–673.
3. Øiseth E., Refsdal G. Lightweight aggregates as frost insulation in roads – Design chart // *Proceedings of the International Conference on Cold Regions Engineering*. 2007. Pp. 63
4. Hoff I., Want A., Øiseth E., Emdal A., Amundsgård K.O. Light Weight Aggregate (LWA) used in road pavements // *Proceedings of the 6th International Conference on the Bearing Capacity of Road and Airfields*. 2002. Pp. 1013–1022.
5. Frydenlund T.E., Aabøe R. Foamglass – A New Vision in Road Construction // *Proceedings of the 22th World Road Congress*. 2003. Pp. 96.
6. Haghi N.T., Hashemian L., Bayat A. Effects of seasonal variation on the load-bearing capacity of pavements composed of insulation layers // *Transportation Research Record*. 2016. № 2579. Pp. 87–95.
7. Xu J., Niu F.-J., Li A.-M., Lin Z.-J. Analysis of the prevention effect of thermal-insulation method on frost heave of railway subgrade in seasonal frozen regions // *Journal of the China Railway Society*. 2010. № 32(6). Pp. 124–131.
8. Yin Y., Zhang D., Feng C., Ji C., Yang H. Insulation and anti-freezing test research of channel lining project in Linhe district of Inner Mongolia // *Journal of Drainage and Irrigation Machinery Engineering*. 2016. № 34(10). Pp. 867–871.
9. Tatarniuk C., Lewycky D. A case study on the performance of high load polystyrene as roadway insulation in Edmonton, Alberta, Canada // *Conference and Exhibition of the Transportation Association of Canada - Transportation Successes: Let's Build on Them*. 2011. Pp. 121.
10. Изучение пучин железнодорожного полотна. Двенадцатый сборник. М.: Огиз-Гострансиздат, 1932. 110 с.
11. Nurmikolu A., Kolisoja P. Extruded polystyrene (XPS) foam frost insulation boards in railway structures // *Proceedings*

- Geotechnical Engineering: Geotechnology in Harmony with the Global Environment*. 2005. Pp. 1761–1764.
12. Xu J., Niu F.-J., Niu Y.-H., Lin Z.-J., Xu Z.-Y. The design parameters of roadbed with insulation in seasonal frozen ground. *Journal of Civil, Architectural and Environmental Engineering*. No. 31(3). Pp. 83–89.
 13. Edgar T., Potter C., Mathis R. Frost Heave Mitigation Using Polymer Injection and Frost Depth Prediction. *Proceedings of the International Conference on Cold Regions Engineering*. 2015. Pp. 416–427.
 14. Liu G., Zhang B. Experimental study on the thermal conductivity of light soil mixed with EPS particles. *5th Asian Regional Conference on Geosynthetics: Geosynthetics for Sustainable Adaptation to Climate Change*. 2012. Pp. 463–466.
 15. Ivanov K.S. Novyy izolyatsionnyy material dlya termostabilizatsii gruntov [New insulating material for thermostabilization of soils]. *Kriosfera Zemli*. 2011. No. 4. Pp. 120–122. (rus)
 16. Korotkov Ye.A., Ivanov K.S. Penosteklo v dorozhnom stroitelstve – novoye napravleniye ispolzovaniya materiala [Foam glass in road construction - a new direction of using the material]. *Vestnik Moskovskogo avtomobilno-dorozhnogo gosudarstvennogo tekhnicheskogo universiteta (MADI)*. 2016. No. 1(44). Pp. 87–97. (rus)
 17. Ivanov K.S., Korotkov E.A. Investigation of the effect of a layer of granulated foam-glass ceramics on the temperature conditions of frozen soil. *Soil Mechanics and Foundation Engineering*. 2017. Vol. 54. No. 5. Pp. 349–355.
 18. Korotkov Ye.A., Ivanov K.S., Patkina I.A. Granulirovanny teploizolyatsionnyy material na osnove opalovogo syrya dlya ustroystva morozozashchitnykh sloev dorozhnoy odezhdyy [Granular heat-insulating material on the basis of opal raw material for the device of frost protection layers of pavement]. *Vestnik SIBADI*. 2015. No. 6(46). Pp. 65–70.
 19. Korotkov Ye.A., Konstantinov A.O., Smirnov P.V., Ivanov K.S. Yevropeyskiy opyt primeneniya penostekla v dorozhnom stroitelstve. Perspektivy ispolzovaniya analogichnykh materialov v Rossiyskoy Federatsii [European experience in the use of foam glass in road construction. Prospects for the use of similar materials in the Russian Federation]. *Nauchnyye problemy transporta Sibiri i Dalnego Vostoka*. 2015. No. 1. Pp. 58–61. (rus)
 20. Nevzorov A.L., Korshunov A.A., Churkin S.V. Metody otsenki puchinistosti gruntov s ispolzovaniyem sovremennykh priborov [Methods for estimating the soils of soils using modern instruments]. *Inzhenernyye izyskaniya*. 2013. No. 5. Pp. 52–56.
 - of the 16th International Conference on Soil Mechanics and Geotechnical Engineering: Geotechnology in Harmony with the Global Environment. 2005. Pp. 1761–1764.
 21. Xu J., Niu F.-J., Niu Y.-H., Lin Z.-J., Xu Z.-Y. The design parameters of roadbed with insulation in seasonal frozen ground // *Journal of Civil, Architectural and Environmental Engineering*. No. 31(3). Pp. 83–89.
 22. Edgar T., Potter C., Mathis R. Frost Heave Mitigation Using Polymer Injection and Frost Depth Prediction // *Proceedings of the International Conference on Cold Regions Engineering*. 2015. Pp. 416–427.
 23. Liu G., Zhang B. Experimental study on the thermal conductivity of light soil mixed with EPS particles // *5th Asian Regional Conference on Geosynthetics: Geosynthetics for Sustainable Adaptation to Climate Change*. 2012. Pp. 463–466.
 24. Иванов К.С. Новый изоляционный материал для термостабилизации грунтов // *Криосфера Земли*. 2011. № 4. С. 120–122.
 25. Коротков Е.А., Иванов К.С. Пеностекло в дорожном строительстве – новое направление использования материала // *Вестник Московского автомобильно-дорожного государственного технического университета (МАДИ)*. 2016. № 1(44). С. 87–97.
 26. Ivanov K.S., Korotkov E.A. Investigation of the effect of a layer of granulated foam-glass ceramics on the temperature conditions of frozen soil // *Soil Mechanics and Foundation Engineering*. 2017. Vol. 54. No. 5. Pp. 349–355.
 27. Коротков Е.А., Иванов К.С., Паткина И.А. Гранулированный теплоизоляционный материал на основе опалового сырья для устройства морозозащитных слоёв дорожной одежды // *Вестник СИБАДИ*. 2015. № 6(46). С. 65–70.
 28. Коротков Е.А., Константинов А.О., Смирнов П.В., Иванов К.С. Европейский опыт применения пеностекла в дорожном строительстве. Перспективы использования аналогичных материалов в Российской Федерации // *Научные проблемы транспорта Сибири и Дальнего Востока*. 2015. № 1. С. 58–61.
 29. Nevzorov A.L., Korshunov A.A., Churkin S.V. Metody otsenki puchinistosti gruntov s ispolzovaniyem sovremennykh priborov // *Inzhenernyye izyskaniya*. 2013. № 5.

Konstantin Ivanov,
+7(922)042-43-52; sillicium@bk.ru

Константин Сергеевич Иванов,
+7(922)042-43-52; эл. почта: sillicium@bk.ru

© Ivanov K.S., 2018

doi: 10.18720/MCE.79.11

Behavior of a hollowed-wood ventilated façade during temperature changes

Деревянный фасад с вентилируемыми каналами для тропического климата

G.B. Vieira,
M.R. Petrichenko,
T.A. Musorina,
D.D. Zaborova,
Peter the Great St. Petersburg Polytechnic University, St. Petersburg, Russia

Студент Г.Б. Виейра,
д-р техн. наук, заведующий кафедрой
М.Р. Петриченко,
аспирант Т.А. Мусорина,
аспирант Д.Д. Заборова,
Санкт-Петербургский политехнический университет Петра Великого, Санкт-Петербург, Россия

Key words: ventilated façade; hollowed wood; energy efficient; thermal performance; enclosure structure

Ключевые слова: вентилируемый фасад; вентилируемые каналы; энергоэффективность; теплофизические характеристики; ограждающая конструкция

Abstract. The Ventilated Façade System is a reasonably new technique, which was developed in Europe with the need of cost savings from the energy for cooling and heating of constructions. This system, established in the 1960's, was an acknowledged as a constructive innovation both for esthetics and functional aims. Therefore, its use has spread not just during buildings' retrofit but also in new constructions. Despite this fact, the applicability of wood with a hollow through it for ventilated façades remain quite unknown, as mainly of these façades are built with conventional materials such as concrete, lightweight concrete, brick, ceramic, wood panels and glasses. Due to that circumstance, this paper will simulate the behavior of a wood-hollowed when submitted to temperature variations (from 10 °C to 30 °C), in a small-scale (1:10). During the trials, the hollowed-wood sample was set in two directions: horizontal and vertical. In addition, trials were carried out with/without insulation material, and with cyclic and non-cyclic temperature variations. The result shows that hollowed-wood presents better behavior when accompanied with thermal insulation materials, reducing the rate, on which the temperature changes inside it. In addition, different orientations of the sample lead to slight difference comportment as well as the increase of the size of the hole in the wood.

Аннотация. Вентилируемая фасадная система-это достаточно новая техника, которая была разработана в Европе с целью экономии затрат энергии на охлаждение и нагрев конструкций. Поэтому его применение распространилось не только во время реконструкции зданий, но и в новых постройках. Несмотря на этот факт, применимость древесины с вертикальным вентилируемым каналом остается довольно неизвестным, по сравнению с наиболее распространенными материалами как бетон, облегченный бетон, кирпич, деревянные панели, стекла и т.д. В данной статье представлен натурный эксперимент поведения деревянного фасада с вентилируемыми каналами при разных колебаниях температур (от 10 °C до 30 °C). Образец представлен в малом масштабе (1:10). Во время испытаний образец древесины с вентилируемыми каналами устанавливался в двух направлениях: горизонтальном и вертикальном. Кроме того, испытания проводились с/без изоляционного материала, а также с циклическими и нециклическими температурными колебаниями. Результат показывает, что пустотелая древесина представляет собой более лучшее поведение в сочетании с теплоизоляционными материалами, уменьшает скорость изменения температуры внутри вентилируемого канала. Различное расположение (горизонтальная/вертикальная) приводит к небольшим различиям температурного распределения.

1. Introduction

The building's segment – i.e. the residential buildings and service sector- is the major consumer of energy and producer of CO in the European Union and is responsible for about 40 % of greenhouse emissions and total final energy consumption as presented in Figure 1 [1].

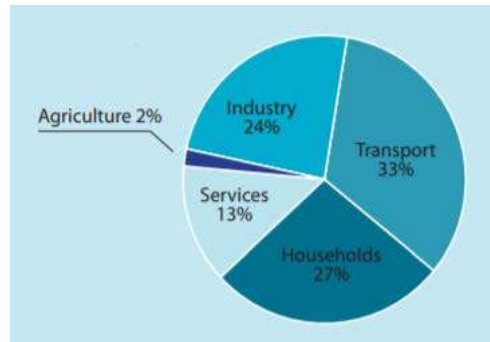


Figure 1. Distribution of energy consumption in Europe by sectors [1]

A similar scenario can be seen in United States, as, according to [2], the combined electricity demand in the residential and commercial sectors made up over 70 % of total electricity demand in 2013, with each sector using approximately the same amount of electricity. Also in Russia, as around 95 % of the buildings of the total housing stock in the country do not meet modern energy efficiency requirements for energy efficiency. Even more, as the physical state of some building façades is also often defective [3].

The residential sector has significant potential for cost-effective energy savings, which, if performed, would drive to a number of benefits, as reduced energy needs, minimize import dependency and climate effects, lower energy bills, raise of job offers and the encouragement of local development [4].

Moreover, a large parcel of European constructions was built before the 1960's – around 40 % – by the time there were basically no requirements for energy efficiency and only a minimum part has undergone any energy retrofits. Hence, it is noticeable that the oldest part of the building stock contributes expressively to the high-energy consumption in the housing sector leading to a large potential of energy saving. According to this context, the European Commission has highlighted the need for increasing the construction energy efficiency for both the new and the existing buildings. Among the most popular responses for this request, it is the improvement of the building thermal insulation. Furthermore, over the last years, ventilated façade systems have gained much attention [5].

Ventilated building façades are an external envelope technique with significant benefits over traditional, single skin façades. These benefits cover almost all building physics topics, from moisture to thermal efficiency, noise, fire resistance and structural efficiency [6].

According to [7], due to it is a non-destructive, quick and clean solution, ventilated façades have been widely used in retrofitting works especially in residential buildings around Europe. Some coating materials might receive a titanium dioxide-based product in order to makes it difficult to get dirt on the surface and simplifies cleaning. In addition, there are coatings which can receive anti-graffiti treatment, which is a problem in big cities around the world. Figure 2 shows a typical ventilated façade and its air convection.

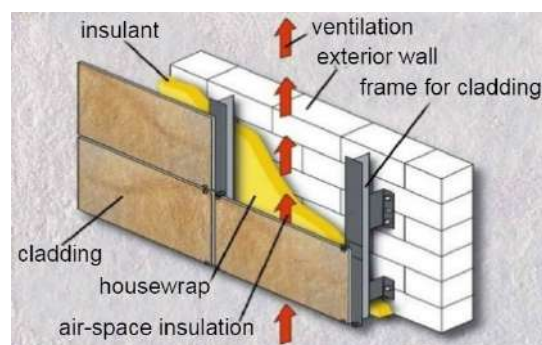


Figure 2. Traditional Ventiladed Façade Scheme [12]

However, some precautions should be taken into consideration while applying this technique in the constructions. There are some minimum requirements that must be valued, such as hygrothermal performance, energy efficiency, sound proof and fire resistance.

Diverse studies were carried out in order to evaluate the efficiency of ventilated façades in edifications and application of new technologies. In [8], a wide range of solutions lead to solving energy saving problems when using ventilated façade. In addition, [9] and [10] analyze, respectively, problems related to hinged ventilated façades and structural design importance on its behavior. Work [11] studies advantages of the applicability of new technologies in standard ventilated façades.

According to [5], the maximum U-value allowed differs not just from country to country but also if a new construction is under progress or if it is a retrofit. Also, some other criteria as type of building (residential, tertiary, i.e.) or indoor temperature can lead to a different maximum U-Value allowed. Therefore, for new residential buildings, Ireland established, for example, a maximum U-Value of 0.21 W/(m²K), while in Latvia U-value may drop slightly below 0.20 W/m²K, but not below 0.15 W/(m²K). For moisture-related some general recommendations and descriptive requirements regarding avoidance of surface condensation and mold formation are provided per country.

The recommended fire resistance criteria (fire propagation time) should be at least 120 min [5]. Nevertheless, at most national building regulations the required length of time against fire is below or equivalent to 60 min. In most countries across Europe, for extensive façade, testing requirements are not mandatory by national regulations.

Energy Performance requirements applies when the ventilated façade system has to work in mutual cooperation with other energy conservation measures in order to reach a particularly strict energy performance standard [13].

However, as long as this paper analyzed, during laboratory trials, a natural ventilated façade the criteria of energy performance was ignored.

During the previous years, many authors have studied different approaches for sustainable ventilated façades. In [14], was evaluated the use of wood-based materials (wood, cardboard and cork) as ventilated façade. Authors considered the system satisfactory in thermal and acoustic parameters and emphasized the short time of construction. Still, the cost and time for processing and assembling it in industries require further studies.

However, [15] states that the use of timber with bonded joints in ventilated façades represents a viable option in comparison with aluminium structure i.e. Nevertheless, the installation procedure needs to be followed very strictly as the adhesion of wood plastic is very unstable.

Another concept investigated related to the use of wood/trees refers to biofaçade by [16], where its application had a better thermal performance during the daytime due to its shading, photosynthesis and evapo-transpiration, contributing for reducing the indoor temperature of the studied object. On the other hand, during the night the results did not represent any gain and even obstruct heat dissipation. Moreover, different types of climbing families give different results, as the geometrical properties will influence the air velocity and room temperature.

In [17], Nore and Thue developed studies about the relation of moisture content with wood claddings and the influence of ventilation gap design in Norway, making recommendations about the openings of wood claddings. The air gap openings should be fully open when the wooden cladding will be exposed to heavy wind driven rain loads. In a dry climate, where the wall will be mostly dry, the results indicate that a design with the air gap openings closed will give the driest wood cladding.

In addition to [17–18], states that, to obtain properties that allowed it to withstand to weathering conditions it has to be properly modified in order to be able to be applied and to remain unchanged even in adverse climatic conditions without requiring great maintenance. The modification process submits the raw wood at elevated temperatures that most of the moisture will evaporate, increasing the wood resistance (up to 30 %), in a process called Thermowood.

Therefore, as long as almost all the studies about the use of wood in ventilated façade leads to the applicability of wood panels, this paper focus on laboratory experiments for verifying the feasibility of using woods with hollows as a ventilated façade in a climate which the temperature varies from 10 °C to 30 °C (subtropical climate). The trials carried out had two different approaches: with the hollows set on the vertical orientation and on the horizontal orientation. Moreover, it will be evaluated the heat losses during the air convection through the hollows made in the wood.

2. Methods

The experiment has been conducted in an isothermal chamber "CHALLENGE 250" with an approximated volume of 20 liters and dimensions of 0.60 x 0.75 x 0.52 m (W x H x L). The standard sensors «Dallas DS18B20» carried the measurement of instantaneous temperature. This sensor is also designed to measure the temperature of liquids, and temperature measurement in a humid environment. The sensor is enclosed in a metal flask measuring 6x50 mm. It is equipped with a sealed lead cable 1 meter length. The cable consists of 3 wires: red (VCC), blue (DATA), black (GND) [22].

The wood-hollowed sample has the following dimensions:

- L = 14 cm;
- W = 3 cm;
- H = 21 cm;
- Diameter of the holes: 1.0–1.5 cm.

The sketch of the sample with rock wool and reinforced concrete is presented on the Figure 3.

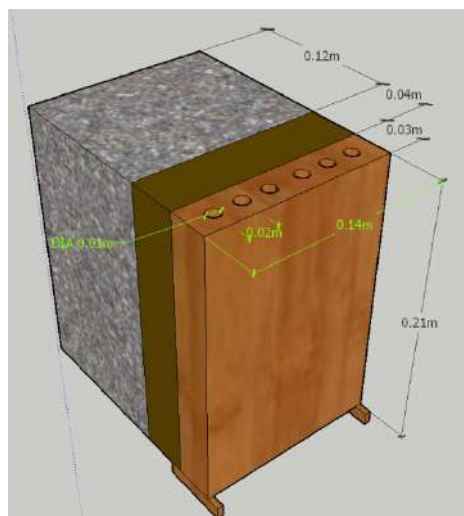


Figure 4. Sketch of the wood sample with rock wool glued and reinforced concrete attached on it

The temperature of the sensor were collected every 3 minutes, both for periodic (cyclic) and non-periodic (non-cyclic) regime. It was placed sensors inside the material, between layers and, even, one outside, in the outer surface, in order to double check the temperature of the chamber and the precision of the sensor, avoiding potential mistakes during the measurements.

The laboratory trials were carried out during the months of October and November of 2017 and different approaches were tested as shown in the scheme below in the figure 4.

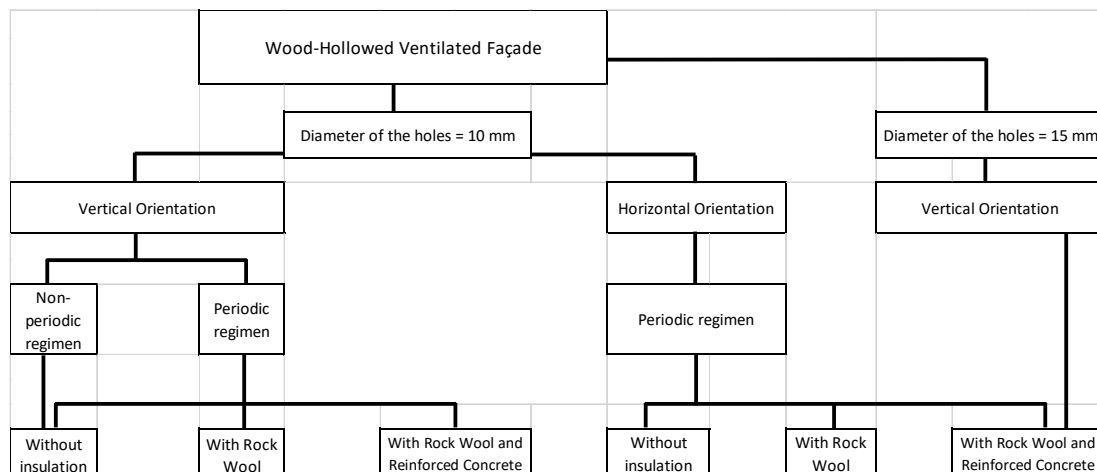


Figure 4. Scheme of the laboratory tests

During the non-cyclic regimen, the temperature of the chamber was set at zero degrees Celsius and was heated up to thirty degrees Celsius, heating to 10 °C and to 20 °C (30 minutes on each).

For the periodic regimen, the temperature varied from 10 °C to 30 °C, typical from a subtropical highland climate, which is the location of the city of Curitiba – Brazil, and one the motivations for this paper.

The picture below show the sample during the trials with different configurations of layers.



Figure 5. Different configurations during the trials: (a) without insulation and vertical orientation (d=10mm); (b) with insulation and concrete and vertical orientation (d=15mm); (c) with insulation and concrete and horizontal orientation (d=10mm)

As the Figure 5 shows, in the top of the chamber two pieces of Styrofoam (expanded polystyrene) were glued in order to simulate a disturbed movement of air inside the chamber, being more similar of what happens in an outdoor area.

The sensors were placed in the following positions:

- Sensor 1: Top of the wood;
- Sensor 2: Inside (h = 10 cm) the middle left hollow (front view) made in the wood (Figure 5b);
- Sensor 3: Inside (h = 10 cm) the middle right hollow (front view) made in the wood (Figure 5b);
- Sensor 4: Outer part of the wood;
- Sensor 5: Bottom of the wood;
- Sensor 6: Between the rock wool layer and the wood-hollowed ventilated façade;
- Sensor 7: Between the rock wool layer and the reinforced concrete layer;

The following materials were used in the samples during the experiments:

- Pine Wood – Dimensions 210 x 140 x 30 mm;
- RockWool Insulation – Dimensions 210 x 140 x 40 mm;
- Reinforced concrete block (Cement B20, steel diameter: 14 mm);

It is important to mention that the wood sample was made in a scale of 1:10. The dimensions were based in the giant bamboo tree called *Guadua Angustifolia*, widely spread in the forests of South America.

3. Results and Discussion

The graphics obtained from the experiments are showed below and three analysis are made related to the behaviour of the wood hollowed ventilated façade:

- Comparison between the vertical orientation without insulation layer, with insulation layer and with insulation layer + reinforced concrete on its configuration;
- Evaluation between horizontal and vertical orientation (both with insulation + reinforced concrete);
- Comparison according to the different diameters adopted (d = 10 and 15 mm).

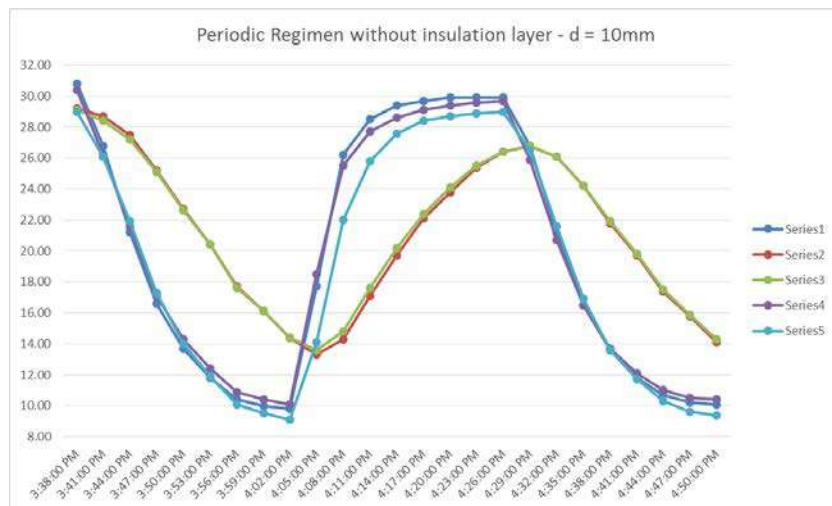


Figure 6. Periodic Regimen without insulation layer and vertical orientation – d = 10mm

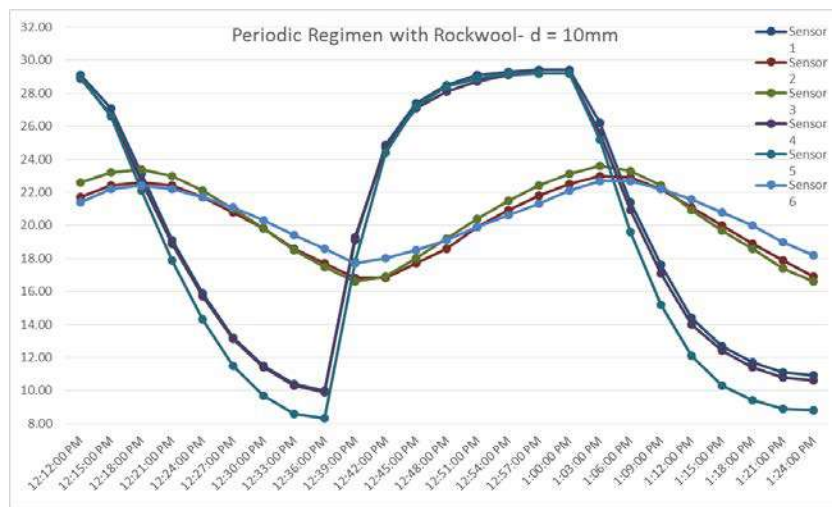


Figure 7. Periodic Regimen with Rockwool and vertical orientation – d=10cm

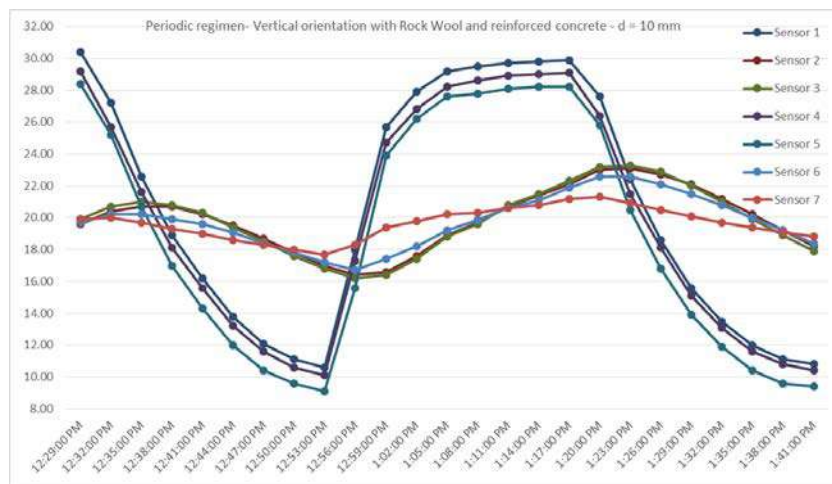


Figure 8. Periodic Regimen with Rock Wool and reinforced concrete, vertical orientation – d=10 mm

Analyzing the Figures 6–8, leads to the conclusion that the use of Rockwool, as insulation material, reduces the speed on which the temperature changes inside the ventilated façade. While the temperature varies in an average rate of $0.62\text{ }^{\circ}\text{C}/\text{min}$ (sensor 2) and $0.60\text{ }^{\circ}\text{C}/\text{min}$ (sensor 3) without the insulation layer, with the insulation glued to the ventilated façade, the temperature changes in a velocity of $0.24\text{ }^{\circ}\text{C}/\text{min}$ (sensor 2) and $0.28\text{ }^{\circ}\text{C}/\text{min}$ (sensor 3). Therefore, with the reinforced concrete added in the configuration, the ratio reduces even more: $0.20\text{ }^{\circ}\text{C}/\text{min}$ (sensor 2) and $0.23\text{ }^{\circ}\text{C}/\text{min}$ (sensor 3).

Vieira G.B., Petrichenko M.R., Musorina T.A., Zaborova D.D. Behavior of a hollowed-wood ventilated façade during temperature changes. *Magazine of Civil Engineering*. 2018. No. 3. Pp. 103–111. doi: 10.18720/MCE.79.11.

Another result that should be highlighted is the fact that, in all the configurations above (Figure 6–8), the sensor 1 (located in the top of the sample) read higher temperatures than sensor 5 (located in the bottom of the sample).

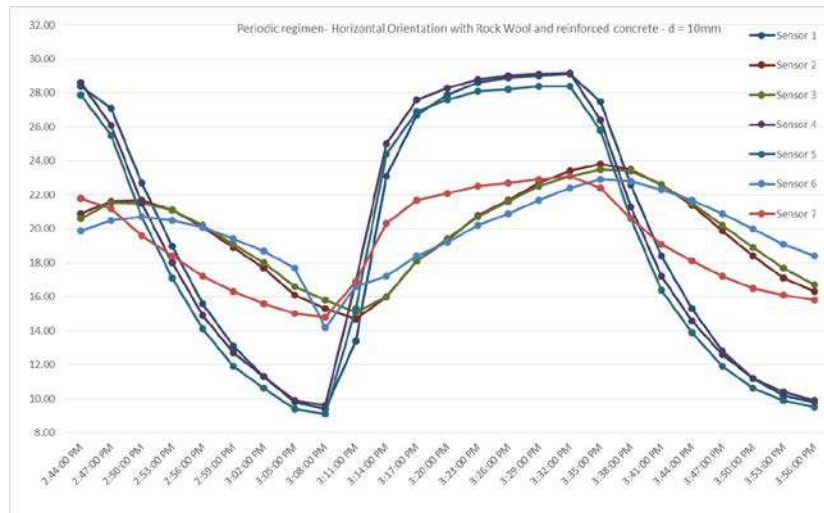


Figure 9. Periodic Regimen with Rock Wool and reinforced concrete, horizontal orientation – d=10 mm

The horizontal and vertical orientation presented similar results when comparing the temperature measured in the boundaries of the wood-hollowed sample in both sensors 1 and 5. The sensors 2 and 3 presented more discrepancies, as the vertical orientation has a temperature, which changes in an average rate for both sensors of 0.22 °C/min and in the horizontal position in a rate of 0.33 °C/min.

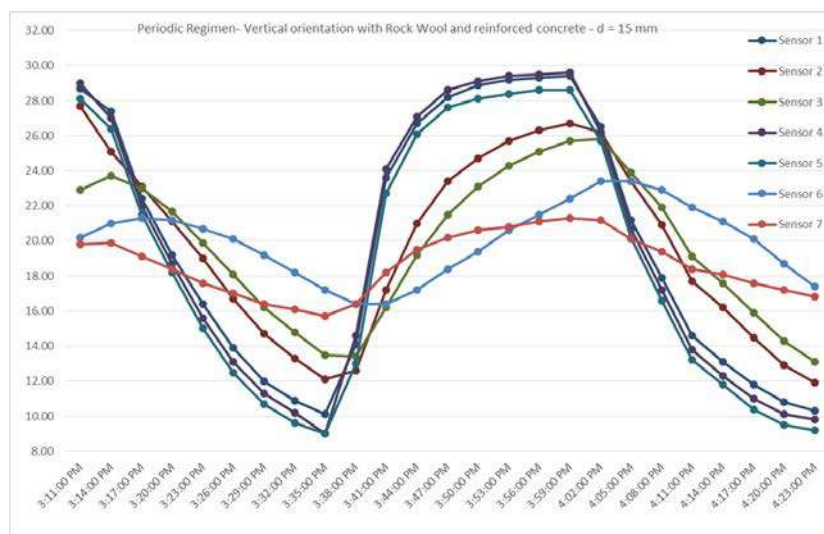


Figure 10. Periodic Regimen with Rock Wool and reinforced concrete, vertical orientation – d=15 mm

Due to the increase of 50 % of the diameter in the holes performed in the wood, the temperature inside the ventilated diverse considerably more when comparing with the same configuration but with 10 mm of diameter. While in the 10 mm diameter-wood-hollowed ventilated façade, the temperature changes, as mentioned above, has a rate of 0.22 °C/min, with diameters of 15 mm, the rate sky rises to 0.60 °C/min average. The sensor 6 read some small differences between both experiments, as the bigger diameter sample oscillated more the temperature than the 10 mm diameter.

Moreover, some topics should be take into consideration and are important for guaranteeing the safeness and the energy efficiency of the building. Firstly, the installation of the insulation layer, wooden ventilated façade and others should be appropriate in order to reach the maximum performance avoiding the presence of thermal bridges, through leaks or the use of improperly material in the construction, as highlighted per [19].

By the end, as wood is not a fireproof material, the need of treating it against fire is undeniable. According to [20], [21] there are a wide range of coating materials that can be used in order to improve the fire properties of the materials and meet the requirements already mentioned. Amongst those materials can be cited: epoxy, water-based materials, latex and intumescent coating. Finally yet importantly, according to [17], it is significant to evaluate the use of wood claddings for each building design as the measured moisture content in the wood claddings demonstrate the influence of ventilation gap design [23].

4. Conclusion

As conclusion, the wood-hollowed ventilated façade presents some benefits since working together with an insulation material layer. As wood has a good thermal resistance and thermal stability, the variation rate of temperature inside the wood is not elevated, when installed together with Rock Wool. Furthermore, the use of bigger holes provided a greater temperature exchange between air and wood. When comparing horizontal and vertical orientations is important to evaluate the commonly wind direction in the location which the project will be settled, as the results can be distinguished as mentioned in the results. Therefore, the use of this solution for ventilated façades are viable, but should be attentively evaluated according to the temperatures, thermal amplitude, wind flow direction and humidity.

However, the size of the sample (1:10), due to space limitation, is considered not big enough for guaranteeing the success of its use in real cases. Due to this fact, it is recommended for further analysis, to enlarge the sample.

5. Acknowledgement

Thanks to the laboratories of the Institute of Civil Engineering from Peter the Great St. Petersburg Polytechnic University, which provided all equipment and materials and assisted doing the experiments.

References

Литература

1. Capros P., Mantzos L., Papandreou V., Tasios N. *Trends to 2030 - Update 2009*. Brussels: Directorate-General for Energy and Transport. Belgium, 2009.
2. U.S. Energy Information Administration, Annual Energy Outlook 2015 – DOE/EIA-0383. USA, 2015. Pp. 01–10.
3. Kostenko V., Gafiyatullina N., Zulkarneev G., Gorshkov A., Petrichenko M., Movafagh S. Solutions to improve the thermal protection of the administrative building. *MATEC Web of Conferences*. 2016. Pp. 02011.
4. EU Directive 2010/31/EU of the European Parliament and of the Council, Energy performance of buildings (recast). Brussels: Official Journal of the European Communities, 2010. Publication 135. Pp. 13–35.
5. Bikas D. et al. Ventilated facades: requirements and specifications across Europe. *Procedia Environmental Sciences* 38, International Conference on Sustainable Synergies from Buildings to the Urban Scale, SBE16. Greece, 2017. Pp. 148–154.
6. Theodosiou T. et al. Analysis of the thermal bridging effect on ventilated facades. *Procedia Environmental Sciences* 38, International Conference on Sustainable Synergies from Buildings to the Urban Scale, SBE16. Thessaloniki, Greece, 2017. Pp. 397–404.
7. *TÉCHNE REVISTA*. Fachadas respirantes. Breathing Facades. (Brazilian Technical Magazine) Edition 144. Brazil, 2009. (pt.). Pp. 42–49.
8. Petrichenko M.R. *Rasshcheplyayushchie razlozheniya v predel'nyh zadachah dlya obyknovennykh kvazilinejnykh differencial'nykh* [The splitting decomposition in limit tasks for the ordinary quasilinear differential equations]. Second Edition. St. Petersburg State Polytechnical University Journal. Physics and Mathematics. 2012. Pp. 143–149. (rus)
9. Vatin N., Petrichenko M., Nemova D., Kharkov N., Korsun A. Numerical modeling of thermogravitational convection in air gap of system of rear ventilated facades. *Applied Mechanics and Materials*. 2014. Vols. 672–674. Pp. 1903–1908.
10. Vatin N., Petrichenko M., Nemova D. Hydraulic methods for
1. Capros P., Mantzos L., Papandreou V., Tasios N. *Trends to 2030 - Update 2007*. Brussels: Directorate-General for Energy and Transport.
2. U.S. Energy Information Administration (EIA), Annual Energy Outlook 2015 (AEO2015).
3. Kostenko V., Gafiyatullina N., Zulkarneev G., Gorshkov A., Petrichenko M., Movafagh S. Solutions to Improve the Thermal Protection of the Administrative Building // *MATEC Web of Conferences*. 2016. Pp. 02011.
4. EU. Directive 2010/31/EU of the European Parliament and of the Council of 19 May 2010 on the energy performance of buildings (recast). Brussels: Official Journal of the European Communities; 2010.
5. Bikas D. et al. Ventilated facades: requirements and specifications across Europe // *Procedia Environmental Sciences* 38, International Conference on Sustainable Synergies from Buildings to the Urban Scale, SBE16. 2017. Pp. 148–154.
6. Theodosiou T. et al. Analysis of the thermal bridging effect on ventilated facades // *Procedia Environmental Sciences* 38, International Conference on Sustainable Synergies from Buildings to the Urban Scale, SBE16. Thessaloniki, Greece, 2017. Pp. 397–404
7. *TÉCHNE REVISTA*. Fachadas respirantes. Edição 144. Brazil, 2009. Pp. 42–49. (pt.)
8. Петриченко М.Р. Расщепляющие разложения в предельных задачах для обыкновенных квазилинейных дифференциальных уравнений // *Научно-технические ведомости Санкт-Петербургского государственного политехнического университета. Физико-математические науки*. 2012. № 2(146). С. 143–149.
9. Vatin N., Petrichenko M., Nemova D., Kharkov N., Korsun A. Numerical modeling of thermogravitational convection in air gap of system of rear ventilated facades // *Applied Mechanics and Materials*. 2014. Vols. 672–674. Pp. 1903–1908.
10. Vatin N., Petrichenko M., Nemova D. Hydraulic methods for calculation of system of rear ventilated facades // *Applied Mechanics and Materials*. 2014. Vol. 633–634.

Vieira G.B., Petrichenko M.R., Musorina T.A., Zaborova D.D. Behavior of a hollowed-wood ventilated façade during temperature changes. *Magazine of Civil Engineering*. 2018. No. 3. Pp. 103–111. doi: 10.18720/MCE.79.11.

- calculation of system of rear ventilated facades. *Applied Mechanics and Materials*. 2014. Vol. 633-634. Pp. 1007–1012.
11. Nemova D.V. Systemy ventilyacii v zhilyh zdaniyah kak sredstvo povysheniya ehnergoehffektivnosti [Systems of ventilation in residential buildings as means of increase of energy efficiency. *Construction of Unique Buildings and Structures*. 2012. No. 3. Pp. 83–86. (rus)
 12. Barbosa S., Ip K. *Double Skin Façade for Naturally ventilated office Buildings in Brazil*. University of Brighton, 2014.
 13. Buildings Performance Institute Europe (BPIE), Europe's Buildings Under the Microscope: A country-by-country review of the energy performance of buildings. 2011. Part 2.
 14. Bianco L., Callegari G., Serra V., Spinelli A. Timber solar facade: A responsive façade for the refurbishment of existing buildings. *10th Conference on Advanced Building Skins*. Bern – Switzerland, 2015. Pp. 402–412.
 15. Nečasová B., Liška P., Jiří Š. *Wooden Facade and Determination of Strength of Bonded Timber Joints*. Technical University of Brno, Czech Republic, 2014.
 16. Sunakom P., Yimprayoon C. *Thermal Performance of Biofacade with Natural Ventilation in the Tropical Climate*. 2011.
 17. Nore K., Thue J.V. *Ventilated Wooden Claddings - A Field Investigation*. Norwegian Institute of Wood Technology. Norway. 2015.
 18. Pinto H. *Dossiê Técnico Econômico. Fachadas Ventiladas*. Brazil, 2006. Vol. 2. Pp. 03–11. (pt.)
 19. EN 13164:2012. Thermal insulation products for buildings. Factory made products of extruded polystyrene foam (XPS). Specification, ISBN 978-0-580-59853-1.
 20. White R. *Use of Coatings to Improve Fire Resistance of Wood*. American Society for Testing and Materials. Standard Technical Publication 826. Philadelphia, USA, 1984. Pp. 24–39.
 21. Hakkarainen T. *Thin thermal barriers for wood based products to improve fire resistance*. Report Code: VTT-R-07061-09. Espoo, Finland, 2010. Pp. 2–11.
 22. Zaborova D., Vieira G., Musorina T., Butyrin A. Experimental study of thermal stability of building materials. *Advances in Intelligent Systems and Computing*. 2017. Vol. 692. Pp. 482–489.
 23. Ruzgys A., Volvačiovas R., Ignatavičius Č., Turskis Z. Integrated evaluation of external wall insulation in residential buildings using SWARA-TODIM MCDM method. *Journal of Civil Engineering and Management*. 2014. Vol. 20. No. 1. Pp. 103–110.
- Pp. 1007–1012.
11. Немова Д.В. Системы вентиляции в жилых зданиях как средство повышения энергоэффективности // Строительство уникальных зданий и сооружений. 2012. № 3. С. 83–86.
 12. Barbosa S., Ip K. *Double Skin Façade for Naturally ventilated office Buildings in Brazil*. University of Brighton, 2014.
 13. Buildings Performance Institute Europe (BPIE), Europe's Buildings Under the Microscope: A country-by-country review of the energy performance of buildings. 2011. Part 2.
 14. Bianco L., Callegari G., Serra V., Spinelli A., Timber solar facade: A responsive façade for the refurbishment of existing buildings // 10th Conference on Advanced Building Skins. Bern, Switzerland. 2015.
 15. Nečasová B., Liška P., Jiří Š. *Wooden Facade and Determination of Strength of Bonded Timber Joints*. Technical University of Brno, Czech Republic, 2014.
 16. Sunakom P., Yimprayoon C., Thermal Performance of Biofacade with Natural Ventilation in the Tropical Climate. 2011.
 17. Nore K., Thue J.V. *Ventilated Wooden Claddings - A Field Investigation*. Norwegian Institute of Wood Technology. Norway. 2015.
 18. Pinto H. *Dossiê Técnico Econômico // Fachadas Ventiladas*. Brazil, 2006. Vol. 2. Pp. 03–11. (pt.)
 19. EN 13164:2012. Thermal insulation products for buildings. Factory made products of extruded polystyrene foam (XPS). Specification, ISBN 978-0-580-59853-1.
 20. White R. *Use of Coatings to Improve Fire Resistance of Wood*. American Society for Testing and Materials. Philadelphia, USA. 1984.
 21. Hakkarainen T. *Thin thermal barriers for wood based products to improve fire resistance*. Espoo, Finland, 2010.
 22. Zaborova D., Vieira G., Musorina T., Butyrin A. Experimental study of thermal stability of building materials // *Advances in Intelligent Systems and Computing*. 2017. Vol. 692. Pp. 482–489.
 23. Ruzgys A., Volvačiovas R., Ignatavičius Č., Turskis Z. Integrated evaluation of external wall insulation in residential buildings using SWARA-TODIM MCDM method // *Journal of Civil Engineering and Management*. 2014. Vol. 20. № 1. Pp. 103–110.

Gabriel Vieira,
+7(911)177-32-31; gabriel.vieira@poli.ufrj.br

Mikhail Petrichenko,
+7(921)330-04-29; fonpetrich@mail.ru

Tatiana Musorina,
+7(952)286-03-76; flamingo-93@mail.ru

Daria Zaborova,
+7(911)180-60-33; zaborova-dasha@mail.ru

Габриэль Беренгуер Виейра,
+7(911)177-32-31;
эл. почта: gabriel.vieira@poli.ufrj.br

Михаил Романович Петриченко,
+7(921)330-04-29; эл. почта: fonpetrich@mail.ru

Татьяна Александровна Мусорина,
+7(952)286-03-76;
эл. почта: flamingo-93@mail.ru

Дарья Дмитриевна Заборова,
+7(911)180-60-33;
эл. почта: zaborova-dasha@mail.ru

© Vieira G.B., Petrichenko M.R., Musorina T.A., Zaborova D.D., 2018

Виейра Г.Б., Петриченко М.Р., Мусорина Т.А., Заборова Д.Д. Деревянный фасад с вентилируемыми каналами для тропического климата // Инженерно-строительный журнал. 2018. № 3(79). С. 103–111.

doi: 10.18720/MCE.79.12

Compressed-bent masonry walls reinforced with composite materials

Сжато-изгибаемые каменные стены, армированные композитными материалами

R.B. Orlovich,*West Pomeranian University of Technology
Szczecin, Szczecin, Poland***V.V. Bepalov,***Peter the Great St. Petersburg Polytechnic
University, St. Petersburg, Russia***V.N. Derkach,***Branch of RUE Institute BelNIIS – Scientific-
technical Centre, Brest, Belarus***Д-р техн. наук, зав. кафедрой****Р.Б. Орлович,***Западно-Померанский технологический
университет Щецин, г. Щецин, Польша***студент В.В. Беспалов,***Санкт-Петербургский политехнический
университет Петра Великого,**Санкт-Петербург, Россия***д-р техн. наук, заместитель директора****В.Н. Деркач,***Филиал РУП "Институт БелНИИС" –**Научно-технический центр, г. Брест,**Республика Беларусь***Key words:** masonry walls; bending
compression; composite reinforcement; load
bearing capacity; interaction curves**Ключевые слова:** каменные стены; сжато-
изогнутые элементы; композитное
армирование; несущая способность; кривые
интеракции

Abstract. Despite the wide spread of surface composite reinforcement of masonry structures, there is not enough information concerning methods of calculating such reinforced structures in the actual normative literature. The article proposes a numerical model for estimating the effect of composite reinforcement on the bearing capacity of a compressed-bent masonry wall which is constructed on the basis of experimental studies of walls from cellular concrete blocks. The numerical model takes into account the plastic work of the masonry under compression and the possibility of crack formation. Theoretical curves are obtained for the dependence of the bearing capacity of reinforced and non-reinforced masonry on the relationship between the compressive force and the bending moment. It is shown that the accepted reinforcement gives the greatest effect in the range of loads from pure bending to compression with bending at a compressive load value equal to half the failure load under pure compression. Such numerical design model can be used to evaluate the effect of reinforcing vaults and walls loaded eccentrically, or from the plane, and other similar structures.

Аннотация. Несмотря на широкое распространение поверхностного композитного армирования каменных конструкций, в современной нормативной литературе не хватает информации, касающейся методов расчёта таких армированных конструкций. В статье предложена численная модель оценки влияния композитного армирования на несущую способность сжато-изгибаемой каменной стены, построенная на основе экспериментальных исследований стен из ячеистобетонных блоков. Численная модель учитывает пластическую работу кладки при сжатии и возможность образования трещин. Получены теоретические кривые зависимости несущей способности армированной и не армированной кладки от соотношения между сжимающей силой и изгибающим моментом. Показано, что принятое армирование даёт наибольший эффект в диапазоне нагружений от чистого изгиба до сжатия с изгибом при величине сжимающей нагрузки в половину от разрушающей при чистом сжатии. Подобная численная модель конструкции может быть использована для оценки эффекта армирования сводов, стен, нагруженных внецентренно, либо из плоскости, и других подобных конструкций.

1. Introduction

Except vertical load masonry walls can be exposed to horizontal actions that can be caused for example from wind, lateral pressure of the ground on the walls of basements, etc. In this case, the wall should be calculated as compressed-bent element. Compression with a bend can also occur in walls at their eccentric loading by overlapping.

The methodology for calculating these walls is described in the technical and normative literature [1]. Bearing capacity of walls limits by resistance of the masonry in the compressed zone of the cross sections or by the loss of their stability under certain combinations of compression and bending. In some cases, the bending moments that cause tension of the masonry parallel to horizontal mortar joints can be defining value (Figure 1).



Figure 1 - Typical damages of eccentric-compressed masonry walls:
a) horizontal cracks on the tensile surface of the partition wall;
b) loss of stability of the facing layer of masonry

In general, bearing capacity of masonry walls subjected both vertical and horizontal loads depends on their flexibility, the values of the eccentricities of the place of applying of the vertical load, flexural stiffness of the masonry and its mechanical parameters and resistance to vertical and horizontal loads, i.e. from their interaction. It should be noted that the walls with their eccentric loading are most often studied in the scientific and technical literature [2–10]. The study of walls on the simultaneous action of horizontal and vertical loads is very rare. This is associated with the difficulties of experiment conducting. The increased sensitivity to cracking is one of their defects, especially in action of horizontal loads. In this regard, according to [1], the design of masonry structures elements that works on bending parallel to horizontal mortar joints is not allowed.

The problem can be solved by surface reinforcement of walls with a meshes from composite materials.

According to this technology, the moistened masonry surface should be covering with a thin layer of a mortar of inorganic mineral materials with modified polymeric additives, into which a reinforcement mesh from composite materials is embedded. Then protection plaster layer should be applying with thickness of 8–10 mm, and then its surface is subjected to finishing treatment. If it's necessary, the second reinforcement mesh can be deposited in the protective layer that will be providing increased strength of strengthening zone [11]. This system is known abroad as FRCM (Fiber Reinforced Cementitious Matrix) and one of its varieties is the system Ruredilx Mesh. A carbon fiber reinforcement meshes can be used in this strengthening system with the following mechanical properties: tensile strength – 4800 MPa; modulus of elasticity – 240 GPa; tensile break strain – 1.8 %. Aramid and glass fiber reinforcement meshes are also used. Recently, basalt fibers reinforcement meshes have been used in Russia [12].

The way that is considered has the following advantages:

- simple technology;
- high adhesion of reinforcement plaster layer to the surface of masonry;

- high compatibility of reinforcement layer with masonry; i.e. approximate deformation characteristics, such as modulus of elasticity, thermal expansion coefficients;
- high fire resistance, corrosion resistance, water resistance and vapor permeability, which makes it possible to reinforce masonry structures both inside and outside buildings.

The advantages of this method of are its universality and the possibility of using it for all shapes of structures.

Composite reinforcement is used not only for surface reinforcement, but also in some cases inside the masonry joints to increase the shear resistance [13].

For brick walls, studies were carried out on the out-of-plane load with reinforcement by this technology. [14–20]. These studies showed a significant dependence of the form of failure on the properties of the solution used. It was also shown that additional strengthening of the compressed side of the masonry does not affect its strength.

The strengthening improvement in the behavior of the masonry in the zone of plastic deformations was also shown in [21] using a similar technology with a GFRP mesh.

An alternative to reinforcing composite materials is the traditional surface reinforcement with a steel mesh [22]. This solution can also be effective, but it has very limited field of utilization.

To analyze the strengthening of the masonry by surface reinforcement, known finite-element models are used [23–28], which take into account plastic deformations and the possibility of initiation and development of cracks. In this study, the simulation is performed to obtain interaction curves of the ultimate bending moment and the compressive force.

It should be noted that, in spite of the available practical experience and wide variety of experimental and theoretical studies, very limited data on methods of calculating masonry structures that are reinforced with composite materials are contained in the foreign, as well as in the domestic normative literature. In many cases, reinforcement is assigned by the so-called "engineering intuition" method without proper calculation justification.

In this paper, the results of experimental and theoretical studies of walls of cellular concrete blocks, which have recently become increasingly practical, have been presented. The main task of the research was to build a numerical model on the basis of experimental data to assess the effect of composite reinforcement on the load-carrying capacity of a compressed-bent masonry wall, depending on the ratio of the compressive force and the bending moment.

2. Methods

A known simulation models of reinforced masonry structures constructed by analogy with reinforced concrete structures (based on static balance of external and internal loads in the calculated cross sections) make it possible to obtain a relatively good convergence with experiments only for the simplest cases, for example, of bent elements [29]. In this regard, the experimental studies of reinforced and unreinforced masonry specimens from cellular concrete blocks, which were tested for compression with bending according to the scheme shown in Figure 2, have been carried out by the authors. Specimens were made from blocks with dimensions $12 \times 50 \times 24 \text{ cm}$ and a density $\gamma = 700 \text{ kg/m}^3$, connected together on thin glue mortar joints. Compressive strength of cellular concrete blocks was $R_c = 3.24 \text{ MPa}$, and tensile strength $R_t = 0.39 \text{ MPa}$ according to laboratory tests.

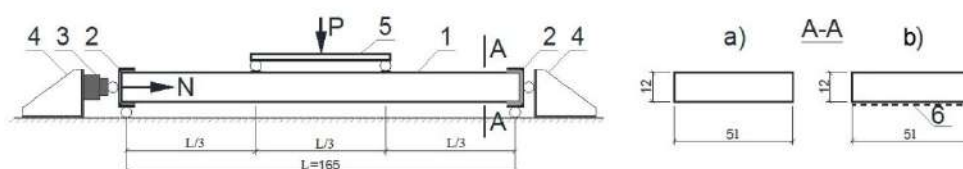


Figure 2. Scheme of tests of unreinforced (a) and reinforced (b) masonry compression specimens with bending (dimensions in cm)

- 1 – test specimen, 2 – steel frame, 3 – hydraulic jack that creates a compressive force N ,
4 – steel seats, 5 – distributing beam for force transfer P ,
6 – mesh reinforcement from composite materials**

As a reinforcement we used fiberglass meshes of the trade mark Mapegrid G220 of the Italian company Mapei. The tensile strength of the grids that was declared by the company is 45 kN per 1 m of width, and the tensile break strain of 3 %.

We tested one specimen with reinforcement and without reinforcement (specimens No. 1) in order to determine the load-carrying capacity M_{RD} at bending. The same number of specimens was tested to determine their load-bearing capacity N_{RD} in compression (specimens No. 5). The rest of the specimens (3 – without reinforcement and 3 – with reinforcement) were tested under the combined action of the longitudinal force and the bending moment $M = PL/6$ caused by the action of the force P . At the same time during loading, the force N was maintained at the same level, and the force P increased until the specimens were destroyed.

The calculations were carried out using the ABAQUS software in a non-linear setting. An iterative procedure was used, according to which the values of the modulus of elasticity of the material of the cellular concrete blocks were refined for each loading level. The plastic behavior of the masonry was also taken into account, which was specified for cases of exceeding the modulus of elasticity limit. A model of the so-called expanded finite element method was also used, which took into account the possibility of crack formation in the masonry and their effect on the stress-strain state of the structure. The design scheme was adopted similar to that depicted in Figure 2, in a plane stress condition using rectangular finite elements. The contact of the steel frame with the masonry specimen was simulated by a free contact “surface to surface” [30] without a rigid interface of the contact zone. The contact of the reinforcement and masonry was taken rigid. In this case, modulus of elasticity were set for reinforcement, taking into account the possibility of its work only in one direction – tension. This was necessary to exclude the possibility of incorporating reinforcement into compression work. When calculating an appropriate limiting moment was selected by iteration with an increment of 0.05 kNm for each level of the compressive force, with a step of 10–20 kN.

3. Results and Discussion

The main results of testing the experimental specimens are presented in Table 1, from which it follows that the load-bearing capacity of the specimens increases with increasing axial compressive force to the level $N = (0.4 \dots 0.5)N_{RD}$, and the load-bearing capacity decreases at a higher level N . At the same time, the reinforced specimens showed a higher load-bearing capacity with bending compression in comparison with unreinforced specimens.

Table 1. The values of the limiting bending moments $M = PL/6$ as a function of the compressive force N

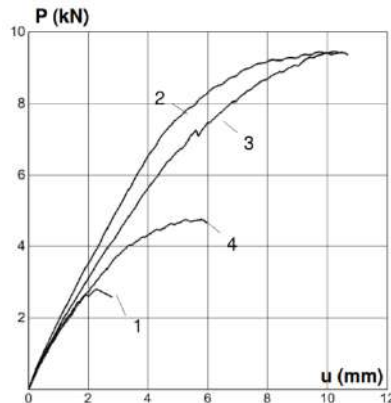
No. of specimen		1	2	3	4	5
Specimens without reinforcement	M (kN·m)	0.39	1.18	1.95	0.98	0
	N (kN)	0.0	40.0	80.0	120.0	165.4
Reinforced specimens	M (kN·m)	0.77	2.60	2.59	1.30	0
	N (kN)	0.0	40.0	80.0	120.0	178.9

As an example, the type of unreinforced specimen No. 3 before and after failure from the combined action of longitudinal force and bending moment have been showed on the Figure 3. The failure was fragile and occurred as a result of crushing the aerated concrete in a compressed zone.



Figure 3. Type of test specimens during loading and after failure

Figure 4 shows the experimental dependences of the maximum deflections reinforced specimens u on the load P . At the level of the compressive force $N=(0...0.25) \cdot N_{RD}$, the failure of the specimens occurred as a result of tension breaking of the reinforcement meshes, and at higher levels – as a result of the exhaustion strength of cellular concrete on the compression. It also follows from the dependences that the compression of specimens by a force $N=(0.25...0.5) \cdot N_{RD}$ leads to a substantial increase of the failure load P .



1 – $N=0$; 2 – $N=0.25 \cdot N_{RD}$; 3 – $N=0.50 \cdot N_{RD}$; 4 – $N=0.75 \cdot N_{RD}$

Figure 4. Experimental dependences of the maximum deflections u of reinforced specimens on the load P at a constant value of the compressive force N

Figure 5 shows the interaction curves “ $M_{Rd}-N_{Rd}$ ” that were obtained by calculation. Experimental values of the load-bearing capacity of the specimens less than the calculated values by 10...25 %. This discrepancy can be explained by the fact that the calculations did not take into account such factors as a variation of the geometric dimensions of the specimens, the effect of deflections on the change in the design scheme, and the idealized form of the applied loads.

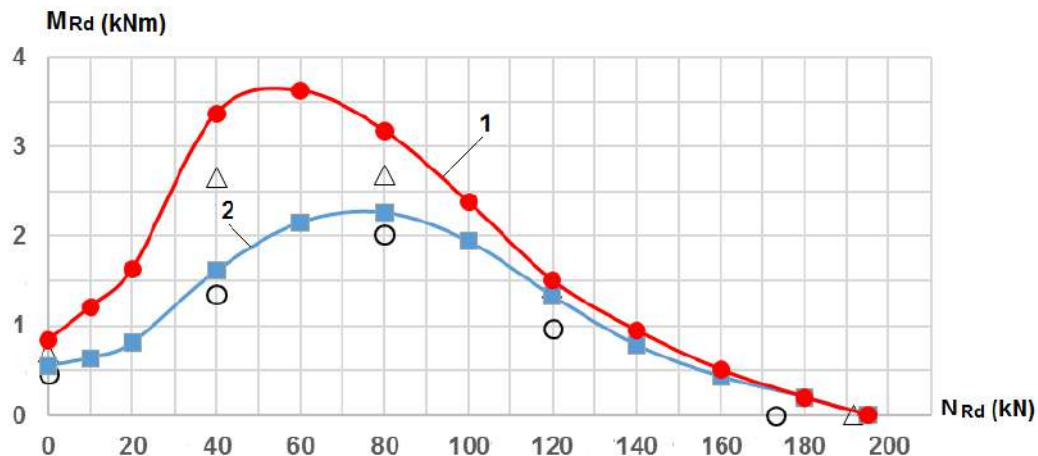


Figure 5. Interaction curves “ $M_{Rd}-N_{Rd}$ ”

1 – for reinforced specimens; 2 – for unreinforced specimens;
 Δ – experimental values for reinforced specimens; \circ – experimental values for unreinforced specimens

An example of the stress-strain state of a reinforced specimen that corresponds to the forces $N = 120 \text{ kN}$ and $M = 1.51 \text{ kN}\cdot\text{m}$ is shown in the Figure 6. In this case, we see a nonuniform distribution of stresses caused by the appearance of plastic deformations in the compressed zone, corresponding to the crushing of the masonry area and the subsequent occurrence of tensile stresses on the lower surface of the specimen.

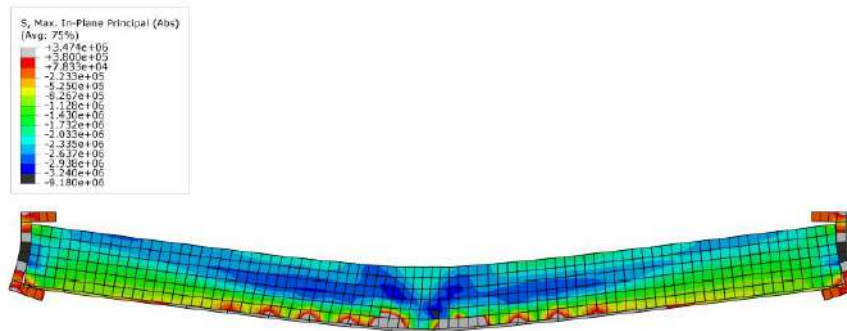


Figure 6. Stress-strain state of a reinforced specimen under action $N=120\text{ kN}$ и $M=1.51\text{ kN}\cdot\text{m}$

It is characteristic, that for load level $N=(0.0\dots0.5)\cdot N_{RD}$, the bending load capacity increased more than 2 times, while at a higher level of force N this increase did not exceed 30 %. In specimens that work only in bending, the availability of reinforcement has increased the bearing capacity of the M_{RD} almost by 100 %, while specimens that work only in compression – only by 8 %. The reinforcement effects for different loading levels correlate with mechanical fracture of the specimens. At low levels of force N , the failure occurred as a result of tension breaking of the reinforcement meshes, and at higher levels – as a result of crushing the masonry in the compressed zone. The results of an experimental study of masonry specimens with eccentric loading, carried out by I. Talero and I. Delgado [31].

Despite some excess the data of the numerical simulation are in qualitative agreement with the experimentally obtained values. Sections of the interaction curves for stress states that are close to pure compression ($0.75\dots1\cdot N_{RD}$) have relationships between the maximum loads for reinforced and unreinforced specimens, which differ slightly from the experimental data, up to the coincidence of theoretical curves at $0.9\dots1\cdot N_{RD}$. Presumably this is caused by the possibility of cracks formation in the direction along the compressive force that has not been considered in the numerical model. The interaction curves that were obtained from the results of numerical simulation are in good agreement with the data of the studies T. Hrynyk and J. Myers [32].

4. Conclusion

The results of experimental study showed that strengthening the compressed-bent masonry from cellular concrete blocks with glass fiber reinforcement meshes causes a significant increase in its bearing capacity. The greatest effect with strengthening is achieved in the action of a compressive load, equal to $0.25\dots0.5$ from the failure load.

A nonlinear finite element model that was calibrated on the basis of experimental data was developed. The model that was presented gives the possibility for a better qualitative understanding of the failure mechanism of the reinforced specimen for various combinations of longitudinal and lateral loads. The transition from failure due to the formation of cracks in the tensile zone to failure from loss of stability due to nonuniform plastic deformations of the masonry in the compressed zone is very evident.

The numerical results that were obtained are in good agreement with both the experimental data and with similar studies of compressed-bent masonry elements that were performed by other authors. Such numerical simulation models can be used in assessing the behavior of various compressed-bent masonry structures, such as vaults loaded eccentrically or from the plane of the wall and other similar structures. At the same time, this numerical model does not take into account the possibility of crack formation in the direction of the compressive force, which causes insufficient accuracy of the results for stress states close to pure compression. It is recommended to apply classical methods of strength evaluation for such states.

Experimental and theoretical study of reinforced vault structures and vertical masonry walls when they loaded from the plane is assumed as a further development of the study.

References

1. Russian Construction Set of Rules SP 15.13330.2012 Kamennyye i armokamennyye konstruksii [Masonry and reinforced masonry structures]. Moscow, 2012. 81 p. (rus)
2. Orlovich R.B., Chakalidi V.Kh., Bepalov V.V. Strengthening of masonry elements with composite mesh under compression and compression combined with bending. *Construction and reconstruction*. 2017. No. 5(73).

Литература

1. СП 15.13330.2012 Каменные и армокаменные конструкции. Москва, 2012. 81 с.
2. Орлович Р.Б., Чакалиди В.Х., Беспалов В.В. Усиление сжатых и сжато-изгибаемых каменных элементов сетками из композитных материалов // Строительство и реконструкция. 2017. № 5(73). С. 45–49.
3. Martin A., Esnault J.-B., Massin P. About the use of

- Pp. 45–49. (rus)
3. Martin A., Esnault J.-B., Massin P. About the use of standard integration schemes for X-FEM in solid mechanics plasticity. *Computer Methods in Applied Mechanics and Engineering*. 2015. No. 283. Pp. 551–572.
 4. Orlovich R.B., Chakalidi V.Kh. Strengthening methods for cylindrical masonry vaults. *Construction and reconstruction*. 2017. No. 1(69). Pp. 51–54. (rus)
 5. Orłowicz R., Jaworski R., Drobiec Ł. Influence of reinforcement on the load-bearing capacity of cellular concrete walls subjected to compression with bending. *Building Inspection*. 2015. No. 10. Pp. 31–33.
 6. McGinley W.M., Corzo A.M., Gergely J., Foster P.B., Young D.T. A design methodology for FRP systems for masonry structures. *10th Canadian Masonry Symposium, Banff, Alberta*. 2005. Pp. 34–44.
 7. Garmendia L., San-Mateos R., García D., Gandini A., San-José J.T., Marcos I. Retrofitting of masonry vaults with composite materials. *Structural Analysis of Historical Constructions*. Leuven, Belgium. 2016. Pp. 351–356.
 8. Hamed E., Rabinovitch O. Failure characteristics of FRP-strengthened masonry walls under out-of-plane loads. *Engineering Structures*. 2010. No. 32. Pp. 2134–2145.
 9. Anania L., Agata G., Giaquinta C., Badala A. Out of Plane Behavior of Calcareous Masonry Panels Strengthened by CFRP. *APCBEE Procedia*. 2014. No. 9. Pp. 401–406.
 10. Furtado A., Rodrigues H., Arede A., Varum H. Experimental Characterization of the In-plane and Out-of-Plane Behaviour of Infill Masonry Walls. *Procedia Engineering*. 2015. No. 114. Pp. 862–869.
 11. Orlovich R.B., Derkach V.N. Zarubezhnyy opyt armirovaniya kamennykh konstruksiy [Foreign experience of reinforcement of masonry structures]. *Zhishchnoye stroitel'stvo*. 2011. No. 11. Pp. 35–39. (rus)
 12. *Al'bum tekhnicheskikh resheniy po primeneniyu bazal'tovoy setki GRIDEX v stroitel'stve* [Album of technical solutions for the application of the GRIDEX basalt grid in construction]. Moscow, 2016. (rus)
 13. Miccoli L., Mueller U., Fontana P. In-plane shear behaviour of earthen materials panels strengthened with polyester fabric strips. *10th International Conference on Structural Analysis of Historical Constructions*. Leuven, Belgium. 2016. Pp. 1099–1105.
 14. Bernat-Maso E., Escrig C., Aranha C. A. Gil L. Experimental assessment of Textile Reinforced Sprayed Mortar strengthening system for brickwork wallettes. *Construction and Building Materials*. 2014. No. 50. Pp. 226–236.
 15. Gattesco N., Boem I. Out-of-plane behavior of reinforced masonry walls: Experimental and numerical study. *Composites Part B: Engineering*. 2017. No. 128. Pp. 39–52.
 16. Anil O., Tatayoğlu M., Demirhan M. Out-of-plane behavior of unreinforced masonry brick walls strengthened with CFRP strips. *Construction and Building Materials*. 2012. No. 35. Pp. 614–624.
 17. Dizhur D., Griffith M., Ingham J. Out-of-plane strengthening of unreinforced masonry walls using near surface mounted fibre reinforced polymer strips. *Engineering Structures*. 2014. No. 59. Pp. 330–343.
 18. Kadam S., Singh Y., Li B. Out-of-plane behaviour of unreinforced masonry strengthened using ferrocement overlay. *Materials and Structures*. 2014. No. 48(10). Pp. 3187–3203.
 19. Bengi A., Emre E., Ali D. Strengthening of brick masonry with PVA fiber reinforced cement stucco. *Construction and Building Materials*. 2015. No. 79. Pp. 255–262.
 20. Sachin B.K., Yogendra S., Bing L. Strengthening of unreinforced masonry using welded wire mesh and micro-standard integration schemes for X-FEM in solid mechanics plasticity // *Computer Methods in Applied Mechanics and Engineering*. 2015. № 283. Pp. 551–572.
 4. Орлович Р.Б., Чакалиди В.Х. Способы усиления цилиндрических каменных сводов // *Строительство и реконструкция*. 2017. № 1(69). С. 51–54.
 5. Orłowicz R., Jaworski R., Drobiec Ł. Influence of reinforcement on the load-bearing capacity of cellular concrete walls subjected to compression with bending // *Building inspection*. 2015. № 10. Pp. 31–33.
 6. McGinley W.M., Corzo A.M., Gergely J., Foster P.B., Young D.T. A design methodology for FRP systems for masonry structures // *10th Canadian Masonry Symposium, Banff, Alberta*. 2005. Pp. 34–44.
 7. Garmendia L., San-Mateos R., García D., Gandini A., San-José J.T., Marcos I. Retrofitting of masonry vaults with composite materials // *Structural Analysis of Historical Constructions, Leuven, Belgium*. 2016. Pp. 351–356.
 8. Hamed E., Rabinovitch O. Failure characteristics of FRP-strengthened masonry walls under out-of-plane loads // *Engineering Structures*. 2010. № 32. Pp. 2134–2145.
 9. Anania L., Agata G., Giaquinta C., Badala A. Out of Plane Behavior of Calcareous Masonry Panels Strengthened by CFRP // *APCBEE Procedia*. 2014. № 9. Pp. 401–406.
 10. Furtado A., Rodrigues H., Arede A., Varum H. Experimental Characterization of the In-plane and Out-of-Plane Behaviour of Infill Masonry Walls // *Procedia Engineering*. 2015. № 114. Pp. 862–869.
 11. Орлович Р.Б., Деркач В.Н. Зарубежный опыт армирования каменных конструкций // *Жилищное строительство*. 2011. № 11. С. 35–39.
 12. Альбом технических решений по применению базальтовой сетки ГРИДЕКС в строительстве. Москва, 2016.
 13. Miccoli L., Mueller U., Fontana P. In-plane shear behaviour of earthen materials panels strengthened with polyester fabric strips // *10th International Conference on Structural Analysis of Historical Constructions, Leuven, Belgium*. 2016. Pp. 1099–1105.
 14. Bernat-Maso E., Escrig C., Aranha C. A. Gil L. Experimental assessment of Textile Reinforced Sprayed Mortar strengthening system for brickwork wallettes // *Construction and Building Materials*. 2014. № 50. Pp. 226–236.
 15. Gattesco N., Boem I. Out-of-plane behavior of reinforced masonry walls: Experimental and numerical study // *Composites Part B: Engineering*. 2017. № 128. Pp. 39–52.
 16. Anil O., Tatayoğlu M., Demirhan M. Out-of-plane behavior of unreinforced masonry brick walls strengthened with CFRP strips // *Construction and Building Materials*. 2012. № 35. Pp. 614–624.
 17. Dizhur D., Griffith M., Ingham J. Out-of-plane strengthening of unreinforced masonry walls using near surface mounted fibre reinforced polymer strips // *Engineering Structures*. 2014. № 59. Pp. 330–343.
 18. Kadam S., Singh Y., Li B. Out-of-plane behaviour of unreinforced masonry strengthened using ferrocement overlay // *Materials and Structures*. 2014. № 48(10). Pp. 3187–3203.
 19. Bengi A., Emre E., Ali D. Strengthening of brick masonry with PVA fiber reinforced cement stucco // *Construction and Building Materials*. 2015. № 79. Pp. 255–262.
 20. Sachin B.K., Yogendra S., Bing L. Strengthening of unreinforced masonry using welded wire mesh and micro-

- concrete. Behaviour under in-plane action. *Construction and Building Materials*. 2014. No. 54. Pp. 247–257.
21. Gattesco N., Gubana A., Melotto M. GFRP to strengthen masonry walls: Numerical analysis and evaluation of the different mechanical parameters role. *10th International Conference on Structural Analysis of Historical Constructions*. Leuven, Belgium. 2016. Pp. 357–364.
 22. Shermi C., Dubey R.N. Study on out-of-plane behaviour of unreinforced masonry strengthened with welded wire mesh and mortar // *Construction and Building Materials*. 2017. № 143. Pp. 104–120.
 23. Pourfalah S., Suryanto B., Cotsovos D.M. Enhancing the out-of-plane performance of masonry walls using engineered cementitious composite // *Composites Part B: Engineering*. 2018. No. 140. Pp. 108–122.
 24. Bellini A., Mazzotti C. Bond behavior and tensile properties of FRCM composites applied on masonry panels. *Composite Structures*. 2016. No. 143. Pp. 322–329.
 25. Reboul N., Si Larbi A., Ferrier E. Two-way bending behaviour of hollow concrete block masonry walls reinforced by composite materials. *Composites Part B: Engineering*. 2018. No. 137. Pp. 163–177.
 26. Natalino G., Ingrid B. Out-of-plane behavior of reinforced masonry walls: Experimental and numerical study. *Composites Part B: Engineering*. 2017. No. 128. Pp. 39–52.
 27. Sarkar N.-E.-K., Manicka D., David P.T. Out-of-plane deformation and failure of masonry walls with various forms of reinforcement. *Composite Structures*. 2016. No. 140. Pp. 262–277.
 28. Alessia M., Giovanni M., Calogero C., D'Anna J., La Mendola L. Finite element analysis of the out-of-plane behavior of FRP strengthened masonry panels. *Composites Part B: Engineering*. 2017. No. 115. Pp. 188–202.
 29. Papanikolaou C., Triantafillou T., Fabregat P.R. Increase of load-carrying capacity of masonry with textile reinforced rendering. *Mauerwerk*. 2015. No. 19. Pp. 40–51.
 30. *Abaqus documentation user manual*, v. 6.14, Dassault Systems, 2014.
 31. Valetta G., Pedemonte G., Fontana J.J., Talero R., Delgado A. Fibreglass Reinforcement in Brick Bearing Walls // *7th international masonry conference*. London, UK. 2006. Pp. 142–149.
 32. Hrynyk T., Myers J. J. Comparative study on the out-of-plane behavior of retrofitted masonry wall systems with arching action. *10th North American Masonry Conference*. 2007. Pp. 305–316.
- Conference on Structural Analysis of Historical Constructions. Leuven, Belgium. 2016. Pp. 357–364.

Romuald Orlovich,
+48(661)86-88-50; orlowicz@yandex.ru

Vladimir Bepalov,
+7(981)785-08-99; chanchullero@yandex.ru

Valery Derkach,
+375(296)41-19-62; v-derkach@yandex.ru

Ромуальд Болеславович Орлович,
+48(661)86-88-50; эл. почта: orlowicz@yandex.ru

Владимир Владимирович Беспалов,
+7(981)785-08-99;
эл. почта: chanchullero@yandex.ru

Валерий Николаевич Деркач,
+375(296)41-19-62;
эл. почта: v-derkach@yandex.ru

© Orlovich R.B., Bepalov V.V., Derkach V.N., 2018

doi: 10.18720/MCE.79.13

The formation of the seabed surface relief near the gravitational object

Формирование рельефа донной поверхности у гравитационного объекта

**V.V. Lebedev,
I.S. Nudner,**

23 State Marine Design Institute – branch of
«31 State Design Institute of Special
Construction», St. Petersburg, Russia

**N.D. Belyaev,
K.K. Semenov,**

Peter the Great St. Petersburg Polytechnic
University, St. Petersburg, Russia

D.I. Schemelinin,

23 State Marine Design Institute – branch of
«31 State Design Institute of Special
Construction», St. Petersburg, Russia

**Канд. техн. наук, ведущий научный
сотрудник В.В. Лебедев,**

**д-р техн. наук, ведущий научный
сотрудник И.С. Нуднер,**

23 Государственный морской проектный
институт – филиал ОАО «31 ГПИСС»,
Санкт-Петербург, Россия

**канд. техн. наук, доцент Н.Д. Беляев,
канд. техн. наук, доцент К.К. Семенов,**
Санкт-Петербургский политехнический
университет Петра Великого,

Санкт-Петербург, Россия

инженер Д.И. Щемелинин,

23 Государственный морской проектный
институт – филиал ОАО «31 ГПИСС»,
Санкт-Петербург, Россия

Key words: gravity-type structure; flow; waves;
ship waves; sand waves; interference

Ключевые слова: гравитационное
сооружение; течение; волнение; судовые
волны; песчаные волны; интерференция

Abstract. During the interaction of waves and currents with objects established in the shallow offshore areas, scour of their base may occur. At the same time, it is always necessary to exclude the appearance of significant seabed scour near supporting parts of gravity-type platforms during the process of their design. The article presents the results of experimental studies of processes occurring under the impact of flows of various types on gravity-type structures and their foundations. The model of Prirazlomnaya platform and the model of drilling barge, which were performed on a scale of 1:60, were used as typical models of offshore structures of gravitational type. Analogies between ship and sand waves are revealed, conditions of appearance of soil waves interference from the rear face of platforms are analyzed.

Аннотация. При взаимодействии волн и течений с объектами, установленными на мелководных участках шельфа, может происходить размыв их основания. При проектировании платформ гравитационного типа необходимо исключить возникновение значительного размыва дна вблизи их опорных частей. В статье представлены результаты экспериментальных исследований процессов, происходящих при воздействии потоков различного типа на гравитационные сооружения и их основания. В качестве типовых моделей шельфовых сооружений гравитационного типа были использованы модель платформы «Приразломная» и модель буровой баржи, выполненные в масштабе 1:60. Выявлены аналогии между судовыми и грунтовыми волнами, проанализированы условия возникновения интерференции грунтовых волн со стороны тыльной грани платформ.

1. Introduction

Gravity-type platforms are one of the most common types of hydraulic engineering structures for the offshore development. The possibility of formation and development of local scour has to be considered during the process of platforms design. The identification of the basic mechanisms underlying the processes that occur in the water flow around hydrotechnical structures and its consideration during

design should reduce the risks of emergencies and increase the safety of operation of the offshore objects [1–5].

Sand waves are the most common factor in the formation of the seabed surface relief in shallow water [6–9]. Two types of sand waves with different reasons of formation on an underwater slope in the vicinity of the location of a large-scale gravity-type object are distinguished in this article. An object whose characteristic linear dimension (for example, the width B or the length L of the object) is greater than the depth of water d in the place of its location will be called an object of large size.

The possibility of formation of sand waves like a transverse ship waves is the first occasion identified in this study. As it is known, ship-induced waves are formed when a partially submerged vessel moves in calm water. Divergent and transverse waves are formed in this case [10, 11]. Divergent waves form an echelon of waves approximately parallel to each other, originating in both the bow and the stern of the vessel. Transverse waves are formed along the vessel at the bow and stern parts of the sides, as well as behind the stern. The group of transverse waves formed in the bow begins with the crest of the wave, and the group formed in the stern part begins from the trough. Such waves can be obtained according to the principle of motion relativity if the vessel is stationary and the flow of water will be uniform. Formation of sand waves like a ship's waves is possible in the case under consideration when the stream of water-saturated soil flows around stationary gravitational object and along its sides.

The second case is the formation of forced sand waves arising in consequence of the transfer of part of the water flow energy to the seabed surface causing a certain movement of seabed soil particles. Periodic structures (sand waves) are formed on the seabed surface and move along the underwater slope at a certain rate because of this displacement of soil particles.

A large object located on the underwater slope under its own weight, for example, a gravity platform, interacts with both the water flow and the flow of seabed soil moving along the underwater slope. Thus, in this case, the seabed surface relief formation occurs as a result of the development of all the above-mentioned sand waves.

2. Methods

Experimental investigations were held in order to obtain and analyze information on changes in the relief of the seabed surface caused by the frontal water flow formed by regular waves and currents impact on the gravity-type platforms [12–15]. It was assumed that the frontal action of the water flow on the platform is carried out during one design storm; the slope of the seabed surface in the vicinity of the platform was assumed to be zero before the start of the experiment; the current during the considered period of time is assumed to be constant; there are no suspended sediments in the water flow approaching to the considered seabed surface.

Experimental studies of the seabed surface relief changes in the gravitational-type model location caused by the frontal action of regular waves and currents were performed on an experimental setup that was organized using the enclosing working area inside the test basin (with overall dimensions 40.0×6.2 m). Waves were generated by a mobile beam-type wavemaker with a beam length of 6.1 m, which was placed on the basin floor at 7 m from the outlet of water supply to the test setup. At 17 m from water supply outlet, a test area began in a form of underwater ledge with height from the basin floor equal to 0.4 m and with length equal to 12 m (Figure 1). In the middle of the ledge, a test section was placed measuring $4.0 \times 4.0 \times 0.4$ m, which was filled with fine-grained sand with average diameter of particles equal to 0.22 mm (Table 1). The sand was wetted and compacted. The sand surface top level was constant everywhere and equal to 0.4 m from the basin floor. In the center of the test section, the models made of bakelite plywood were placed on rigid base with the level that was accurately equal to 0.4 m with respect to the basin floor. The rest of the ledge is covered with bakelite plywood. The pipe 0.1 m diameter with removable plug on the upper side was laid on floor along the basin wall for convenient filling of the experimental setup with water (Figure 1).

Table 1 – Granulometric composition of sand used in the experimental studies in percentage, the shape of the grain is semicircular

Sieve size									
0.63	0.4	0.315	0.2	0.16	0.1	0.063	0.05	Residual	Clay
0.40	6.40	16.20	44.80	15.80	9.94	4.86	0.50	0.40	0.86

At a distance of 11 m from the test area with the flow, a metal wall was established (Figure 1) in which, up to a mark of 0.45 m relative to the basin bottom, two rectangular spillways each 1.2 m wide were cut.

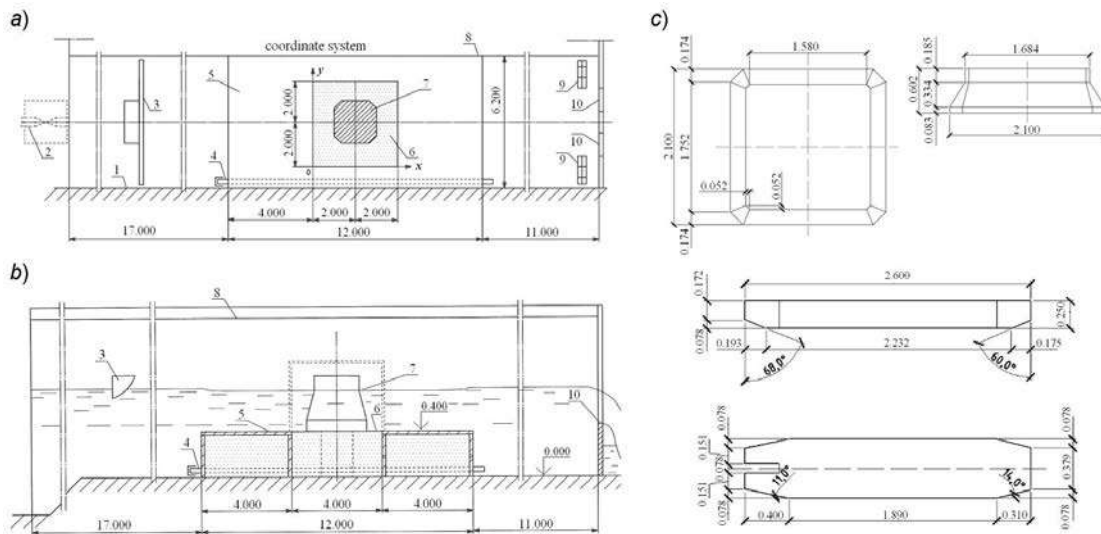


Figure 1. Test setup:
a – plan; b – longitudinal section; c – gravity-type Platform and Barge models:
1 – wave basin wall; 2 – supply pipeline with stop valve; 3 – beam-type wavemaker;
4 – pipeline with plug; 5 – test area; 6 – test section; 7 – platform model; 8 – enclosure;
9 – wave suppressor; 10 – weir with thin wall

Thus, two thin-plate weirs were formed. The marks of the weirs crests were variable and were established depending on the conditions of the experiments. These weirs were used to determine the average water flow velocity V . The inclined wave suppressors were installed before the metal wall of the enclosure and from the side of the pool wall (Figure 1). The water supply to the experimental setup was carried out by a centrifugal pump from an underground reservoir through a system of pipelines and valves. A valve installed before experimental facility regulated the change in flow rate. As exemplary models of the gravity platforms, the model of the offshore ice-resistant fixed platform *Prirazlomnaya* (hereinafter referred to as the Platform) and the model of the drilling barge (hereinafter referred to as the Barge), made on a scale of 1:60, were used.

Physical modeling of the processes of seabed surface changing near the gravity-type platforms under the impact of the water flow formed by waves and current was carried out on the assumptions that the motion of the water and soil flows satisfies the Navier-Stokes equations and that modeling should be conducted without distortion of scales, geometric similarity, both artificial structures, and parameters of water flows in order to obtain a qualitative correspondence between the processes taking place in nature and on the model. In the described studies, the modeling of the soil composing the seabed was carried out by fine-grained sand with an average particle diameter of 0.22 mm.

The kinematic similarity of the occurring processes was due to the equality in the model and in nature of the Froude numbers $Fr_V = V^2/gd$ that were determined with respect to the depth d and the average flow velocity V of the water flow acting on the object.

In order to study the beginning of the formation of the seabed relief of the underwater slope in the intended conditions of the action of the water flow on the gravity-type platform, experimental studies were carried out at values of the Shields parameter θ less than the critical ones (Table 2).

To fulfill this condition, the values of the Shields parameter were calculated by the formula

$$\theta = U_f^2 / (g(\rho_s - \rho)D_0),$$

where U_f is the dynamic velocity; ρ_s is the density of the particles of the soil composing the seabed; ρ is the density of water.

At the same time, the values of the Reynolds number for the dynamic velocity were calculated from expression

$$\text{Re}_f = U_f D_0 / \nu,$$

where ν is the kinematic viscosity of water.

The relationship between U_f and the velocity of the water flow $U = (V + U_{w_{\max}})$ was taken in the following form [16]:

$$U_f = U \sqrt{f/2},$$

where f is the coefficient of hydraulic friction; $U_{w_{\max}}$ is the maximum orbital velocity in the wave.

The hydraulic friction coefficient for water flows formed by waves and currents moving above the eroded seabed was determined as follows accordingly to [17]:

$$f = (f_c^2 V^2 + f_w^2 U_{w_{\max}}^2) / (f_c V^2 + f_w U_{w_{\max}}^2),$$

where f_c is the coefficient of hydraulic friction for the water flow moving above the eroded seabed with an average velocity (it was determined according to [18]); f_w is the coefficient of hydraulic friction for the water flow formed by waves with the maximum orbital velocity $U_{w_{\max}}$ moving above the eroded seabed (its value was determined according to [16, 17, 19]).

Table 2. Conditions of tests

Test No.	Water depth d , m	Average speed of current V , m/s	Wave height, h , m	Wave period T , s	Froude number Fr_v	Reynolds number Re_f	Shields parameter θ
1	0.330	0.067	0.053	1.7	0.0014	2.07	0.012
2	0.330	0.067	0.095	1.7	0.0014	4.08	0.029
3	0.175	0.125	0.074	1.7	0.0091	3.24	0.089
4	0.175	0.125	0.064	1.7	0.0091	2.14	0.022
5	0.330	0.067	0.095	1.3	0.0014	3.86	0.060
6	0.330	0.067	0.107	1.3	0.0014	3.60	0.080
7	0.160	0.105	0.068	1.3	0.0070	3.57	0.042
8	0.175	0.124	0.080	1.3	0.0090	3.88	0.049
9	0.162	0.108	0.081	1.3	0.0073	4.21	0.060
10	0.177	0.129	0.065	1.3	0.0096	2.84	0.026

The values of the Shields parameter calculated for the conditions of carried out experimental studies were sufficiently close to the critical values determined for the corresponding Reynolds numbers Re_f from the Shields curve given in [20].

The experimental setup was drained and the formed bottom relief was fixed using the GOM ATOS 2 Triple Scan measuring information system after the end of each of the tests. The cloud of coordinates of the points obtained during each experiment was used to measure the relief plan of the seabed surface and to measure its profiles in the intended cross sections [12, 14, 15].

3. Results and Discussion

The frontal impact of the water flow formed by regular waves and current on the gravity-type platform changes the seabed relief by forming the movement of sand waves on the bottom surface adjacent to the platform.

The stream around a gravity-type construction formed by a soil flow caused by the simultaneous frontal action of regular waves and currents contributes to the formation of sand waves of the ship waves

type at the side faces of the object and behind its stern. The formation of these waves was observed both at the sides of the Platform model and at the sides of the Barge model (Figures 2–7, 9–12).

Analysis of the relief of the bottom surface formed as a result of experiment No. 1 indicates the presence of groups of sand waves at the side faces of the Platform (Figure 2). Groups of sand waves formed closer to the frontal face begin with a crest (area 1 in Figure 2), while groups of sand waves formed closer to the rear side begin with a trough (area 2 in Figure 2). The fronts of these waves are practically perpendicular to the direction of motion of the water stream. Thus, it can be argued that for the values of the water flow parameters in experiment No. 1 (Table 2), the movement of the bottom soil begins, in interaction with which lateral sand waves like a transverse ship waves begin to form at the lateral faces of the Platform. Behind the Platform, there is also the formation of a group of transverse waves (area 3 in Figure 2).

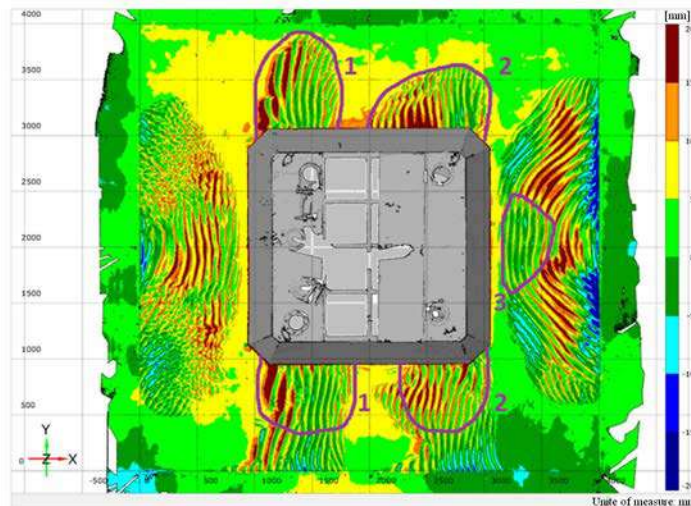


Figure 2. Bottom profile near the Platform model after experiment No. 1:

- 1 – formation of transverse sand waves at the bow parts of the side faces;
- 2 – formation of transverse sand waves at the stern parts of the side faces;
- 3 – formation of transverse sand waves astern of the Platform

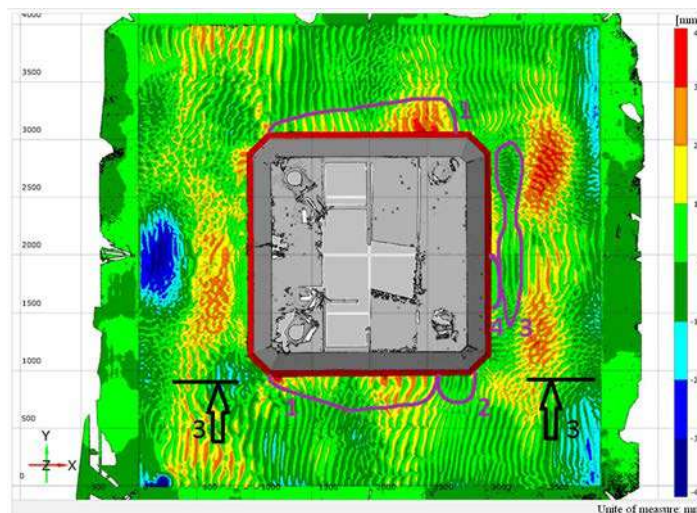


Figure 3. Bottom profile near the Platform model after experiment No. 2:

- 1 – formation of transverse sand waves at the bow parts of the side faces;
 - 2 – formation of transverse sand waves at the stern parts of the side faces;
 - 3 – formation of transverse sand waves astern of the Platform;
 - 4 – not deformed seabed surface behind the stern of the Platform;
- 3-3 is a cross-section, through which the seabed surface profile is made shown in Figure 8

As the parameters of the water flow (wave heights and flow velocities) increase and, consequently, as growth in the parameters of the soil stream flowing around the Platform, the groups of transverse sand waves at the lateral sides merge near the frontal face with the formation of a common transverse sand

wave with a complex-shaped crest (areas 1 in Figures 3–8). One or more crests of transverse waves (areas 1 in Figures 4–7) form at the frontal part of the Platform side faces depending on the nature of flow around. At the stern part of the Platform along the lateral faces, transverse waves begin to form, starting from the trough (areas 2 in Figures 4–7). Simultaneously, the water flow contributes to formation and movement of sand waves of shorter length along the side faces of the Platform along the resulting relief of the bottom surface (Figure 8).

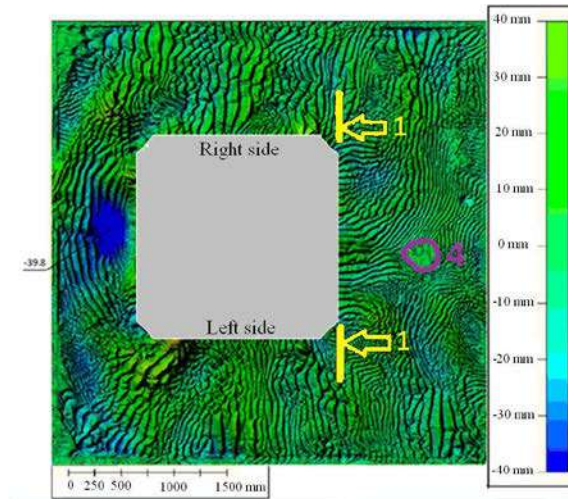


Figure 4. Bottom profile near the Platform model after experiment No. 3:

- 1 – formation of transverse sand waves at the bow parts of the side faces;
- 2 – formation of transverse sand waves at the stern parts of the side faces;
- 3 – formation of transverse sand waves astern of the Platform;

3-3 is a cross-section, through which the seabed surface profile is made shown in Figure 8

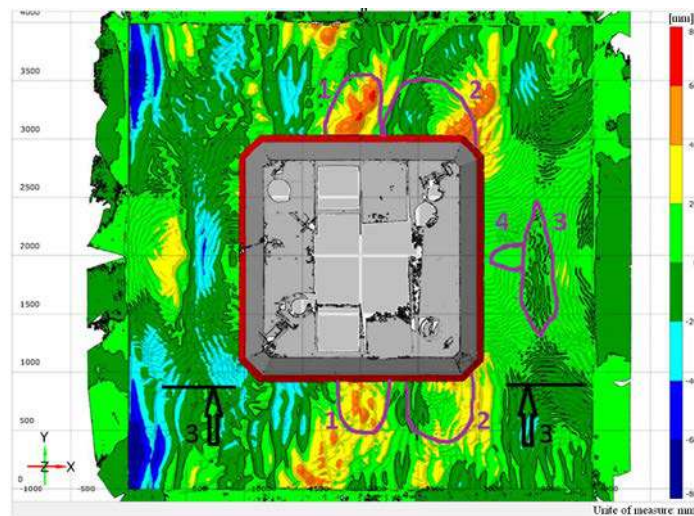


Figure 5. Bottom profile near the Platform model with a protective skirt with a length of penetration into the soil $H = 0.20$ m after experiment No. 4:

- 4 – not deformed seabed surface behind the stern of the Platform;

1-1 is a cross-section, through which the seabed surface profile is made shown in Figure 14

Figure 8 presents bottom surface profiles along the left lateral face of the Platform formed as a result of experiments NoNo. 2, 3 and 5 (cross-section 3-3 in Figures 3, 4, 6). The conditions for experiments NoNo. 2 and 5 are identical in depth and flow velocity of the water flow, as well as in the height of the generated regular waves, and differ only in the period of these waves (Table 2). The conditions of experiment No. 3 differed from the conditions for experiments NoNo. 2 and 5 (Table 2), only the period of regular waves was the same as in test No. 2. The distance l between the top of the first crest of the transverse sand wave in the bow part of the Platform and the maximum depth of the first trough of the transverse sand wave in the stern of the Platform, divided by the characteristic size of the

Platform, was selected as a characteristic value η_l to analyze the bottom surface profiles shown in Figure 8. In this case, the width B of the side face of the Platform is used (Figure 1), so $\eta_l = l/B$.

Consequently, $\eta_{l2} = 0.55$ for the experiment No. 2, $\eta_{l3} = 0.23$ for the experiment No. 3, $\eta_{l5} = 0.75$ for the experiment No. 3.

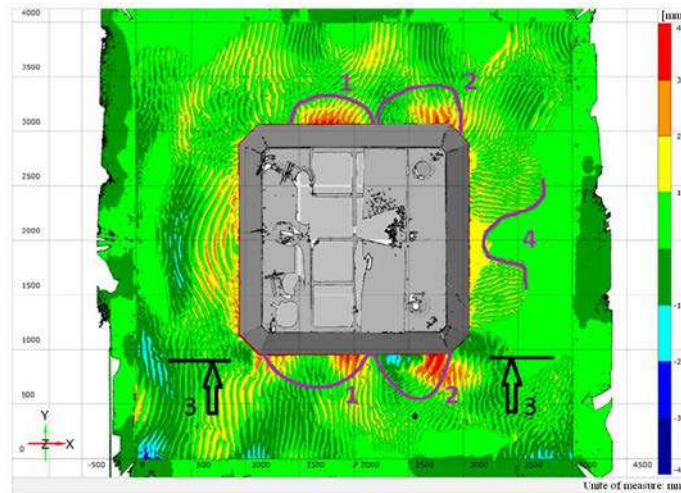


Figure 6. Bottom profile near the Platform model after experiment No. 5:
 1 – formation of transverse sand waves at the bow parts of the side faces;
 2 – formation of transverse sand waves at the stern parts of the side faces;
 4 – not deformed seabed surface behind the stern of the Platform;
 3-3 is a cross-section, through which the seabed surface profile is made shown in Figure 8

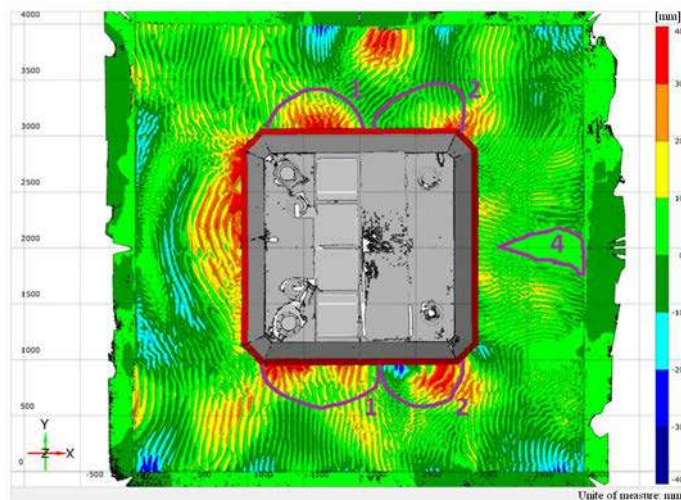


Figure 7. Bottom profile near the Platform model after experiment No. 6:
 1 – formation of transverse sand waves at the bow parts of the side faces;
 2 – formation of transverse sand waves at the stern parts of the side faces;
 4 – not deformed seabed surface behind the stern of the Platform

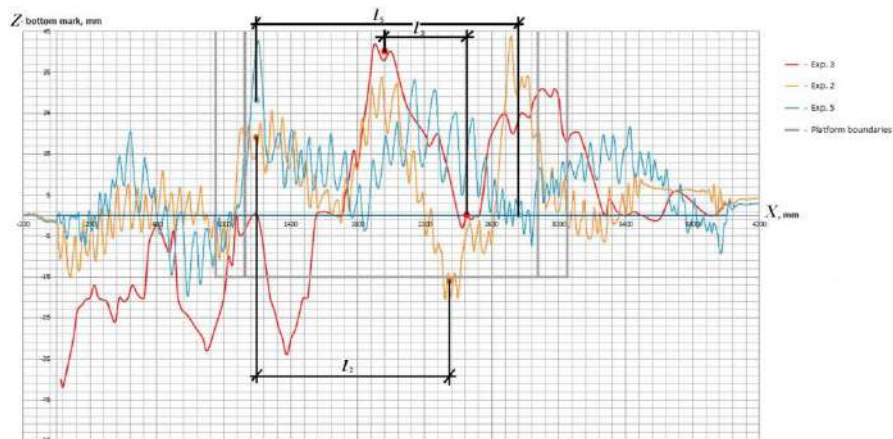


Figure 8. The profiles of the bottom surface along the left side of the Platform in the cross-section 3-3 along the side of the Platform model as a result of experiments NoNo. 2, 3 and 5

Analysis of the bottom surface profiles considered (Figure 8) and the values η_l obtained show that the magnitude η_l depends on all parameters of the water flow, but the value η_l is greater for larger sizes of the wave period, when all other parameters of the water flow are equal. It should be noted that when the parameters of the soil stream caused by the water flow increase, the first crest of the sand transverse wave is shifted toward the stern (comparison of the curves for the Experiments NoNo. 2 and 3 in Figure 8).

A similar relief of the bottom surface in the form of transverse sand waves is created along the lateral faces in the case of the frontal action of the water flow formed by regular waves and currents on a gravity platform of the Barge type (Figures 9–11). The formation of transverse sand waves in the bow parts of the Barge sides beginning at the crest (areas 1 in Figures 9–11) and at the stern parts starting from the trough (areas 2 in Figures 9–11) was also observed in this case. The flow around the Barge with a high parameters generate transverse waves with a common crest of a complex shape near the bow (areas 1 in Figures 9–11) and form transverse waves beginning with troughs with large depths at the stern part just as in the case of the flow around the Platform (areas 2 in Figures 9–11). Experiment No. 10 with the impact of the water flow formed by regular waves and currents on the Barge with protective underwater riprap prism showed that sandy transverse waves are formed along the sides as in the cases already considered (Figure 12).

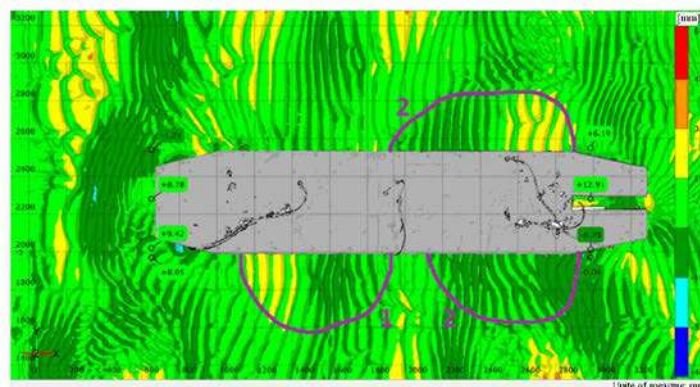


Figure 9. Bottom profile near the Barge model after experiment No. 7:
 1 – formation of transverse sand waves at the bow parts of the side faces;
 2 – formation of transverse sand waves at the stern parts of the side faces

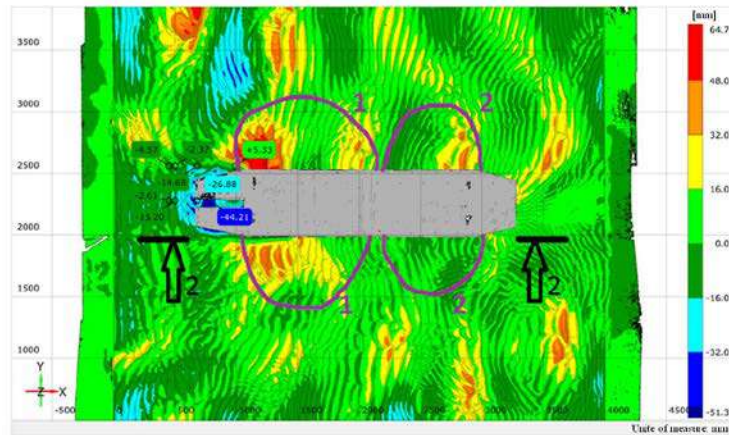


Figure 10. Bottom profile near the Barge model after experiment No. 8:

- 1 – formation of transverse sand waves at the bow parts of the side faces;
- 2 – formation of transverse sand waves at the stern parts of the side faces;
- 2-2 is a cross-section, through which the seabed surface profile is made shown in Figure 13

Figure 13 shows the bottom surface profiles along the side of the Barge (cross-sections 2-2 in Figures 10 and 11) formed as a result of experiments NoNo. 8 and 9. As it can be seen from Table 2, the conditions for experiments NoNo. 8 and 9 differ in the values of water depths and flow velocities, while the wave parameters (wave heights and periods) are practically the same.

The distance l between the top of the first crest of the transverse sand wave in the bow part of the Barge and the maximum depth of the first trough of the transverse sand wave in the stern of the Barge, divided by the length of the barge underwater base L , was selected as a characteristic value η_l to analyze the bottom surface profiles shown in Figure 13, so $\eta_l = l/L$.

Consequently, $\eta_{l8} = 0.54$ for the experiment No. 8 and $\eta_{l9} = 0.50$ for the experiment No. 9.

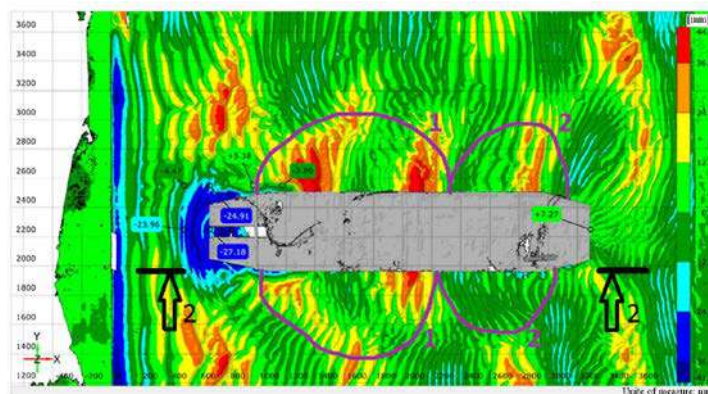


Figure 11. Bottom profile near the Barge model after experiment No. 9:

- 1 – formation of transverse sand waves at the bow parts of the side faces;
- 2 – formation of transverse sand waves at the stern parts of the side faces;
- 2-2 is a cross-section, through which the seabed surface profile is made shown in Figure 13

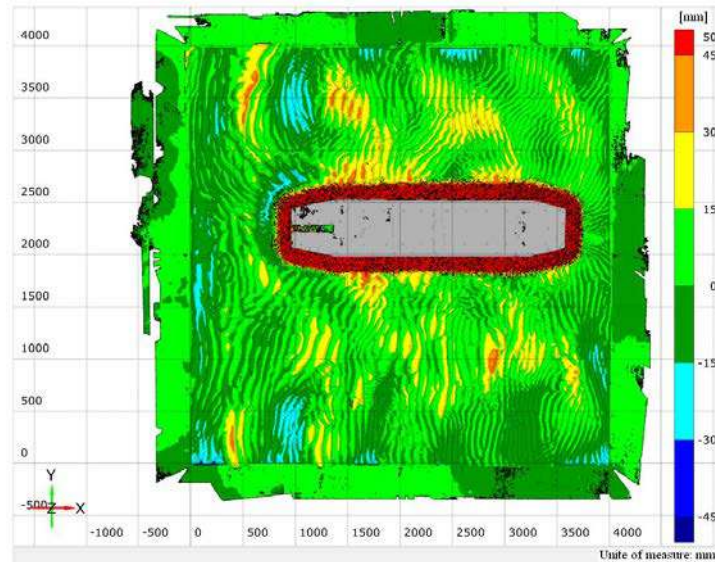


Figure 12. Bottom profile near the Barge model with protective underwater riprap prism after experiment No. 10

Analysis of the bottom surface profiles under consideration (Figure 13) shows that in the cases of water flow impact on the Barge, the values η_l for experiments NoNo. 8 and 9 remain close to each other, but at higher water flow velocities the value η_l will be greater.

Against the background of the formation of transverse waves similar to ship waves along the sides of the Barge, sand waves of smaller length are formed by the moving water flow just as in the experiments with the Platform (Figure 13). It should be noted that the flow around a large-sized object by the water stream generates movement of sand waves along the underwater slope that promotes the appearance of diffraction and interference of sand waves in specific areas near the object [21].

The interference of sand waves is a phenomenon of amplification or weakening of the amplitude of the resultant wave, depending on the relation between the phases of two sand waves forming in space or, in other words, the addition of several coherent oscillations of sand waves, in which they either strengthen or weaken each other [22, 23].

Sand waves move along the side faces of the Platform as already noted. The sand waves unfold at the cut corners and move along the back face (Figures 4–7). Sand waves from the left and right sides move towards each other along the back face. Interference of sand waves is possible in sum of these motions. The position of the interfered waves can be traced along the area of the unperturbed bottom surface, which divides the motion from the left and right sides.

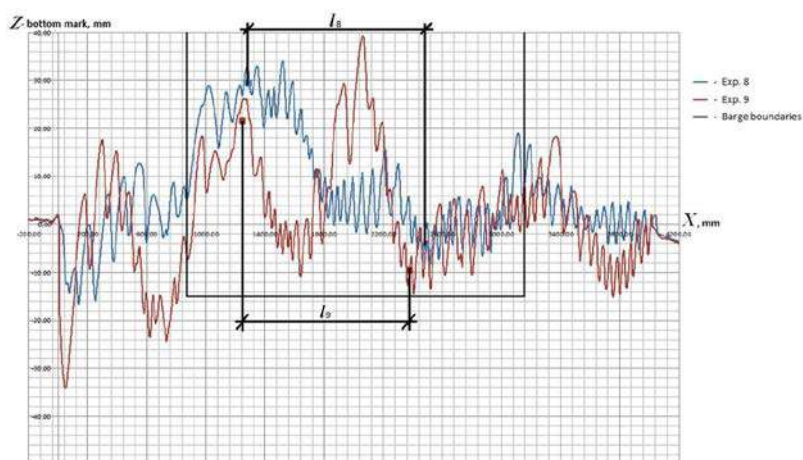


Figure 13. The longitudinal profiles of the bottom surface in cross-section 2-2 along the side of the Barge model as a result of experiments NoNo. 8 and 9

There will be an area of the unperturbed bottom surface (areas 4 in Figures 4, 6, 7) between the fronts of the sand waves moving both from the left and right sides of the Platform, if the energy of the water flow transmitted to the bottom surface is not sufficient to move sand waves along the entire length of its back face. The interaction of sand waves moving towards each other from the left and right sides does not occur. The interaction between sand waves moving from the left and right sides of the Platform is possible if this energy is sufficient (Figure 5). And if the rays of sand waves are parallel to the rear face, then interference occurs in the interaction area (Figure 14).

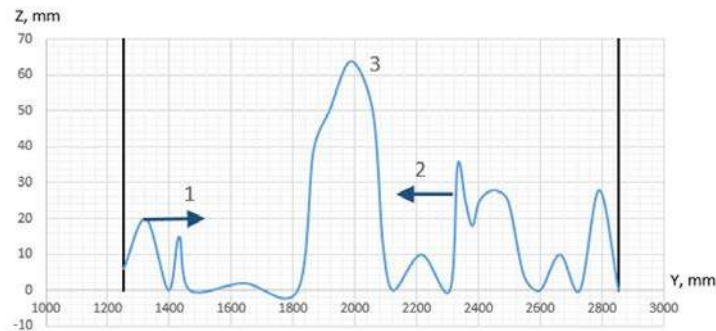


Figure 14. Interference (3) during the movement of sand waves (1, 2) along the rear edge of the Platform as a result of the experiment No. 4 (Cross-section 1-1 in Figure 5)

4. Conclusions

The presented results indicate that when interacting of a frontal water flow formed by regular waves and current with a gravity-type platform of a large size, the relief of the seabed surface adjacent to the platform is formed by sand waves.

The formation of sand waves is caused by the various reasons, among which it is necessary to allocate water and soil motion. Waves formed by soil flows are similar in nature to ship waves.

The ground flows moving around the platform contribute to the formation of larger waves, on which surface sand waves formed by the water flow move. Because of the movement of sand waves formed by the water flow, their interference behind the back of the platform is possible.

References

1. Bellendir Ye.N. *Naychnoe obosnovaniye proyektirovaniya gravitatsionnykh opornykh blokov morskikh ledostoykykh platform i ikh sopriazheniya s gruntovym osnovaniem* [Scientific substantiation of the gravitational support block's design for offshore ice-resistant platforms and coupling them with foundation]. Doctoral dissertation. Saint-Petersburg: VNIIG, 2006. 284 p. (rus)
2. Khalfin I.Sh. *Vozdeystvie voln na morskije neftegazopromyslovyje sooruzheniya* [The impact of waves on the offshore oil and gas facilities]. Moscow: Nedra, 1990. 313 p. (rus)
3. Belyaev N.D., Lebedev V.V., Nudner I.S. [et al.]. Selection of protective measures against scouring at the foundations of offshore gravity platforms. *Magazine of Civil Engineering*. 2015. No. 3(55). Pp. 79–88 (rus)
4. Makarov K.N., Chebotarev A.G. Breakwater placement at the root of a seawall. *Magazine of Civil Engineering*. 2015. No. 3(55). Pp. 67–78
5. Klimovich V.I., Pariev K.V. Design reliability for scour protection of the bottom near the platform "Prirazlomnaja". *Magazine of Civil Engineering*. 2017. No. 7. Pp. 52–65. doi: 10.18720/MCE.75.5.
6. *Sediments, Morphology and Sedimentary Processes on Continental Shelves: Advances in Technologies, Research and Applications*. ISBN: 978-1-118-31120-2. Feb 2012, Wiley-Blackwell. 440 p.
7. Ashley G.M. Classification of large-scale subaqueous bedforms: a new look at an old problem. *Journal of*

Литература

1. Беллендир Е.Н. Научное обоснование проектирования гравитационных опорных блоков морских ледостойких платформ и их сопряжения с грунтовым основанием. Дисс. ... докт. техн. наук. СПб., 2006. 284 с.
2. Халфин И.Ш. Воздействие волн на морские нефтегазопромисловые сооружения. М.: Недра, 1990. 312 с.
3. Беляев Н.Д., Лебедев В.В., Нуднер И.С. [и др.]. Выбор мероприятий по защите от размыва оснований гравитационных платформ для освоения шельфа // Инженерно-строительный журнал. 2015. № 3(55). С. 79–88.
4. Макаров К.Н., Чеботарев А.Г. Волнозащитные наброски в корневых частях портовых молов // Инженерно-строительный журнал. 2015. № 3(55). С. 67–78.
5. Климович В.И., Парьев К.В. Надежность конструкции защиты от размывов дна вблизи платформы «Приразломная» // Инженерно-строительный журнал. 2017. № 7(75). С. 52–65.
6. *Sediments, Morphology and Sedimentary Processes on Continental Shelves: Advances in Technologies, Research and Applications*. ISBN: 978-1-118-31120-2. Feb 2012, Wiley-Blackwell. 440 p.
7. Ashley G.M. Classification of large-scale subaqueous bedforms: a new look at an old problem // *Journal of Sedimentology Petrology*. 1990. Vol. 60(1). Pp. 160–172.
8. Knaapen M.A.F., Hulscher S.J.M.H., De Vriend H.J., Stolk A. A new type of bedwaves // *Geophysical Research*

Лебедев В.В., Нуднер И.С., Беляев Н.Д., Семенов К.К., Щемелинин Д.И. Формирование рельефа донной поверхности у гравитационного объекта // Инженерно-строительный журнал. 2018. № 3(79). С. 120–131.

- Sedimentology Petrology*. 1990. Vol. 60(1). Pp. 160–172.
8. Knaapen M.A.F., Hulscher S.J.M.H., De Vriend H.J., Stolk A. A new type of bedwaves. *Geophysical Research Letters*. 2002. Vol. 28. No. 7. Pp. 1323–1326. 2001.
 9. Nemeth A.A., Hulscher S.J.M.H., de Vriend H.J. Offshore sand wave dynamics, engineering problems and future solutions. *Pipeline and Gas Journal*. 2003. Vol. 230(4). Pp. 67–69.
 10. Noblesse F., Delhommeau G., Liu H., Wan D.-c., Yang C. Ship bow waves. *Journal of Hydrodynamics. Ser. B*. 2013. Vol. 25. No. 4. Pp. 491–501.
 11. Maxeiner E. *Physics of Breaking Bow Waves: A Parametric Investigation Using a 2D+T Wavemake*. Dissertation for the degree of Doctor of Philosophy. University of Maryland, 2009. 156 p.
 12. Babchik D., Belyaev N., Lebedev V. [et al.]. Experimental investigations of local scour caused by currents and regular waves near drilling barge foundations with cutout in stern. *Application of Physical Modelling to Port and Coastal Protection. Book of Proceedings of 5th International Conference "Coastlab14"*. Vol. 2. Varna, Bulgaria, 2014. Pp. 114–124.
 13. Gaydarov N.A., Zakharov Y.N., Ivanov K.S. et al. Numerical and Experimental Studies of Soil Scour Caused by Currents near Foundations of Gravity-Type Platforms. *Proceedings of 2014 International Conference on Civil Engineering, Energy and Environment (CEEE 2014)*. Hong Kong, 2014. Pp. 190–196.
 14. Semenov K.K., Lebedev V.V., Nudner I.S. [et al.]. Impact of waves and currents on the soil near gravity-type offshore platform foundation: numerical and experimental studies. *Proceedings of the International Offshore and Polar Engineering Conference*. 2015. Pp. 807–814.
 15. Shchemelinin L.G., Utin A.V., Belyaev N.D. [et al.]. Experimental studies regarding the efficiency of sea bed soil protection near offshore structures. *Proceedings of the ISOPE*. 2014. TPC-0320. Pp. 625–631.
 16. Thomsen J.M. *Scour in a marine environment characterized by current and waves*. Aalborg University, Denmark, 2006.
 17. Van Rijn L. C. Sand transport by currents and waves: General approximation formulae. *Proceeding of Coastal Sediments*. 2003. Vol. 3.
 18. Knoroz V.S. Nerazmyvayushchaya skorost' dlya nesvyaznykh gruntov i faktory, yeye opredelyayushchiye [Non-eroding speed for disconnected soils and the factors that determine it]. *Proceedings of the VNIIG*. 1958. Vol. 59. Pp. 62–81. (rus)
 19. Le Roux J.P. Wave friction factor as related to the Shields parameter for steady currents. *Sedimentary Geology*. 2003. Vol. 155. Pp. 37–43.
 20. Shields A. Anwendung der Ahnlichkeitsmechanik und der Turbulenzforschung auf die Geschiebewegung. *Mitt. der Preuss. Versuchsanst. fur Wasserbau und Schiffbau*. Heft 26. Berlin, Deutschland. 1936.
 21. Knaapen M.A.F., Hulscher S.J.M.H., de Vriend H.J. Data analysis of sand waves in the North Sea. *Proceeding of Marine Sandwave Dynamics*. Lille, France. 2000. Pp. 97–100.
 22. Boccotti P. *Wave Mechanics and Wave Loads on Marine Structures*. Butterworth-Heinemann. 2014. 344 p.
 23. Триккер, Р. Бор, прибой, волнение и корабельные волны. Л.: Гидрометеиздат, 1969. 286 с.
 - Letters. 2002. Vol. 28. No. 7. Pp. 1323–1326, 2001.
 9. Nemeth A.A., Hulscher S.J.M.H., de Vriend H.J. Offshore sand wave dynamics, engineering problems and future solutions // *Pipeline and Gas Journal*. 2003. Vol. 230(4). Pp. 67–69.
 10. Noblesse F., Delhommeau G., Liu H., Wan D.-C., Yang C. Ship bow waves // *Journal of Hydrodynamics. Ser. B*. 20013. Vol. 25. № 4. Pp. 491–501.
 11. Maxeiner E. Physics of Breaking Bow Waves: A Parametric Investigation Using a 2D+T Wavemake. Dissertation for the degree of Doctor of Philosophy. University of Maryland, 2009. 156 p.
 12. Babchik D., Belyaev N., Lebedev V. [et al.]. Experimental investigations of local scour caused by currents and regular waves near drilling barge foundations with cutout in stern // *Application of Physical Modelling to Port and Coastal Protection. Vol. 2. Book of Proceedings of 5th International Conference "Coastlab14"*. Varna, Bulgaria, 2014. Pp. 114–124.
 13. Gaydarov N.A., Zakharov Y.N., Ivanov K.S. et al. Numerical and Experimental Studies of Soil Scour Caused by Currents near Foundations of Gravity-Type Platforms // *Proceedings of 2014 International Conference on Civil Engineering, Energy and Environment (CEEE 2014)*. Hong Kong, 2014. Pp. 190–196.
 14. Semenov K.K., Lebedev, V.V., Nudner, I.S. [et al.]. Impact of Waves and Currents on the Soil near Gravity-Type Offshore Platform Foundation: Numerical and Experimental Studies // *Proceedings of the International Offshore and Polar Engineering Conference*. 2015. Pp. 807–814.
 15. Shchemelinin, L.G., Utin, A.V., Belyaev, N.D. [et al.]. Experimental studies regarding the efficiency of sea bed soil protection near offshore structures // *Proceedings of the ISOPE*. 2014. TPC-0320. Pp. 625–631.
 16. Thomsen J.M. Scour in a marine environment characterized by current and waves. Aalborg University, Denmark, 2006.
 17. Van Rijn, L. C. Sand transport by currents and waves: General approximation formulae // *Proceeding of Coastal Sediments* 2003. Vol. 3.
 18. Knoroz В.С. Неразмывающая скорость для несвязных грунтов и факторы, ее определяющие. // *Известия ВНИИГ им. Б. Е. Веденеева*. 1958. Т. 59. С. 62–81.
 19. Le Roux J. P. Wave friction factor as related to the Shields parameter for steady currents // *Sedimentary Geology*. 2003. Vol. 155. Pp. 37–43.
 20. Shields A. Anwendung der Ahnlichkeitsmechanik und der Turbulenzforschung auf die Geschiebewegung // *Mitt. der Preuss. Versuchsanst. fur Wasserbau und Schiffbau*, Heft 26. Berlin, Deutschland. 1936.
 21. Knaapen M.A.F., Hulscher S.J.M.H., de Vriend H.J.. Data analysis of sand waves in the North Sea // *Proceeding of Marine Sandwave Dynamics*. Lille, France. 2000. Pp. 97–100.
 22. Boccotti P. *Wave Mechanics and Wave Loads on Marine Structures*. Butterworth-Heinemann. 2014. 344 p.
 23. Триккер, Р. Бор, прибой, волнение и корабельные волны. Л.: Гидрометеиздат, 1969. 286 с.

Lebedev V.V., Nudner I.S., Belyaev N.D., Semenov K.K., Schemelinin D.I. The formation of the seabed surface relief near the gravitational object. *Magazine of Civil Engineering*. 2018. No. 3. Pp. 120–131. doi: 10.18720/MCE.79.13.

Vladimir Lebedev,
+7(921)649-83-67; *vladimir.v.lebedev@mail.ru*

Igor Nudner,
+7(911)752-84-99; *igor_nudner@mail.ru*

Nikolay Belyaev,
+7(921)982-72-44; *dnd@mail.ru*

Konstantin Semenov,
+7(911)732-01-71; *semenov.k.k@gmail.com*

Dmitry Schemelinin,
+7(911)291-84-96; *dimabens@gmail.com*

Владимир Валентинович Лебедев,
+7(921)649-83-67;
эл. почта: *vladimir.v.lebedev@mail.ru*

Игорь Сергеевич Нуднер,
+7(911)752-84-99;
эл. почта: *igor_nudner@mail.ru*

Николай Дмитриевич Беляев,
+7(921)982-72-44; эл. почта: *dnd@mail.ru*

Константин Константинович Семенов,
+7(911)732-01-71;
эл. почта: *semenov.k.k@gmail.com*

Дмитрий Игоревич Щемелинин,
+7(911)291-84-96;
эл. почта: *dimabens@gmail.com*

© Lebedev V.V., Nudner I.S., Belyaev N.D., Semenov K. K., Schemelinin D.I., 2018

doi: 10.18720/MCE.79.14

Ultra-light hybrid composite wood-polymer structural materials in construction

Сверхлегкие гибридные композитные древесно-полимерные конструкционные элементы в строительстве

A.S. Rassokhin,
A.N. Ponomarev,
Peter the Great St. Petersburg Polytechnic University, St. Petersburg, Russia
O.L. Figovsky,
International Nanotechnology Research Center Polymate, Migdal Haemek, Israel

Аспирант А.С. Рассохин,
канд. техн. наук, профессор
А.Н. Пономарев,
Санкт-Петербургский политехнический университет Петра Великого, г. Санкт-Петербург, Россия
д-р техн. наук, директор О.Л. Фиговский,
International Nanotechnology Research Center Polymate, г. Мигдаль ха-Эмек, Израиль

Key words: hybrid wood-polymer composites; impregnation; gradient toughening; external reinforcement; sulfo adducts of the carbon nanoclusters

Ключевые слова: гибридные древесно-полимерные композиты; пропитка; градиентное упрочнение; внешне армирование; сульфoadдукты нанокластеров углерода

Abstract. In the 21st century, wood construction is again widespread. Industrial wood ceased to be perceived as a material for household buildings and low-rise rural houses and began to be used in the construction of large-span, high-rise and unique buildings and structures. The paper analyzes the use of wood for the construction of large-span, high-rise and unique buildings and structures. The results of experimental studies of hollow wooden parts, developed by the authors, impregnated with epoxy compositions, modified by sulfoadducts of nanoclusters of carbon ("Ugleron C") are given. The possibility of external reinforcement of wood with high-strength carbon fiber grids is considered. The technology of additional strengthening of wooden parts by an external membrane from a multifunctional composite water compatible coating "EpoxyPAN" has also been proven. The results of physical and mechanical tests of samples of ultralight hybrid wood-polymer components are presented. The spheres of their application in park construction, wooden bridge construction, construction of wooden high-rise, large-span and unique buildings and structures are analyzed.

Аннотация. В 21-ом веке строительство с использованием древесины вновь обрело массовый характер. Древесина перестала восприниматься как материал для хозяйственных построек и малоэтажных домов и стала применяться при строительстве большепролетных, высотных, уникальных зданий и сооружений. В статье проведен анализ сфер использования древесины при строительстве большепролетных, высотных, уникальных зданий и сооружений. Приводятся результаты экспериментальных исследований полых деревянных деталей, пропитанных эпоксициановыми композициями, модифицированными сульфoadдуктами нанокластеров углерода («Углерон С»). Рассматривается возможность внешнего армирования древесины сетками из высокопрочного углеродного волокна. Отработана технология дополнительного усиления деревянных деталей внешней мембраной из многофункционального композиционного водосовместимого покрытия «ЭпоксипАН». Приводятся результаты физико-механических испытаний образцов сверхлегких гибридных древесно-полимерных деталей. Проанализированы сферы их применения в парковом строительстве, деревянном мостостроении, строительстве деревянных высотных, большепролетных, уникальных зданий и сооружений.

1. Introduction

Since ancient times, in geographic forest-rich areas, wood has been used as the main building material due to its availability, good strength characteristics, ease of processing and low price. Solid

Рассохин А.С., Пономарев А.Н., Фиговский О.Л. Сверхлегкие гибридные композитные древесно-полимерные конструкционные элементы в строительстве // Инженерно-строительный журнал. 2018. № 3(79). С. 132–139.

wood and sawn timber were used in construction, ranging from simple farm buildings to unique structures, such as wooden fortresses in towns and temples, some of which are extant at the present and overcame the mark of 300 years [1].

But in the 19th century, due to the development of industrial technologies, brick and steel structures became more accessible, and concrete also reinforced. The concrete became the most common material in the construction industry in the 20th century. As a result, the wood fell by the wayside and began to be considered a finishing material, a material for household outbuildings and cottage housing construction

But by the end of the 20th century, due to the rapid development of chemical technology of woodworking, the scope of the use of wood in load-bearing building structures has significantly expanded. In addition, the construction has reached a new level, as more attention was paid to the issues of ecology, resource saving and comfort of human habitation. Wood is one of the most environmentally friendly materials, as it creates a useful indoor microclimate for humans and is a renewable natural resource.

Laminated wood structures came into common use in the construction [2–5]. Their history began with glued beams from individual slats (Glulam) [2, 3]. At the moment, a veneer beam (LVL) [3], as well as panels and veneer blocks (CLT) [4–8] are already widely used.

Due to the development of wooden architecture technologies, as well as the improvement of legislation, which in many countries has previously banned the building of multistore blocks from wood, pilot constructions have been built that show the applicability of wood for the construction of large-span, high-rise and unique buildings and structures.

In 2015 the first multistore (8 floors) apartment block using CLT technology, which is operated without any complaints, was built in Finland.

Among the large-span laminated wood structures, Zenith Concert Hall (France), Bern railway station (Switzerland), the Arena in Salzburg (Austria) should be mentioned.

Also, high efficiency of wood structures in the construction regions with high seismic activity is known [9–11].

The widespread introduction of structures with load-bearing elements on the basis of wood is hampered by the established belief about fragility, increased fire hazard of timber-based structures, as well as its low bearing capacity. This makes actual the work on improving the properties of wood structures. Different aspects of this issue were covered by researchers around the world. The issues of impregnation are covered in the publications [11–14], protective coatings are analyzed in the publications [13, 16–20], external and interlayer reinforcement and the issues of glued laminated wood is covered in the publications [2–5, 21–43].

Based on the analysis, it can be concluded that construction requires lightweight, high-strength construction materials based on wood with equally high fire and technical characteristics for the construction of large-span, high-rise and unique buildings and structures.

2. *Materials and methods*

In order to carry out research on the physical and mechanical characteristics of HWPC, hollow test samples from coniferous wood veneer with humidity no more than 10% have been developed and manufactured. The test samples were in the form of hexahedrons inscribed in a circle of 185 mm and 1200 mm long.

The wood hexahedrons were assembled from a 10 mm thick veneer with preliminary impregnation. For the impregnation, a composition based on 75.53 % mass. of alcohol-acetone mixture (with a weight ratio of alcohol to acetone 1:1), 20 % mass. of epoxy resin SR 8100 from Sicomin (France), 4.47 % mass. of amine hardener SD 8824 from Sicomin (France). The hardener was modified with sulfoadducts of the carbon nanoclusters ("Ugleron C") in an amount of 1.6 % by weight of the amount of hardener. The efficiency of the modified epoxy compositions with sulfoadducts of the carbon nanoclusters ("Ugleron C") [42], as well as their optimal concentrations, have been specified in the previous work of the authors [13].

The impregnation was made in the sleeve of vacuum film PO180, air evacuation was provided by a two-stage plate-rotor vacuum pump with an oil seal Ulvac GLD-137A.

After the impregnation, the drying of the preparations was continued for 7 days in a room with heated floors without access of damp air. Additional drying was necessary to ensure uniformity in temperature moisture-induced deformations after gluing.

As glue structure the composition from 53 % mass. of epoxy resin ED-20 (Russian State Standard GOST 10587-84), 47 % mass. of water soluble amine hardener was used. The water soluble amine hardener has been modified by carbon nanoporous microfibers (CNPMF) in number of 0.8 % of mass. relatively the mass of the hardener. The efficiency of the modification of epoxy compositions with carbon nanoporous microfibers (CNPMF) [43], as well as their optimal concentrations, have been specified in the previous work of the authors [13].

After the polymerization of the glued joint of the wood sample, under normal conditions, external reinforcement in the form of a grid of carbon fiber UKN-M-12K according to Russian Specification TU 1916 -146-05763346-96 produced by LLC Argon (Russia) was made. As a binder, a composition consisting of SR 8100 epoxy resin from Sicomin (France) and SD 8824 amine hardener of Sicomin (France) in a ratio of 25:6, respectively, was used. The composition was modified with sulfoadducts of the carbon nanoclusters ("Ugleron C") in an amount of 1.6 % by weight of the amount of hardener. Photo of a wood sample with a carbon fiber grid external reinforcement is given in Figure 1.



Figure 1. HWPC sample with external reinforcement in the form of a carbon fiber grid

Upon completion of polymerization process of glue connection, the continuous membrane from polymer nanocomposite material EpoxyPAN was applied on an external surface of preparations for additional strengthening of HWPC and protection against possible action of hostile environment, water and fire (Fire technical characteristics of EpoxyPAN, according to the existing certificate: G1, If1, Sp1, Fo2, T1). Drawing was made by a pneumatic method by means of the textural sprayer the LC-02 brand PRAKTIKA Ltd company.

Measurements of durability on a tension strength of samples of HWPC on a four-dot bend in accordance with Russian State Standard 16483.12-72 have been taken. Tests were carried out at the stand with the hydraulic test BISS MAGNUM UT-05-3000 module. For a possibility of carrying out tests of samples of the above-stated sizes the industrial technological equipment which drawing is given in Figure 2 has been developed and has been made.

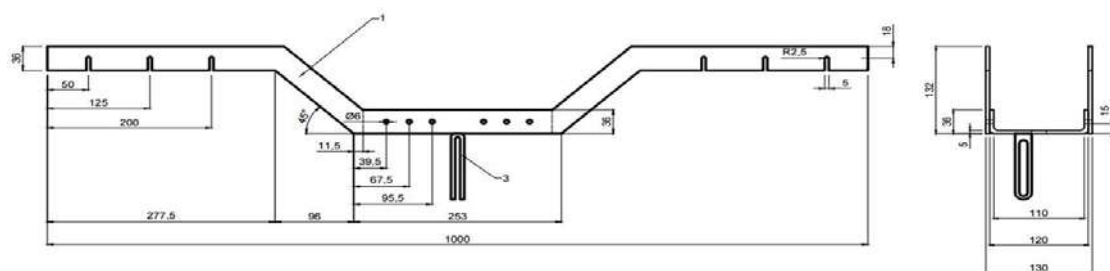


Figure 2. Drawing of the industrial technological equipment

The loading scheme of the test samples is shown in Figure 3.

Axial compression tests were carried out on a universal electromechanical machine Instron 5982 with a maximum force of 100 kN and a test space of 1930 mm. A photo of the process of testing for axial compression is given in Figure 4.

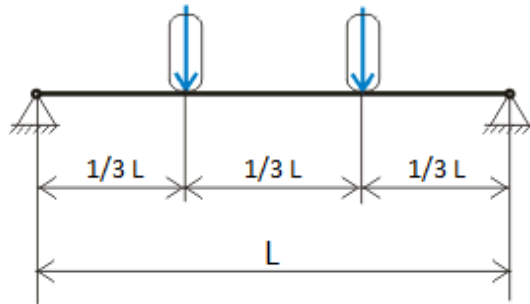


Figure 3. Loading scheme



Figure 4. Compression tests of a HWPC sample on Instron 5982 test machine

3. Results and Discussion

The results of physical and mechanical tests of ultralight hybrid wood-polymer components are given in Figures 5 and 6.

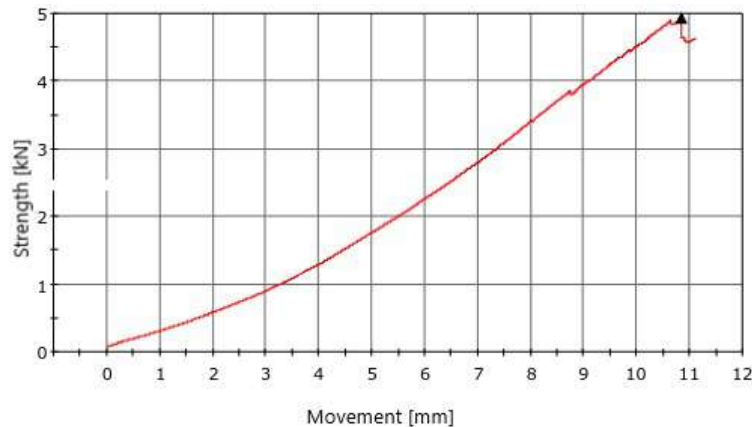


Figure 5. Results of HWPC samples bending tests

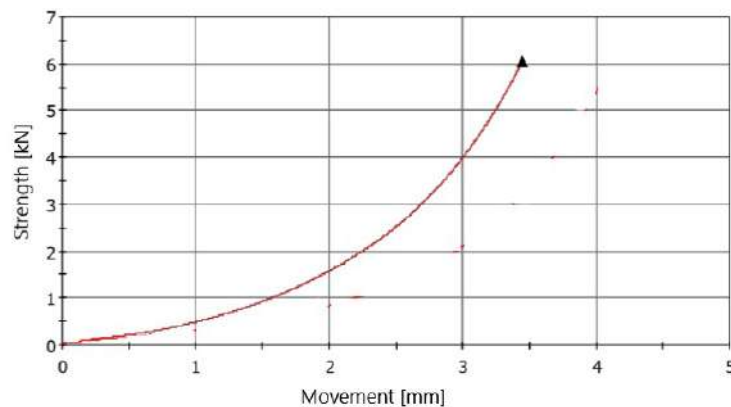


Figure 6. Results of HWPC samples compression tests

Analysis of the results of physical and mechanical tests of the HWPC samples says for their high load-bearing capacity, despite the fact that the weight of 1 linear meter of the HWPC is a hexagonal

hollow structure inscribed in a circle with a diameter of 185 mm is 3.2 kg, which is 4 times lighter than a pine with 10 % humidity and equal volume. It is essential decrease in mass of a structural element of rather previous work of authors [13].

These structures could be used as elements of the frame, rafter systems, columns of wood structures, which would significantly reduce the overall weight of the structure and, consequently, the load on the foundation.

As the construction industry is quite conservative and the legislation is imperfect, ultralight HWPCs will not be able to get a foothold in the housing construction industry fast, it will take some time. But already at the current stage, ultralight HWPCs are able to replace wood, concrete and metal supports of power lines, communications and lighting. This is particularly relevant to hard-to-reach, mountain, marshy places, as well as the extreme north, since the installation of traditional wood, concrete and metal supports requires a lot of labor, special equipment, burial or foundation. HWPC is many times lighter and several of its components can be assembled directly on site.

Impregnation and a protective layer of "EpoxyPAN" provide a greater durability than wood and metal, especially in corrosive environments, and external reinforcement allows to achieve high mechanical characteristics.

Low relative density, high load-bearing capacity, durability, resistance to aggressive environments, ease of assembly at the construction site opens the possibility of constructing towers, masts, antennas from HWPC.

HWPC can also be used as vertical elements of the bearing structures of small pedestrian bridges and transitions. Schematic diagrams are given in Figures 7 and 8.

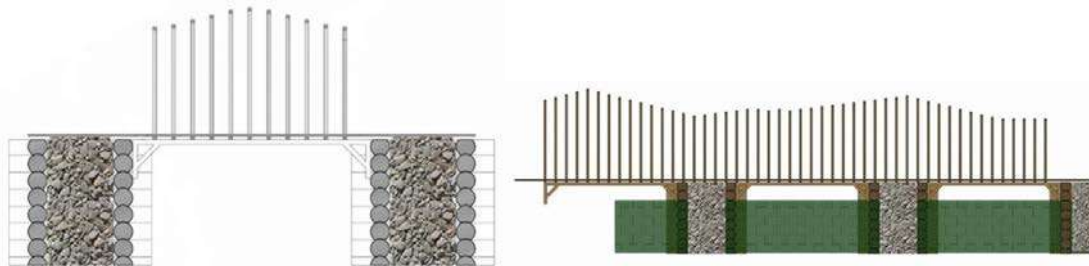


Figure 7. Schemes of park pedestrian bridges, developed by the architect S.I. Gareyev

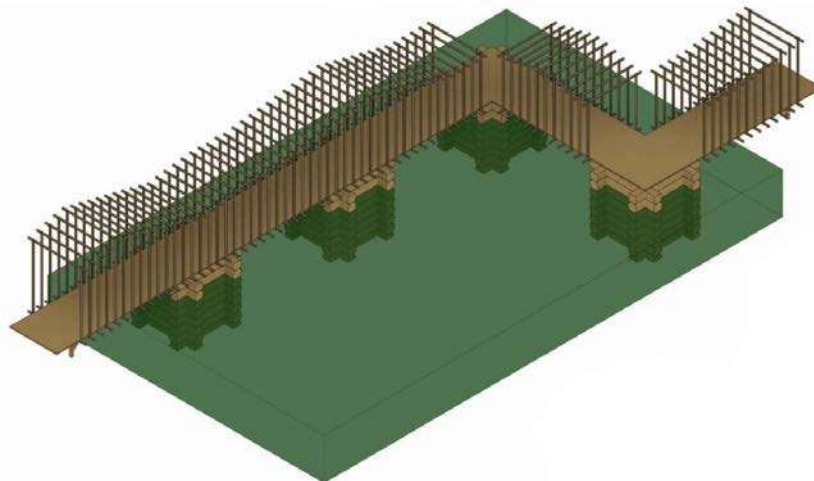


Figure 8. Scheme of the pedestrian bridge across the marshy / mountainous areas, developed by the architect S.I. Gareyev

4. Conclusions

1. The performed data analysis shows an increased interest in wood as a building material, even for high-rise, large-span, unique buildings and structures.

Рассохин А.С., Пономарев А.Н., Фиговский О.Л. Сверхлегкие гибридные композитные древесно-полимерные конструкционные элементы в строительстве // Инженерно-строительный журнал. 2018. № 3(79). С. 132–139.

2. The efficiency of impregnation of wood with compositions on the basis of epoxy compositions by evacuation is specified.
3. The efficiency of external reinforcement of wood by carbon fiber grids is specified.
4. An ultra-light hybrid composite wood-polymer structural element for the construction of high-rise, large-span, unique buildings and structures, lighting poles, power lines, communications, towers and communication towers, etc is developed.
5. Volume density has gone down by 4 times of rather previous work of authors [13].
6. Use of the hollow structural element expands scope of the HWPC as the structural element become more transportable and easily mounted.

5. Acknowledgements

Authors express profound gratitude to the staff of the testing center of St. Petersburg State University of Architecture and Civil Engineering for assistance in conducting the tests and to the architect S.I. Gareev for architectural design of bridge structures and pedestrian crossings from the HWPC.

References

1. Kozlov V. A., Krutov V. I., Kisternaya M. V. Sostoyanie drevesiny preobrazhenskoj cerkvi muzeya-zapovednika «Kizhi» [Condition of wood of Church of the Transfiguration of memorial estate "Kizhi"]. *Transactions of the Karelian Research Centre of RAS*. 1999. No. 1. Pp. 131–139. (rus)
2. Tsoumis G. *Science and Technology of Wood Structure, Properties, Utilization*. Van Nostrand Reinholdy New York, 1991. 494p.
3. Faherty K.F., Williamson T.G. *Wood. Engineering and Construction Handbook*. McGraw-Hill Inc. New York, 1999. 897 p.
4. Brandner R., Flatscher G., Ringhofer A., Schickhofer G., Thiel A. Cross laminated timber (CLT): overview and development. *European Journal of Wood and Wood Products*. 2016. No. 3.
5. Ringhofer A., Schickhofer G. Timber in Town—current examples for residual buildings in CLT and task for the future. *European Conference on Crosslaminated timber (CLT)*. 2013.
6. Sliseris J., Gaile L., Pakrastins L. Numerical analysis of behaviour of cross laminated timber (CLT) in blast loading. *IOP Conference Series: Materials Science and Engineering*. 2017. No. 251(1). Art. no. 012105.
7. Frolovs G., Rocens K., Sliseris J. Shear and tensile strength of narrow glued joint depending on the grain direction of plywood plies. *Procedia Engineering*. 2017. No. 172. Pp. 292–299.
8. Frolovs G., Rocens K., Sliseris J. Optimal design of plates with cell type hollow core. *IOP Conference Series: Materials Science and Engineering*. 2017. No. 251(1). Art. no. 012075.
9. Belash T.A., Ivanova Zh.V. Derevyannye konstrukcii v sejsmostojkom stroitel'stve zdaniij i sooruzhenij (otechestvennyj i zarubezhnyj opyt) [Wooden Designs in Aseismic Construction of Buildings and Constructions (Domestic and Foreign Experience)]. *Magazine "Earthquake engineering. Constructions safety"*. 2015. No. 3. Pp. 57–60.(rus)
10. Arnold C., Reitherman R. *Building Configurarian and Seismic Design*. John Wiley and Sons, Inc. New York, 1982.
11. Inan Z. Runner beams as a building element of masonry walls in Eastern Anatolia, Turkey. *Vernacular Heritage and Earthen Architecture: Contributions for Sustainable Development*. London. 2014. Pp. 721–726.
12. Kosheleva N.A., Shejkmán D.V. Issledovanie processa propitki polimerami pri modifikacii malocennyh porod drevesiny [Research of process of impregnation by polymers at modification of invaluable breeds of wood]. *Newsletter of KSTU*. 2015. No. 14. Pp. 126–130. (rus)
13. Ponomarev A.N., Rassokhin A.S. Hybrid wood-polymer composites in civil engineering. *Magazine of Civil*

Литература

1. Козлов В.А., Крутов В.И., Кистерная М.В. Состояние древесины Преображенской церкви музея-заповедника // Труды Карельского научного центра Российской академии наук. 1999. № 1. С. 131–139.
2. Tsoumis G. *Science and Technology of Wood Structure, Properties, Utilization*. Van Nostrand Reinhold. New York, 1991. 494 p.
3. Faherty K.F., Williamson T.G. *Wood. Engineering and Construction Handbook*. McGraw-Hill Inc. New York, 1999. 897 p.
4. Brandner R., Flatscher G., Ringhofer A., Schickhofer G., Thiel A. Cross laminated timber (CLT): overview and development // *European Journal of Wood and Wood Products*. 2016. № 3.
5. Ringhofer A., Schickhofer G. Timber in Town—current examples for residual buildings in CLT and task for the future // *European Conference on Crosslaminated timber (CLT)*. 2013.
6. Sliseris J., Gaile L., Pakrastins L. Numerical analysis of behaviour of cross laminated timber (CLT) in blast loading // *IOP Conference Series: Materials Science and Engineering*. 2017. № 251(1). Art. no. 012105.
7. Frolovs G., Rocens K., Sliseris J. Shear and tensile strength of narrow glued joint depending on the grain direction of plywood plies // *Procedia Engineering*. 2017. № 172. Pp. 292–299.
8. Frolovs G., Rocens K., Sliseris J. Optimal design of plates with cell type hollow core // *IOP Conference Series: Materials Science and Engineering*. 2017. № 251(1). Art. no. 012075.
9. Белаш Т.А., Иванова Ж.В. Деревянные конструкции в сейсмостойком строительстве зданий и сооружений (отечественный и зарубежный опыт) // Сейсмостойкое строительство. Безопасность сооружений. 2015. № 3. С. 57–60.
10. Arnold C., Reitherman R. *Building Configurarian and Seismic Design*. John Wiley and Sons, Inc. New York, 1982.
11. Inan Z. Runner beams as a building element of masonry walls in Eastern Anatolia, Turkey // *Vernacular Heritage and Earthen Architecture: Contributions for Sustainable Development*. London. 2014. Pp. 721–726.
12. Кошелева Н.А., Шейкман Д.В. Исследование процесса пропитки полимерами при модификации малоценных пород древесины // Вестник КНТИУ. 2015. № 14. С. 126–130.
13. Пономарев А.Н., Рассохин А.С. Гибридные древесно-полимерные композиты в строительстве // Инженерно-строительный журнал. 2016. № 8(68). С. 45–57
14. Куницкая О.А., Бурмистрова С.С.

Rassokhin A.S., Ponomarev A.N., Figovsky O.L. The formation of the seabed surface relief near the gravitational object. *Magazine of Civil Engineering*. 2018. No. 3. Pp. 132–139. doi: 10.18720/MCE.79.14.

- Engineering*. 2016. No. 8. Pp. 45–57.
14. Kunickaya O.A., Burmistrova S.S. Eksperimental'nye issledovaniya propitki drevesiny pri pomoshchi gidroudara [Experimental study of wood impregnation with hydraulic impact]. *Systems. Methods. Technologies*. 2015. No4 (28) Pp. 103-108 (rus)
 15. Moore G.R., Kline D.E., Blankenhorn P.R. Impregnation of wood with a high viscosity epoxy resin. *Wood Fiber Sei.* 1983. Vol. 15. No. 3. Pp. 223–234.
 16. Azeez A.A., Rhee K.Y., Park S. J., Hui D. Epoxy clay nanocomposites – processing, properties and applications: a review. *Compos. Part B Eng.* 2013. No. 45. Pp. 308–320.
 17. Sprenger S. Epoxy resins modified with elastomers and surface-modified silica nanoparticles. *Polymer*. 2013. No. 18(54). Pp. 4790–4797.
 18. Pearson R., Liang Y. Polymer nanocomposites. *Woodhead Publishing Ltd.* 2010. No. 13. Pp. 773–786.
 19. Islam M.E., Mahdi T.H., Hosur M.V., Jeelani S. Characterization of carbon fiber reinforced epoxy composites modified with nanoclay and carbon nanotubes // *Procedia Engineering*. 2015. № 105. Pp. 821–828.
 20. Deka M., Saikia C.N. Chemical modification of wood with thermosetting resin: effect on dimensional stability and strength property. *Bioresource Technology*. 2000. Vol. 73. No. 2. Pp. 179–181.
 21. Plevris N., Triantafillou T. Time-dependent behavior of RC members strengthened with FRP laminates. *Journal of Structural Engineering*. 1994. No. 120. Pp. 1016–1042.
 22. Biblis E.J. Analysis of wood-fiber glass composite beams within and beyond the elastic region. *Forest Prod. J.* 1965. No. 2(15). Pp. 81–88.
 23. Triantafillou T., Deskovic N. Prestressed FRP sheets as external reinforcement of wood members. *Journal of Structural Engineering, ASCE*. 1992. Vol. 118. No. 5. Pp. 1270–1284.
 24. Plevris N., Triantafillou T. Creep behavior of FRP reinforced wood members. *Journal of Structural Engineering*. 1995. No. 121(2). Pp. 174–186.
 25. Triantafillou T. Shear reinforcement of wood using FRP materials. *Journal of Materials in Civil Engineering*. 1997. No. 9. Pp. 65–69.
 26. Dagher H.J. High-performance wood composites for construction // VII EBRAMEM, São Carlos – Brasil. 2000. Pp. 154–163.
 27. Tingley D., Cegelka S. High-strength-fiber-reinforced plastic reinforced wood. *Internacional Wood Engineering Conference*. New Orleans, Louisiana, USA. 1996. Vol. 3. Pp. 57–64.
 28. Davids W., Nagy E., Richie M. Fatigue behavior of composite-reinforced glulam bridge girders. *Journal of Bridge Engineering*. 2008. Vol. 13. No. 2. Pp. 183–191.
 29. Fiorelli J., Dias A.A. Analysis of the strength and stiffness of timber beams reinforced with carbon fiber and glass fiber. *Materials Research*. 2003. Vol. 6. No. 2. Pp. 193–202.
 30. Kliger I.R., Haghani R., Brunner M., Harte A.M., Schober K.-U. Wood-based beams strengthened with FRP laminates: improved performance with pre-stressed systems. *European Journal of Wood and Wood Products*. 2016. Vol. 74. No. 3. Pp. 319–330.
 31. Barreto A.M.J.P., Campilho R.D.S.G, De Moura M.F.S.F, Morais J.J.L., Santos C.L. Repair of wood trusses loaded in tension with adhesively bonded carbon-epoxy patches. *The Journal of Adhesion*. 2010. Vol. 86. No. 5–6. Pp. 630–648.
 32. Chang W.-S. Repair and reinforcement of timber columns and shear walls – A review. *Construction and Building Materials*. 2015. Vol. 97. Pp. 14–24.
 - Экспериментальные исследования пропитки древесины при помощи гидроудара // *Системы. Методы. Технологии*. 2015. № 4(28) С. 103–108.
 15. Moore G.R., Kline D.E., Blankenhorn P.R. Impregnation of wood with a high viscosity epoxy resin // *Wood Fiber Sei.* 1983. Vol. 15. № 3. Pp. 223–234.
 16. Azeez A.A., Rhee K.Y., Park S. J., Hui D. Epoxy clay nanocomposites – processing, properties and applications: a review // *Compos. Part B Eng.* 2013. № 45. Pp. 308–320.
 17. Sprenger S. Epoxy resins modified with elastomers and surface-modified silica nanoparticles // *Polymer*. 2013. № 18(54). Pp. 4790–4797.
 18. Pearson R., Liang Y. Polymer nanocomposites // *Woodhead Publishing Ltd.* 2010. No. 13. Pp. 773–786.
 19. Islam M.E., Mahdi T.H., Hosur M.V., Jeelani S. Characterization of carbon fiber reinforced epoxy composites modified with nanoclay and carbon nanotubes // *Procedia Engineering*. 2015. № 105. Pp. 821–828.
 20. Deka M., Saikia C.N. Chemical modification of wood with thermosetting resin: effect on dimensional stability and strength property // *Bioresource Technology*. 2000. Vol. 73. № 2. Pp. 179–181.
 21. Plevris N., Triantafillou T. Time-dependent behavior of RC members strengthened with FRP laminates // *Journal of Structural Engineering*. 1994. № 120. Pp. 1016–1042.
 22. Biblis E.J. Analysis of wood-fiber glass composite beams within and beyond the elastic region // *Forest Prod. J.* 1965. № 2(15). Pp. 81–88.
 23. Triantafillou T., Deskovic N. Prestressed FRP sheets as external reinforcement of wood members // *Journal of Structural Engineering, ASCE*. 1992. Vol. 118. № 5. Pp. 1270–1284.
 24. Plevris N., Triantafillou T. Creep behavior of FRP reinforced wood members // *Journal of Structural Engineering*. 1995. № 121(2). Pp. 174–186.
 25. Triantafillou T. Shear reinforcement of wood using FRP materials // *Journal of Materials in Civil Engineering*. 1997. № 9. Pp. 65–69.
 26. Dagher H.J. High-performance wood composites for construction // VII EBRAMEM, São Carlos – Brasil. 2000. Pp. 154–163.
 27. Tingley D., Cegelka S. High-strength-fiber-reinforced plastic reinforced wood // *Internacional Wood Engineering Conference*. New Orleans, Louisiana, USA. 1996. Vol. 3. Pp. 57–64.
 28. Davids W., Nagy E., Richie M. Fatigue behavior of composite-reinforced glulam bridge girders // *Journal of Bridge Engineering*. 2008. Vol. 13. № 2. Pp. 183–191.
 29. Fiorelli J., Dias A.A. Analysis of the strength and stiffness of timber beams reinforced with carbon fiber and glass fiber // *Materials Research*. 2003. Vol. 6. № 2. Pp. 193–202.
 30. Kliger I.R., Haghani R., Brunner M., Harte A.M., Schober K.-U. Wood-based beams strengthened with FRP laminates: improved performance with pre-stressed systems // *European Journal of Wood and Wood Products*. 2016. Vol. 74. № 3. Pp. 319–330.
 31. Barreto A.M.J.P., Campilho R.D.S.G, De Moura M.F.S.F, Morais J.J.L., Santos C.L. Repair of wood trusses loaded in tension with adhesively bonded carbon-epoxy patches // *The Journal of Adhesion*. 2010. Vol. 86. № 5–6. Pp. 630–648.
 32. Chang W.-S. Repair and reinforcement of timber columns and shear walls – A review // *Construction and Building Materials*. 2015. Vol. 97. Pp. 14–24.

Рассохин А.С., Пономарев А.Н., Фиговский О.Л. Сверхлегкие гибридные композитные древесно-полимерные конструкционные элементы в строительстве // *Инженерно-строительный журнал*. 2018. № 3(79). С. 132–139.

33. Schober K.U. *Innovative Timber Composites – Improving Wood with Other Materials*. Bath, UK: Schober, K.U. (ed.), University of Bath. 2013. 48 p.
34. Lobov D.M., Kricin A.V., Tihonov A.V. Osobennosti armirovaniya derevjannyh elementov, usilennyh uglernodnym voloknom, pri staticheskom izgibe [Features of reinforcing of the wooden elements strengthened by carbon fiber]. *Izvestija KGASU*. 2013. No. 2(24). Pp. 132–138. (rus)
35. Yahyaei-Moayyed M., Taheri F. Experimental and computational investigations into creep response of AFRP reinforced timber beams. *Composite Structures*. 2011. Vol. 93. No. 2. Pp. 616–628.
36. Davalos J.F., Kim Y., Barbero E.J. A layerwise beam element for analysis of frames with laminated sections and flexible joints. *Finite Elements in Analysis and Design*. 1995. Vol. 19. No. 3. Pp. 181–194.
37. Dolan C.W., Galloway T.L., Tsunemori A. Prestressed glued-laminated timber beam—pilot study. *Journal of Composites for Construction*. 1997. Vol. 1. No. 1. Pp. 10–16.
38. Nadir Y., Nagarajan P., Ameen M., Arif M.M. Flexural stiffness and strength enhancement of horizontally glued laminated wood beams with GFRP and CFRP composite sheets. *Construction and Building Materials*. 2016. Vol. 112. Pp. 547–555.
39. Franke S., Franke B., Harte A. Failure modes and reinforcement techniques for timber beams – State of the art. *Construction and Building Materials*. 2015. Vol. 97. Pp. 2–13.
40. Svecova D., Eden R.J. Flexural and shear strengthening of timber beams using glass fibre reinforced polymer bars – an experimental investigation. *Canadian Journal of Civil Engineering*. 2004. Vol. 31. No. 1. Pp. 45–55.
41. Kim Y.J., Harries K.A. Modeling of timber beams strengthened with various CFRP composites. *Engineering Structures*. 2010. Vol. 32. No. 10. Pp. 3225–3234.
42. Ponomarev A.N., Judovich M.E., Kozeev A.A. Sulfoaddukt nanoklasterov ugljeroda i sposob ego poluchenija [Sulfoadduct of nanoclusters of carbon and way of his receiving]. *Russian Patent no. 2478117*. 2013. (rus)
43. Ponomarev A.N. Nanoporistoe uglernodnoe mikrovolokno dlja sozdaniya radiopogloshhajushhh materialov [Nanoporous carbon microfiber for creation of the radiosorption materials]. *Russian Patent no. 2570794*. 2014. (rus)
- Building Materials. 2015. Vol. 97. Pp. 14–24.
33. Schober K.U. *Innovative Timber Composites – Improving Wood with Other Materials*. Bath, UK: Schober, K.U. (ed.), University of Bath. 2013. 48 p.
34. Лобов Д.М., Крысин А.В., Тихонов А.В. Особенности армирования деревянных элементов, усиленных углеродным волокном, при статическом изгибе // Известия КГАСУ. 2013. № 2(24). С. 132–138.
35. Yahyaei-Moayyed M., Taheri F. Experimental and computational investigations into creep response of AFRP reinforced timber beams // *Composite Structures*. 2011. Vol. 93. No. 2. Pp. 616–628.
36. Davalos J.F., Kim Y., Barbero E.J. A layerwise beam element for analysis of frames with laminated sections and flexible joints // *Finite Elements in Analysis and Design*. 1995. Vol. 19. No. 3. Pp. 181–194.
37. Dolan C.W., Galloway T.L., Tsunemori A. Prestressed glued-laminated timber beam—pilot study // *Journal of Composites for Construction*. 1997. Vol. 1. No. 1. Pp. 10–16.
38. Nadir Y., Nagarajan P., Ameen M., Arif M.M. Flexural stiffness and strength enhancement of horizontally glued laminated wood beams with GFRP and CFRP composite sheets // *Construction and Building Materials*. 2016. Vol. 112. Pp. 547–555.
39. Franke S., Franke B., Harte A. Failure modes and reinforcement techniques for timber beams – State of the art // *Construction and Building Materials*. 2015. Vol. 97. Pp. 2–13.
40. Svecova D., Eden R.J. Flexural and shear strengthening of timber beams using glass fibre reinforced polymer bars – an experimental investigation // *Canadian Journal of Civil Engineering*. 2004. Vol. 31. No. 1. Pp. 45–55.
41. Kim Y.J., Harries K.A. Modeling of timber beams strengthened with various CFRP composites // *Engineering Structures*. 2010. Vol. 32. No. 10. Pp. 3225–3234.
42. Пономарев А.Н., Юдович М.Е., Козеев А.А. Сульфоддукт нанокластеров углерода и способ его получения // Патент по. 2478117. 2013.
43. Пономарев А.Н. Нанопористое углеродное микроволокно для создания радиопоглощающих материалов // Патент по. 2570794. 2014.

Aleksandr Rassokhin,
+7(911)526-68-59; rassokhinaleksandr@gmail.com

Andrey Ponomarev,
+7(911)929-35-22; 9293522@gmail.com

Oleg Figovsky,
+972(50)577-99-20; figovsky@gmail.com

Александр Сергеевич Рассохин,
+7(911)526-68-59;
эл. почта: rassokhinaleksandr@gmail.com

Андрей Николаевич Пономарев,
+7(911)929-35-22;
эл. почта: 9293522@gmail.com

Олег Львович Фиговский,
+972(50)577-99-20;
эл. почта: figovsky@gmail.com

© Rassokhin A.S., Ponomarev A.N., Figovsky O.L., 2018

doi: 10.18720/MCE.79.15

Environmental impact of the tunnel construction

Влияние строительства тоннелей на окружающую среду

R.V. Vvedenskij,*Open joint stock company scientific, research,
design and surveying institute**«Lenmetrogioprotrans», Saint Petersburg,
Russia***S.G. Gendler,***Saint-Petersburg Mining University,
St. Petersburg, Russia***T.S. Titova,***Emperor Alexander I St. Petersburg State
Transport University, St. Petersburg, Russia***младший научный сотрудник****Р.В. Введенский,***«Научно-исследовательский, проектно-
изыскательский институт**«Ленметрогипротранс», Санкт-Петербург,
Россия***д-р техн. наук, профессор С.Г. Гендлер,***Санкт-Петербургский горный университет,
Санкт-Петербург, Россия***д-р техн. наук, заведующая кафедрой,
проректор по научной работе****Т.С. Титова,***Петербургский государственный
университет путей сообщения Императора
Александра I, Санкт-Петербург, Россия***Key words:** traffic tunnels; environment; unique environmental and geographic conditions; detrimental impact; monitoring; pollutants**Ключевые слова:** транспортные тоннели; окружающая среда; уникальные природно-географические условия; негативное воздействие; мониторинг; атмосферный загрязняющие вещества

Abstract. The object of research are traffic tunnels at the combined road (motorway and railway) the city of Adler to the Alpica Servis alpine resort, which construction and operation was bound up with negative environmental impact. Analysis of the environmental impact of technological processes during the construction and operation of tunnels was carried out data-driven of field study. Scientific and methodical bases of performance mining and environmental monitoring in the unique natural and geographical conditions of the Caucasian Reserve are developed. Nomenclature of monitored indicators, points and frequency of their measurement, as well as the requirements for instrumentation are defined. The measurement result of the pollution content in the air and soil during the construction and operation of traffic tunnels are presented. The objective laws of adverse impact on various components of the environment depending on the construction phase are established.

Аннотация. Объектом исследования являются транспортные тоннели на совмещённой (автомобильной и железной) дороге Адлер – горноклиматический курорт «Альпика - Сервис», строительство и эксплуатация которых была связана с негативным воздействием на окружающую среду. Анализ влияния технологических процессов, сопровождающих строительство и эксплуатацию тоннелей на окружающую среду, был осуществлен на основе данных натурных наблюдений. Разработаны научно-методические основы проведения горно-экологического мониторинга окружающей среды в уникальных природно-географических условиях Кавказского заповедника, определяющие перечень контролируемых показателей, точки и частоту их измерения, а также требования к приборному обеспечению. Приведены результаты измерений содержания загрязняющих веществ в атмосферном воздухе и почво-грунтах в периоды строительства и эксплуатации транспортных тоннелей. Установлены закономерности, характеризующие уровни негативного воздействия на различные компоненты природной среды в зависимости от периода строительства.

1. Introduction

At the beginning of the 21st century, the volume of traffic tunnels construction in Russia has increased manyfold. Due to the demand for traffic infrastructure construction for hosting of the 2014 Winter Olympic Games, the 2017 FIFA Confederations Cup and the 2018 FIFA World Cup, as well as for creating favourable conditions for the development of the modern sport and resort centres, the construction has moved to the regions with unique environmental and geographic conditions, above all to the Krasnodar region districts (Adler, Tuapse and Anapa) [1]. Besides the railroad tunnels construction, motorroad tunnels construction has initiated in these districts. The most typical example of this trend is the city of Adler, where 9 traffic tunnels, among them 6 railroad tunnels and 3 motorroad tunnels, were constructed for hosting the 2014 Winter Olympic Games (Figure 1).



Figure 1. Tunnel routes layout

These tunnel routes pass through the premises of The Western Caucasus nature reserve, rich in rare flora and fauna species and unique in its relief, which includes the Mzymty river flowing in the vicinity of the motorway. In accordance with the existing regulations, anthropogenic impact in this area is permissible provided that it does not incur a long-term disruption of the environment that would spread beyond the construction sites during the construction period and buffer zones during the operation period [2].

As for the peculiarities of assessing the environmental impact of tunnels under construction and of working out impact reduction measures, it should be noted that a significant difference exists between the reference admissible concentration limit concentrations in the working area air and their maximum one-time concentrations used for environmental impact assessment. These two values can be significantly different. For instance, the admissible concentration limit of sulphur dioxide for the working areas is 10 mg/m^3 . The maximum one-time concentration is 0.5 mg/m^3 . The difference between these reference values further increases in the atmosphere of cities with the population over 200000 people and in the resort districts, where the pollutants concentration should not exceed 80 % of the maximum one-time concentration value, considering the dispersion of the pollutants.

Compared to the construction of the surface facilities, the construction and the further operation of traffic tunnels has important specific features that influence the limit and the result of the detrimental environmental impact.

The following are the specific characteristics of such impact during the construction period:

- simultaneous construction works on the ground surface and underground, which influences all the biosphere components: the atmosphere, the soil, the surface and ground water, the flora and the fauna, and the population;

- application of various technologies for the construction of tunnels and surface facilities, such as: manual mining operations, use of tunnel boring machines, roadheaders; drilling and blasting operations, digging, drilling and pile insertion works, and concrete works;
- use of a large variety of construction machines and equipment;
- considerable duration of works, which can last up to 5 years with a temporary change in the detrimental impact limits [6].

The assessment of detrimental environmental impact in the period of construction was performed in 2009–2013 as regular quarterly observations during the construction of traffic tunnels at the combined road (motorroad and railroad) connecting Adler and the Alpika-Servis alpine resort. In the course of observations, simultaneous measurements of the thermodynamic and chemical parameters of the air in the tunnel excavations and at the construction sites were made, as well as the analyses of the chemical composition of the drainage and the waste water, and of the soil in the part of the road that are adjacent to the tunnel portals [7].

During the operation period, the number of factors that determine the environmental impact of the traffic tunnels decreases [8]. Besides, while during the construction period the environmental impact is almost similar for railroad and motorroad tunnel construction, provided that similar tunneling techniques are applied, during the operation of motorroad tunnels the main detrimental factor is the polluting vehicle exhausts that increase the pollutants concentration in the tunnel air and in the atmosphere and, consequently, in the soils in the portal areas [9]. Railroad tunnels have minimal impact on the atmosphere, however, the noise impact of the train in the portal areas is significant [10].

In 2014–2017, the assessment of the traffic tunnels detrimental environmental impact was completed with the instrumental measurements of the pollutants concentration in the atmosphere and the soil during the operation period.

The study reveals that national and foreign literature does not cover environmental issues enough as to traffic tunnels [11]. The absence of scientifically based data challenges evaluation and choice of environmentally safe construction technology [12]. Given the unique nature and geography, this may wreak significant social and economic damage [13].

The field study performed was marked by a large number of measurement tools used in a limited construction space of nine traffic tunnels (six railway tunnels and three road tunnels) from 128 to 4572 m long, as well as by unique nature and geography of the construction area. The results of the study will serve as a basis for the development of environmentally friendly construction of traffic tunnels under similar conditions.

2. Methods

2.1. Monitoring during tunnels construction

When providing monitoring during tunnels construction, the emphasis was made on measuring the pollutants concentration in the atmosphere [14]. The monitoring technique was tested and adjusted during the tunnels construction for the first tunnel ensemble consisting of relatively parallel motorroad and railroad tunnels and a service adit located between the tunnels. The tunnels and the adit were linked by a breakthrough connection. The railroad tunnel measured 2535 metres long, and the motorroad tunnel — 2298 metres long.

The tunnels were created by mined tunneling. Thus, the first railroad tunnel was built with the use of the Voest Alpine Miner AM75 roadheaders that allow to do machine mining of soils with various rock strength of the tunnel bearing rocks; the motorroad tunnel was built in a similar way. The sources of environmental impacts were identical: motor transport and excavation equipment, which produce a considerable share of pollutants while functioning.

The ecological monitoring during tunnels construction was done every quarter between 2009 and 2013. The monitoring activities included the assessment of construction impact on the atmosphere, on the water, and on the soil of the near-portal sites.

The assessment of the impact on the atmosphere consisted in determining the concentration of the suspended substances, of carbon oxide (CO), sulphur dioxide (SO₂) and nitrogen dioxide (NO₂) in the air. The measurement were made at various sites in the excavation (face, middle of the tunnel, portal and construction site). Following portable hardware were used:

- portable gas analyzer PGA-200 (CO, SO₂, NO₂). Original equipment manufacturer – Russia; limit percentage error is 25 %;
- dust meter ICP-4 (suspended substances). Original equipment manufacturer – Russia; limit percentage error is 25 %.

In order to assess the tunnels construction impact on the near-portal sites soil, samples of the surface layer at the depth of 0.0–0.2 m were analysed. The analysis looked for oil products and heavy metals [15]. The soil type is chernozem with stony inclusions.

This interval allowed determining the areas and periods of works that have the highest or the lowest environmental impact [16]. As well as allowed discovering the correlation between the exhausts and the pollutants dispersion in the atmosphere and establishing the dynamics of the pollutants accumulation and wash-out from the soil.

2.2. Monitoring during tunnels operation

The methodology of the study at that period of time implied the measurement of physical, chemical and thermodynamic characteristics of ambient air and chemical analysis of soils. Since the main contamination source is motor vehicles, most measurements were focused on road tunnels [17]. Since contaminated air is emitted into the atmosphere through tunnel portals, measurement points were arranged directly at the portals and around right-of-way areas adjacent to the highway at a 50 m distance from the portals. The choice of measurement points and tools met the requirements of the construction period [18].

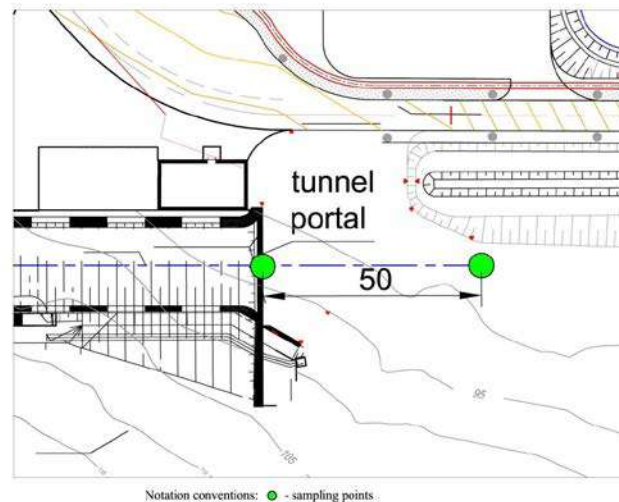


Figure 2. Sampling points chart

3. Results and Discussion

At the initial stage of construction, the pollutants concentration at the tunnel portal is around 0–0.2 mg/m³. As the length of the tunnel increased, an increase in the pollutants concentration was observed (up to 5.0 mg/m³), which may be explained by the increase in the amount of mining and conveyor equipment operating in the tunnel simultaneously. The drop in the pollutants concentration occurred after the creation of a breakthrough in the tunnel (February 2011) and after the completion of the main excavation works, as the result of the change in the ventilation system (Figure 3).

Before the creation of the breakthrough, the railroad and the motorroad tunnels were aired through plenum ventilation system. After the breakthrough connection was created between the tunnel sections with opposed egresses, in the central part of the tunnels airway stoppings were built, dividing thus the tunnels into two separate parts, each of them aired through plenum ventilation. In the period of equipping of the mined excavations they were aired with a ventilator installed at the airway stopping and supplying air depending on the direction of the natural draught towards the northern or the southern portal.

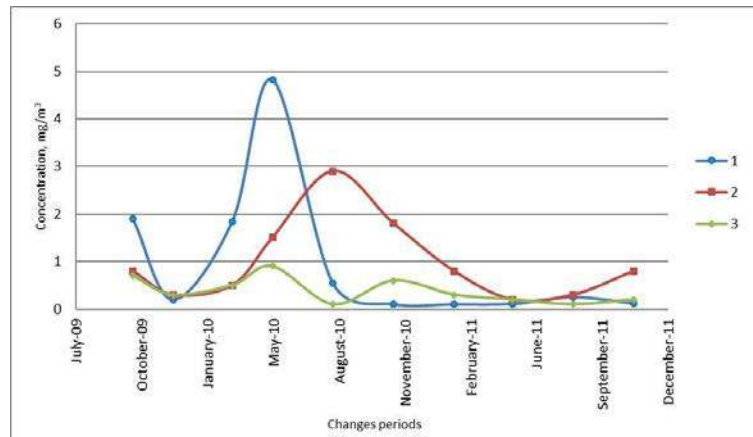


Figure 3. Pollutants concentrations at the tunnel portal, where 1 – suspended substances concentration; 2 – carbon oxide concentration; 3 – sulphur dioxide concentration

During the motorroad tunnel construction results similar to those of the railroad tunnel were obtained. During the initial construction stage, a stronger environmental impact was observed. After the creation of a breakthrough and the completion of the main tunnel excavation works, the impact decreased.

The described atmosphere environmental load dynamics may be explained by the increase in the amount of the load-haul-dump units as the length of the mined tunnel section grew and, consequently, the pollutants dumping into the tunnel air intensified.

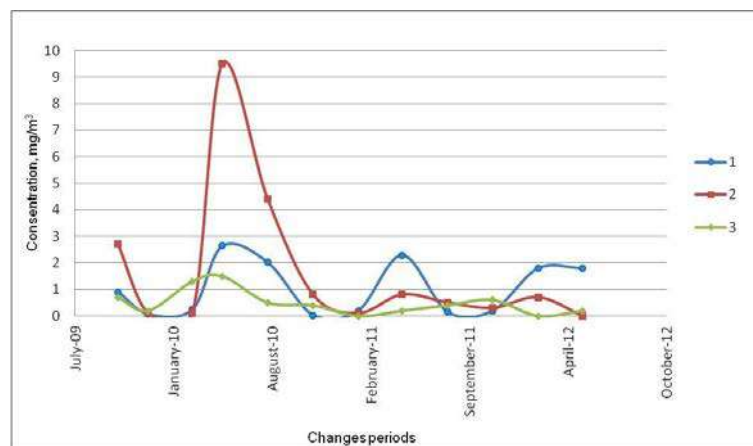


Figure 4 — Pollutants concentrations at the tunnel portal, where 1 – suspended substances concentration; 2 – carbon oxide concentration; 3 – sulphur dioxide concentration

Accordingly, the analysis of the monitoring results obtained during the construction period demonstrated that in the course of traffic tunnels construction the environmental load, in particular that of the atmosphere, is not uniform. The environmental load is minimal at the initial construction period and increases as the mined tunnel sections grow in length and the mining works intensify. After the completion of the main construction stage, during the tunnel equipping, the environmental load drops again.

3.1. The results of the pollutants concentration measurement in the atmosphere during operation

The results of the measurements demonstrated that in the course of the railroad tunnels operation at the section connecting Adler and Alpika-Servis alpine resort, no sources of atmosphere impact were detected, while the impact on the drainage industrial water evacuated from the tunnel is minimal.

In the course of motorroad tunnels operation the main source of detrimental impact on the atmosphere were the pollutants exhausts of the motor transport. The final pollutants concentration in the air flow exiting the tunnel depends on the motor vehicles traffic, which changes throughout the day: maximal during the "rush hour" and minimal at night; it also depends on the amount of air moving along the tunnels.

The measurements were made at different moments of the day in different air flow density conditions. Thus, the "rush hour" was set from 10.00 till 12.00. The regular traffic period was defined as 22.00 to 00.00.

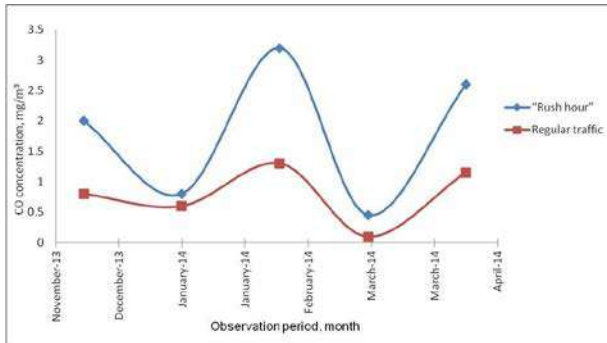


Figure 5. CO concentration at the southern portal of motorroad tunnel No. 1 during operation

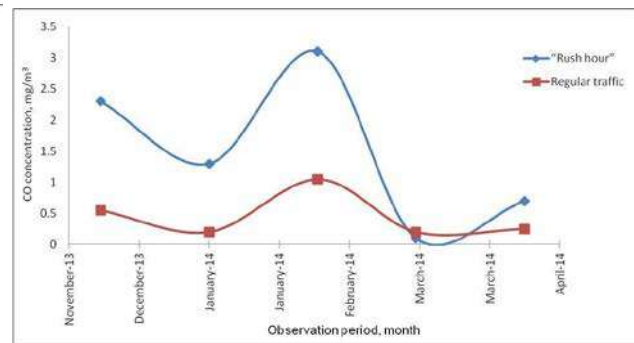


Figure 6. CO concentration at the northern portal of motorroad tunnel no. 1 during operation

The increase in the traffic causes a certain degradation of the environmental conditions. However, even in the periods of busy traffic typical for the "rush hour", the CO concentration in the atmosphere at the tunnel portals and near-portal sites does not exceed the recommended values stipulated by Hygienic Regulations GN 2.1.6.1338-03 " Admissible concentration limits Concentrations in the Atmosphere of Inhabited Areas". In the periods of decreased traffic (regular period) the pollutants concentrations drop even lower than the "rush hour" values (Fig. 5 and 6).

3.2. Results of measurements of pollutants concentration in the soil at near-portal sites during construction

According to the results of the measurements, the pollutants concentration in the air depends on the amount of motor transport and construction equipment operating in the tunnel and at the construction site at the time of measurement. Due to this, the concentration value may be significantly different for different periods. For more detailed assessment of the environmental impact, the oil products and heavy metals concentrations in the surface soil layers in the near-portal tunnel areas were measured; these areas may over time accumulate part of the pollutants settling down on their surface after exiting the tunnel in the tunnel air flow [19]. The pollutants accumulation in the soil has wavelike character (with peaks of concentration). The periods of accumulation are succeeded by periods of pollutants wash-out from the soil [20].

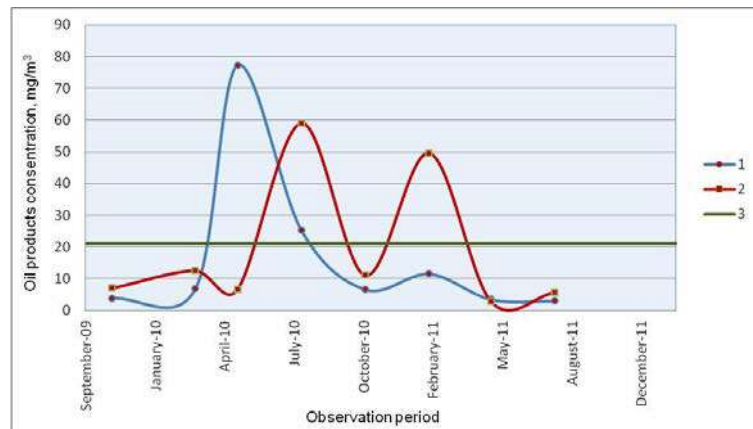


Figure 7. Oil products concentration in the soils at the near-portal areas of the railroad tunnel no. 1. 1 – southern portal; 2 – northern portal; 3 – background concentration

In order to determine the extent of the surface soil layer chemical pollution the overall pollution indicator (Z_c) was used (1).

$$Z_c = K_{c_1} + \dots + K_{c_i} + \dots K_{c_n} - (n - 1) \quad (1)$$

where n – quantity of analytes;

C_i – concentration of the i -th pollutant component.

Z_c is a sum of the concentration coefficients K_c (2) of the toxic substances (pollutants) of the I, II and III class of toxicologic hazard (mostly metals) divided by the background values.

$$K_c = \frac{C_i}{C_{NBC}} \quad (2)$$

where C_{NBC} – natural background concentration.

The changes in the Z_c values with time determine the dynamics of change in the heavy metals concentrations in the soil compared to the background concentration. As well as can identify the periods of metals accumulation and migration in the soil.

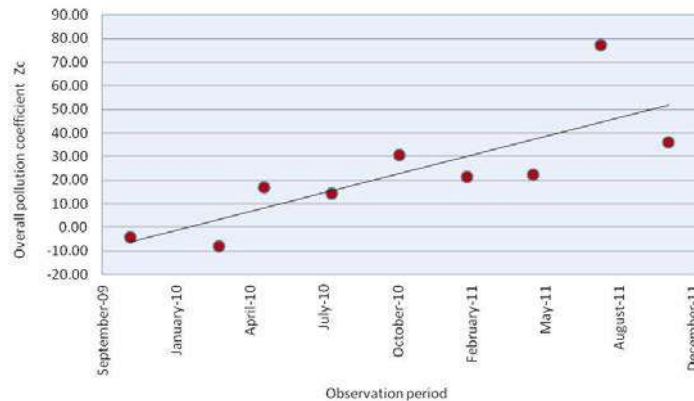


Figure 8. Changes in Z_c during railroad tunnel construction

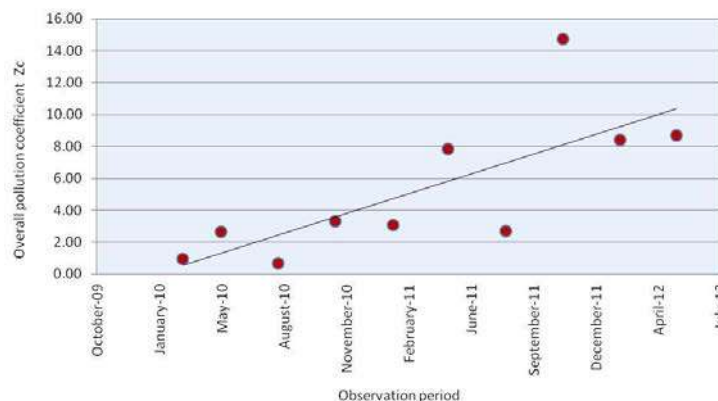


Figure 9. Changes in Z_c during motorroad tunnel construction

As demonstrated by the preceding diagrams, depending on the samples collection period, the metals concentration in soil tends to increase. This trend is confirmed by the linear correlation between the Z_c coefficients and the time of impact. The linear correlation coefficients for the railroad and the motorroad tunnels were 0.79 and 0.75 respectively.

However, as it turns out, the oil products and the heavy metals soil concentrations dynamics is influenced not only by the technological processes related to tunnel construction, but also by the environmental factors related to the alternation of the dry and rainy seasons.

3.3. Results of measurements of pollutants concentration in the soil at near-portal sites during operation

In order to determine the concentration of pollutants that settle down on and accumulate in the daylight surface of the right-of-way area of the tunnels, surface soil layer samples were collected. The samples were analysed to determine the presence of heavy metals (Table 1).

Table 1. Comparative of heavy metals concentration in the surface soil layer of the near-portal areas of the motorroad and the railroad tunnels

Indicator	Concentration, mg/kg	
	Railroad tunnel	Motorroad tunnel
1	2	3
Copper, Cu	14.1	34.2
Zink, Zn	43.7	77.1
Lead, Pb	9.6	19.3
Cadmium, Cd	0.69	1.01
Mercury, Hg	0.05	0.05
Arsenic, As	2.22	8.12
Nickel, Ni	22.5	74.4
Manganese, Mn	1211	2730
Cobalt, Co	8.1	30.5

The comparison of heavy metals concentrations in the soil allows making a conclusion regarding the environmental situation during the operation of motorroad and railroad tunnels.

Thus, based on Table 1, the heavy metals concentration in the soils of areas adjacent to the motorroad tunnel are considerably higher than those of the areas near the railroad tunnel.

The data obtain confirms the higher level of detrimental impact during operation of motorroad tunnels than during the operation of the railroad tunnels.

4. Conclusion

1. Evaluation of the negative impact of tunnel construction and operation of transportation tunnels and the designing measures to reduce it should be carried out on the basis of data from mining and environmental monitoring including periodic observations of all the environmental conditions both at construction sites and in the adjacent territory.

2. Mining and environmental monitoring revealed that the level of anthropogenic impact on environment in case of tunnel construction depends on the technology of tunnel digging, construction stages and mining, conveying and tunneling equipment.

3. The analysis of measurements of the content of pollutants in the atmospheric air at the tunnel portals and around them made during construction period showed that the environmental impact on was unbalanced. Being minimal at the initial construction stage, it increased together with the length of the tunnel dug and the intensity of tunneling works. After the completion of the main construction, environmental impact decreased while tunnels were being finished.

4. The dynamics of pollutant concentration in soil and ground in areas adjacent to the excavation sites on the day surface is wavelike, what is associated with the accumulation of pollutants during the dry period and with their washing and transfer into the Mzymta river during by rains;

5. A distinctive feature of the environmental impact from the operation of road tunnels in comparison with railway tunnels is the increased concentration of pollutants in the ambient air near the portals that depends on the traffic intensity, and higher concentrations of heavy metals in soil and ground.

6. The correlations revealed make it easier to forecast the negative environmental impact during the construction and operation of transportation tunnels depending on their type, construction technology and the specifics of their usage at different periods.

References

1. Pinchuk A.P., Teslya V.O. Ehkologicheskoe sostoyanie atmosfery Krasnodarskogo kraja [Ecological state of the atmosphere Krasnodar territory]. *Scientific works of KubSTU*. 2016. No 11. Pp.66-75. (rus)
2. Samysheva I.M., Pavlova L.V. Ehkologicheskij aspekt ehkspluatatsii stroitelstva I rekonstrukcii avtomobilnyh mostov dorog, tonnelej [Ecological aspect of operation,

Литература

1. Пинчук А.П., Тесля В.О. Экологическое состояние атмосферы Краснодарского края // Научные труды Кубанского государственного технологического университета. 2016. № 11. С. 66–75.
2. Самышева И.М., Павлова Л. В. Экологический аспект эксплуатации, строительства и реконструкции автомобильных мостов, дорог, тоннелей // Экология и

- construction and reconstruction of highways, bridges, tunnels]. *Ecology and scientific-technical progress. Urbanology*. 2015. Vol.1. Pp. 498-503. (rus)
3. Gendler S.G., Dompalm E.I., Vvedenskiy R.V., Kotomina A.Y., Mogilnyy M.V., Ryzhova L.V. Ehkologicheskoe soprovozhdenie stroitelstva i ehkspluatatsii transportnyh tonnelej i metropolitenov – osnova dlya minimizatsii negativnogo vozdeystviya na okruzhayushchuyu sredu [The ecological accompaniment construction and exploitation transport tunnel and subways - basis for minimization negative environmental impact]. *Metro and tunnels*. 2016. No 6. Pp 25-31. (rus)
 4. Gendler S.G., Rogalev V.A. Ocenka zagryazneniya atmosfernogo vozduha pri stroitelstve i ehkspluatatsii transportnyh tonnelej [Estimation of atmospheric air pollution at construction and operation of traffic tunnel] *Journal of Mining Institute*. 2012. Vol. 195. Pp. 152-155. (rus)
 5. Scoba V.A., Surnina E. K. Ehkologicheskaya bezopasnost pri stroitelstve i ehkspluatatsii transportnyh tonnelej [Environmental safety during the construction and operation of transport tunnels] *Technical regulation in transport construction*. 2016. No 6 (20). Pp. 10-13. (rus)
 6. Yong Y. Construction and environmental protection of Geleshan tunnel. *Modern Tunnelling Technology*. 2004. No. 41(1). Pp. 68–72.
 7. Ryzhova L.V., Titova T.S., Gendler S.G. Ensuring environmental safety during the construction and operation of tunnels in residential areas. *Procedia Engineering*. 2017. Vol. 189. Pp. 404–410.
 8. Gendler S.G., Dompalm E.I., Kotomina A.Y. Ocenka zagryazneniya atmosfery pri ehkspluatatsii transportnyh tonnelej [The estimation of atmosphere pollution during transport tunnel exploitation]. *Mining informational and Analytical Bulletin (scientific and technical journal)*. 2009. No 5. Pp. 377-381. (rus)
 9. Trofimenko Y., Kruchkov D. Ehksperimentalnaya ocenka zagryazneniya vozduha v gorodskih avtotransportnyh- onnelyah [Experimental estimation of air pollution in city road tunnels]. *Vestnik Moskovskogo avtomobilno-dorozhnogo gosudarstvennogo tehnikeskogo universiteta (MADI)*. 2005. No 4. Pp. 116-120. (rus)
 10. Xiankun W. Countermeasures against environmental impact in the construction of Zhongnanshan extra-long tunnel. *Modern Tunnelling Technology*. 2003. No. 40(6). Pp. 31–38.
 11. Ridley P. Modelling pollution dynamics of longitudinally ventilated road tunnels. *Journal of Wind Engineering and Industrial Aerodynamics*. 2017. Vol. 163. Pp. 55–64.
 12. Attanayake P.M., Waterman M.K. Identifying environmental impacts of underground construction. *Hydrogeology Journal*. 2006. Vol. 14. No. 7. Pp. 1160–1170.
 13. Aruna kumari N., Paul S. Impact of Tunnels in Environment. *International Journal of Engineering Trends and Technology (IJETT)*. 2013. Vol. 4. No. 8. Pp. 3429–3433.
 14. Bezrodnyj K.P., Lebedev M.O. Gorno-ehkologicheskij monitoring pri stroitelstve i ehkspluatatsii transportnyh tonnelej Severnogo Kavkaza [Minind and ecological monitoring during construction and operation North Caucasus transport tunnels]. *Science studies*. 2014. No 5 (24). [Electronic source]. System requirements: AdobeAcrobatReader. URL: <https://naukovedenie.ru/PDF/12KO514.pdf> (access date: 07.06.2017). (rus)
 15. Derkachev V.A., Dmitrienko V.A. Snizhenie zagryaznenij grunta pri stroitelstve avtodorozhnogo tonnelya [Decrease in pollution of soil at construction road tunnel]. *Mining science and technology*. 2013. No 8. Pp.12-16. (rus)
 16. Vaníček I., Jirásko D. Vaníček M. Transportation and Environmental Geotechnics. *Procedia Engineering*. 2017. научно-технический прогресс. Урбанистика. 2015. Т. 1. С. 498–503.
 3. Гендлер С.Г., Домпальм Е.И., Введенский Р.В., Котомина А.Ю., Могильный М.В., Рыжова Л.В. Экологическое сопровождение строительства и эксплуатации транспортных тоннелей и метрополитенов - основа для минимизации негативного воздействия на окружающую среду // *Метро и тоннели*. 2016. № 6. С. 25–31.
 4. Гендлер С.Г., Рогалев В.А. Оценка загрязнения атмосферного воздуха при строительстве и эксплуатации транспортных тоннелей // *Записки Горного института*. 2012. Т. 195. С. 152–155.
 5. Скоба В.А., Сурнина Е.К. Экологическая безопасность при строительстве и эксплуатации транспортных тоннелей // *Техническое регулирование в транспортном строительстве*. 2016. № 6(20). С. 10–13.
 6. Yong Y. Construction and environmental protection of Geleshan tunnel // *Modern Tunnelling Technology*. 2004. № 41(1). Pp. 68–72.
 7. Ryzhova L.V., Titova T.S., Gendler S.G. Ensuring environmental safety during the construction and operation of tunnels in residential areas // *Procedia Engineering*. 2017. Vol. 189. Pp. 404–410.
 8. Гендлер С.Г., Домпальм Е.И., Котомина А.Ю. Оценка загрязнения атмосферы при эксплуатации транспортных тоннелей // *Горный информационно-аналитический бюллетень (научно-технический журнал)*. 2009. № 5. С. 377–381.
 9. Трофименко Ю.В., Крючков Д.В. Экспериментальная оценка загрязнения воздуха в городских автотранспортных тоннелях // *Вестник Московского автомобильно-дорожного государственного технического университета (МАДИ)*. 2005. № 4. С. 116–120.
 10. Xiankun W. Countermeasures against environmental impact in the construction of Zhongnanshan extra-long tunnel // *Modern Tunnelling Technology*. 2003. № 40(6) Pp. 31–38.
 11. Ridley P. Modelling pollution dynamics of longitudinally ventilated road tunnels // *Journal of Wind Engineering and Industrial Aerodynamics*. 2017. Vol. 163. Pp. 55–64.
 12. Attanayake P.M., Waterman M.K. Identifying environmental impacts of underground construction // *Hydrogeology Journal*. 2006. Vol. 14. № 7. Pp. 1160–1170.
 13. Aruna kumari N., Paul S. Impact of Tunnels in Environment // *International Journal of Engineering Trends and Technology (IJETT)*. 2013. Vol. 4. № 8. Pp. 3429–3433.
 14. Безродный К.П., Лебедев М.О. Горно-экологический мониторинг при строительстве и эксплуатации транспортных тоннелей Северного Кавказа // *Интернет-журнал Науковедение*. 2014. No 5 (24). [Электронный ресурс]. Систем. требования: AdobeAcrobatReader. URL: <https://naukovedenie.ru/PDF/12KO514.pdf> (дата обращения: 07.06.2017).
 15. Деркачев В.А, Дмитриенко В.А. Снижение загрязнений грунта при строительстве автотрoжного тоннеля // *Горные науки и технологии*. 2013. № 8. С. 12–16.
 16. Vaníček I., Jirásko D. Vaníček M. Transportation and Environmental Geotechnics // *Procedia Engineering*. 2017. Vol. 189. Pp. 118–125.
 17. Гендлер С.Г. Экологические аспекты проветривания транспортных тоннелей в условиях мегаполисов // *Записки Горного института*. 2016. Т. 218. С. 313–321.
 18. Allen J., May P., Hughes L., Salmon L.G., Cass G.R. Emissions of size- segregated aerosols from on-road vehicles in the Caldecott Tunnel // *Environmental Science & Technology*. 2001. № 35. Pp. 4189–4197.
 19. Zhuravleva M.A., Zubrev N.I., Kokin S.M. Contamination of roadside areas with heavy metals // *World of Transport and*

Введенский Р.В., Гендлер С.Г., Титова Т.С. Влияние строительства тоннелей на окружающую среду // *Инженерно-строительный журнал*. 2018. № 3(79). С. 140–149.

- Vol. 189. Pp. 118–125.
17. Gendler S.G. Ehkologicheskie aspekty provetrivaniya transportnyh tonnelej v usloviyah megapolisov [Ecological aspects of vehicle tunnels ventilation in the conditions of megalopolises] *Journal of Mining Institute*. 2016. Vol. 218. Pp. 313–321. (rus)
18. Allen J., May P., Hughes L., Salmon L.G., Cass G.R. Emissions of size- segregated aerosols from on-road vehicles in the Caldecott Tunnel. *Environmental Science & Technology*. 2001. No. 35. Pp. 4189–4197.
19. Zhuravleva M.A., Zubrev N.I., Kokin S.M. Contamination of roadside areas with heavy metals. *World of Transport and Transportation*. 2014. Vol. 6(55). Pp. 174–181.
20. Baydarashvili M., Shrednik N., Spasovskaia A. Detection Method of Pollution with Heavy Metals Ions of the Soil. *Procedia Engineering*. 2017. Vol. 189. Pp. 630–636.
- Transportation. 2014. Vol. 6(55). Pp. 174–181.

Roman Vvedenskij,
+7(911)261-56-28; romanvvedenskij@gmail.com

Semen Gendler,
+7(812)328-86-21; sgendler@mail.ru

Tamila Titova,
+7(812)457-81-34; t.s.titova@gmail.com

Роман Владимирович Введенский,
+7(911)261-56-28;
эл. почта: romanvvedenskij@gmail.com

Семен Григорьевич Гендлер,
+7(812)328-86-21; эл. почта: sgendler@mail.ru

Тамила Семеновна Титова,
+7(812)457-81-34;
эл. почта: t.s.titova@gmail.com

© Vvedenskij V.R., Gendler S.G., Titova T.S., 2018



ПОЛИТЕХ
Санкт-Петербургский
политехнический университет
Петра Великого

Инженерно-строительный институт
Центр дополнительных профессиональных программ

195251, г. Санкт-Петербург, Политехническая ул., 29,
тел/факс: 552-94-60, www.stroikursi.spbstu.ru,
stroikursi@mail.ru

Приглашает специалистов проектных и строительных организаций,
не имеющих базового профильного высшего образования
на курсы профессиональной переподготовки (от 500 часов)
по направлению «Строительство» по программам:

П-01 «Промышленное и гражданское строительство»

Программа включает учебные разделы:

- Основы строительного дела
- Инженерное оборудование зданий и сооружений
- Технология и контроль качества строительства
- Основы проектирования зданий и сооружений
- Автоматизация проектных работ с использованием AutoCAD
- Автоматизация сметного дела в строительстве
- Управление строительной организацией
- Управление инвестиционно-строительными проектами. Выполнение функций технического заказчика

П-02 «Экономика и управление в строительстве»

Программа включает учебные разделы:

- Основы строительного дела
- Инженерное оборудование зданий и сооружений
- Технология и контроль качества строительства
- Управление инвестиционно-строительными проектами. Выполнение функций технического заказчика и генерального подрядчика
- Управление строительной организацией
- Экономика и ценообразование в строительстве
- Управление строительной организацией
- Организация, управление и планирование в строительстве
- Автоматизация сметного дела в строительстве

П-03 «Инженерные системы зданий и сооружений»

Программа включает учебные разделы:

- Основы механики жидкости и газа
- Инженерное оборудование зданий и сооружений
- Проектирование, монтаж и эксплуатация систем вентиляции и кондиционирования
- Проектирование, монтаж и эксплуатация систем отопления и теплоснабжения
- Проектирование, монтаж и эксплуатация систем водоснабжения и водоотведения
- Автоматизация проектных работ с использованием AutoCAD
- Электроснабжение и электрооборудование объектов

П-04 «Проектирование и конструирование зданий и сооружений»

Программа включает учебные разделы:

- Основы сопротивления материалов и механики стержневых систем
- Проектирование и расчет оснований и фундаментов зданий и сооружений
- Проектирование и расчет железобетонных конструкций
- Проектирование и расчет металлических конструкций
- Проектирование зданий и сооружений с использованием AutoCAD
- Расчет строительных конструкций с использованием SCAD Office

П-05 «Контроль качества строительства»

Программа включает учебные разделы:

- Основы строительного дела
- Инженерное оборудование зданий и сооружений
- Технология и контроль качества строительства
- Проектирование и расчет железобетонных конструкций
- Проектирование и расчет металлических конструкций
- Обследование строительных конструкций зданий и сооружений
- Выполнение функций технического заказчика и генерального подрядчика

По окончании курса слушателю выдается диплом о профессиональной переподготовке
установленного образца, дающий право на ведение профессиональной деятельности

